Loughborough University

This item was submitted to Loughborough's Research Repository by the author.
Items in Figshare are protected by copyright, with all rights reserved, unless otherwise indicated.

An investigation into the design parameters of expanding mandrel sleeves

PLEASE CITE THE PUBLISHED VERSION

PUBLISHER

Loughborough University of Technology

LICENCE

CC BY-NC 4.0

REPOSITORY RECORD

Knight, J.A.G.. 2021. “An Investigation into the Design Parameters of Expanding Mandrel Sleeves”. Loughborough University. https://doi.org/10.26174/thesis.lboro.15015201.v1.

AN INVESTIGATION INTO THE DESIGN PARAMETERS OF EXPANDING MANDREL SLEEVES.

BY

J.A.G. KNIGHT
B.Sc., C.ENG., M.I.PROD.E.

A THESIS

SUBMITTED IN PARTIAL FULFILMENT OF THE REQUIREMENTS

FOR THE AWARD OF THE DEGREE OF

MASTER OF SCIENCE

OF

LOUGHBOROUGH UNIVERSITY OF TECHNOLOGY

JUNE 1976

SUPERVISOR: D.J. BILLAU, M.Sc., C.ENG., M.I.MECH.E., F.I.PROD.E.

CENTRE FOR INDUSTRIAL STUDIES,

DEPARTMENT OF ENGINEERING PRODUCTION.

ACKNOWLEDGEMENTS

The author wishes to express his gratitude to Mr. D.J. Billau, his supervisor, for his understanding, concern and his continued help and encouragement without which this thesis would never have been written.

The author's thanks are also due to

Professor R.J. Sury, for his permission to undertake this research.

Mr. H. Baxter, for his fruitful suggestions and his technical help during the experimental work.

To his former colleagues in the Centre for Industrial Studies for encouragement and helpful discussion throughout.

To the undergraduates of Loughborough University of Technology who manufactured many of the specimens and apparatus used in this research.

Finally, the author expresses his sincere gratitude to his wife for the many hours she has spent in the production of this thesis.

Synopsis

The aim of the present investigation was to establish the influence of the design parameters on the performance of a proprietary expanding mandrel. For the mandrel system investigated the parameters have been identified as the diameter and length of the mandrel sleeve and the number of slots contained within the mandrel sleeve.

To enable the action of the sleeve to be understood more simply linear models of the mandrel sleeve have been manufactured from steel and Araldite, the latter being used in comparative photoelastic studies. The results achieved from the load/ extension tests upon the steel linear models enabled a mathematical model of the action of the mandrel sleeve in the free state to be established. Close correlation between the predicted and experimental radial expansion of the mandrel sleeve has been obtained. The mathematical model allows the influence of the design parameters on the free radial expansion of the mandrel sleeves to be established at a design stage.

The second phase of the investigation was the performance of the mandrel in a simulated working environment. Stiff rings have been manufactured to represent the workpiece, transducer elements were embedded into the rings which enabled the contact pressure at the interface of mandrel/ workpiece to be established. Variation of contact pressure down the axial length of the mandrel was found to exist for all the mandrel sleeves tested, the variation was found to reduce as the diameter of sleeve increased. Similarities in the action of a 'shrink-fit' of shaft and ring and the expansion-fit of a mandrel sleeve and workpiece have been established. The efficiency of the mandrel system has been shown to be mainly a function of the

diameter of the sleeve with the number of slots contained within the sleeve a secondary factor. From the data of the contact pressure/ applied load tests an empirical expression has been derived which relates the output of the mandrel sleeve to the diameter and applied load.

CONTENTS

LIST OF FIGURES

LIST OF TABLES

LIST OF PLATES

NOMENCLATURE

A	Constant
b	Breadth
C	Constant, circumferential expansion, linear extension
D	Diameter, diametral expansion
D_{es}	End section diameter
e	Strain
E	Youngs Modulus
f	Stress
F_{CR}	Euler crippling load
F_G	Gripping force
h	Smallest dimension of a rectangle
I	Second moment of area
I_{es}	Second moment of area of end section
k	Radius of gyration
l	Length of mandrel beam element
l_{es}	End section length
L	Length of slender column
L^*	Mandrel length
M	Bending moment
M_r	Beam element 'built in' moment
N	Number of beam elements
P	Pressure
W	Applied load, circumferential tension
W_A	Load applied to mandrel
W_c	Radial load per metreof circumference
W_o	Radial component of load
W_r	Reaction load on conical tapers
W_T	Circumferential tension in thin tube
x	Distance along beam
y	Distance from neutral axis, deflection
y_{es}	End section deflection
y_n	Deflection of one beam element
α	Slope of end section
θ	Half included angle of conical taper
μ	Coefficient of friction
ϕ	$\text{Tan}^{-1}\ \mu$

CHAPTER 1

INTRODUCTION AND LITERATURE REVIEW

1.1 INTRODUCTION

It has been the tendancy in the United Kingdom to neglect the development and associated research of work holding devices for machine tools. Thornley & Wilson(1) have recently stated that, 'Only in the more recent years has chuck development awakened to the surge of progress, and investigations on a scientific basis carried out in order to assess their capabilities and limitations'. Most of this work has been carried out in Germany (2),(3), very little has been published in the United Kingdom. This British complacency can be traced back to before the 1914-18 war (4), when the purchase of German scroll chucks, which was then the current practice, became impossible. Several British machine tool makers were forced by the circumstances to design and manufacture their own chucks (5). This complacency again returned after the war and remained until the more recent and notable investigations (1),(6).

If the investigations on a scientific basis, of chucks, have been limited it can be said that the investigations concerning mandrels are negligible. Indeed the analysis of the replies received from a survey of manufacturers showed that the present 'design methods' were based on empirical information and experience in the field, obtained over many years. No scientific approach to the design was found to exist.

It is from this basis of 'What we did yesterday, scaled up or down, will do today', that this research project was initiated. The research being part of a larger research programme, at Loughborough University of Technology, to investigate work holding devices so that the performance of such work holding devices can be better designed to match the improved accuracy, performance, tolerances and faster speeds,

which are expected from today's machine tools.

The aim of this research is to investigate and establish relationships between, number of slots, diameter, applied load and corresponding expansion for a proprietary split bush type expanding mandrel, and further to establish the nature and magnitude of the interface pressure between workpiece and mandrel. From the results obtained it is planned to be able to better predict the importance of the relevant design parameters and to so develop simple design criterea for the first time.

Mandrels, or shafts for holding work to be machined, are commonly used on machine tools for the purpose of correctly positioning the component to be machined and to maintain this location against the cutting forces and reactions. Mandrels are of two types plain and expanding, the plain mandrel is the simplest workholder for round workpieces. The main characteristic of the mandrel is a slightly tapered chucking surface with a taper of the order of .49mm per metre (.006 inches per foot). The workpiece diameter must be smaller than the largest diameter of the mandrel, and the workpiece is forcibly pushed endwise onto the mandrel. This produces a gripping force all around the hole in the workpiece, decreasing axially in relation to the interference produced between the outer diameter of the mandrel and the workpiece (7). The driving torque that can be transmitted depends on the radial gripping and the tangential friction forces produced.

With plain mandrels it is not always easy to obtain the same driving power or to position the workpiece to a definite stop when trying to control the resulting interference between workpiece and madrel. Pressing the workpiece onto the mandrel requires an arbor press, is slow, and may damage the finish of

the workpiece bore and score the mandrel and if the bore is not round and straight, the workpiece and mandrel will mutually distort under the forces used to press on the workpiece.

Expanding mandrels overcome many of the problems associated with plain mandrels, it is possible to mount and dismount the work with ease and without seizing or scoring of the work or mandrel. The workpiece does not have to be pressed onto the mandrel to produce the gripping force. The force is produced by some mechanism giving a mechanical advantage to the operator and can be applied completely remote from the expanding mandrel itself as in the use of pneumatically or hydraulically operated expanding mandrels.

Expanding mandrels also require a smaller number of operations to mount the workpiece and they have increased the useful range of manufacturing tolerances (the functional lack of precision of the plain mandrel limits the useful range of manufacturing tolerances). Many designs of expanding mandrels are available ranging from the stationary collet type through to the hydraulically operated expanding mandrel with 'incompressible plastic mass'. The many types of expanding mandrel available give rise to a wide application in industry. Alignment and assembly of body and wings in the Aerospace Industry, inspection and balancing in the Automotive Industry, and in the turning, milling and grinding operations on machine tools, these are all typical of todays use of expanding mandrels.

1.2 LITERATURE REVIEW

1.2.1 Early History of Expanding Mandrels.

During the early part of the 19th Century the fastening of boiler tubes to the smokebox and firebox tubeplates of locomotives was a constant source of trouble. There were at that early time two methods in common use, the tube could be riveted in position, with a protruding length hammered down over the surrounding metal. Alternatively, a tapered steel ferule could be driven into one end of the tube with the effect of expanding it and holding it firmly in place.

A third method (8) was intrduced by a Dr Church, an amateur engineer in Birmingham, who in 1838 invented what was probably the first expanding mandrel, which enabled the end of the tube to be expanded manually in situ in the tubeplate. Although designed for a work-forming purpose and not a work-holding the mandrel has all the features of the stationary collet type of expanding mandrel used today (9).

The workforming type of mandrel and other similar ones, which probably developed from Dr Church's, became a common tool in a boiler makers tool kit and over the years became accepted as a standard piece of equipment, the rights and name of the original inventor being forgotten.

Some 27 years after Dr Church's invention a letter appeared in the Engineer (10) requesting information about the origin of the invention of an expanding mandrel for fixing brass tubes in boilers. Royalties were now having to be paid by all users of this type of expanding mandrel, to a single railway company who claimed patent rights of the design.

The letter provoked a lively correspondance (11)-(21) with claims and counterclaims as to the originator of the expanding mandrel. The matter was finally brought to a conclusion by

the editor of the Engineer after some 10 months (November 1860-August 1861) when illustrations of the original mandrels, made by Dr Church in 1833, were published (10).

During the 50 year period (1860 - 1910) that followed the letters in the Engineer the expanding mandrel evolved from a workforming tool into a workholding device, very little evidence of how this took place is available, indeed the author was unable to find any references concerning expanding mandrels over this 50 year period, during his literature survey.

We do know however, that by the 1914 - 18 war many forms of expanding mandrels were available, (22), (23), and from this time until the present, numerous references concerning expanding mandrels are available all following the similar pattern of being either of a descriptive nature, rather than of a technical nature, or being advertising literature. The details of the former being published in many instances to enable similar mandrels to be manufactured by the readers of the journals.

1.2.2 Stationary Collet Mandrels

The stationary collet mandrel can consist in its simplest form of a body bored internally with a female conical taper and being slit in two or four places to permit it to deflect in expanding and collapsing (28). Usually into the internal female taper fits a male tapered plug which has either an internal or external thread at one end. The mandrel is expanded by tightening the taper plug. Many lathe operators who have needed to locate off a turned bore for second operation work have made themselves a simple expanding mandrel of this type (24).

By 1915 the collet type expanding mandrels of this simple design were being manufactured as proprietary items, Dowd (23) reviewed the design of an expanding collet which could be held on the spindle of a turret lathe. Chapman (25) designed a rather special collet type mandrel for long work. The arbor had two male tapers and the split collet sleeve having two internal female tapers to match the arbor. The sleeve had three slots cut axially from each end to a point 25mm (1 inch) from the centre. The result was in fact two split collets back to back.

Hall (26) conducted some work into the optimum angle of the conical taper on the tapered plug. After experimentation he came out in favour of three designs. For the first he recommended an angle of slightly less than that used regularly on spring collets, 15 degrees. On the second design he chose a smaller angle to increase the gripping power and to accomodate smaller work. His third design, for very small work which precluded the use of a threaded plug, used a plain taper plug to expand it. The taper recommended being Brown and Sharp or Morse. Dixie (27) recommended an included angle of 16° for the tapered plug.

An included angle of 60° was suggested by Gitter (29),

this was to enable a roller bearing centre, fixed into a tailstock, to actuate the mandrel. The design being a simple mandrel split longitudinally two ways. Mulholland (30) used a similar large included angle for his design of an expanding mandrel which tightens into blind holes. Wevers (31) and Courtney (32) suggested included angles of 18 degrees and 24 degrees respectively, in their designs.

A variation on the split collet design was shown by Baule (33). The mandrel consists of a round bar held in a normal three jaw chuck. This bar has a hole drilled diametrically through the bar, a slot is milled or sawed in the end of the bar axially down the bar to this hole. A further hole is drilled and tapped diametrically on one finger of the mandrel only, a grub screw is fitted in this tapped hole, the screw contacting the underside of the other finger. A third hole is drilled clearance in one finger and tapped in the other for a bolt to pass through. When the grub screw is tightened the mandrel is expanded, sufficient pressure being exerted on the bore of the workpiece. The bolt is used to draw the split fingers together if they over-expand during use.

1.2.3 Hydraulic and Solid Elastic Expanding Mandrels

Hydraulic expanding mandrels do not seem to have been common before the 1940's. During the Second World War (1939-45) several proprietary mandrels were produced, no doubt to facilitate high precision grinding and turning required at this time. The hydraulic type of expanding mandrel is expanded by a self-contained hydraulic system which creates true, accurate centering with an equalised gripping force. By turning an actuating screw a piston is moved forward and hydraulic fluid is forced from the piston chamber up through the parts and into a space between the expanding sleeve and the mandrel body. A single mandrel can be designed to expand in several different sizes of bores of a workpiece or different workpieces.

Schroeder (34) reviewed the design of an hydraulically expanded mandrel which was used during the Second World War, it was developed to give accurate centering. (37) Anon., shows a similar design.

The relative incompressible property of some rubber and plastic material has been utilised in the design of expanding mandrels. Alfred Herbert of Coventry (35) produced an interesting mandrel which is very similar in design to the normal hydraulic expanding mandrel except that the expanding medium (normally hydraulic oil) is replaced by a commercial rubber. The rubber changes its shape under pressure but the volume remains constant. The thrust therefore exerted on the rubber by the actuating screw system is transmitted to the expanding portion of the tool, the degree of expansion being kept within the elastic limit of the material from which the mandrel body is made.

Herriman (36) designed a simple expanding mandrel which used the recovery properties of rubber to hold the workpiece.

1.2.4 Mandrels with Sliding Elements or Inserts

This type of expanding mandrel has been very popular since the First World War, many references are available describing particular designs from individuals. This popularity has culminated in the roller actuated expanding mandrels being produced in commercial quantities (37).

Some interesting early designs which incorporated a sliding jaw up an incline plane are shown by Jones (38) and Wheeler (39). Fletcher (40) gives details of a proprietary mandrel of similar design manufactured in Belfast in 1918. Hohn (41) described a design of a mandrel to accomodate large cylinder bushings for locomotives. The mandrel consisted of a shaft, two spiders, two cone washers, two nuts and sixteen arms, (eight on each spider), bushes of different sizes are accomodated by using interchangeable arms of different length (for bushings ranging from 483 - 762mm (19 - 30in.). The ends of the arms are machined to the same angle as the conical washers. When the nuts are tightened the conical ends of the washers expand (force) the arms outward radially so that they grip the bushing. The arms which fit into radial slots milled in the face of the spiders are held in position by capscrews.

Dick (42) designed an expanding mandrel for holding bushings and pieces of tubing of considerable length. The work is held by six hardened gripping inserts, three at each end of the mandrel. The inserts are carried in slots 120 degrees apart. The inner ends of the inserts are machined to suit the male conical taper of the mandrel body, the outer ends are rounded. Relative movement of the conical tapers, actuated by a screwthread causes the inserts to move out radially and thereby grip the workpiece. This design was claimed to have a big improvement over the expanding mandrel which worked with

a tapered plug driven into a split bushing. Whittle (43), Gerber (44) and Heise (45) proposed mandrels of similar designs.

The cutting forces produced during the machining operation have been utilised in the Pin-Cam type of expanding mandrel (46). The mandrel of solid construction has ramp-type cams ground on it, and a series of rollers are positioned to ride axially across the cams. As the workpiece is turned relative to the mandrel, the pins are forced outwards into contact with the bore and effect the gripping pressure. The ramp-type cam is made with a small angle which becomes a locking angle to secure the workpiece. If the angle is too steep, no locking can be effected, too shallow and difficulty is experienced in loosening. A pin cage retains the rollers with a snap ring to prevent loss. It is claimed that high concentricities can be maintained of the order of 25.4um (.0001 in.) and the action of the pins causes an equal force around the bore. The Efficiency Tool Products Company (47) produced a 'Self Gripping' mandrel of similar design in 1919.

The use of rollers to expand tubular shell which are not split lengthwise is described by Conn (46). These proprietary Roll-lock mandrels expand by the gradual rolling and wedging action of straight rollers between the conically tapered inner diameter of the shell and the conically tapered plug which is turned by a wrench. This type of mandrel which has a chucking area not weakened by axial slots generally has a small range of expansion, of the order of .002mm per mm of diameter (.002 ins. per in. of diameter). Concentricities of 5 - 10um (.0002 - .0004in.) total indicated reading can be obtained.

1.2.5 The Split-Sleeve Expanding Mandrel

This type of mandrel is the most popular of the commercially produced mandrels, Erickson (48) in the United States (Bristol Erickson in the U.K.), Tobler of France (49) being the market leaders in the field. Indeed these mandrels are in use on numerous machine tools in the most important automobile manufacturers works in Europe for all types of machining operations i.e., turning, gear shaping, grinding, inspection etc. This design of mandrel has been fitted out to approximately 70% of the machine tools destined for Togliatigrad in the U.S.S.R.

Charlton (50) in 1919 reviewed the use of the split bush type mandrel and commented on their wide use in industry, he suggested a method of correctly positioning the workpiece on this type of mandrel. Rowell (51) gave a complete review of the materials and processes required to manufacture a split bush type expanding mandrel and gave the angle of taper on the tapered arbor and on the inside of the bushings to be 31.24mm per metre (.375 ins. per foot). Four slits (two from each end of the bushings) were suggested for small diameters and eight for larger diameters.

Gergens (52) dealt with several designs of the split bush type expanding mandrel. He showed that the way in which the sleeve is slotted and the taper of the arbor so designed could affect the operational characteristics of the mandrel. A design was put forward so that uniform expansion of the sleeve could be obtained, an alternative design could effect the ends of the bushing to expand and not the centre. Arrangements which overcame the tendancy of the bushings to lock were also proposed.

Many patent designs of split bush type expanding mandrels

which utilize some special design feature have been reviewed. Holmes (53), Whittles (54) and Hudson (55) are typical of these.

Mason (56) reviewed the design of a split bush type expanding mandrel where the conical taper on the arbor part of the mandrel system is not one continuous taper. The arbor has what is termed a double angle, i.e., widely spaced precision ground male conical surfaces. The spacing of the conical surfaces causes uniform increase in bush diameter when the bush is moved up the taper. The result of this action is to create a uniform gripping pressure along the entire length of the workpiece.

A review of equipment manufactured by the Tobler Corporation Anon. (57) shows the position of expanding mandrels in relation to workholding devices for modern machining methods, Anon. (58) and Anon. (59) point out the close relationship between precision expanding mandrels and increased productivity.

CHAPTER 11

DESIGN AND DESCRIPTION OF EXPERIMENTAL EQUIPMENT

2. Design and Description of Experimental Equipment

2.1 The Split Bush Expanding Mandrel System

It was decided at the outset of the research project that the mandrel system to be investigated would be a proprietary split bush expanding mandrel.

To ascertain what expanding mandrel systems were available in the United Kingdom a detailed survey of the manufacturers and suppliers was undertaken. The results of the survey indicated that the most suitable system for this research project was the one manufactured by the Bristol Erickson Company of Kingswood, Bristol

This mandrel system offered outstanding features over other expanding mandrel systems.

(a) Bristol Erickson is the largest British manufacturer of the split bush expanding mandrel and other associated work holding devices.

(b) This type of mandrel has been supplied to many industries in the United Kingdom and Europe.

(c) The cost and delivery was competitive.

(d) The mandrel system offered was typical of the split bush type expanding mandrel.

(e) The range of mandrels available allowed more design parameters to be studied than any other comparable system.

A comprehensive system was purchased from Bristol Erickson, comprising in total eighteen split bush sleeves and the two associated arbors to complete the mandrel system. The eighteen split bush sleeves consisted of two basic lengths of sleeve 42.86 mm.(1.6875 in.) and 26.98 mm.(1.0625 in.), three different diameters 60.32 mm.(1.375 in.), 50.80 mm.(2.0 in.) and 41.27 mm.(1.625 in.), and three different angular spacings of slots 45°, 36° and 30°. Plate 1 shows the mandrel sleeves and Plate 2 shows an assembly of arbor and mandrel sleeve.

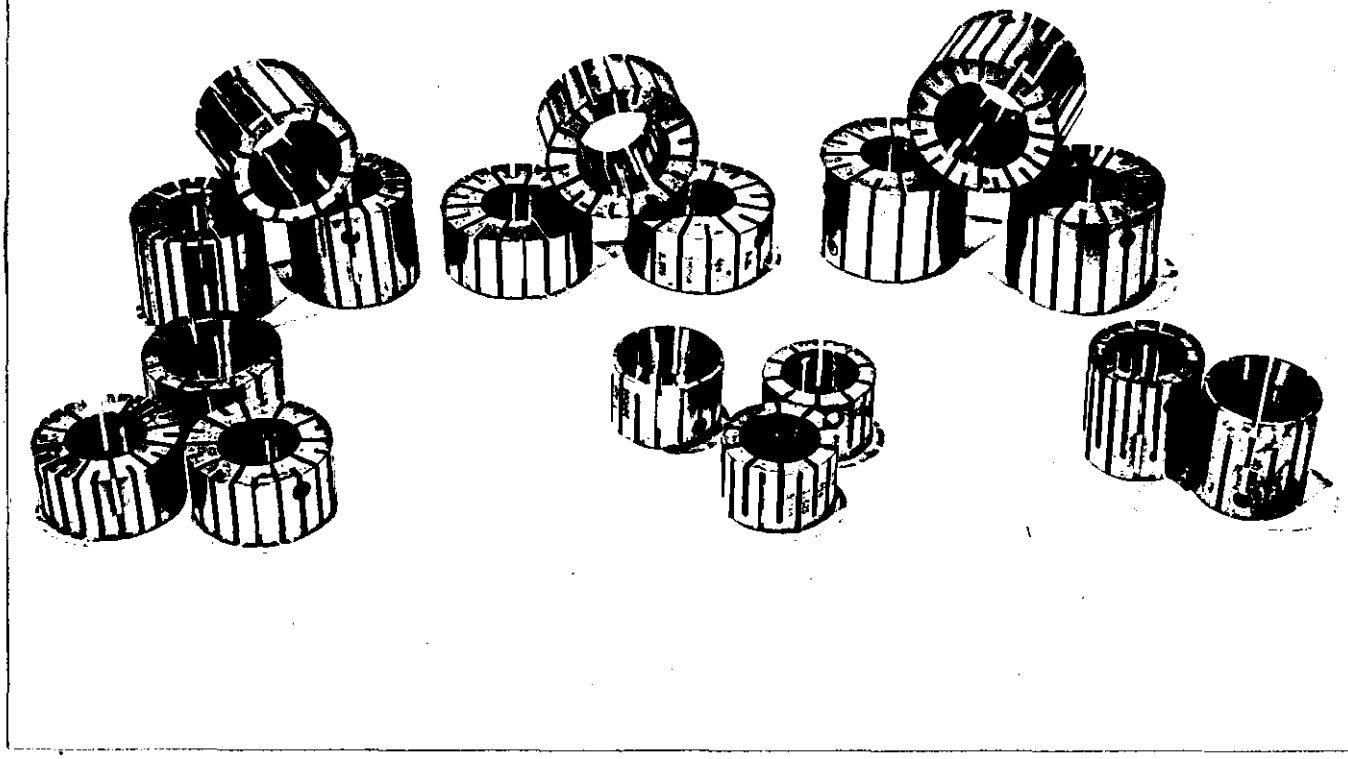

Plate 1. Mandrel sleeves

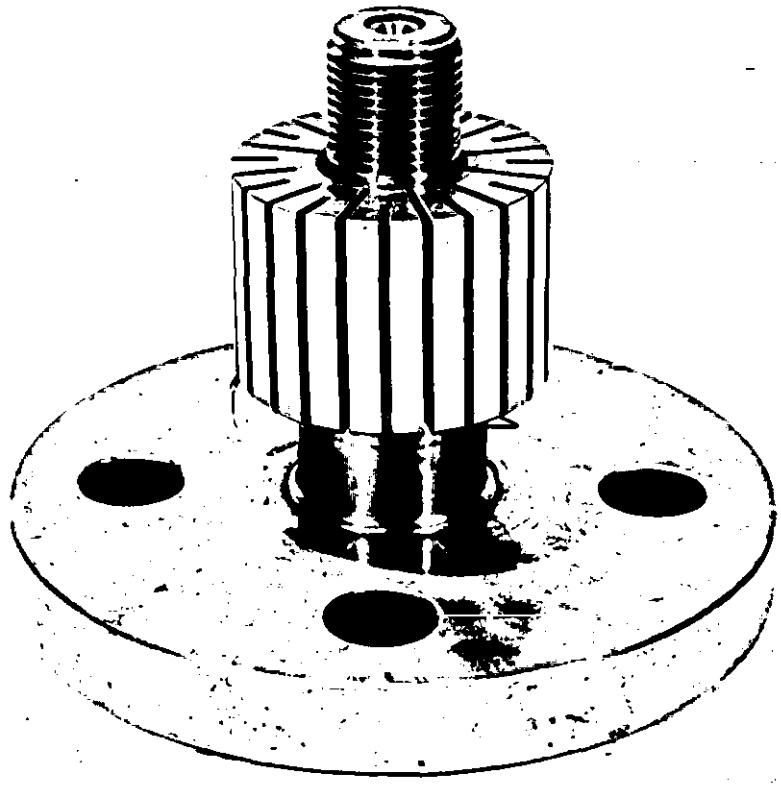

Plate 2. Mandrel assembly

The Bristol Erickson system has as one of its main features the 'double parallel angle principle'. The arbors, shown in figure 2.1, display what is meant by the 'double angle'. There are, on the arbor, two male conical tapered surfaces spaced a set distance apart, these tapered surfaces mate on the corresponding female conical tapered surfaces located at each end of the mandrel sleeves. The included angle (36°) of the two tapered sections is the same, hence the parallel angle. The use of this double parallel angle allows the system to utilize a large enough angle so that the tapers do not lock. Also the physical size of the end sections of the mandrel sleeve are reduced, this limitation will later be shown by the author to have a direct influence on the expansion characteristics of the mandrel sleeves. The use of a non-locking angle is an important feature in a production situation because this gives automatic removal of the gripping force between workpiece and mandrel when the loading on the mandrel is removed, giving easy workpiece removal.

The interchangeable split bush sleeves, shown in figure 2.2, are cylindrical in form, the outside diameter being parallel, with the inside diameter having two female conical sections of 36° included angle located one at each end of the sleeve. The cylinder is split axially from each end to within a short distance of the opposite end, the slots have equal angular spacing.

Figure 2.3. shows a typical assembly of a sleeve and arbor, it is also useful to help to understand the action of the mandrel system. If a force is applied to the top surface, designated X, of the sleeve (note, the actual way in which the force is generated can be of many forms) the sleeve is forced to move downward and by doing so further up the conical

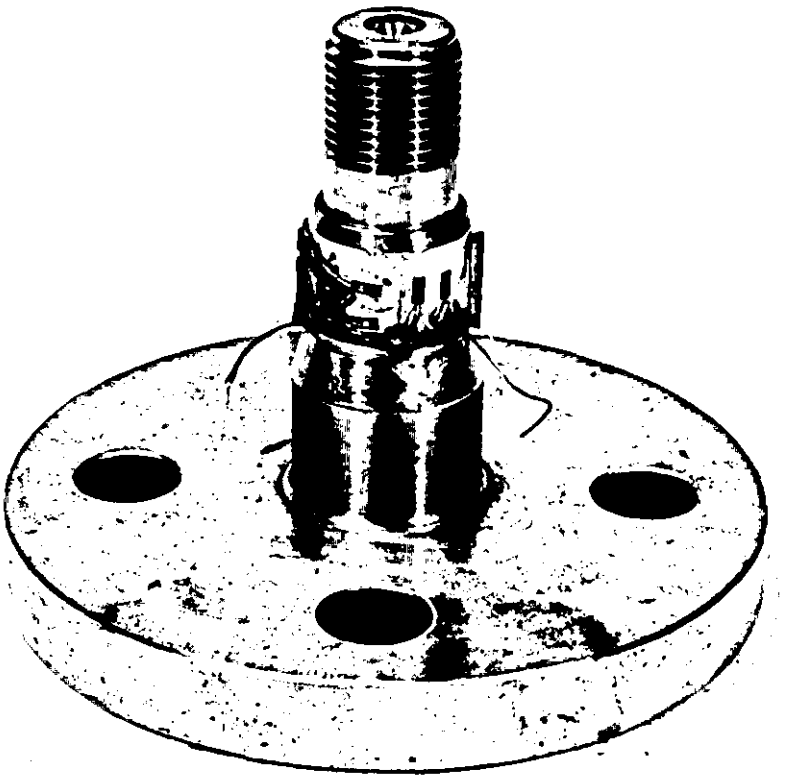

Plate 3. Modification to arbor.

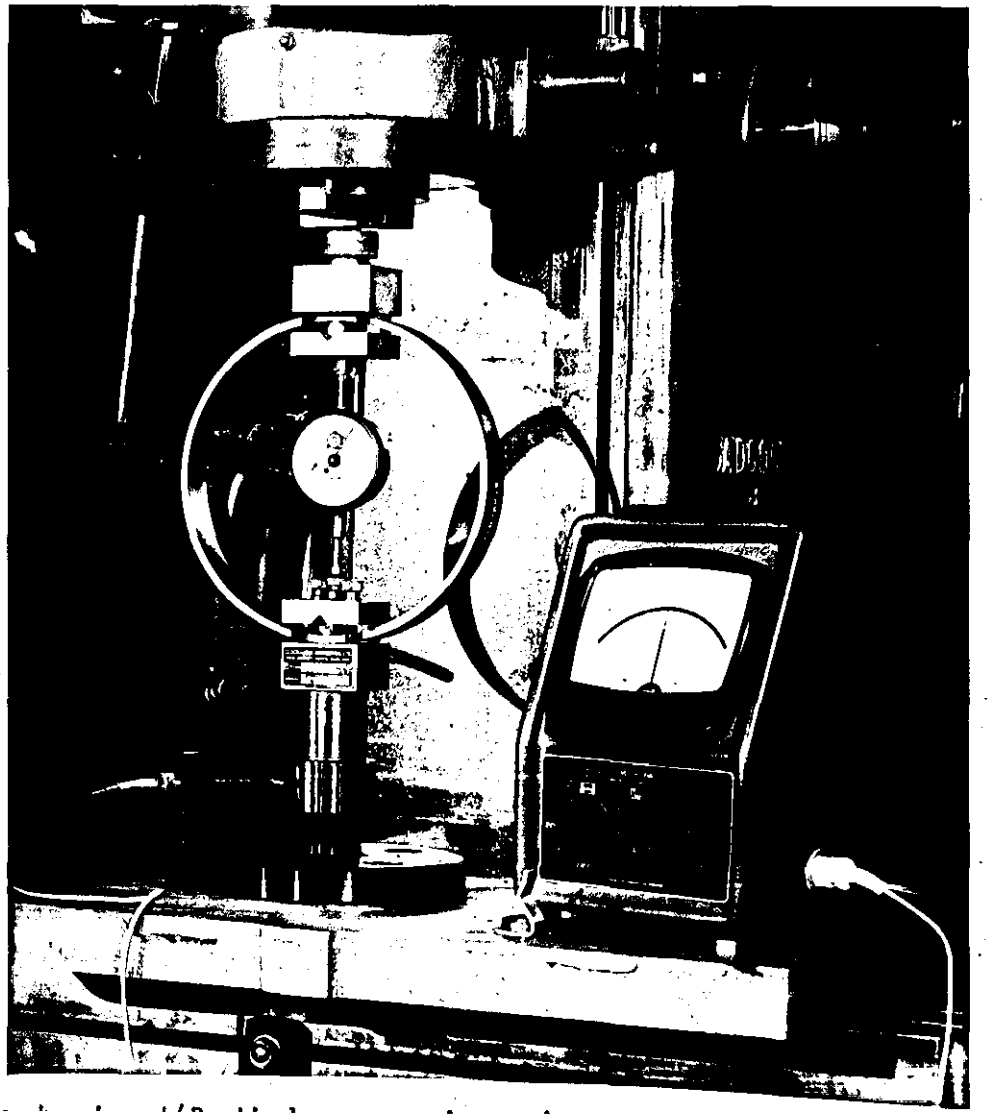

tapers on the arbor. Movement up the taper causes radial pressures to be generated on the mating surfaces between arbor and sleeve, this pressure causes the split sleeve to expand. Equilibrium is reached when the circumferential tension in the sleeve balances the radial pressure. It is the restriction of the radial expansion by a workpiece which causes a pressure to be generated at the interface of the sleeve outside diameter and the workpiece inside diameter. This pressure force generated correctly positions the component to be machined and maintains this location against cutting forces and reactions.

2.1.1 Modification to the Arbor

The 0.53mm. (.021 inch) radial clearance, dimension A on figure 2.3, between the sleeve and the arbor would have created interference and trapping of the strain gauge wiring system to be installed on the arbor. The use of 10/.10 gauge wire, the smallest gauge p.v.c. insulated wire commercially available, required that either the sleeves or the arbor would have to be machined. Small grooves were therefore machined in the arbor using the Wickman Electrical Discharge Machine. The small grooves semicircular in cross-section enabled the wires to be set below the surface of the mandrel. The position of the grooves and the associated strain gauges are shown on plate 3.

Four T.M.L. type FLE-1-11 strain gauges were installed on the arbor between the two tapered sections. The wiring diagram is shown in figure 2.4.

2.2 Experimental Rig for Radial Expansion

Instrument Data.

Rank Taylor Hobson Mitronic Micro-Comparator with axial transducer head.

Full scale deflection ranges .1mm., .030mm., .010mm. and .003mm.

Mean sensitivity on .003mm. F.S.D. = .0001mm.

Clockhouse proving ring type 2000. number 1537.

Dial gauge no. 74562. Last calibrated October 1972.

Mean sensitivity 5.93 Newtons per division.

The experimental set up for the measurement of radial expansion of the mandrel sleeve for a given applied load is shown in plate 4.

The mandrel system is mounted upon a baseplate, also mounted on the baseplate is a brass supporting stand which holds the axial transducer head for the Rank Taylor Hobson Mitronic Micro-Comparator. A hardened steel collar is positioned on top of the sleeve and a Clockhouse proving ring is positioned on the collar, the whole arrangement being in axial alignment.

The rig was designed to be used upon any device which could give uniform and controllable load application to the mandrel system. Tensile testing machines, small presses hydraulic or mechanical, or the movement of the table towards the spindle head on milling machines, were all possible methods considered to apply the load to the mandrel. For convenience, the rig was set up on an Adcock and Shipley vertical milling machine type 18/32, the use of this as the loading medium ensured that

(a) The required accuracy and repeatability was obtained throughout the loading range.

(b) The loading could be applied easily and positively by the upward movement of the table towards the machine spindle head.

(c) The slideways locating the table ensured that the axial alignment of the rig was maintained.

(d) With the machine not running there were no vibration problems.

(e) Easy and rapid manipulation and adjustment of the rig was obtained.

The rig was positioned upon the loading apparatus (Adcock & Shipley vertical milling machine) by placing the baseplate on the worktable, the free end of the Clockhouse proving ring being positioned against a brass thrust bar under the spindle head. Loads were applied to the mandrel system by raising the worktable towards the spindle head, thereby causing a deflection of the proving ring and thus creating a known load to be applied to the mandrel system.

2.3 Manufacture of Linear Models of Mandrel Sleeves for Photoelastic Studies

Linear models of the mandrel sleeves are the physical representation of the cylindrical sleeves in a straight line form. The linear models can be thought of as though one had cut through one side of the cylindrical sleeve and then opened it out into a straight line. Figure 2.5. shows the range of Araldite linear models manufactured.

Araldite CT 200, which is an epoxy resin suitable for photoelastic studies, was purchased ready cured in 9.5mm.(.375in.) sheet form. From the sheet 6 strips were cut, two widths of strips were cut 45mm.(1.8025in.) and 27mm (1.0625in.) wide which represented the two lengths of mandrel sleeves. Slots 1.6mm(.0625in.) wide were then machined into the Araldite strips using a 1.6mm. slitting saw on a Cincinatti 2M1 horizontal milling machine, the machine set up is shown in figure 2.6. The cutting speed 15m/min.(50ft/min.) and feed rate 20mm/min.(.75in/min.) were as recommended by MacDonald & Meek (60) , these were found to give excellent results, i.e., low induced machining stresses, low thermal distortion. The spacing of the centre distance between the slots on the linear models represents the average circumferential distance between the slots on the mandrel sleeves, 3 different centre distances for 3 different angular spacings using a constant 50mm.(2in.) diameter mandrel sleeve for reference.

2.3.1. The Photoelastic Bench

The comparative photoelastic studies were undertaken upon a Jessop-Leech photoelastic bench shown diagramatically in figure 2.7. The bench consists of a mercury discharge lamp housed in a protective cover with a cooling fan. Mounted upon a slideway, which enables movement for correct focussing, are four lenses, a polarizer, analyser and two quarter wave plates. The emitted light passes first through the polarizing lense and secondly, if required, through the quarter wave plate which is mounted immediately behind the polarizing lense, the quarter wave plate is hinged to facilitate removal from the light path. A loading frame is set in the middle of the bench immediately after the first set of lenses, this is to enable the specimens to be subjected to a stress whilst in the light path. Finally, the light passes through the second set of lenses which consist of the second quarter wave plate mounted in front of the analyser. The quarter wave plate is again hinged to facilitate removal from the light path. The fringe pattern of the stressed specimen is finally projected via an angled mirror to a frosted glass screen to enable observation or photographs to be made.

Figure 2.8. shows a simple fixture manufactured from mild steel which the encastré beam was held whilst under study in the photoelastic bench. To facilitate the manufacture of an accurate pair of clamp members, face A was ground first and then the clamps were mounted upon face A whilst faces B and C were ground, this was accomplished without removal from the magnetic table.

2.4 Manufacture of Linear Models of Mandrel Sleeves

Linear models of the mandrel sleeves are as defined in section 2.3, a physical representation of the cylindrical sleeves in a straight line form. Three linear models were manufactured from steel, see figure 2.9, the material chosen for the models was En 3b steel in bright bar form. One model was of rectangular cross section, figure 2.9.(a), and two were machined with the mandrel sleeve cross section profile shown in figure 2.9.(b). The spacing of the slots on the models represents the average circumferential distance between the slots on the cylindrical mandrel sleeves, using a 50mm.(2in.) diameter mandrel sleeve for reference.

The slots 1.6mm.(.0625in.) wide were machined in the bar using a 1.6mm. slitting saw on a Cincinatti 2M1 horizontal milling machine, the machine set up is shown in figure 2.6., and the set up for machining the cross section profile to represent the inside of the cylindrical mandrel sleeves is shown in figure 2.10.

2.4.1 Experimental set up for the determination of the Load-Extension characteristics of the Steel Linear Models

Instrument Data.

Rank Taylor Hobson micro-comparator with axial transducer head.

Full scale deflection ranges .1mm, .030mm, .010mm, and .003mm.

Mean sensitivity on .003mm. F.S.D. = .0001mm.

Houndsfield tensile testing machine type with manual loading.

The steel linear models were designed to enable a standard Houndsfield tensile testing machine to be used for the application of load. An essential requirement for the load-expansion rig for the steel linear models was that the method of load application be such as to produce tensile loading only. One loading system which fulfills this requirement is a Houndsfield tensile testing machine, it also has simple load application and accurate load verification over a wide range of loads.

The experimental set up for the load-extension tests is shown in figure 2.11., the set up consists of a standard Houndsfield testing machine into which is mounted the steel linear model. The axial transducer head is mounted in a holder which is fastened to the steel linear model. The transducer head being positioned in the holder so that the stylus is under a deflection by being placed against the datum face of a precision ground steel block, the block also being fastened to the linear model, the datum face and the stylus are initially set up at 90° to each other. Upon loading, the linear model extends thus moving apart the transducer head (held in the holder) and the datum face on the steel block, the stylus thus moves outward and accurate measurement of the extension obtained.

2.5 Design and Manufacture of Interface Pressure Rigs

Andreev and Shat'ko (64) investigated the contact pressures in joints with interference fits. The shaft deformations caused by radial forces produced by the interference fit of a wheel hub on a shaft, were measured by means of pins onto which were attached wire strain gauges. The cylindrical pins with flats for holding the strain gauges were pressed into holes drilled radially in the shaft, the shaft was then machined to the required diameter. Axial holes were provided on the shaft to facilitate the electrical wire connections to the strain gauges. The shaft was then calibrated and the results were plotted, relating the readings on the strain bridges to the pin pressures and strain.

The action of an expanding mandrel can be considered the reverse of a shrink fit. In a shrink fit the bore in a wheel hub is smaller than its mating shaft. To assemble the components it is necessary to either force the shaft into the hub or to heat the hub until it has expanded by an amount at least as much as the interference, the hub can then be easily placed in position on the shaft. It is the shrinking of the hub when cooling which gives the 'shrink fit' its name, it is also this shrinking which creates the radial pressures between the hub and shaft.

The diameter of the expanding mandrel in its unloaded state is smaller than the bore of the workpiece which is to be loaded onto it. When the workpiece is loaded onto the mandrel, the mandrel sleeve is expanded by the application of a load, to meet the bore of the workpiece. It is this expansion which causes the generation of the radial pressure at the interface of sleeve and workpiece. We can thus consider the action of an expanding mandrel to be the reverse of a shrink fit.

It was from this basis that the design idea for the

interface pressure rigs was originated. It was realised that as Andreev and Shat'ko had placed transducer elements in the shaft to measure radial pressures, equally feasible was the placing of transducer elements in the hub to measure these pressures. It was decided then to build first a trial rig with one central strain gauge transducer element to investigate whether the method gave usable results.

The Bristol Erickson expanding mandrel system is manufacture so that the radius of curvature on the beam elements, making up the mandrel sleeve, exactly conform to the radius of curvature of a workpiece bore that is the same size as the quoted nominal diameter of the mandrel sleeve, i.e., a 50.80mm. diameter sleeve when at its nominal diameter measures across any diameter 50.80mm. To ensure that full contact was established between the two element segments and the rig bore/pressure transducers, the interface pressure rigs were manufactured to have a bore diameter within 1.27 μm of the quoted nominal diameter. A further consideration in the design of the interface pressure rigs is that as the mandrel system is loaded the mandrel expands, the amount the mandrel sleeve expands depends upon the stiffness of the workpiece (ratio of increase in bore diameter to internal pressure applied). For a low stiffness value the expansion of the bore becomes significant and the radius of curvature of the bore becomes greater than the radius of curvature of the mandrel sleeve segments, the contact between segment and bore therefore tending towards line contact. On the other hand, the use of workpieces of high stiffness values restricts the expansion of the bore to amounts which can be neglected in terms of change in radius of curvature, contact between segment and bore are therefore kept to a maximum. The interface pressure rigs were manufactured so as to be of high stiffness values with a bore/O/D ratio of 2.5.

Figure 2.12. shows the first trial interface pressure rig designed for use with the 60.32mm.(2.375in.) diameter mandrel. The rig was manufactured from 152.4mm.(6in.) diameter En3B steel. The 152.4mm. diameter billet was held in a three jaw chuck on a Dean Smith and Grace centre lathe, the bore was drilled and finished turned to .38mm.(.015in.) below the nominal 60.32mm. (2.375in.). Face 1 was faced square to the bore. The ring was then marked out for the position of the 4.76mm.(.18in.) reamed hole and associated holes for electrical connections and for the fixing screws to hold the transducer element. The holes were drilled, reamed and tapped on a Herbert 50 radial drilling machine A strain gauge transducer element was manufactured as described in 2.3.2. and was fitted into the 4.76mm.(.18in.) reamed hole as shown in figure 2.13, a small amount of element was left proud of the bore. The element was fastened in position by a set-screw as shown.

The ring was then loaded into a four jaw chuck on a Jones and Shipman internal grinding machine, the bore being checked for concentricity with the machine spindle axis and Face 1. for squareness to this axis, by the use of a dial test indicator. The bore was then finished ground to size, this consequently ground part of the element left proud to the same size as the bore. After removal from the grinding machine the element was taken out of the ring and strain gauges were attached. The element was then placed back in the ring with the wires being received as shown in figure 2.14. The wiring diagram for the strain gauges is shown in figure 2.21.

The initial trial rig showed that meaningful measurements could be obtained (Experimental results see Table 8.52.). From this information 3 interface pressure rigs, figure 2.15, were manufactured using the above techniques, further transducer elements being added to enable pressure measurements to be made down the length of the mandrels.

2.5.1 Design and Manufacture of Transducer Elements

The function of the transducer elements and the design of the interface pressure rigs, into which the elements were to fit, imposed on the elements the form which they had to take, figure 2.16 shows a typical transducer element.

The loading action on the elements is a column action due to axial loading, because the load is a compressive load then an appropriate column equation has to be used in the design. From Hall et. al. (63)

The Euler equation for the critical load for slender columns of uniform cross section is

$$Fcr. = \frac{C.\pi^2.EA.}{(L/k)^2} \qquad (1)$$

The value of C depends on the end conditions. The lowest value of C, .25, is given for one end fixed and the other free of all restraint, although the transducer elements have greater restraint than this, therefore higher value of C and of Fcr., the true fixing conditions are indeterminate, therefore it was considered prudent to use .25.

$$k = \frac{h\sqrt{3}}{6} = \frac{2.92 \times 10^{-3} \times \sqrt{3}}{6} = .84$$

$$\text{from -(1)} \quad Fcr. = \frac{.25 \times \pi^2 \times 206.9 \times 10^9 \times 9.27 \times 10^{-6}}{\left(\frac{25.4}{.84}\right)^2}$$

$$= 5.2 \times 10^3 \text{ N}$$

The estimated maximum load on the element is 365N and the Euler crippling load is given by (1) as 5.2×10^3 N. This gives a factor of safety of 14.

The transducer elements were manufactured from 4.76mm (.18 in.) diameter Silver Steel. Each element was cut originally to a length of 51.0mm(2 in.) as shown in figure 2.16, this enabled the elements to be held in a fixture, figure 2.17, whilst the square section was ground on the centre of the elements. The elements were ground on a Jones and Shipman surface grinder. After the first flat surface had been ground the elements were unlocked in the fixture and then rotated through 90° and relocked in the fixture, a further flat surface was then ground. This series of operations were continued until the square centre section was obtained. The elements were then cut to length, the sections shown dotted in figure 2.16 being removed and end designated B ground flat and square to the element axis.

2.5.2 Design and Manufacture of Strain Gauge Proving Rings

The function of the strain gauge proving rings was to enable the calibration of the transducer elements whilst in position in the interface pressure rigs.

This constraint dictated the form which the proving rings had to take, figure 2.18. The design therefore was limited to one of strength and deformation.

The maximum load on the proving ring is assumed to be the same as the estimated load on the transducer element, see section 2.5.1., 365N (82 lbf).

The generalized formula for bending moments in a thin ring subjected to equal and diametrically opposite loads given in Roark (61) are,

Maximum Bending Moment +ve at position designated 1

Maximum Bending Moment -ve at position designated 2

$$M_+ = .3183\ W.R.$$

$$M_- = -.1817\ W.R.$$

and the generalized form $M = W.R.\ (.3183 - \frac{1}{2} \sin \Theta)$.

The proving rings are to be manufactured from En8 steel which has a Yield Stress of the order of 432 MN/m^2 (28 ton f/in^2).

Now $M_+ = .3183 \times 365 \times 30.16 \times 10$

$= 3.5$ N-m

and $M_- = .1817 \times 365 \times 30.16 \times 10$

$= 2.000$ N-m

from the Simple Bending Equation Morley (62)

$$\frac{M}{I} = \frac{f}{y} = \frac{E}{R}$$

$$M = \frac{fI}{y} \quad \text{transposing} \quad f = \frac{My}{I} \qquad (2)$$

Second moment of area $I = \frac{bd^3}{12}$

for section at point designated 1

$$I = \frac{7.94 \times 10^{-3} \times (3.57 \times 10^{-3})^3}{12}$$

$$= 3.01 \times 10^{-11} \ m^4$$

from (2) $$f = \frac{3.5 \times 1.78 \times 10^{-3}}{3.01 \times 10^{-11}}$$

$$= 207 \ MN/m$$

207 MN/m^2 is well within the Yield Stress of 432 MN/m^2

Bending moment at change of Section (designated 3) $\theta = 30^\circ$

$$M = WR\,(.3183 - \tfrac{1}{2}\sin\theta)$$

$$= 365 \times 30.16 \times 10^{-3} \times (.3183 - (\tfrac{1}{2} \times \sin 30))$$

$$= .748 \ N\text{-}m$$

This is less than the M_- figure and can be neglected

Bending moment at 2

$$M_- = -2.00 \ N\text{-}m$$

$$I = \frac{bd^3}{12} = \frac{7.94 \times 10^{-3} \times (2.38 \times 10^{-3})^3}{12}$$

$$= 8.93 \times 10^{-12} \ m^4$$

$$f = \frac{My}{I} = \frac{2.00 \times 1.19 \times 10^{-3}}{8.93 \times 10^{-12}}$$

$$= 266.7 \ MN/m^2$$

266.7 MN/m is well within the Yield Stress of 432 MN/m

From Roark the increase in diameter of the ring, Dx., is given by

$$Dx. = \frac{.137\,WR}{EI}$$

$$E = 206.9 \times 10^9 \ N/m^2$$

$$Dx = \frac{.137 \times 365 \times (30.16 \times 10^{-3})^3}{206.9 \times 10^6 \times 8.93 \times 10^{-12}}$$

$Dx = .743$ mm.

Deflection Dx cannot be greater than $D_1 - D_2$

$= 1.19$ mm.

The strain gauge proving rings were manufactured from En8 steel in black bar form. The first operation, of the production method, was to turn the outside diameter D_3 on one end of the bar using a centre lathe. The workpiece was then turned around and held on diameter D_3 in soft jaws, the outside diameter of the ring D_1 was turned and the inside diameter D_4 was drilled and bored to size. The workpiece was then set up in a dividing head on a vertical milling machine, figure 2.19., where the relieved diameter D_2 was machined. Finally, the workpiece was reheld in the soft jaws on the centre lathe and the ring parted off to length.

Two strain gauges were attached to the proving ring in the positions indicated in figure 2.18. The strain gauges were TML type FLA-2, the wiring diagram is shown in figure 2.20.

2.5.3 Experimental set up for Interface Pressure Measurement

Instrument Data.

Techequipment Strain Bridge model 11 and 66 way distribution box.
Manufactured by Techequipment, Nottingham.

Mean sensitivity at gain factor 1 = 1 με

Clockhouse proving ring model 200.

Dial gauge number 1537. Last calibrated 1972.

Mean sensitivity 5.9N (1.3331bf) per division.

The experimental set up for the measurement of radial pressure between the mandrel sleeve and interface pressure rig is shown on plate 5.

The mandrel system is mounted upon a baseplate, the interface pressure rig being positioned around the mandrel sleeve, on top of the mandrel sleeve is placed a hardened steel collar which supports the Clockhouse proving ring, the whole assembly being in axial alignment.

Load application to the experimental set up is effected by subjecting the Clockhouse proving ring to a deflection, this was facilitated by placing the rig upon an Adcock and Shipley type 18/32 vertical milling machine. The baseplate of the rig being positioned on the worktable, the free end of the proving ring being restrained by a brass thrust bar fitted under the machine spindle head, upward movement of the worktable subjects the proving ring to a deflection and hence creates a load of known magnitude on the mandrel sleeve.

The strain gauge transducer elements are wired to the Techequipment strain bridge via the Techequipment 66 way distribution box, see figure 2.2$_1$. The use of the 66 way distribution box enabled the strain gauge elements in all the interface pressure rigs to be wired to the strain bridge

using one channel only, thus enabling simple switching for measurement and maximum utilization of the strain bridge. The strain gauges fitted to the arbor for the 42.86mm. long mandrel sleeves were wired into a separate channel on the strain bridge.

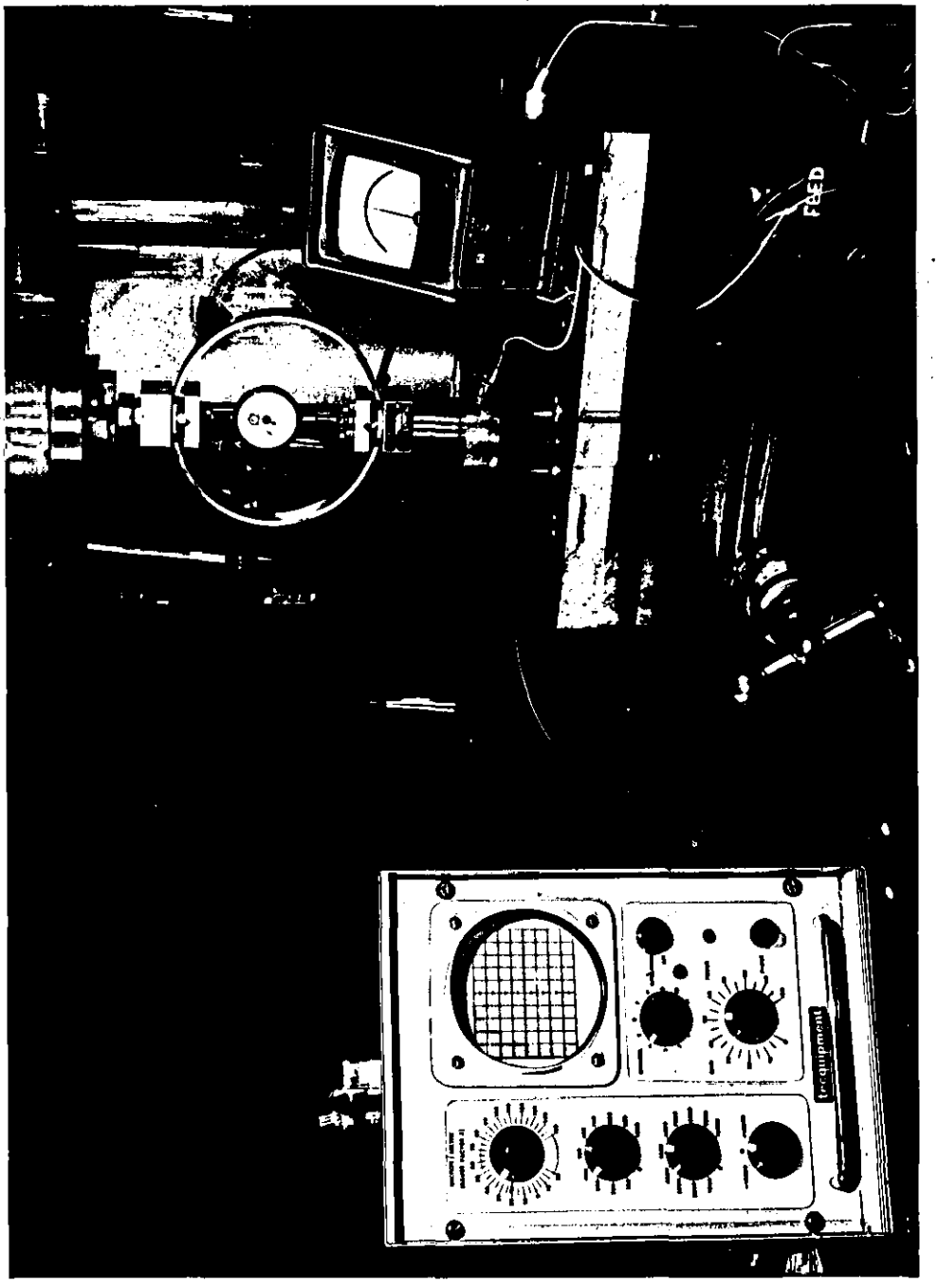

Plate 5. Interface pressure measurement rig.

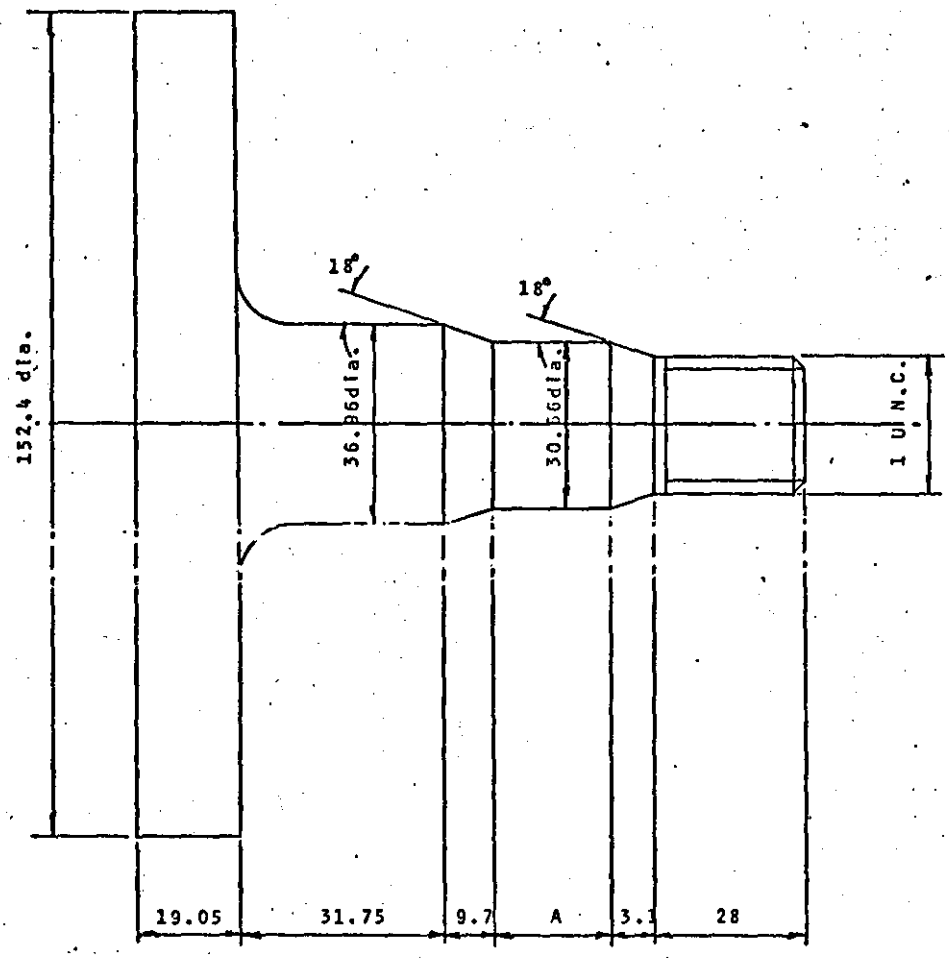

SLEEVE LENGTH	DIMESION A
42.86	21.97
26.98	10.74

FIGURE 2-1. DETAIL OF MANDREL ARBORS

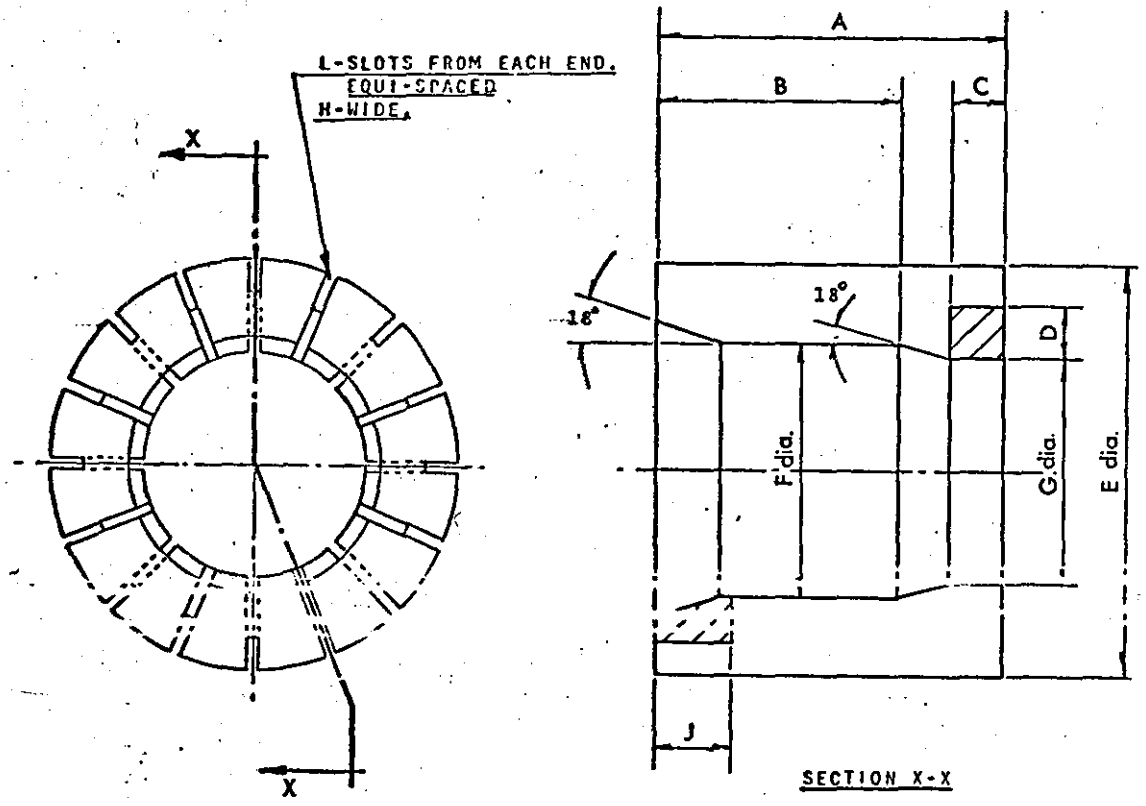

E	L	H	A	B	C	D	G	F	J
60.32	8	1.59	42.86	30.15	6.35	6.35	27.78	31.75	9.53
60.32	10	1.59	42.86	30.15	6.35	6.35	27.78	31.75	9.53
60.32	12	1.59	42.86	30.15	6.35	6.35	27.78	31.75	9.53
60.32	8	1.59	26.98	19.02	4.76	6.35	27.78	31.75	4.76
60.32	10	1.59	26.98	19.02	4.76	6.35	27.78	31.75	4.76
60.32	12	1.59	26.98	19.02	4.76	6.35	27.78	31.75	4.76
50.80	8	1.59	42.86	30.15	6.35	6.35	27.78	31.75	9.53
50.80	10	1.59	42.86	30.15	6.35	6.35	27.78	31.75	9.53
50.80	12	1.59	42.86	30.15	6.35	6.35	27.78	31.75	9.53
50.80	8	1.59	26.98	19.02	4.76	6.35	27.78	31.75	4.76
50.80	10	1.59	26.98	19.02	4.76	6.35	27.78	31.75	4.76
50.80	12	1.59	26.98	19.02	4.76	6.35	27.78	31.75	4.76
41.27	8	1.59	42.86	30.15	6.35	6.35	27.78	31.75	9.53
41.27	10	1.59	42.86	30.15	6.35	6.35	27.78	31.75	9.53
41.27	12	1.59	42.86	30.15	6.35	6.35	27.78	31.75	9.53
41.27	8	1.59	26.98	19.02	4.76	6.35	27.78	31.75	4.76
41.27	10	1.59	26.98	19.02	4.76	6.35	27.78	31.75	4.76
41.27	12	1.59	26.98	19.02	4.76	6.35	27.78	31.75	4.76

FIGURE 2-1 . DETAILS OF MANDREL SLEEVES

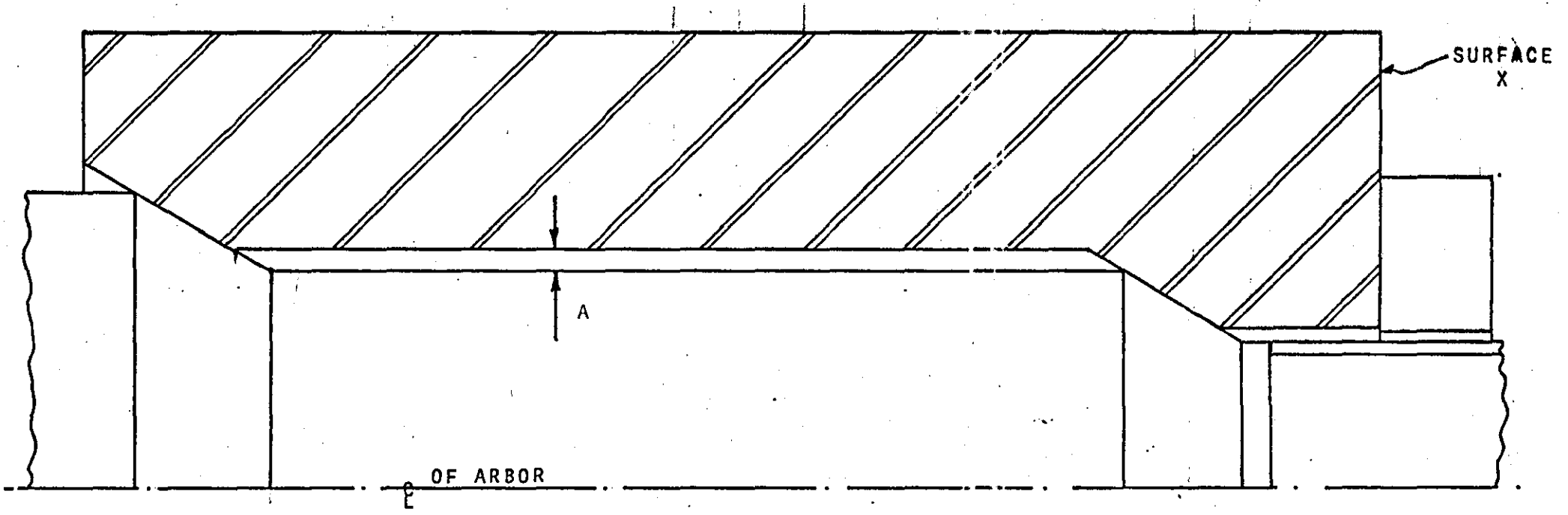

Figure 2.3:ASSEMBLY OF ARBOR AND MANDREL SLEEVE

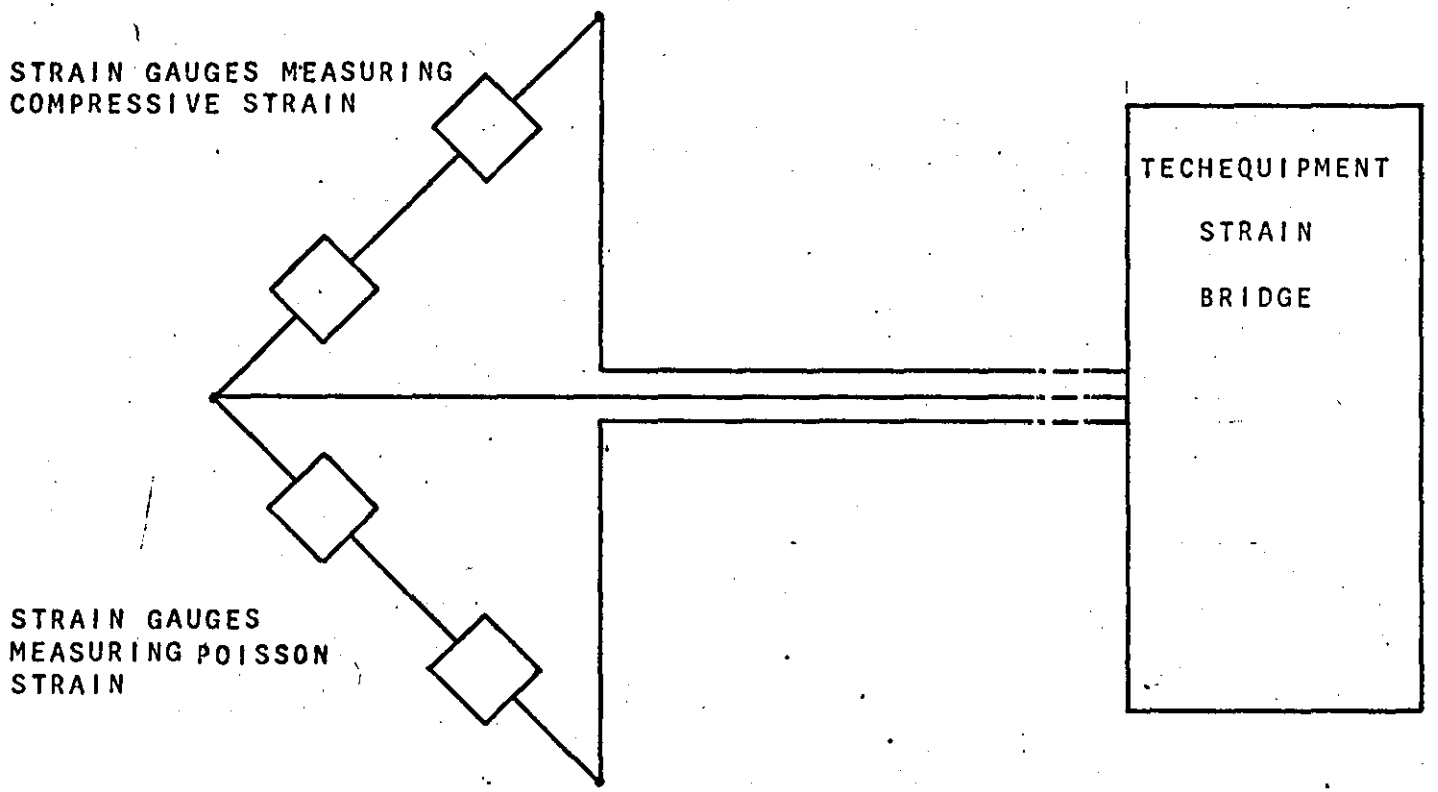

Figure 2.4:WIRING DIAGRAM FOR ARBOR STRAIN GAUGES.

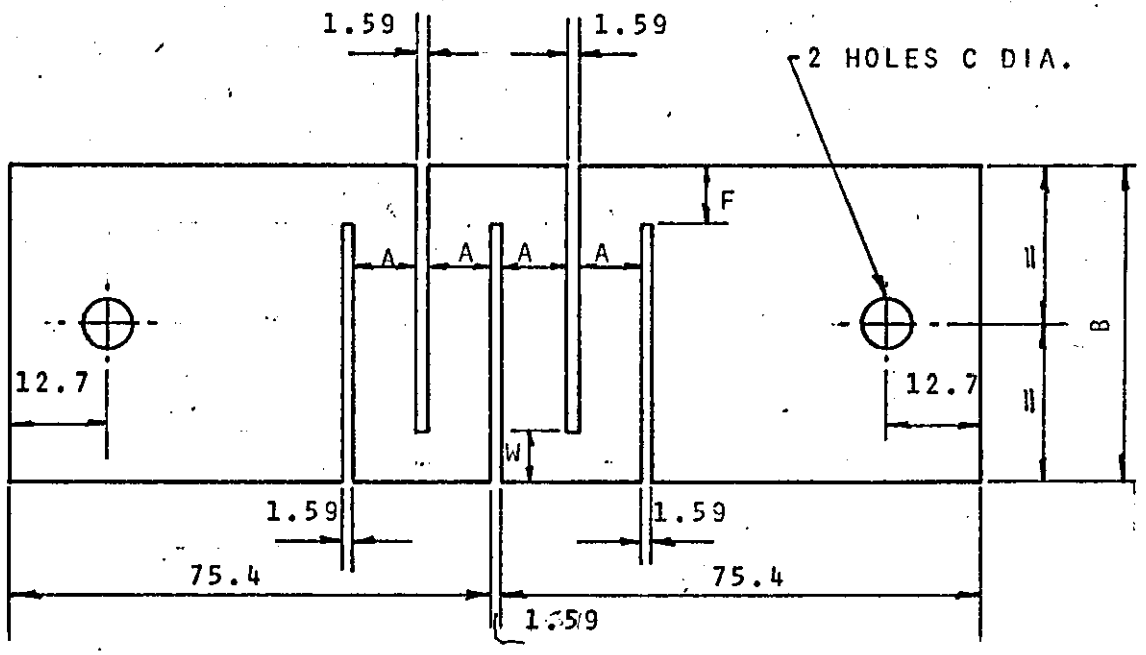

MODEL No.	A	B	C	F	W
1	3.5	41.28	6	3.14	3.14
2	4.5	41.28	6	3.14	3.14
3	6.5	41.28	6	3.14	3.14
4	3.5	26.98	6	2.74	2.74
5	4.5	26.98	6	2.74	2.74
6	6.5	26.98	6	2.74	2.74

Figure 2.5. DETAILS OF ARALDITE LINEAR MODELS.

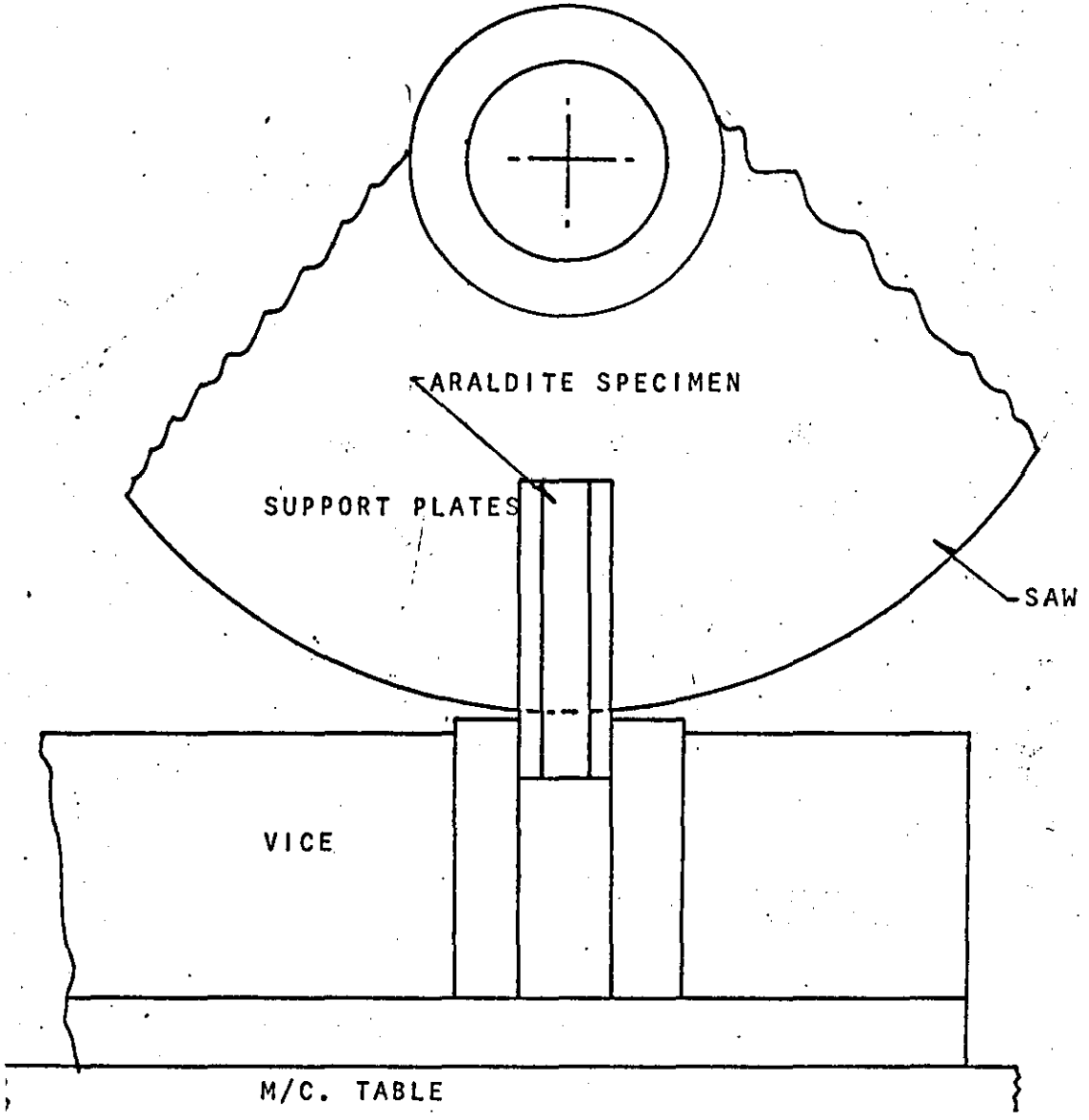

ENLARGED SECTION A-A

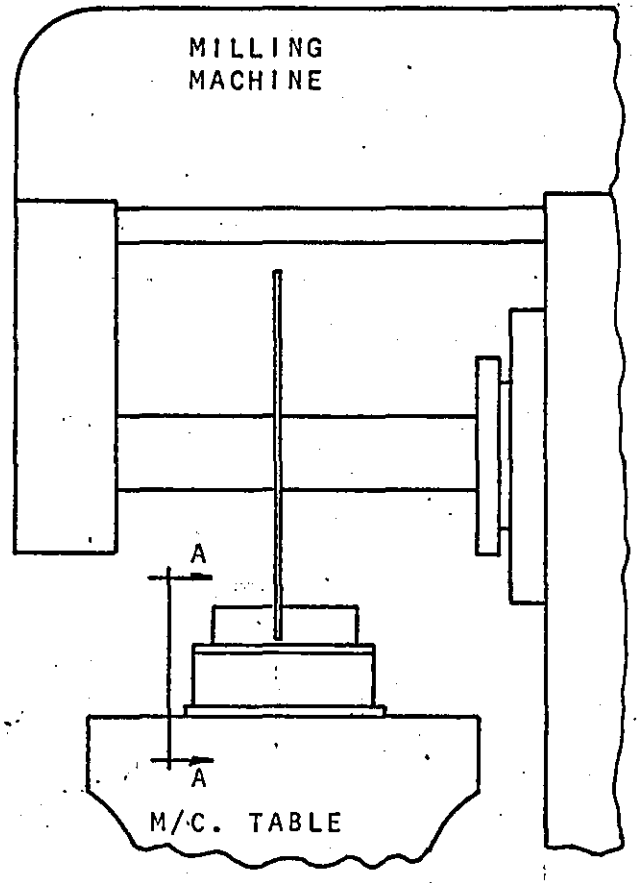

Figure 2.6. MACHINING SET-UP FOR MILLING SLOTS IN ARALDITE LINEAR MODELS.

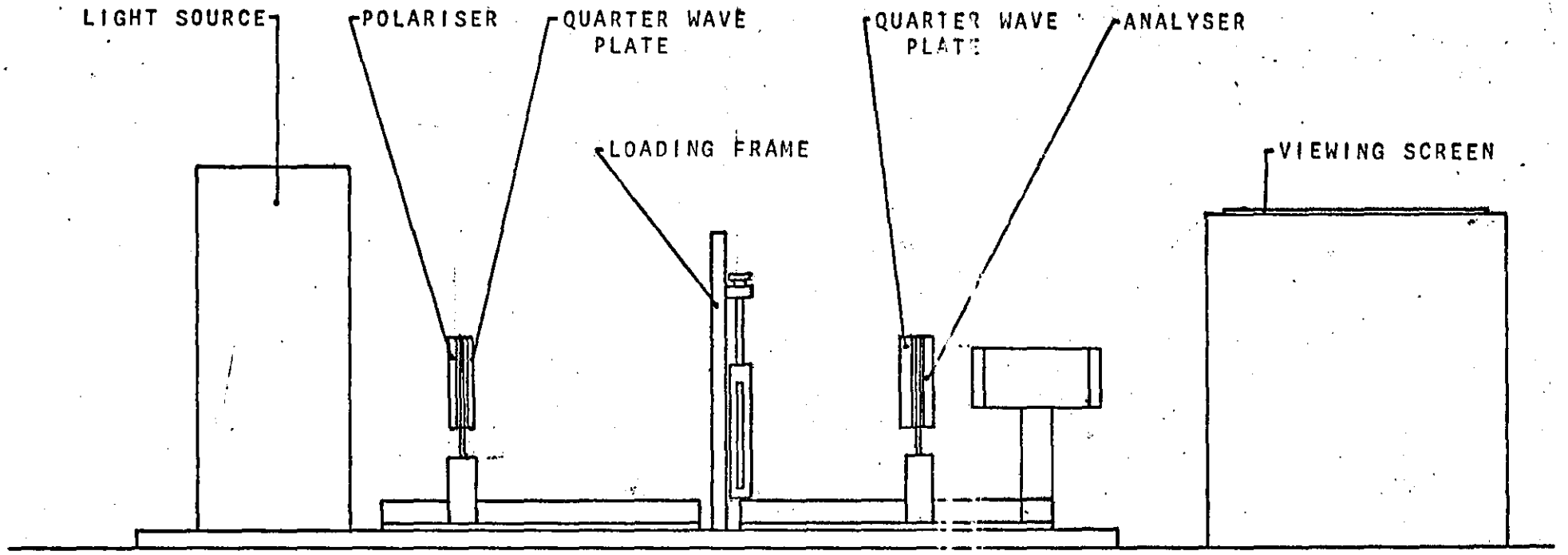

Figure 2.7. PHOTOELASTIC BENCH

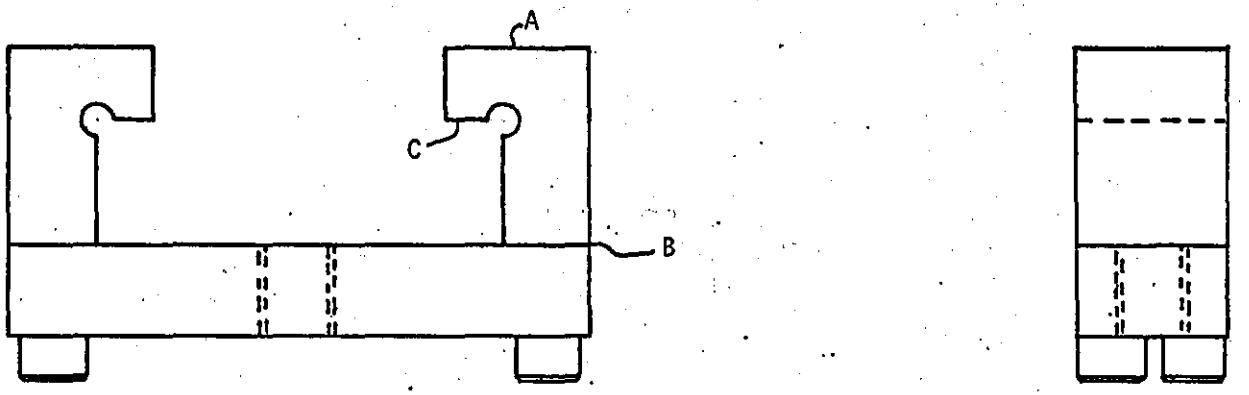

Figure 2.8. FIXTURE FOR HOLDING ARALDITE BEAMS

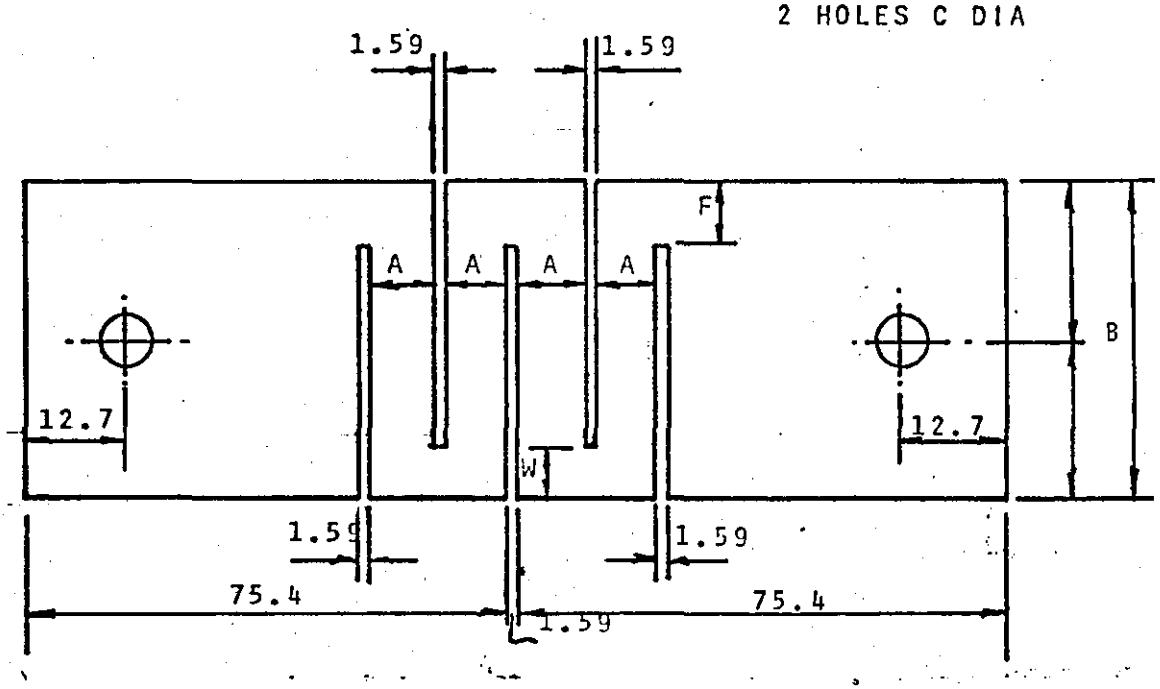

MODEL No.	A	B	C	D	F	W	PROFILE
1	4.57	42.86	6	12.7	6.7	6.7	(a)
2	4.57	42.86	6	6.35	6.35	9.53	(b)
3	4.57	42.86	6	11.11	6.35	9.53	(b)

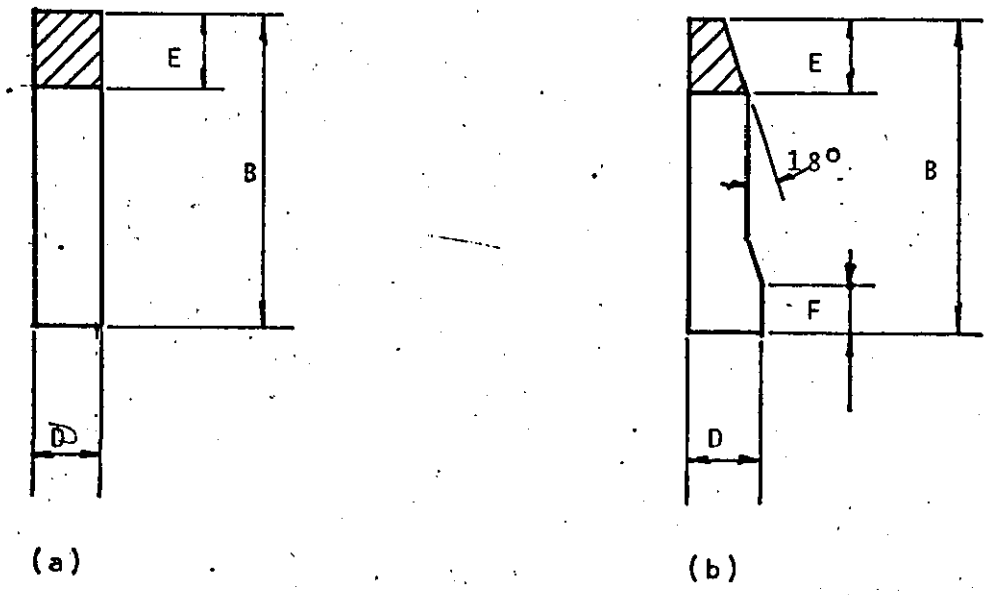

Figure 2.9. DETAILS OF STEEL LINEAR MODELS

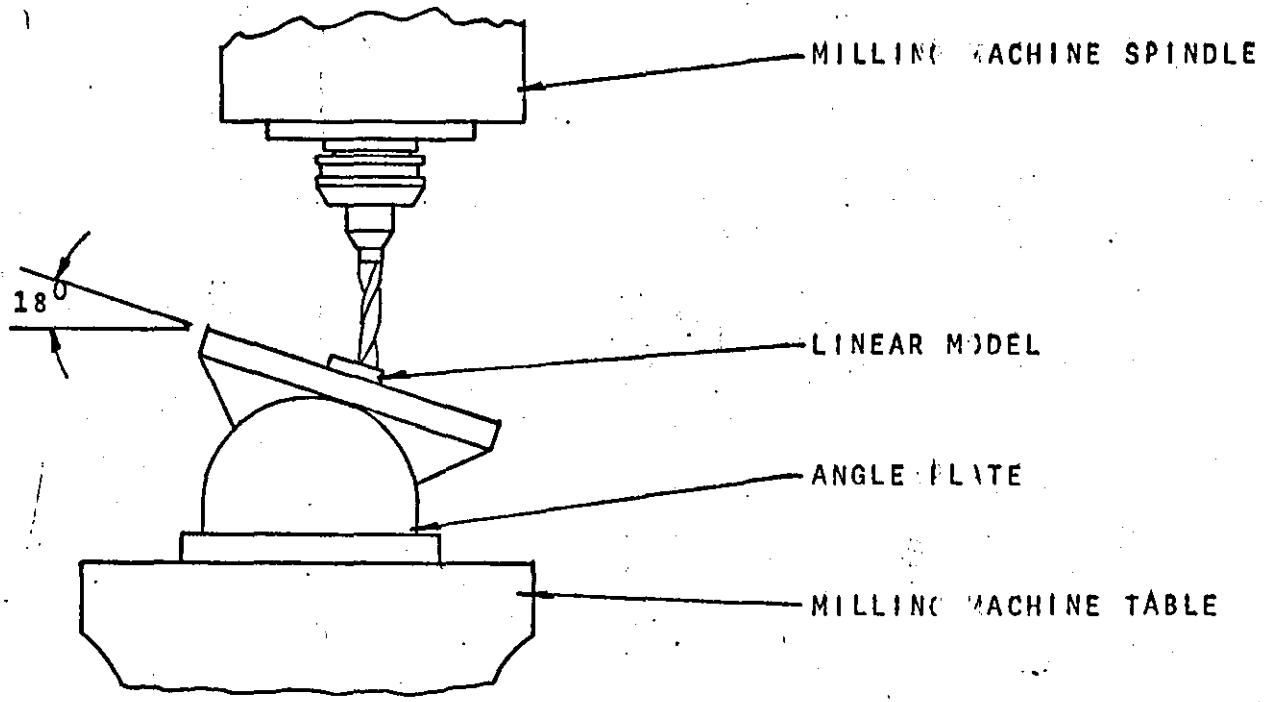

Figure 2.10: SET-UP FOR MACHINING MANDREL PROFILE ON STEEL LINEAR MODELS.

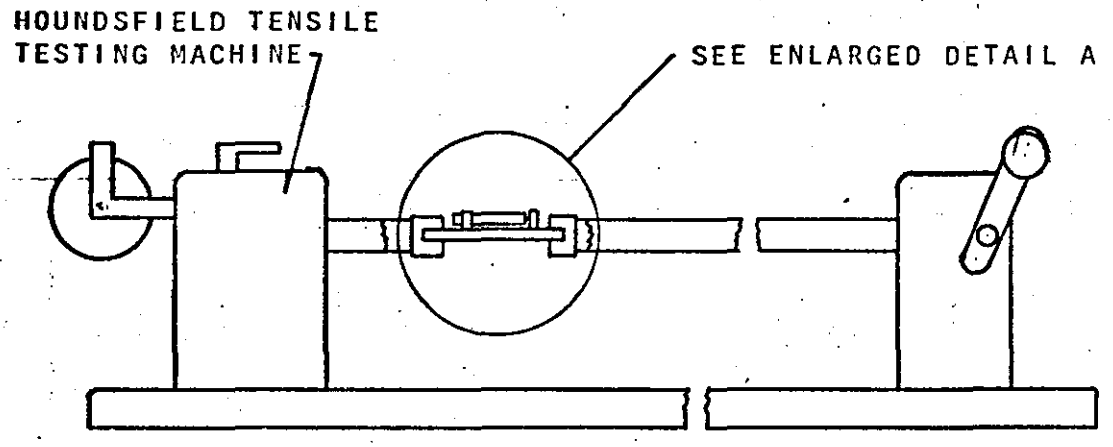

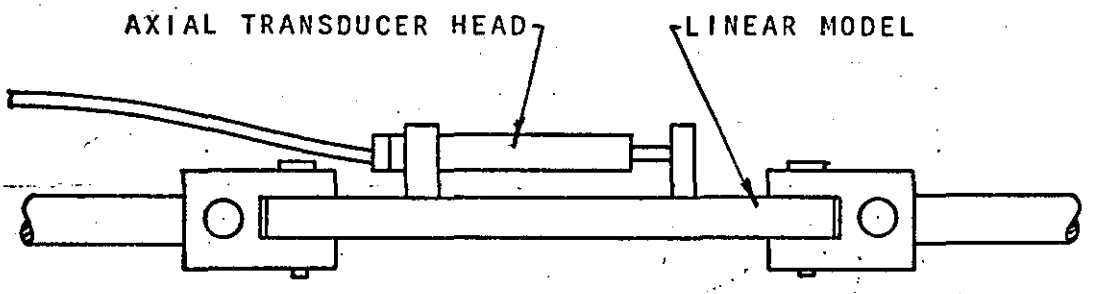

ENLARGED DETAIL A.

Figure 2.11:EXPERIMENTAL SET-UP FOR LOAD-EXTENSION TESTS ON STEEL LINEAR MODELS.

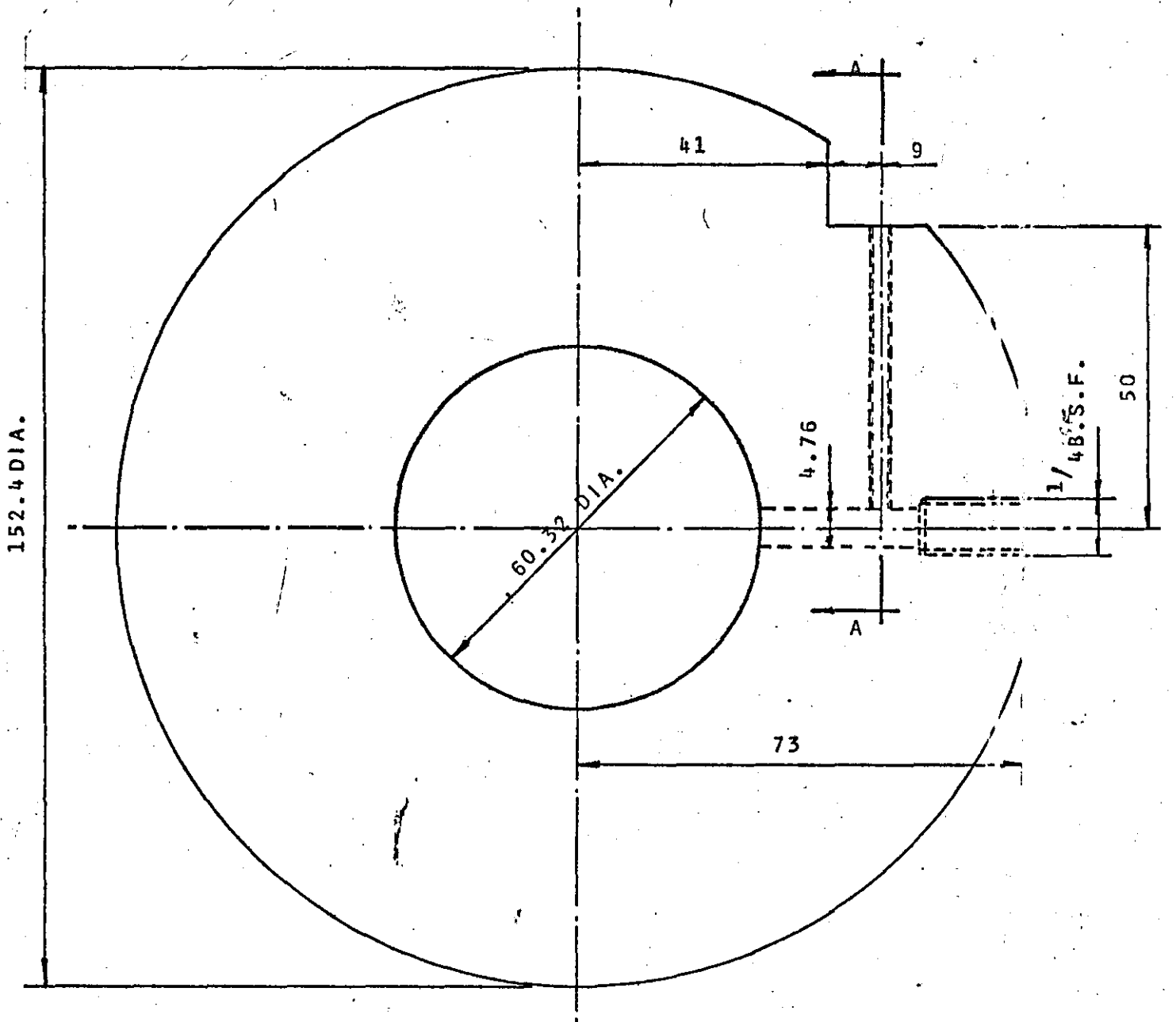

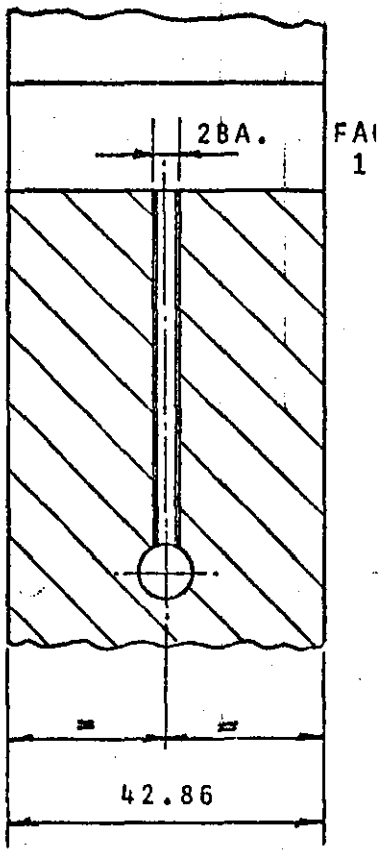

SECTION A-A

Figure 2.12: TRAIL INTERFACE PRESSURE RIG

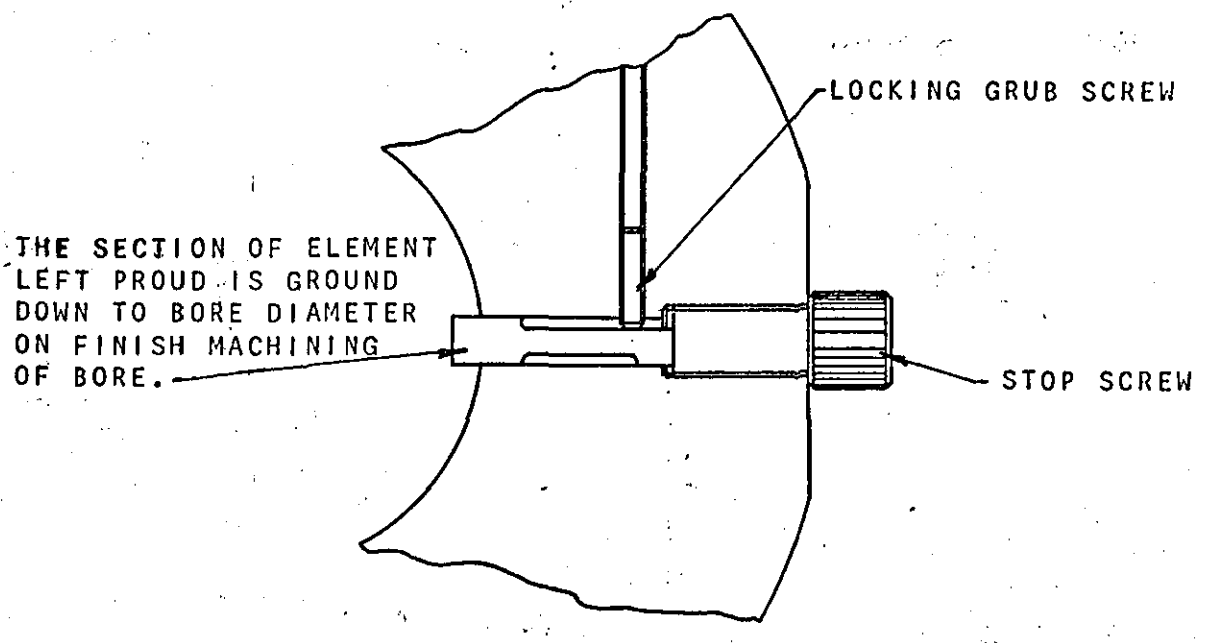

Figure 2.13:FITTING OF STRAIN GAUGE TRANSDUCER ELEMENT

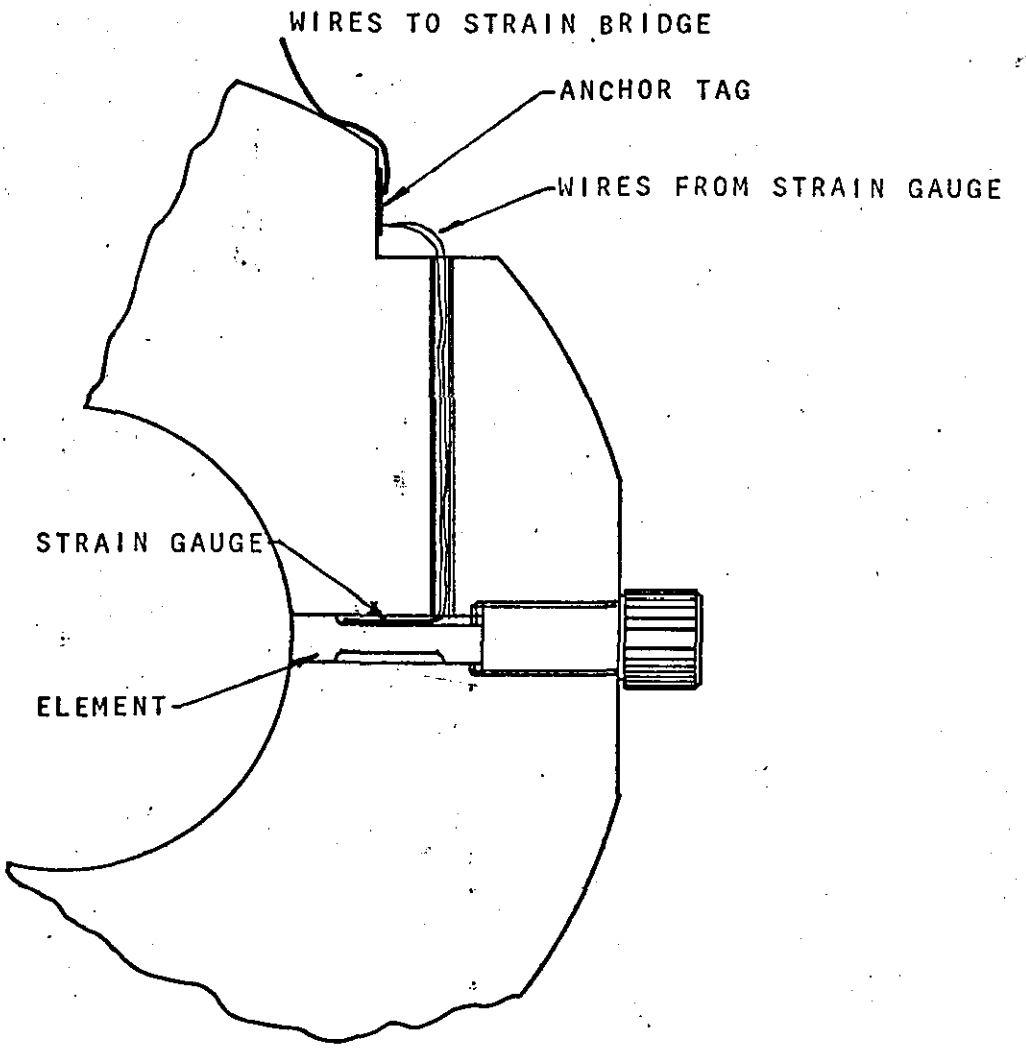

Figure 2.14:FITTING OF STRAIN GAUGE WIRES IN RIG

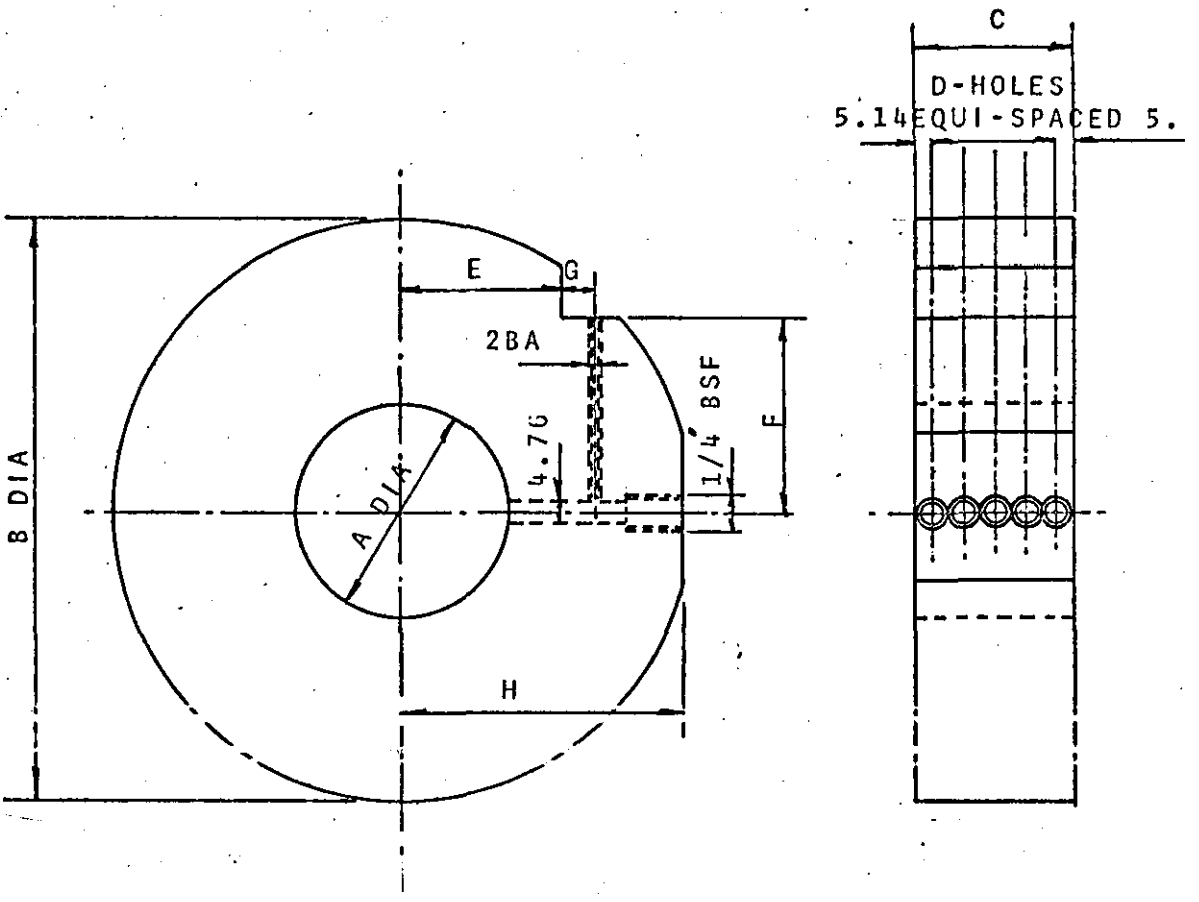

	A	B	C	D	E	F	G	H	ELEMENT No.
RIG 1	41.27	101.6	26.98	3	35	25	6	48	1,2,3.
RIG 2	50.80	127.0	42.86	5	39	36	7	61	4,5,6,7,8.
RIG 3	50.80	127.0	26.98	3	39	36	7	61	9,10,11.
RIG 4	60.32	152.4	42.86	5	41	50	9	73	12,13,14,15,16.

Figure 2.15:DETAILS OF INTERFACE PRESSURE RIGS.

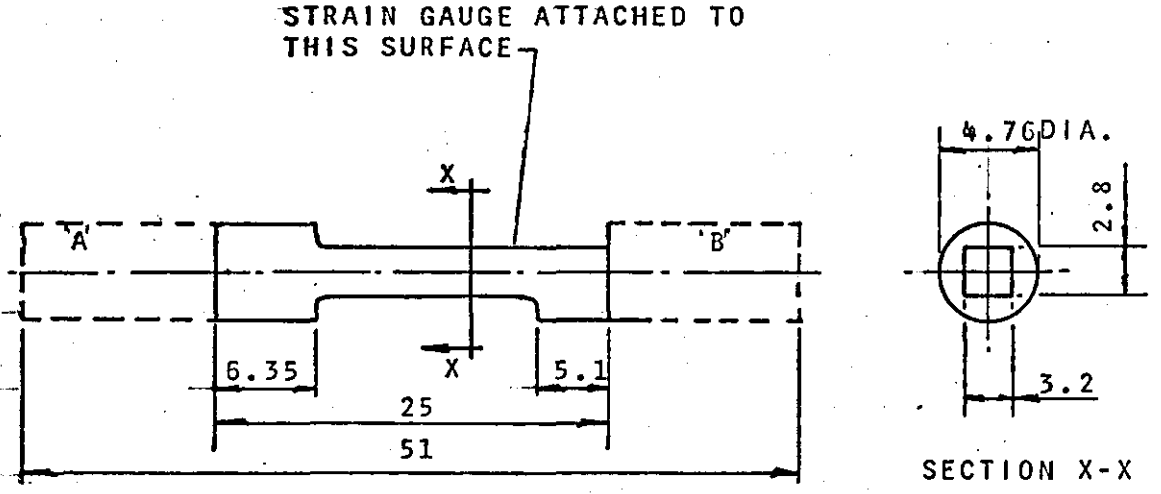

NOTE: 'A' IS REMOVED WHEN BORE OF INTERFACE PRESSURE IS FINISH GROUND.
'B' IS REMOVED WHEN CENTRAL SECTION OF ELEMENT HAS BEEN GROUND TO SIZE

Figure 2.16:TRANSDUCER ELEMENT.

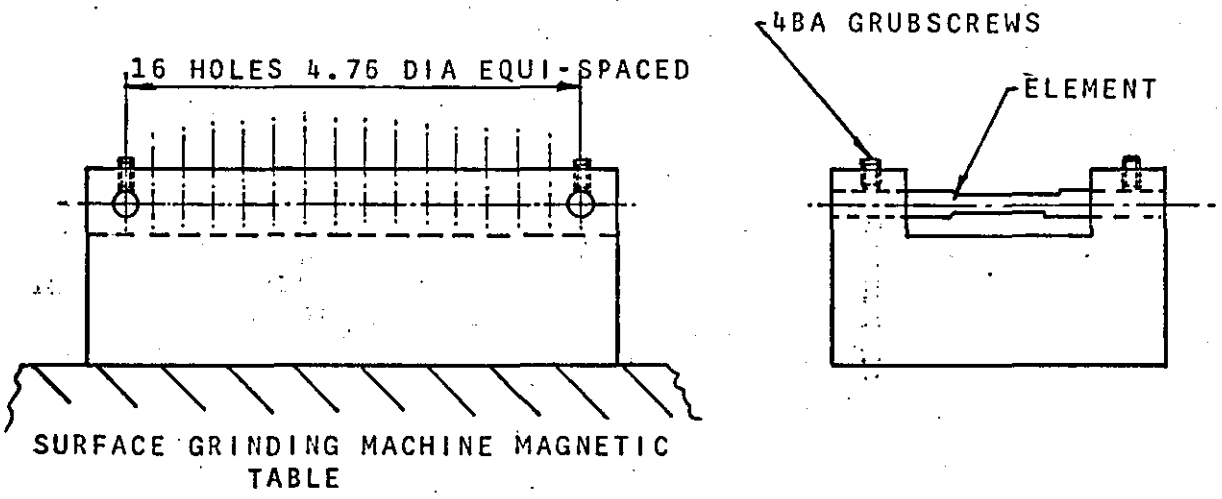

Figure 2.17:FIXTURE FOR GRINDING TRANSDUCER ELEMENTS.

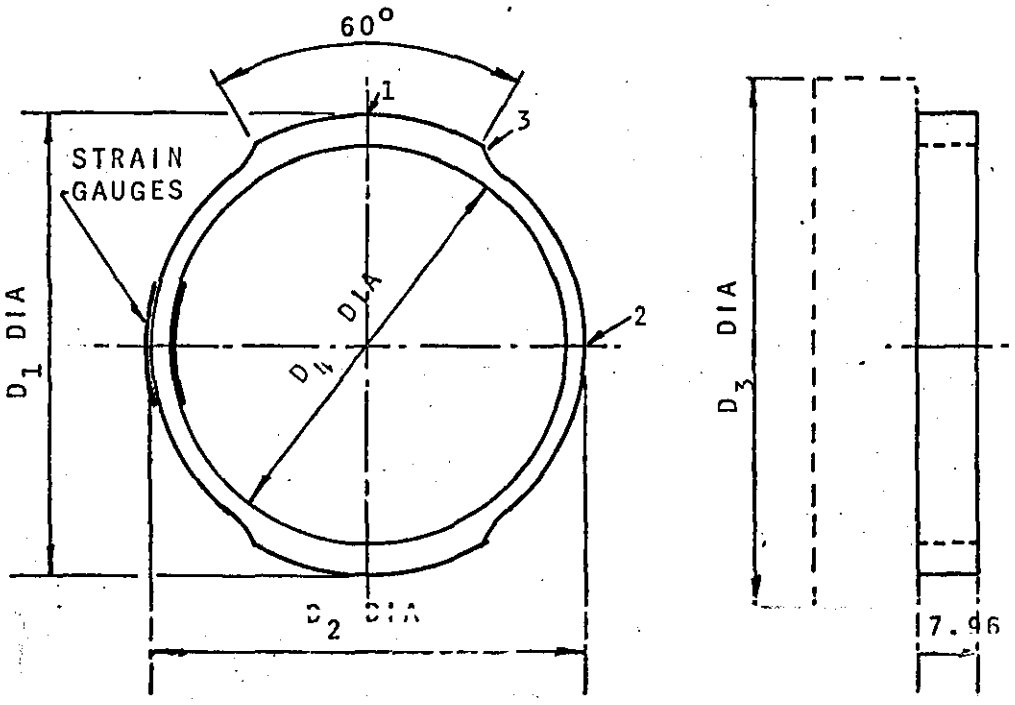

D_1 DIA	D_2 DIA	D_3 DIA	D_4 DIA
60.32	55.56	70.0	53.18
50.8	45.04	60.0	43.66
41.27	36.51	50.0	34.13

Figure 2.18:PROVING RINGS

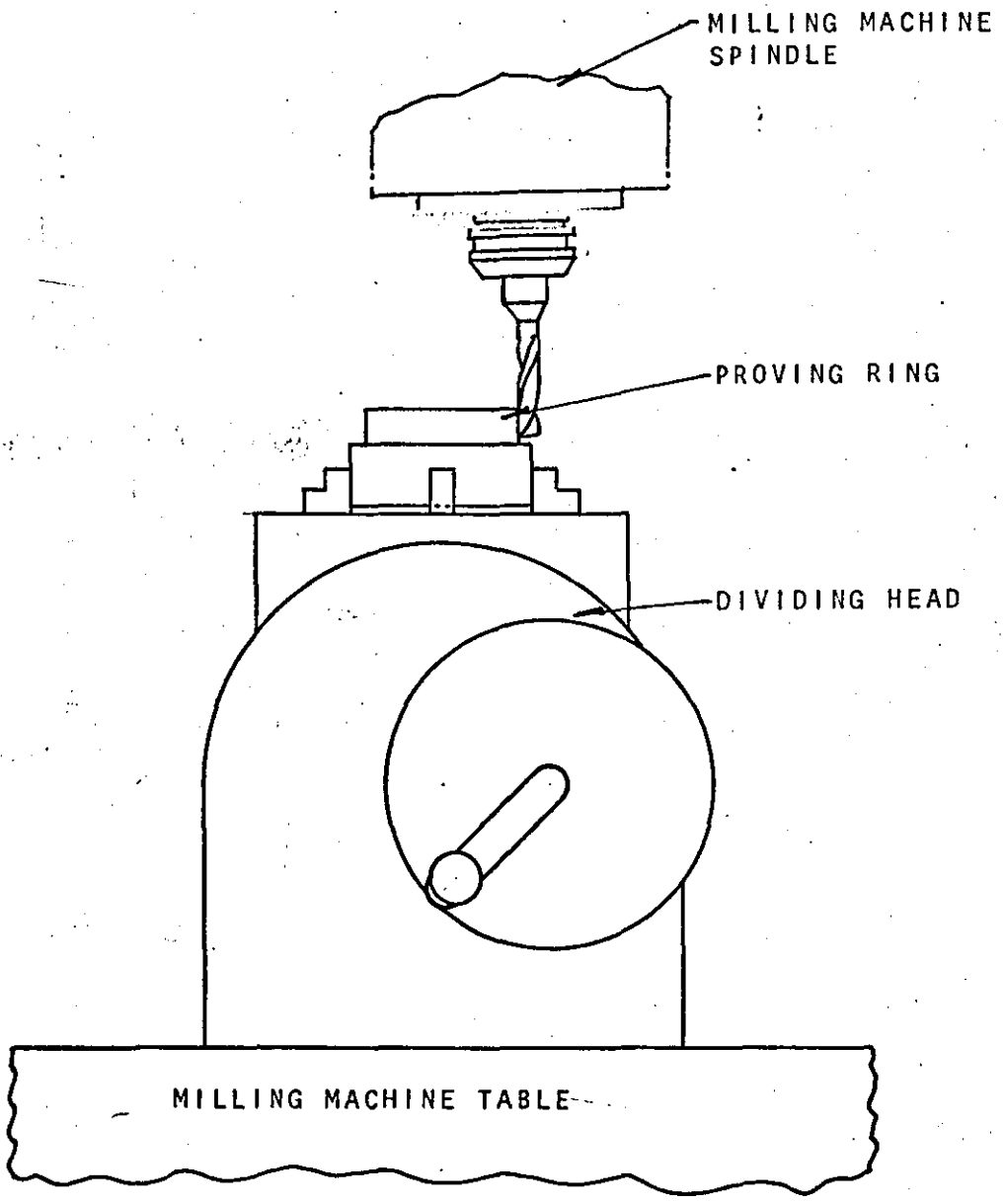

Figure 2.19:MILLING OF RECESS DIAMETER ON STRAIN GAUGE PROVING RING.

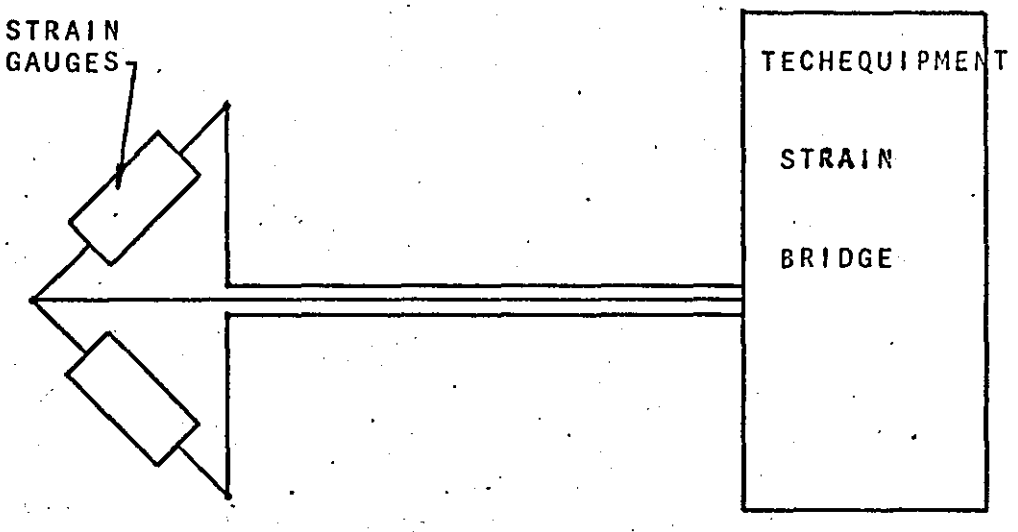

Figure 2.20:WIRING DIAGRAM FOR STRAIN GAUGE PROVING RINGS.

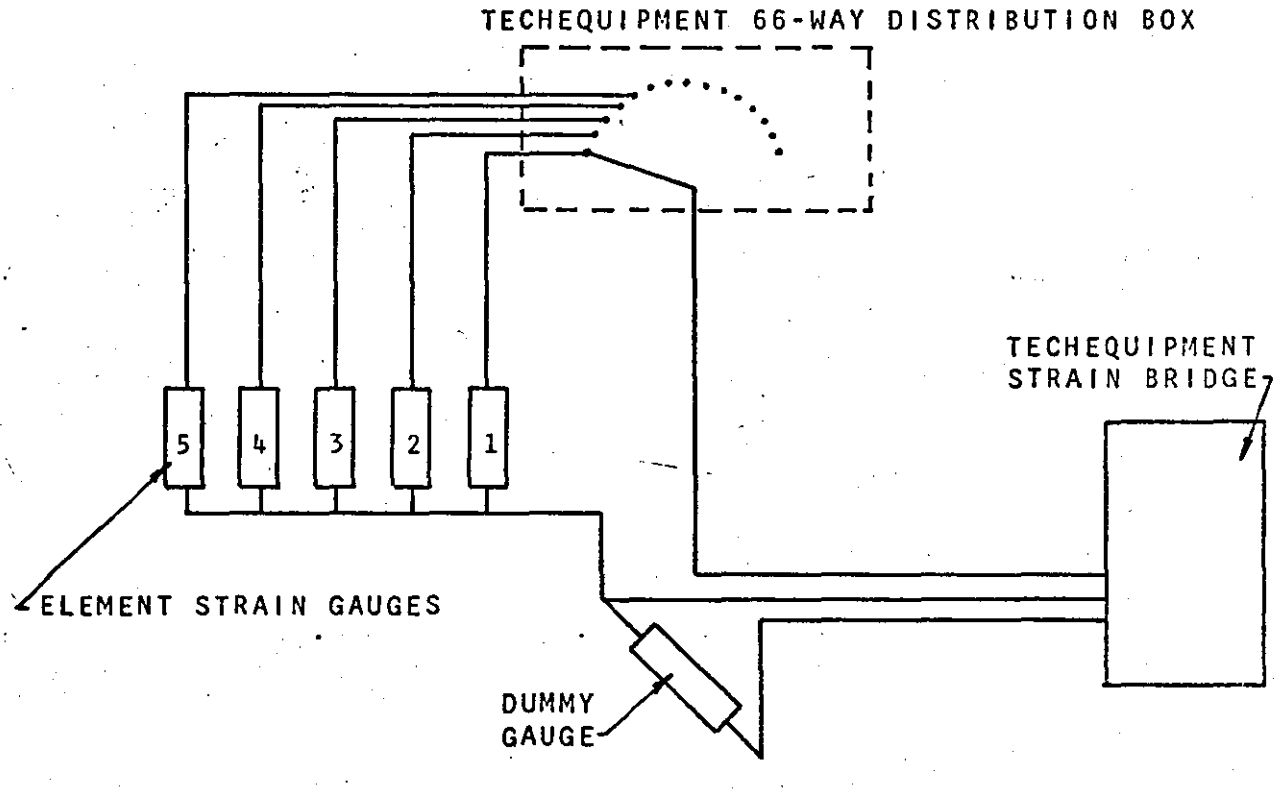

Figure 2.21:TYPICAL WIRING DIAGRAM FOR INTERFACE PRESSURE RIGS

CHAPTER 111

EXPERIMENTAL WORK

3. Experimental Work

3.1 Determination of the Load-Expansion Characteristics of the Mandrel Sleeves.

In this part of the research project the aim was to determine experimentally the relationship between the load applied to the mandrel sleeve and the corresponding radial expansion of the sleeve. To enable large radial expansions to be obtained and to determine the load requirement to expand the mandrel sleeve from its collapsed diameter up to the nominal diameter of a component, this experimentation was conducted without workpieces loaded onto the mandrel. (Under normal operating conditions the expansion of the sleeve is restricted by the positioned workpiece).

In order to establish the above relationships a series of experiments were undertaken which enabled the radial expansion of the mandrel sleeve and load distribution between the two conical tapers to be measured at known values of applied load. The experimentation was in three parts

1. Load-radial expansion measurement.
2. Variation of radial expansion down the length of the mandrel sleeve.
3. Measurement of the distribution of load between the two conical tapers on the arbor for the 42.86m.m(1.6875in.) long mandrel sleeves.

3.1.1 Load-radial Expansion Measurement

The load application apparatus and method, and experimental rig, designed for this experimental work is described in Chapter 2. section 2, and is shown on Plate ?
Sixteen mandrel sleeves and the two associated arbors were subjected to investigation, the experimental procedure followed in each case was to load the required sleeve onto the arbor, ensuring that an adequate film of oil was present upon the conical taper surfaces on the arbor and on the mating female conical taper surfaces in the mandrel sleeve. The oil used being Mobil Vactra recommended for general lubrication situations. The hardened steel collar was then positioned on top of the mandrel sleeve and the Clockhouse proving ring positioned on top of the collar, the free end of the proving ring being positioned against a thrust bar which restrains movement in the upward direction. Loads are applied by moving the table of the loading apparatus upward and toward the restrained thrust bar, this subjects the proving ring to a deflection and creates a load of known magnitude on the arbor. An initial load of 45N (10lbf) was placed upon the sleeve, this was done to give true contact between the mandrel sleeve and arbor and enabled a datum value of diameter to be established on the mandrel sleeve. With the datum value of diameter established the axial transducer head of the Mitronic micro-comparator was then placed in contact with the mandrel sleeve, the transducer head was positioned midway down the length of the sleeve. With the .10mm. full scale deflection range selected on the micro-comparator the system was set to zero.

The sleeve was now loaded in increments which gave an increase in radius of the order of 20 μm.(.0008in.), loading

continued until an increase in radius of the order of 127 um (.005in.) had been obtained, (this is equivalent to an increase in diameter of 254 μm(.010in.) which is of the order to that required in practice. The increase in radius was recorded for every increment in load. The procedure was repeated each time for the sixteen sleeves investigated. Tables 8.21 to 8.36 present the tabulated results and figures 3.3 to 3.18 show the results graphically.

3.1.2 Investigation into the Variation of Radial Expansion down the length of the Mandrel Sleeve

The experimental rig and load application procedure is as described in Chapter 2. section 2. Six mandrel sleeves and two associated arbors were subjected to investigation, the experimental procedure was similar to that described in 3.1.1, with the exception being that the transducer head was raised and lowered to enable measurements of radial expansion to be taken down the length of the mandrel sleeve. The actual procedure consisted of applying a 45N (10lbf) initial preload to the mandrel sleeve and then to position the transducer head of the micro-comparator against the mandrel sleeve at a height 1m.m.(.040in.) below the top edge of the mandrel sleeve, the micro-comparator was then set to zero. A load was now applied to the mandrel until an expansion of 127 μm (.005in.) was obtained, the value of the load was recorded. The load was then removed from the mandrel and the axial transducer head was lowered by 5m.m.(.200in.), reloading of the mandrel now took place until an expansion of 127 μm (.005in.) was again achieved, the value of the load to cause this expansion was recorded. The probe was progressively lowered by 5m.m.(.200in.) until the whole length of the mandrel sleeve had been covered, the load to give a 127 μm (.005in.) radial expansion was recorded at each measuring position. Tables 8.37 to 8.42 present the results.

3.1.3 Measurement of the Load Distribution between the Two Conical Tapers

The experimental set up used in this experimentation was similar to, and the load application apparatus and method, the same as that described in Chapter 2. section 2. Six mandrel sleeves associated to the arbor for the 42.86m.m(1.6875in.) long mandrel sleeves were subjected to experimentation. Strain gauges had been mounted between the two tapers to facilitate the measurement of the load in this section of the arbor, the gauges being wired to the Techequipment strain bridge for the direct reading of the strain (hence load) on the arbor, the strain was initially measured and recorded with no load applied to the arbor.

The experimental procedure was carried out in the following manner, The mandrel sleeve to be investigated was loaded onto the arbor, the wires to the strain gauges being positioned into the slots in the arbor, thus ensuring that the wires were not trapped under the mandrel sleeves. A load was then applied to the mandrel system and the corresponding strain in the arbor measured, the load was then increased in increments suitable for the particular mandrel sleeve until the load required to expand the mandrel sleeve 127 μm was reached (this was known from the results taken in 3.1.1). The resulting strain in the arbor for each load was measured and recorded. The results are presented in Tables 8.43 to 8.48.

3.2. Comparative Photoelastic Studies

The photoelastic studies were undertaken to give a qualitative comparison of the stress pattern to be found in an encastre beam, where one end deflects relative to the other, and the stress pattern to be found in the beam element of a linear model of the mandrel sleeve when such a model is placed under load extension. No attempt was made to determine the magnitude of the stresses present.

The photoelastic studies were undertaken on the Jessop-Leech photoelastic bench as described in Chapter 2. section 3.1. The linear models were placed in the loading frame and subjected to a load of approximately 45 N, the quarter-wave plates were set as shown in figure 3.1. to display the isocromatic (lines of constant stress) on a black background. Photographs of the stress pattern were then taken for later comparison.

The arrangement of fixture and Araldite beam as shown in figure 3.2. enabled the stress pattern of an encastre beam, where one end has been subjected to a deflection relative to the other, to be obtained. To subject the Araldite beam to such a deflection the following method was used. The distance marked Y on figure3.2. was known, the thickness of the Araldite beam was also known, slip blocks of different thickness (approximately .25mm.) were placed under the beam and on top of face D on the fixture base, slip blocks to make up to the height Y + .025mm. were then placed on top of the beam, the fixing screws were then tightened and the face B on the clamp brought down to the face D on the base of the fixture. With the beam now subjected to a deflection the fixture was mounted on the loading frame of the photoelastic bench. Photographs were taken of the resulting stress pattern. Plates 6 and 7

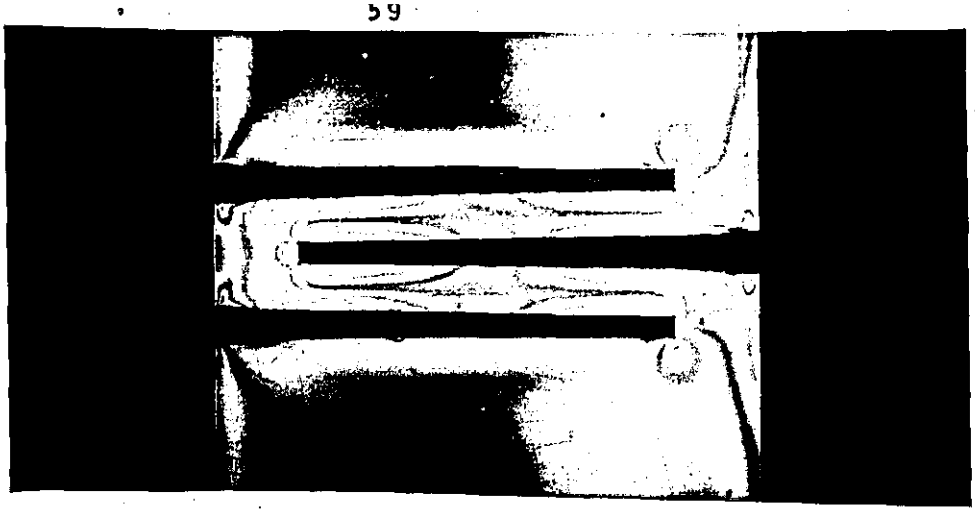

Plate 6. Stress pattern for model 1.

Plate 7. Stress pattern for model 4.

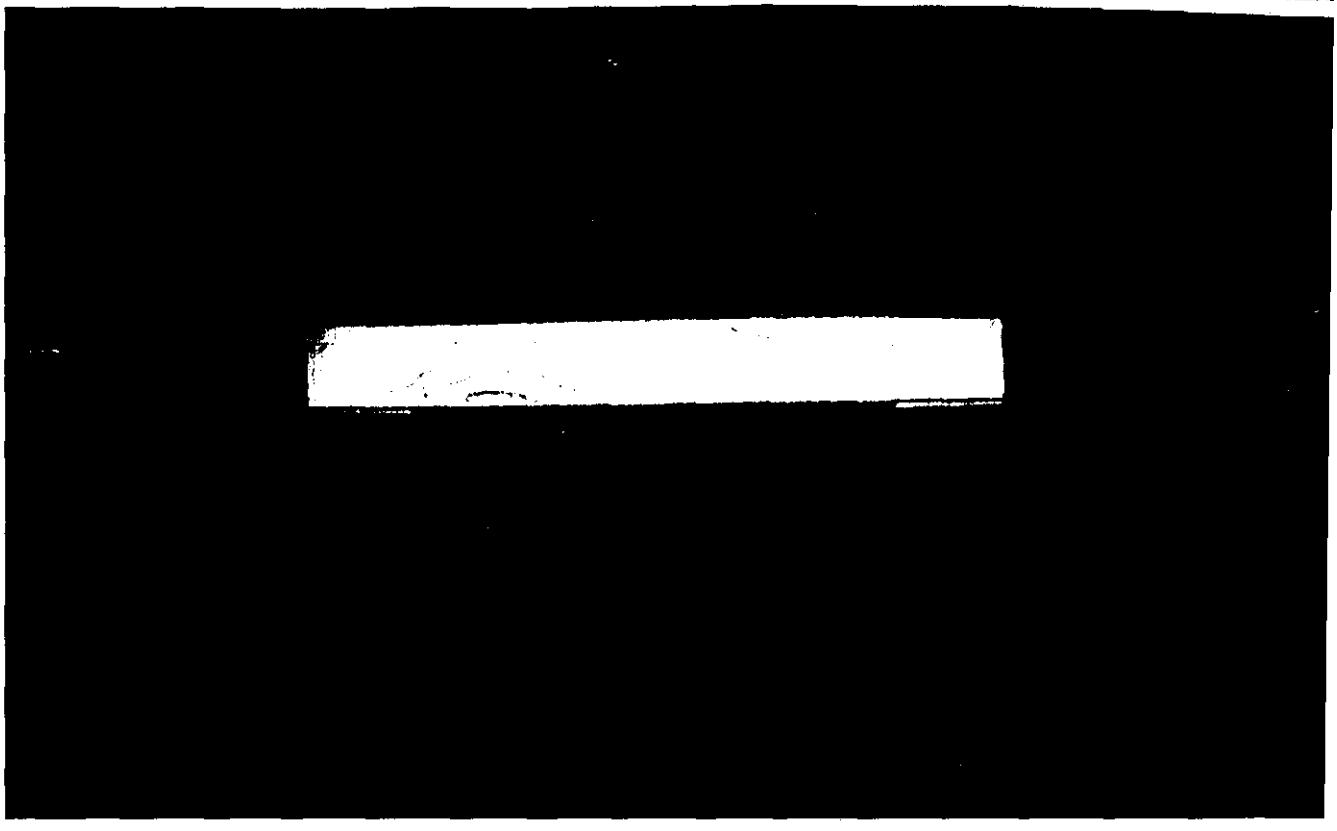

Plate 8. Stress pattern for encastre beam

show the stress pattern for a 43mm. and 27mm. wide linear model and plate 8 shows the stress pattern for the encastre beam. Comparison of plates 6 and 7 with 8 show that there is a similarity between the stress patterns of the encastré beam and beam element section of the linear models.

3.3 Load-Extension tests on the Steel Linear Models

The aim of this experimental work was to establish the relationship between the applied load and the resulting extension of the linear model, the results obtained being used to test the validity of the hypothesis regarding the action of the mandrel sleeves (see Chapter 4).

The experimental equipment and set up for this experimentation is as described in section 2.4.1. and shown in figure 2.11. Three linear models (see figure 2.9.) were subjected to investigation, the method of experimentation being the same in each case. Initially, the linear model was placed under a 19.6N (4.4lbf) preload, the axial transducer head was then adjusted to give full scale deflection on the comparator. The preloading enabled the 'back-lash' of the system to be taken out and this gave more consistent readings. Further loads were now applied in steps of 49N (11lbf), the resulting extension displayed by the comparator being recorded at each load, loading continued until an extension of the order of 250 μm was reached. The model was then unloaded and the above procedure repeated until 5 sets of readings were obtained.

Tables 8.49., 8.50. and 8.51. present the curve of load against extension, the average of the 5 readings (for any one load) being plotted for extension.

3.4 Measurement of Interface Pressure

The measurement of interface pressure was the final part of the experimental work involved in this project. The feasibility of measuring the interface pressure between the mandrel sleeve and a workpiece had been established by the experimental work conducted with the initial trial interface pressure rig, the rig was later converted into interface pressure rig number 4 by the addition of further transducer elements. The results of this initial work are presented in Table 8.52. This final experimental work involved 12 of the 16 mandrel sleeves available, the two arbors associated with these sleeves were also used.

The experimental set up for this work is described in Chapter 2. section 5.2., and shown on plate 5. The experimental method was as follows. The relevant mandrel sleeve was fitted onto the arbor, the interface pressure rig was then placed in position around the sleeve and held in that position until a small load was placed on the sleeve. This initial load was sufficient to radially expand the sleeve until contact with the rig was established and the radial pressure generated at the interface just supported the rig. Alignment of the rig to the sleeve was effected by eye, the rig having a line parallel with the centre line of the transducer elements scribed on its top surface, this line was positioned on the centre of the arc of curve of a segment of the mandrel sleeve. With the 'self-holding' position established the strain reading of all the transducer elements and the arbor strain gauges were measured and recorded, the magnitude of the applied load was also recorded.

The mandrel was now further loaded, the load being

applied in increments which depended on the size of the mandrel being investigated, the load increments were 285N (64lbf) or 569N (128lbf) for the 41.28, 50.8 and the 60.36mm. diameter mandrel sleeves respectively. The criterion which determined the maximum load was that the loading was continued until a value of load was reached which was of the order to that which would be likely to be applied to the mandrel by a workman when using a wrench to tighten a nut on the arbor's 1in. UNF screwthread (see Appendix 8.3.). The strain readings of the elements and arbor were measured and recorded for each load increment.

Upon attaining the maximum load, and after measurement and recording of the strain had taken place, the mandrel was unloaded and the interface pressure rig and mandrel sleeve removed fron the assembly, repositioning of these was then carried out and the mandrel was again placed under an initial load, the above procedure was repeated until 4 sets of readings at each load increment for each of the twelve mandrel sleeves were obtained. The twelve mandrel sleeves subjected to investigation and the interface pressure rigs used are shown in Table 3.1. Tables 8.53. to 8.64. present the results and figures 3.22. to 3.26. show the curves of applied load versus interface pressure.

Table 3.1

Mandrel Sleeve		Interface Pressure Rig		
Diameter	Length	No.	No. of Elements	Element Nos.
41.27	26.98	1	3	1,2,3
50.80	42.86	2	5	4,5,6,7,8
60.32	26.98	3	3	9,10,11
60.32	42.86	4	5	12,13,14,15,16

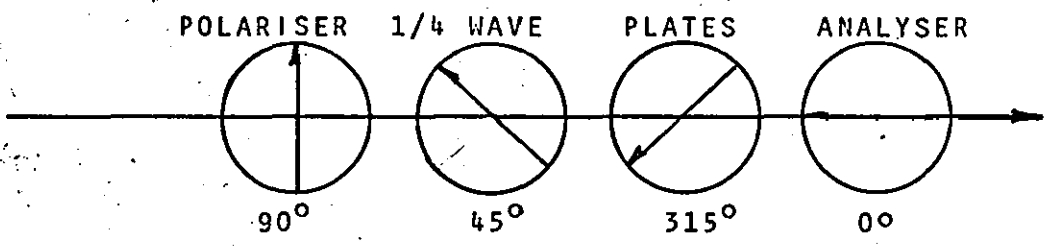

Figure 3.1. SETTING OF LENSES.

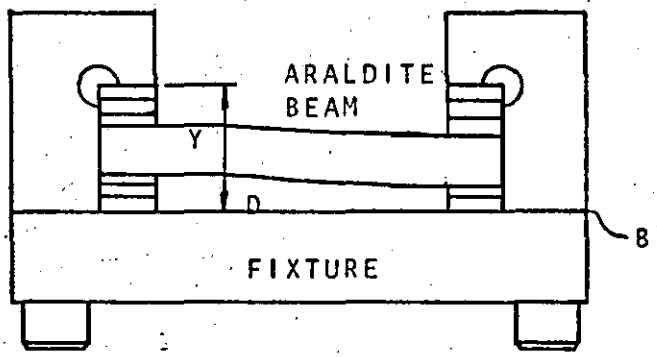

Figure 3.2. METHOD OF HOLDING ARALDITE BEAM.

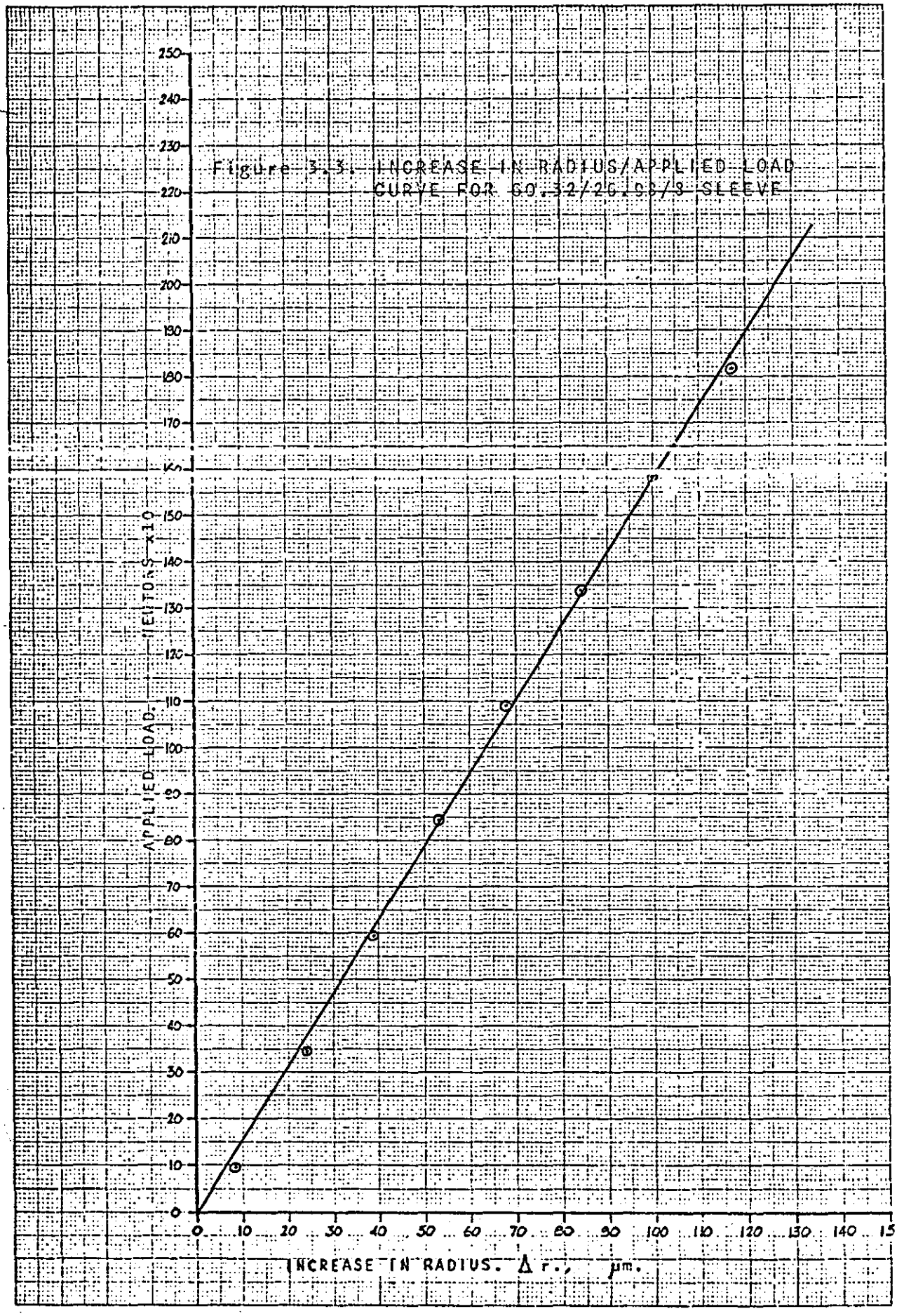

Figure 3.3. INCREASE IN RADIUS/APPLIED LOAD CURVE FOR 60.32/26.08/3 SLEEVE

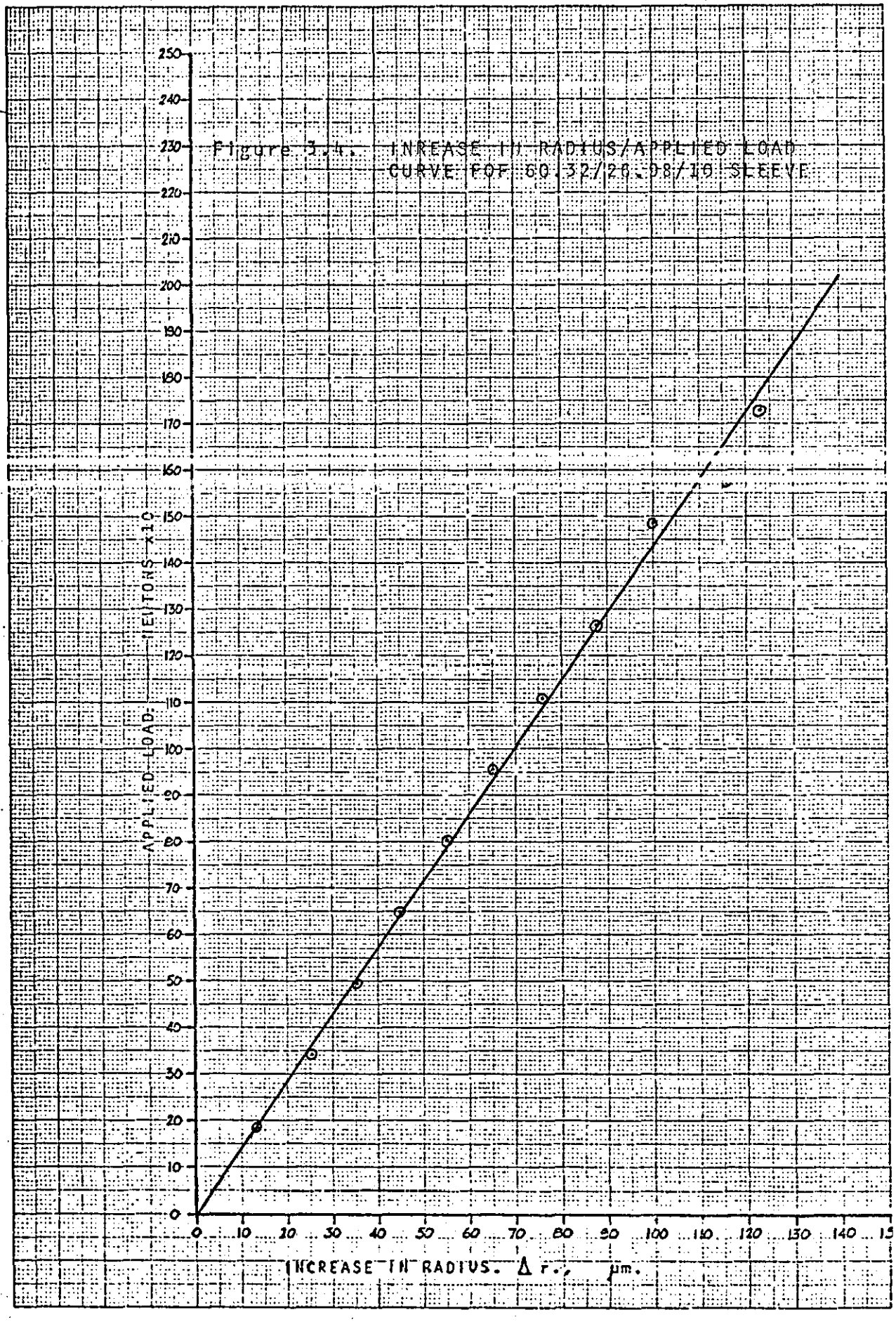

Figure 3.4. INCREASE IN RADIUS/APPLIED LOAD CURVE FOF 60.32/20.08/10 SLEEVE

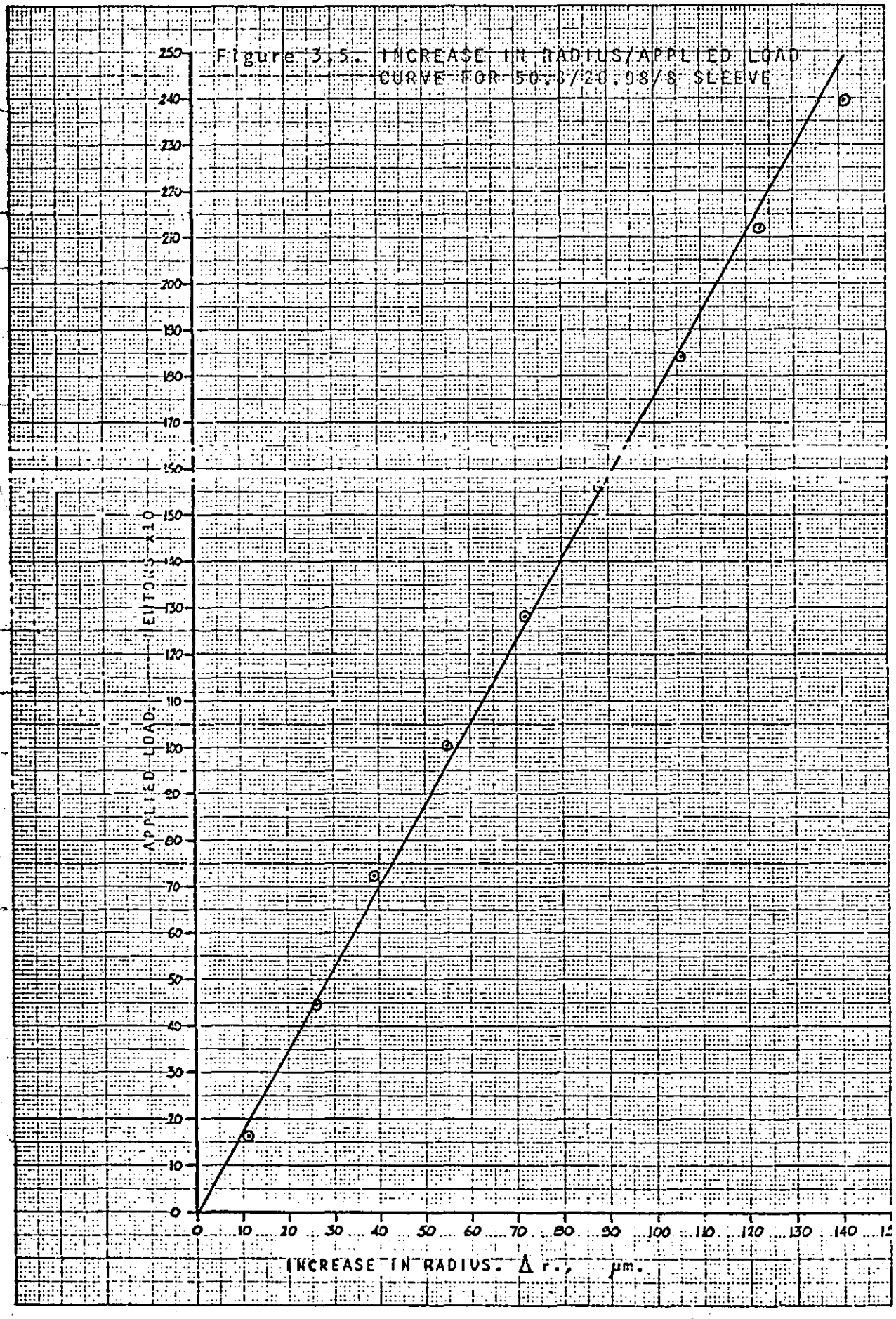

Figure 3.5. INCREASE IN RADIUS/APPLIED LOAD CURVE FOR 50.8/20.98/8 SLEEVE

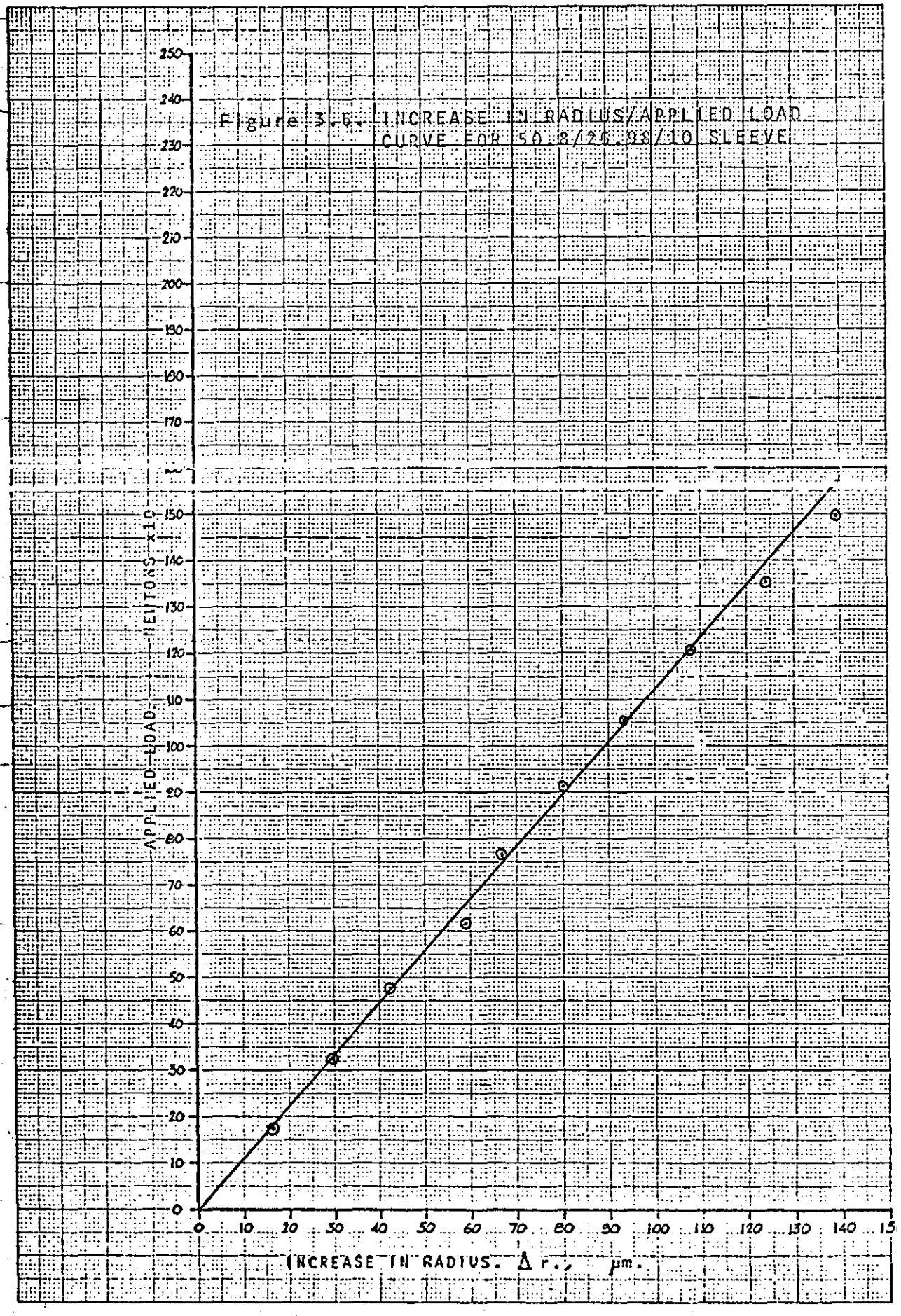

Figure 3.6. INCREASE IN RADIUS/APPLIED LOAD CURVE FOR 50.8/25.98/10 SLEEVE

Figure 3.7 INCREASE IN RADIUS/APPLIED LOAD CURVE FOR 50.8/25.08/12 SLEEVE

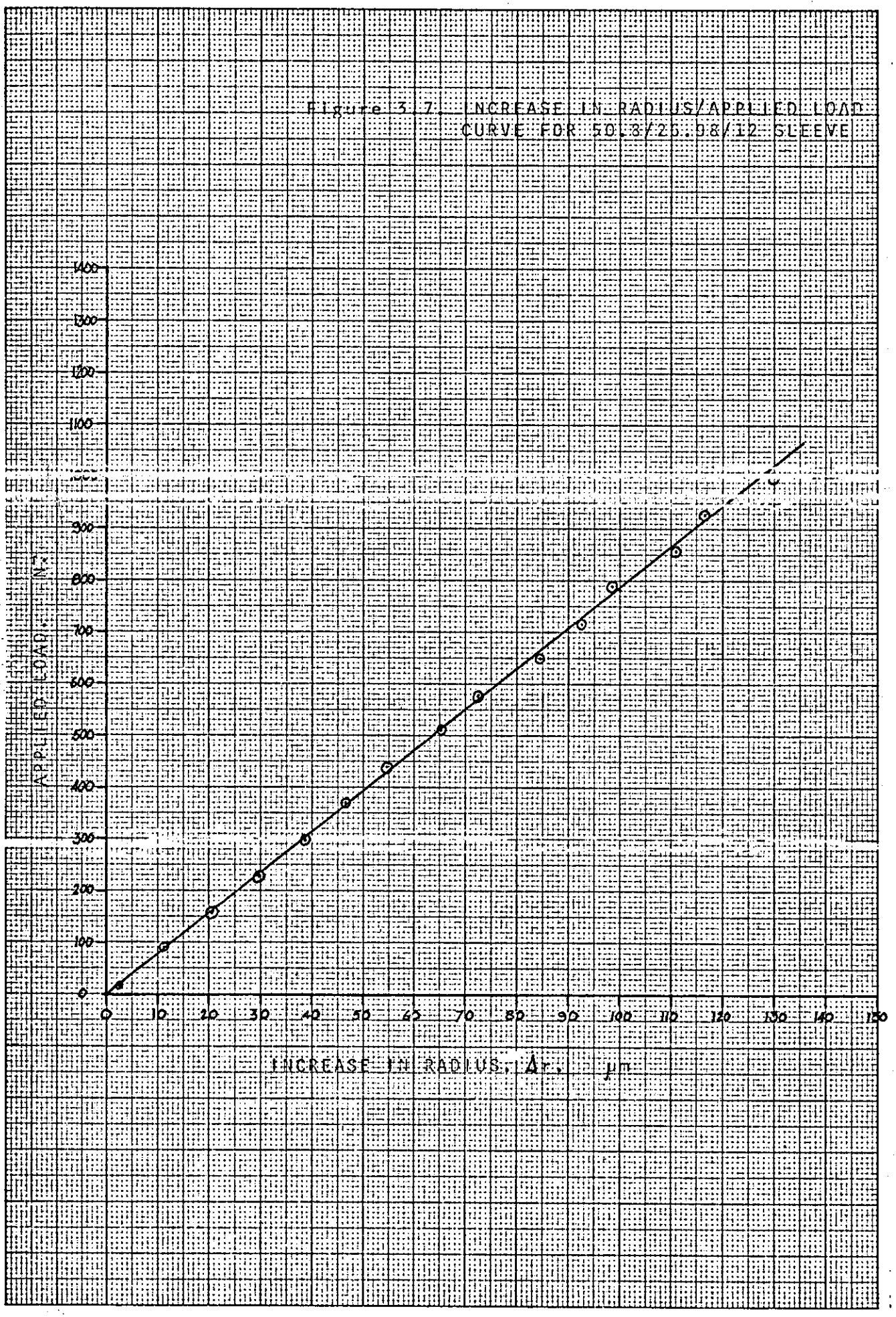

Figure 3.8. INCREASE IN RADIUS/APPLIED LOAD CURVE FOR 41.26/25.93/8 SLEEVE

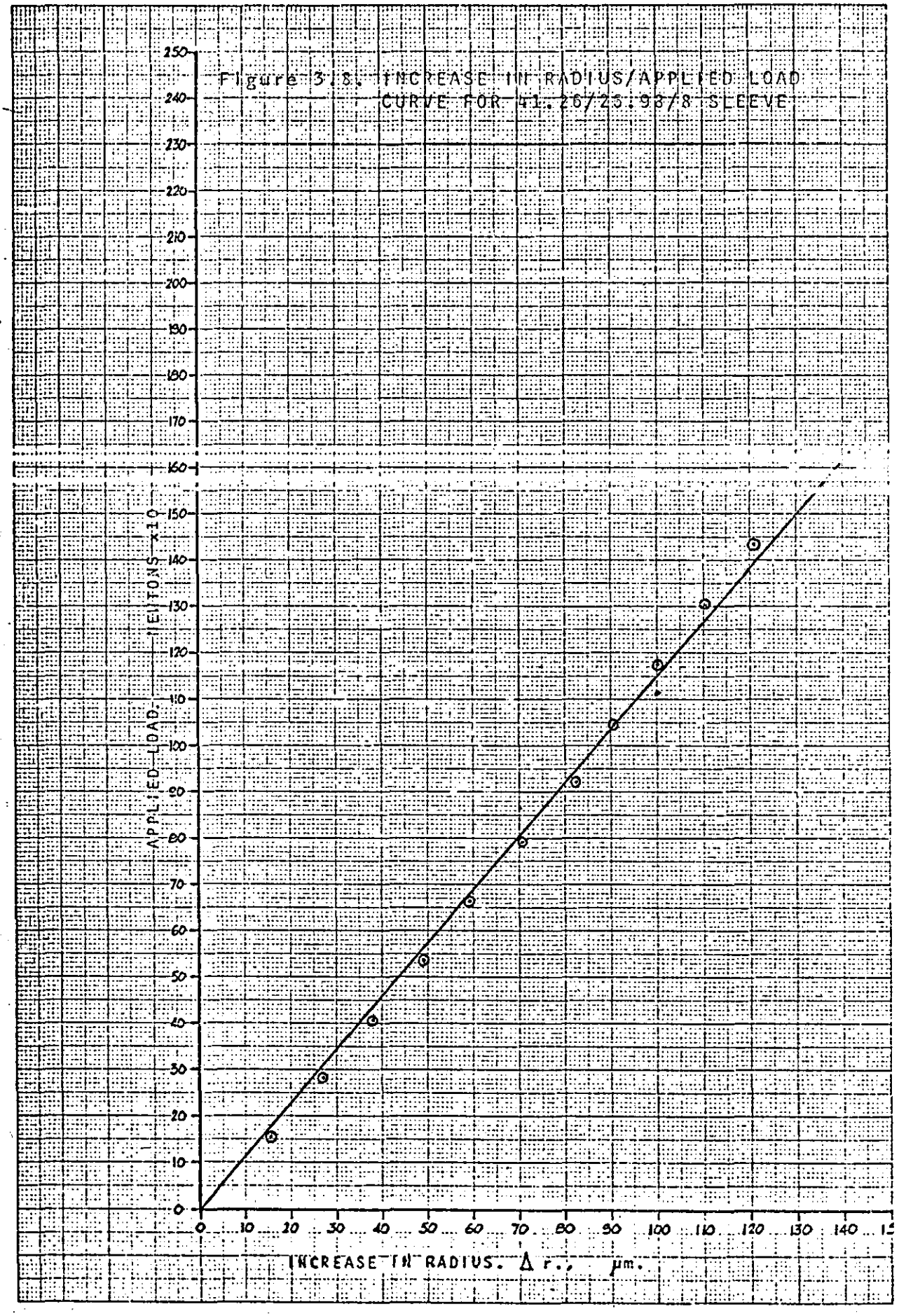

Figure 3.9. INCREASE IN RADIUS/APPLIED LOAD CURVE FOR 41.26/26.98/10 SLEEVE

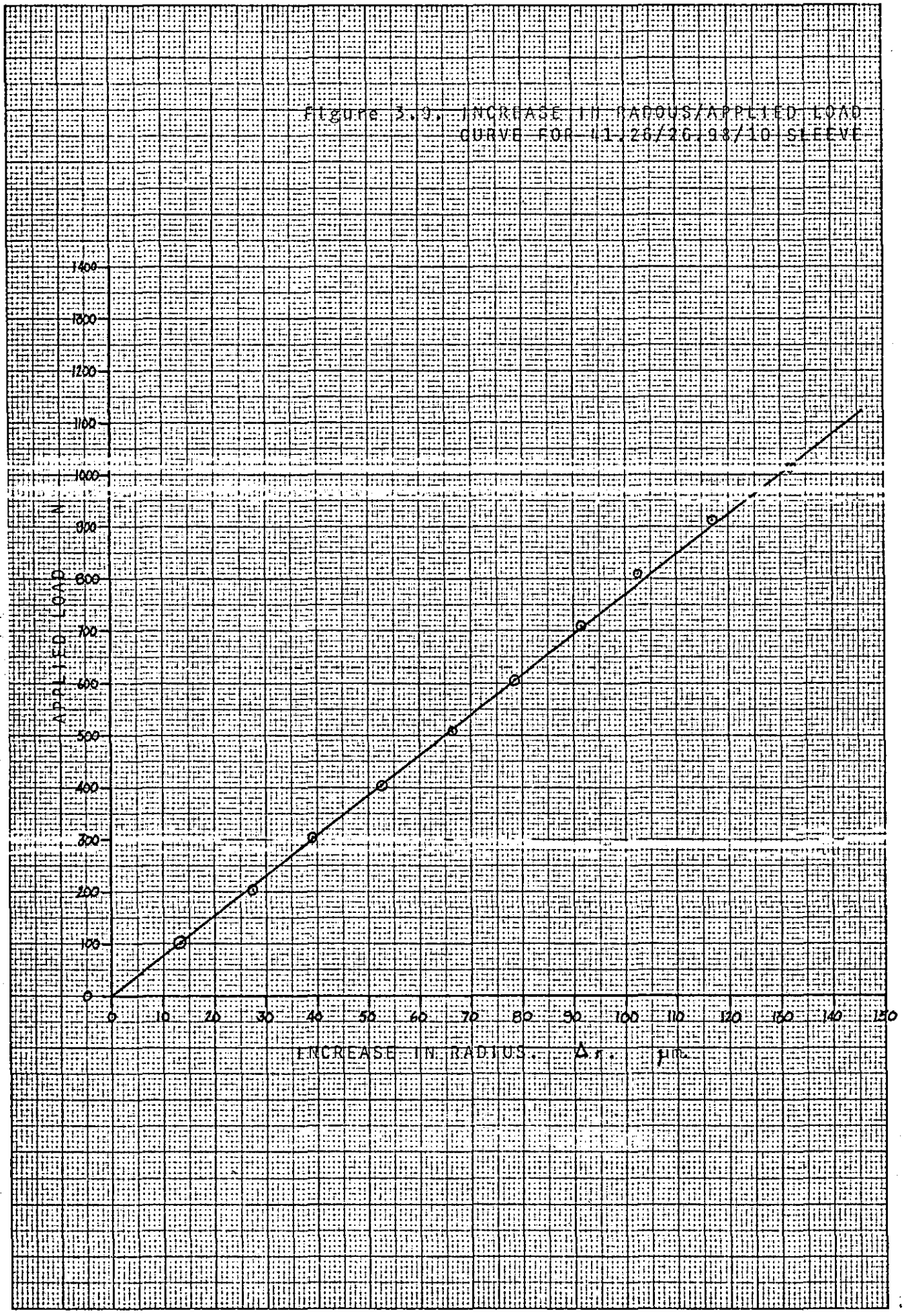

FIGURE 3.10. INCREASE IN RADIUS/APPLIED LOAD CURVE FOR 60.32/42.86/8 SLEEVE

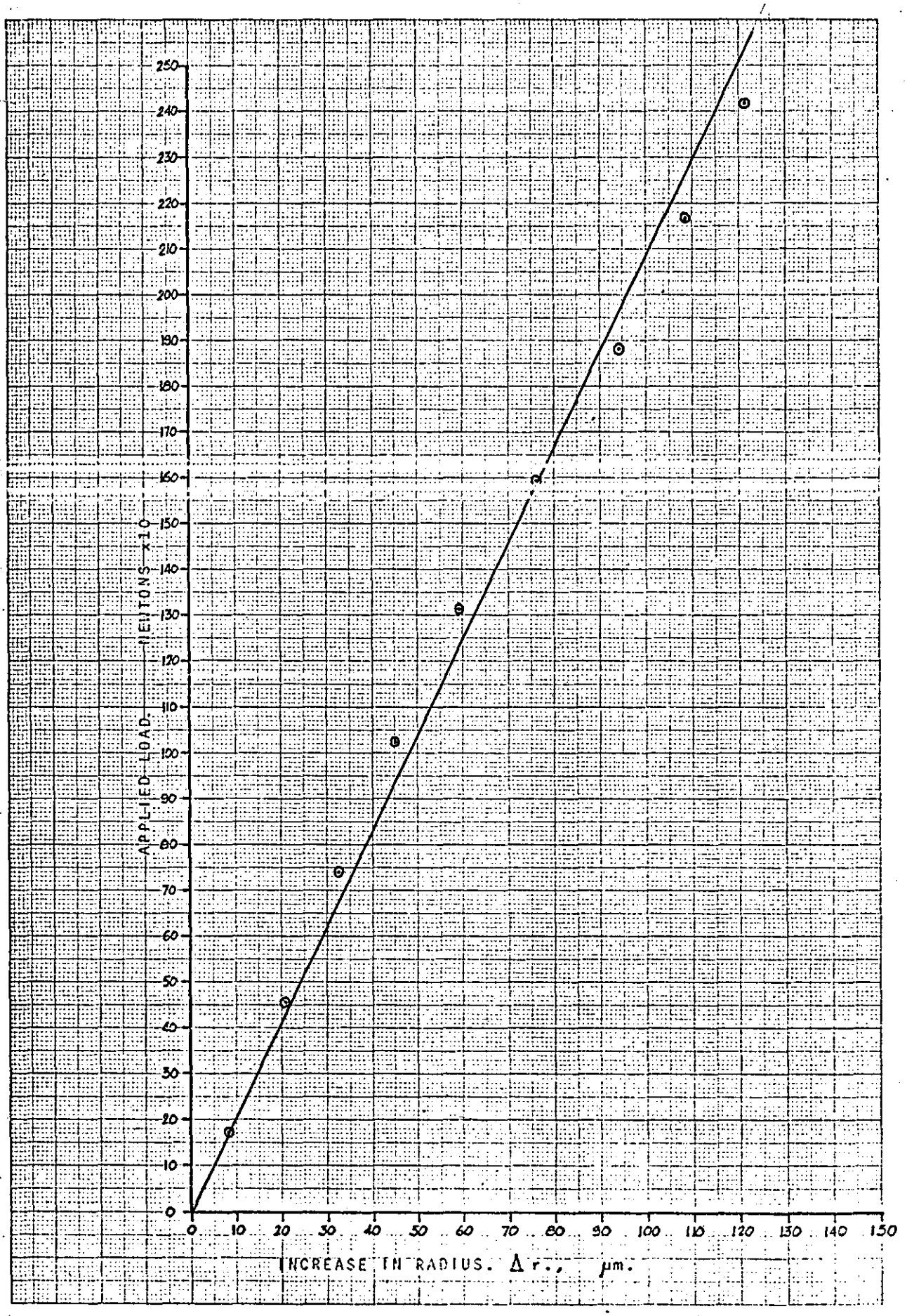

Figure 3.11. INCREASE IN RADIUS/APPLIED LOAD CURVE FOR 60.32/42.86/10 SLEEVE

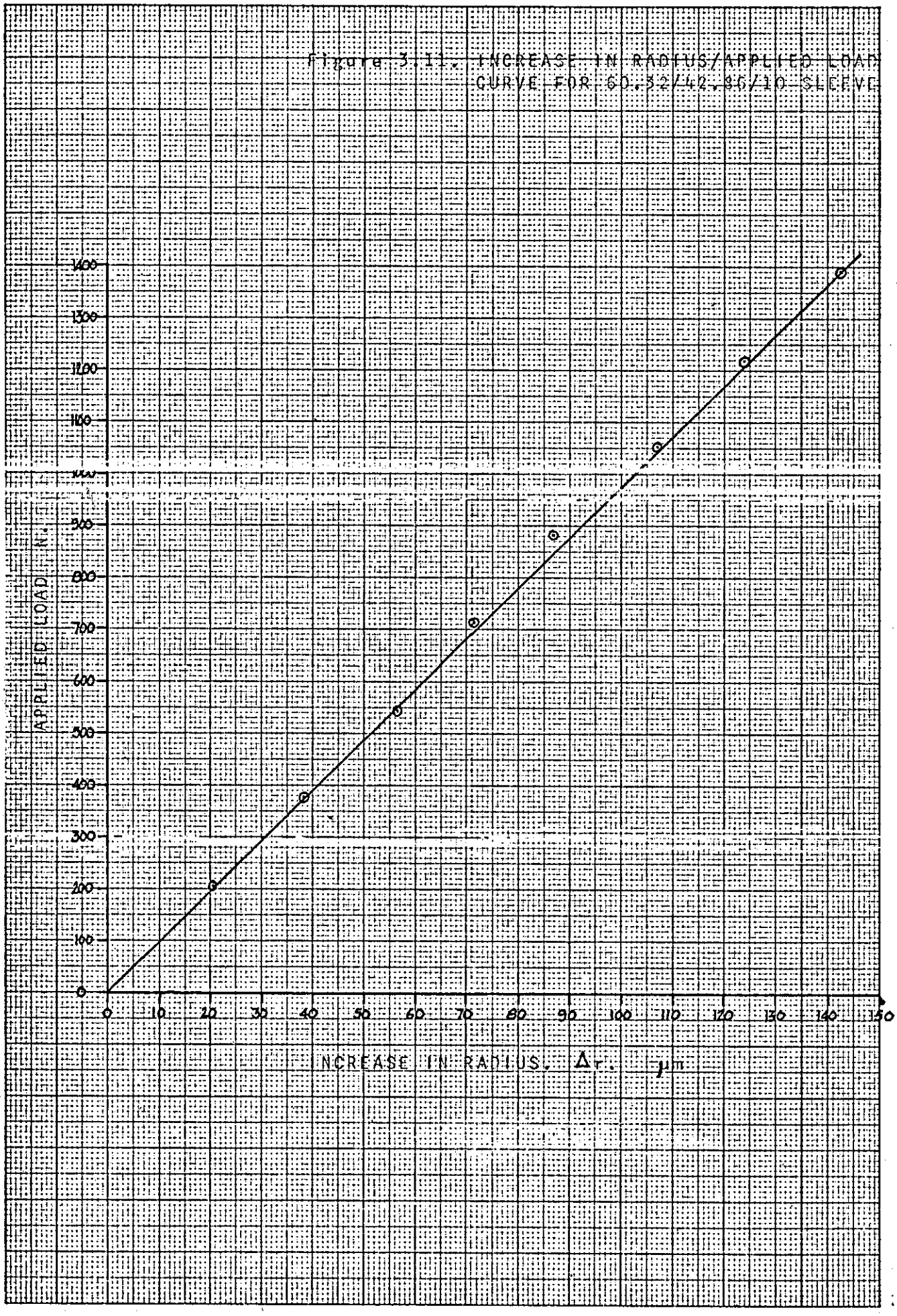

Figure 3.12. INCREASE IN RADIUS/APPLIED LOAD CURVE FOR 60.32/42.86/12 SLEEVE

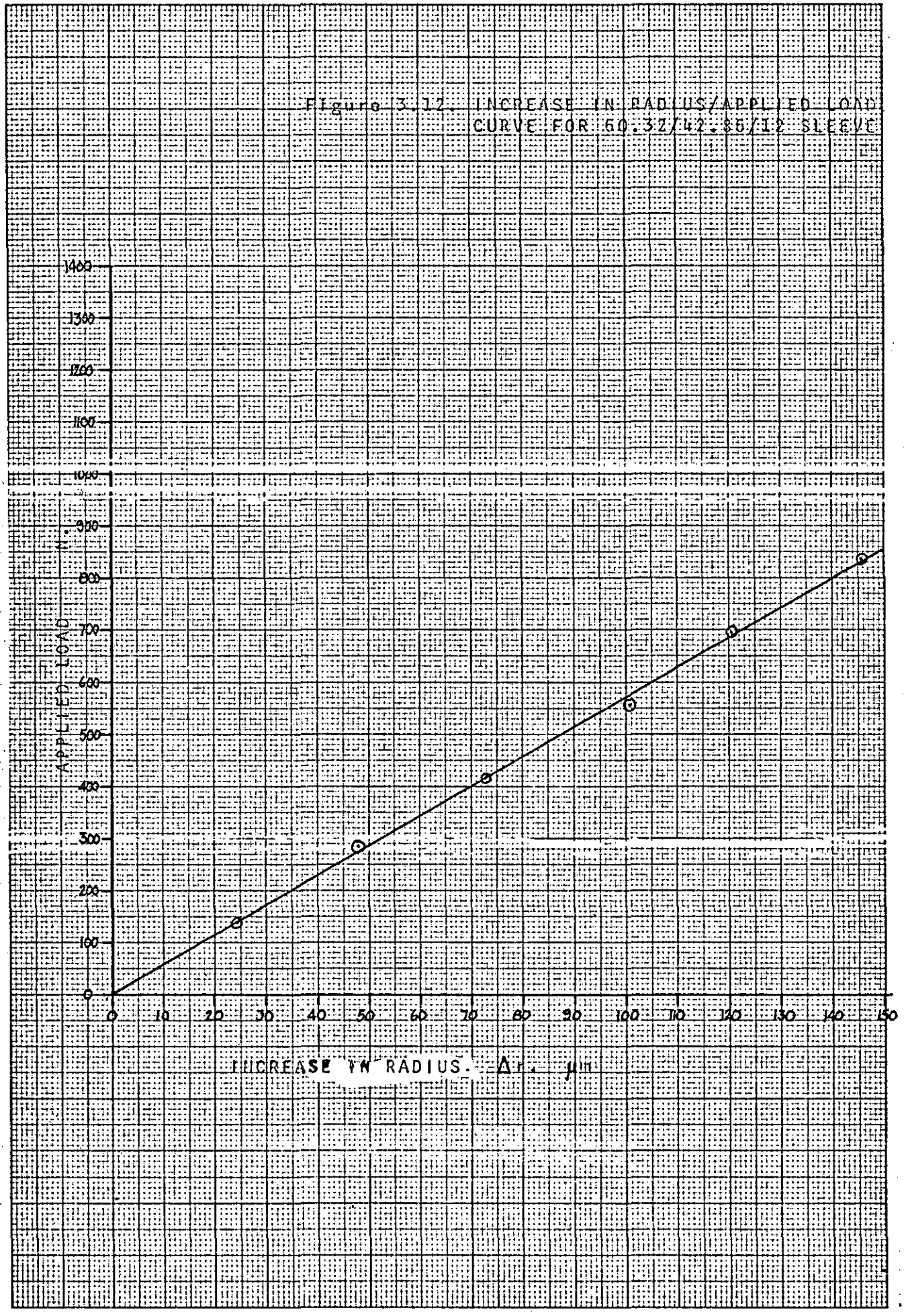

Figure 3.13. INCREASE IN RADIUS/APPLIED LOAD CURVE FOR SC.8/42.80/10 SLEEVE

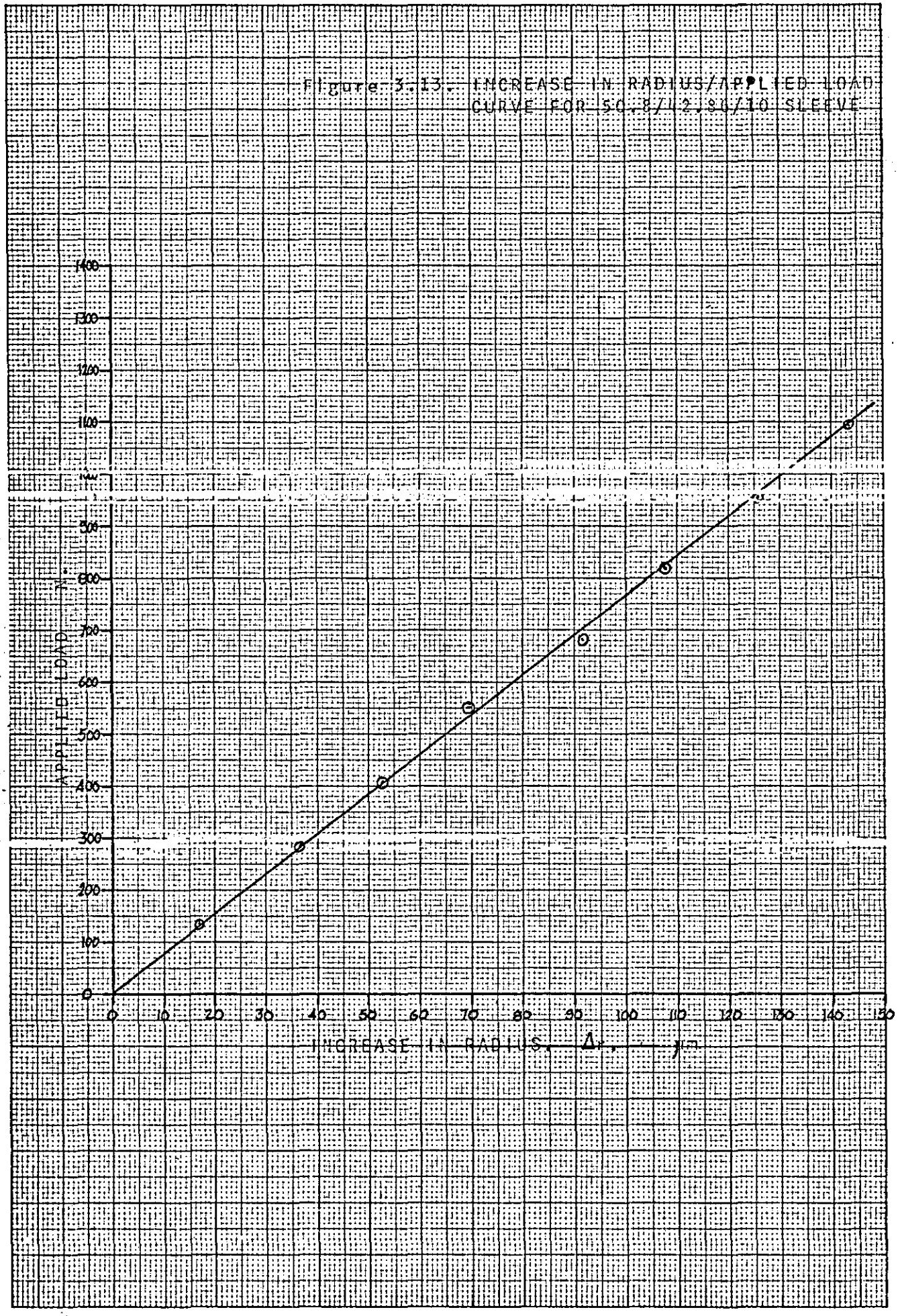

Figure 3.14. INCREASE IN RADIUS/APPLIED LOAD CURVE FOR 50.8/42.86/12 SLEEVE

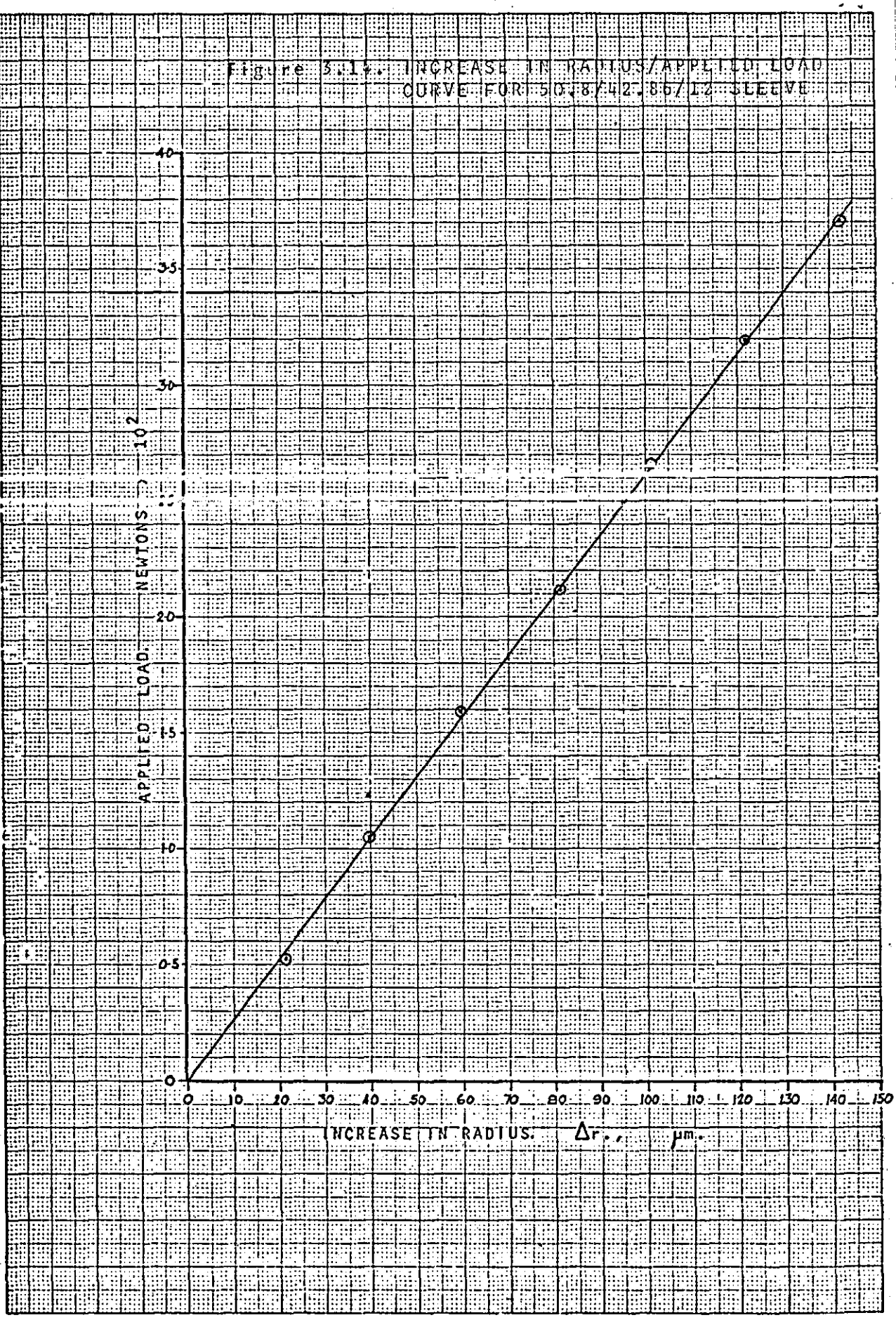

Figure 3.15. INCREASE IN RADIUS/APPLIED LOAD CURVE FOR 41.26/42.98/13 SLEEVE

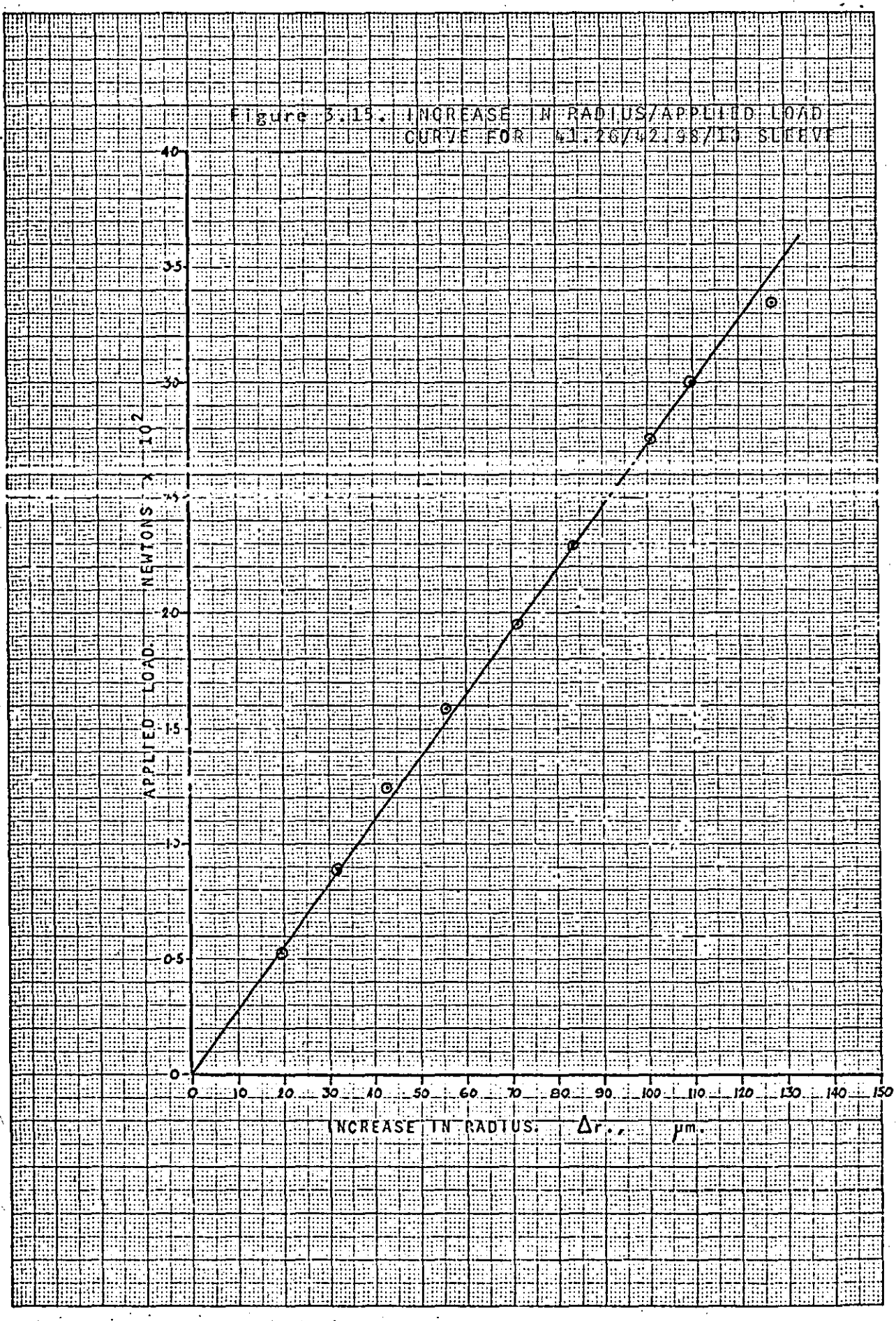

Figure 3-10. INCREASE IN RADIUS/APPLIED LOAD CURVE FOR 41.26/42.98/12 SLEEVE

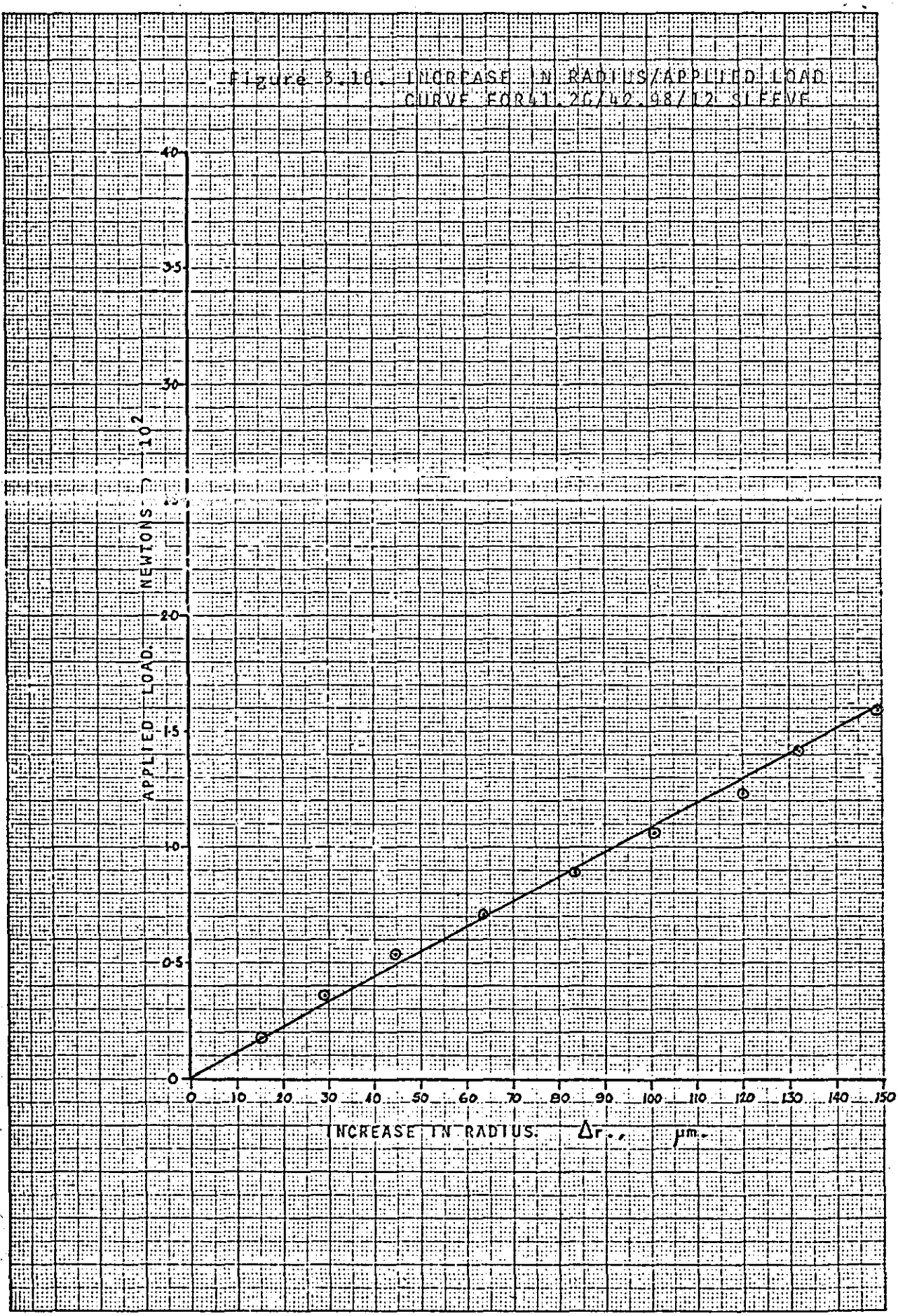

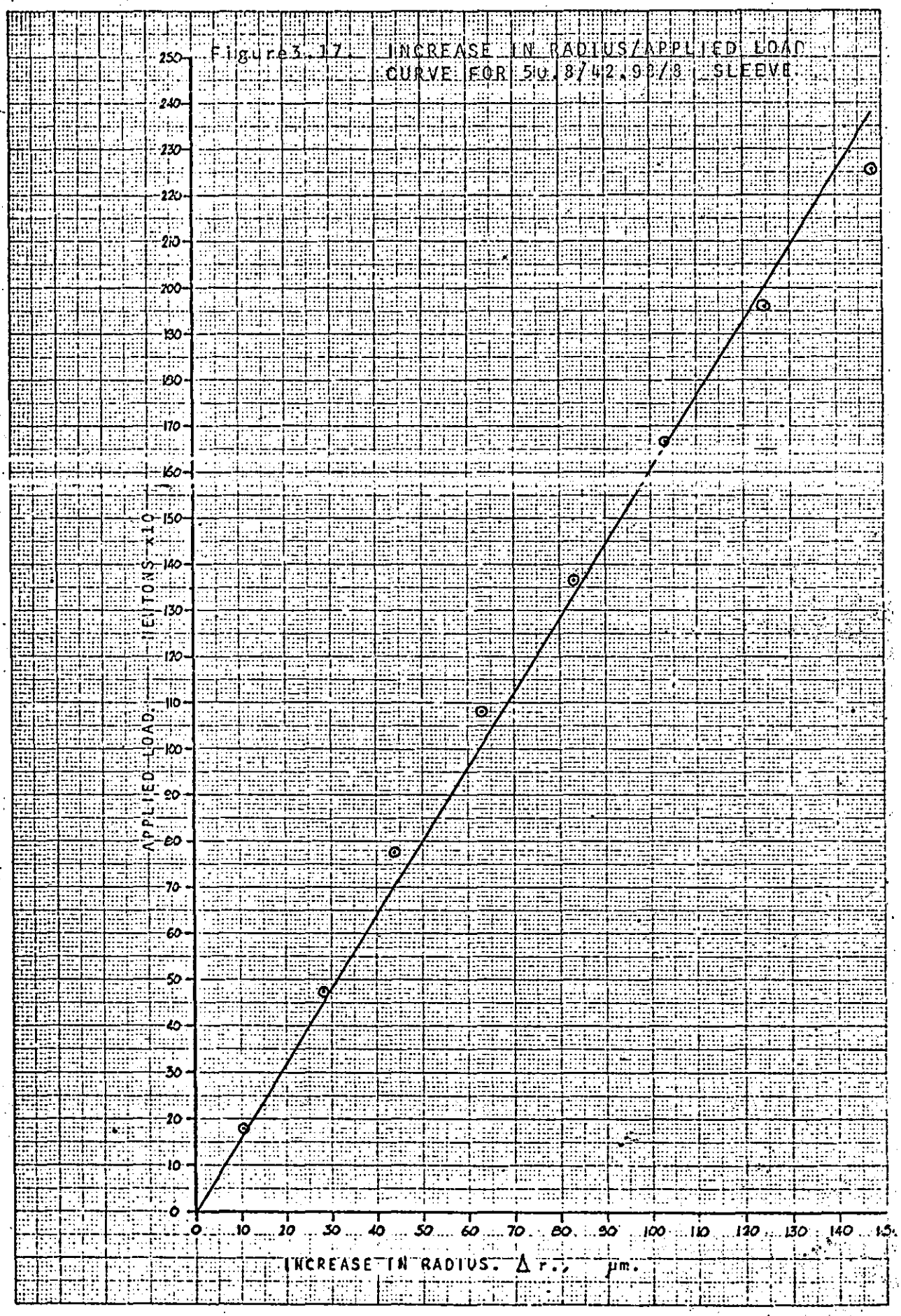

Figure 3.17. INCREASE IN RADIUS/APPLIED LOAD CURVE FOR 50.8/42.90/3 SLEEVE.

Figure 3.19. INCREASE IN RADIUS/APPLIED LOAD CURVE FOR 41:24/42:30/0 SLEEVE

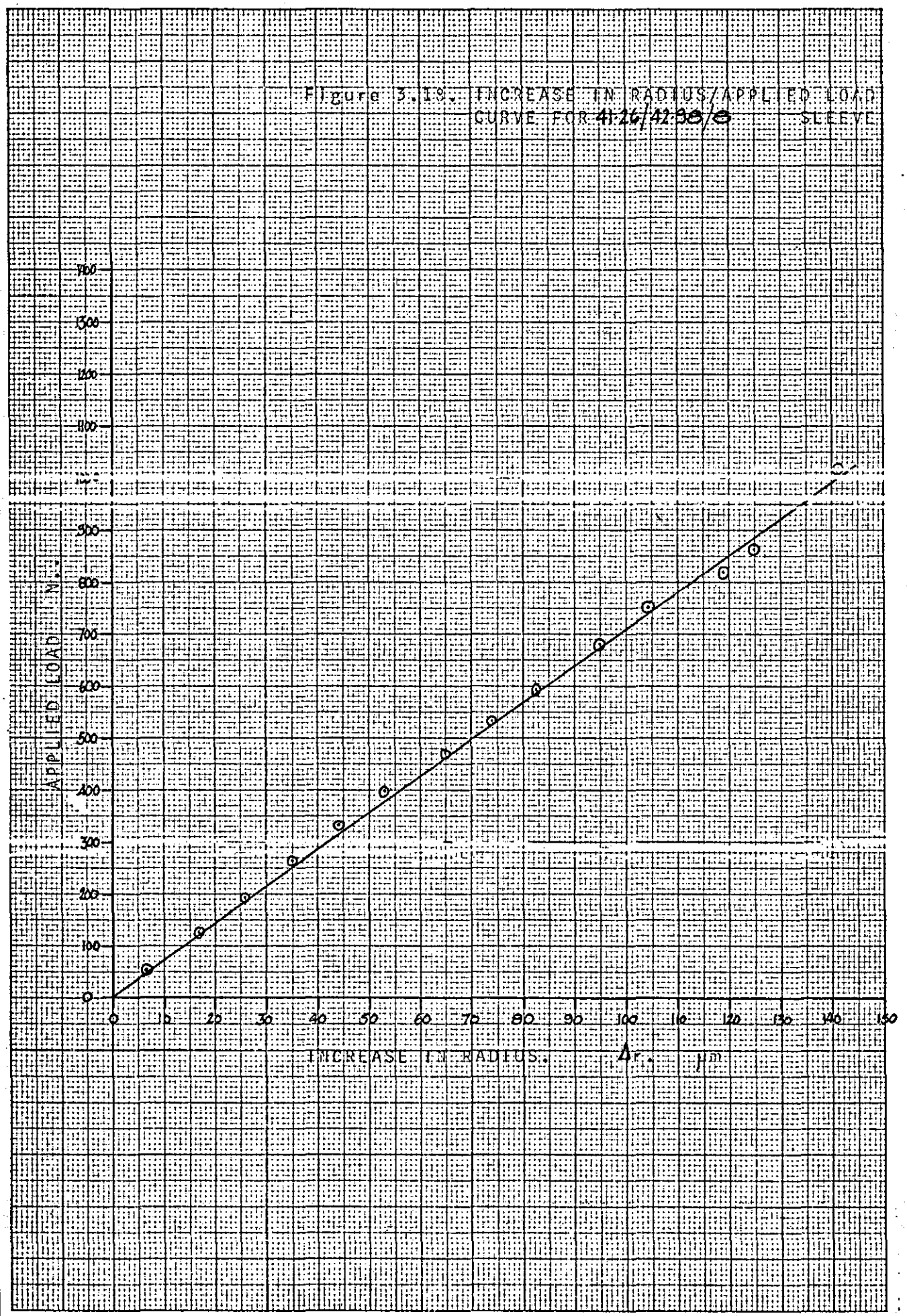

Figure 3.19. LOAD-EXTENSION CURVE FOR LINEAR MODEL 1 (steel)

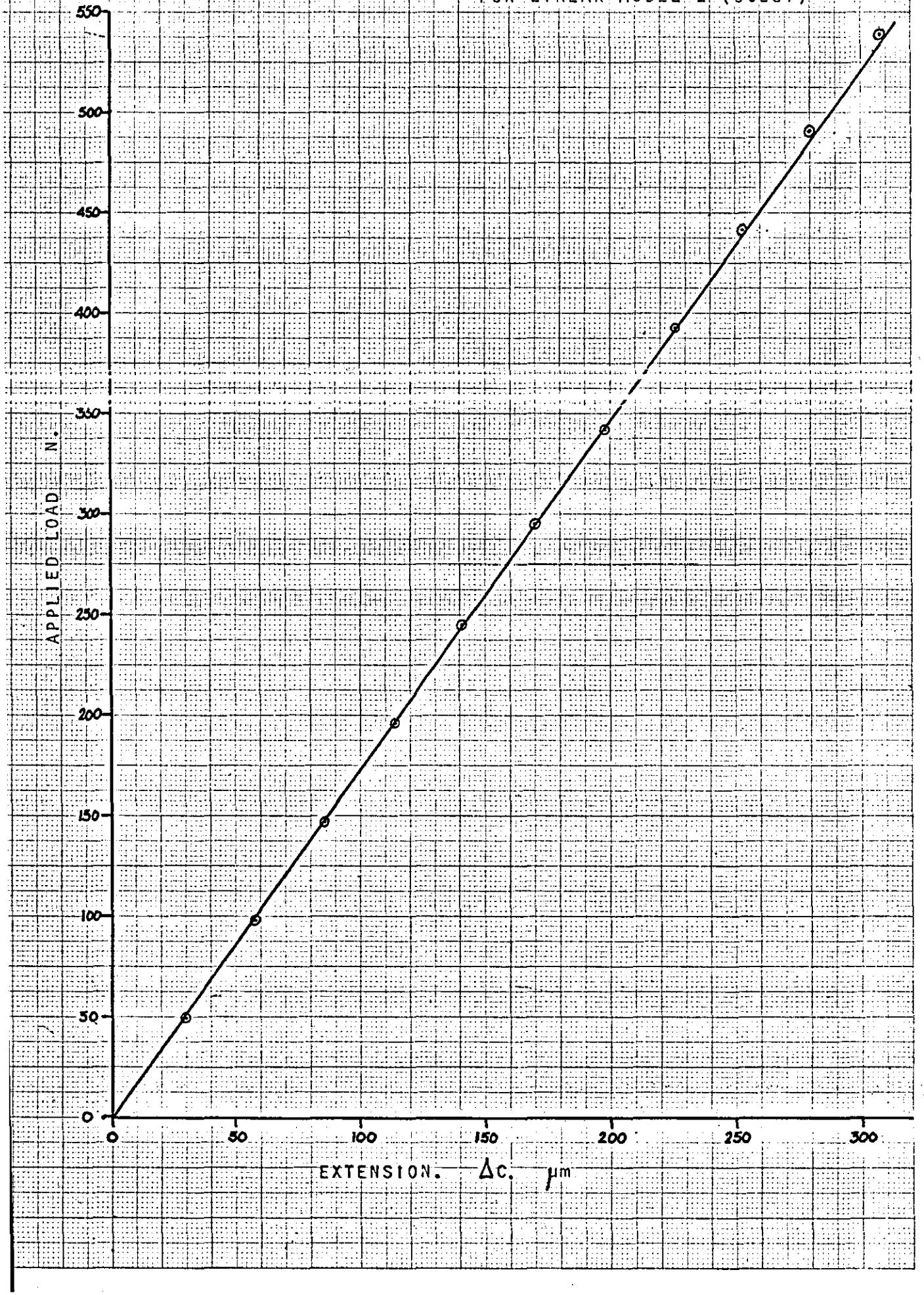

Figure 3.20. LOAD-EXTENSION CURVE FOR LINEAR MODEL 2 (steel)

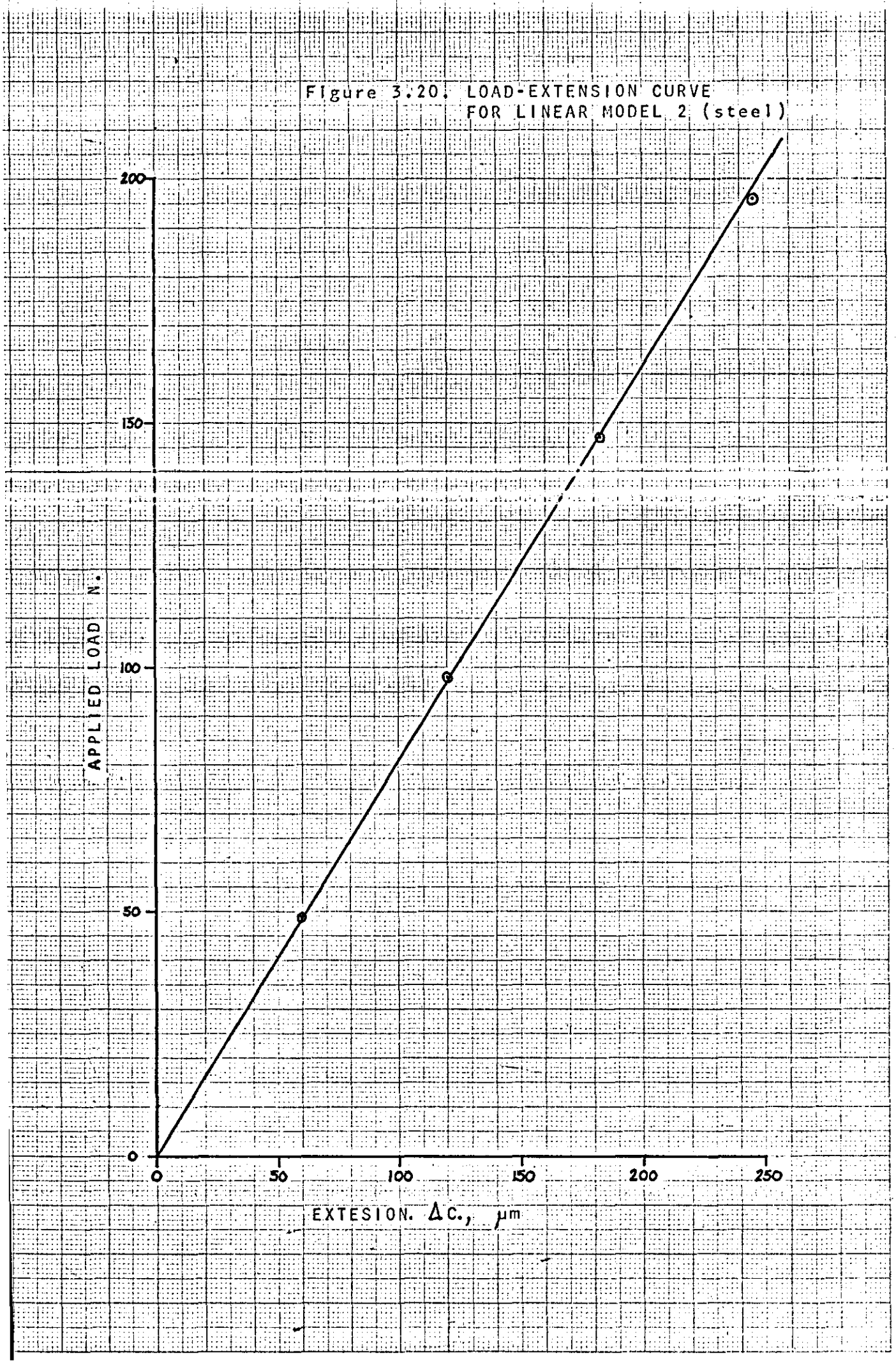

Figure 3.21. LOAD-EXTENSION CURVE FOR LINEAR MODEL 3 (steel)

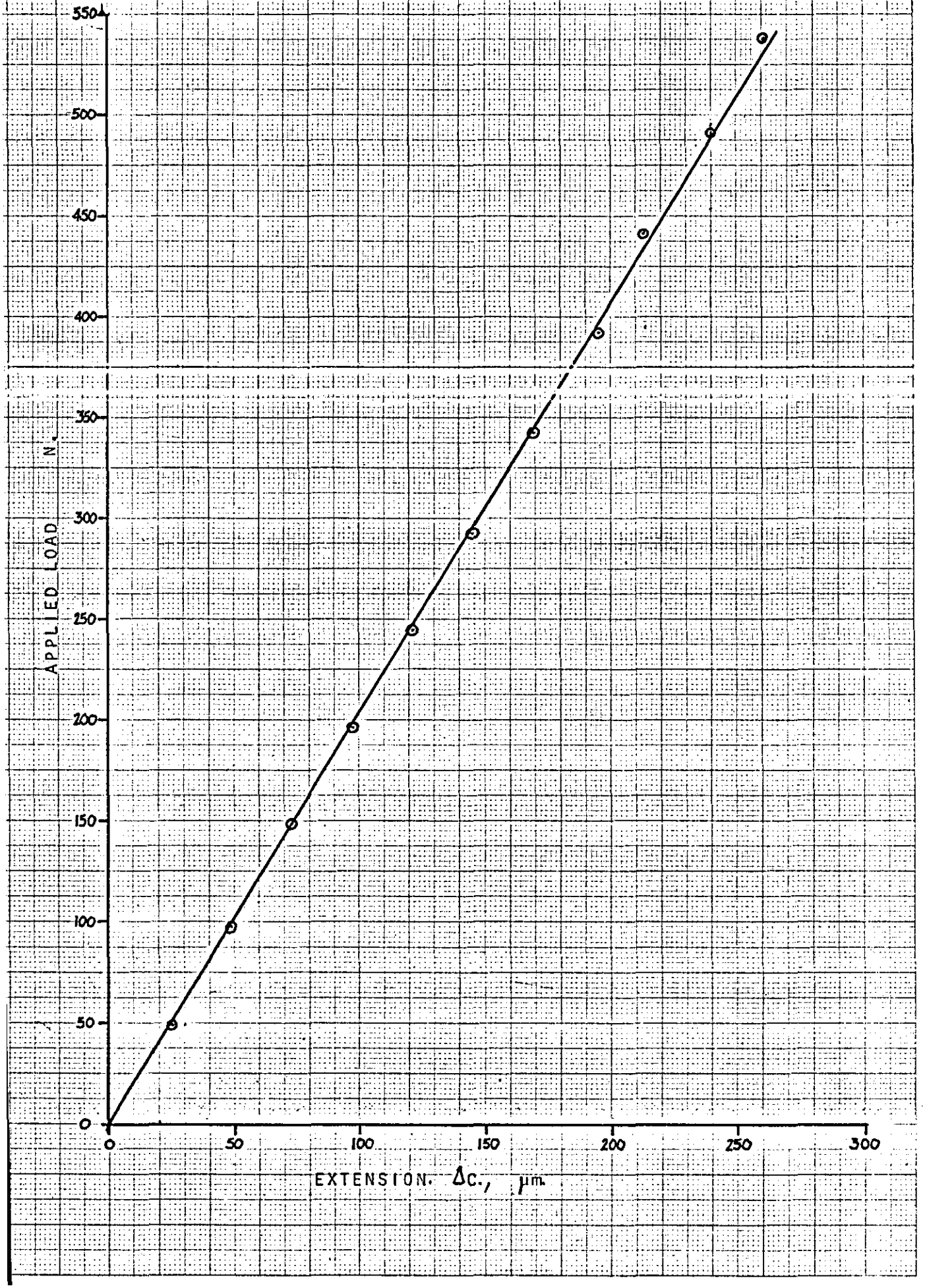

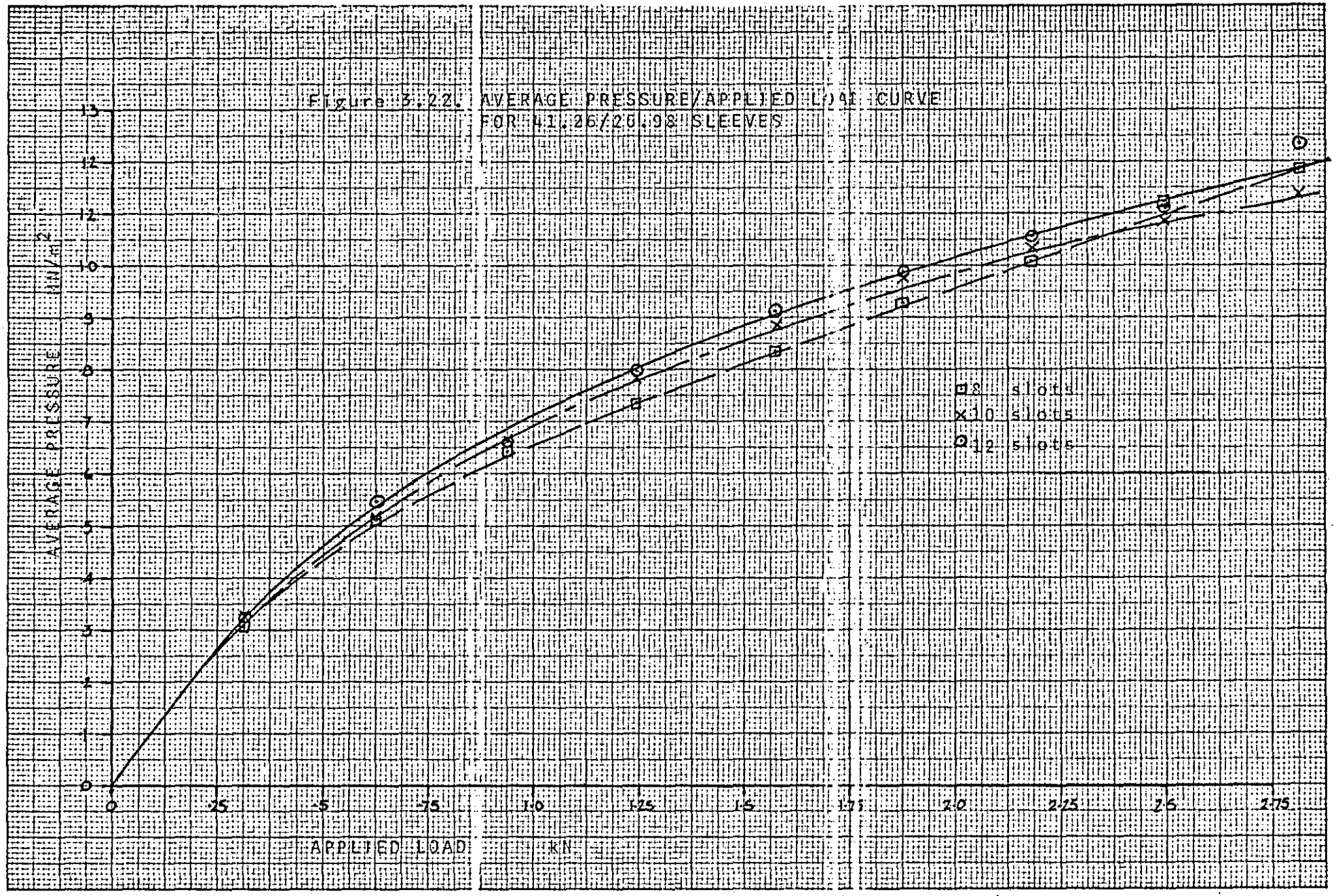

Figure 3.22. AVERAGE PRESSURE/APPLIED LOAD CURVE FOR 41.26/26.98 SLEEVES

Figure 3.23. AVERAGE CONTACT PRESSURE/APPLIED LOAD CURVE FOR 50.8/42.86/ SLEEVE

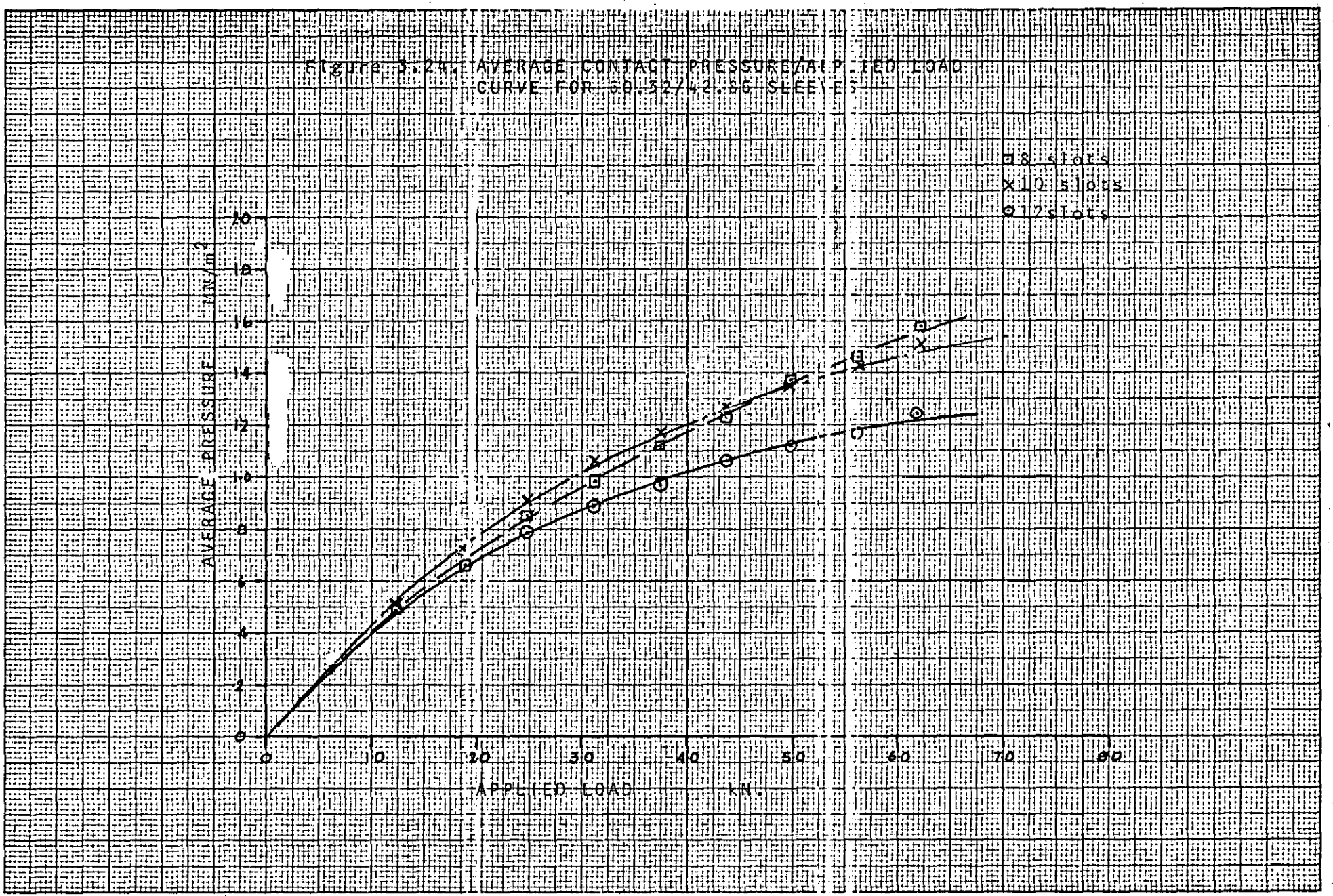

Figure 5.24. AVERAGE CONTACT PRESSURE/APPLIED LOAD CURVE FOR 60,32/42.56 SLEEVE

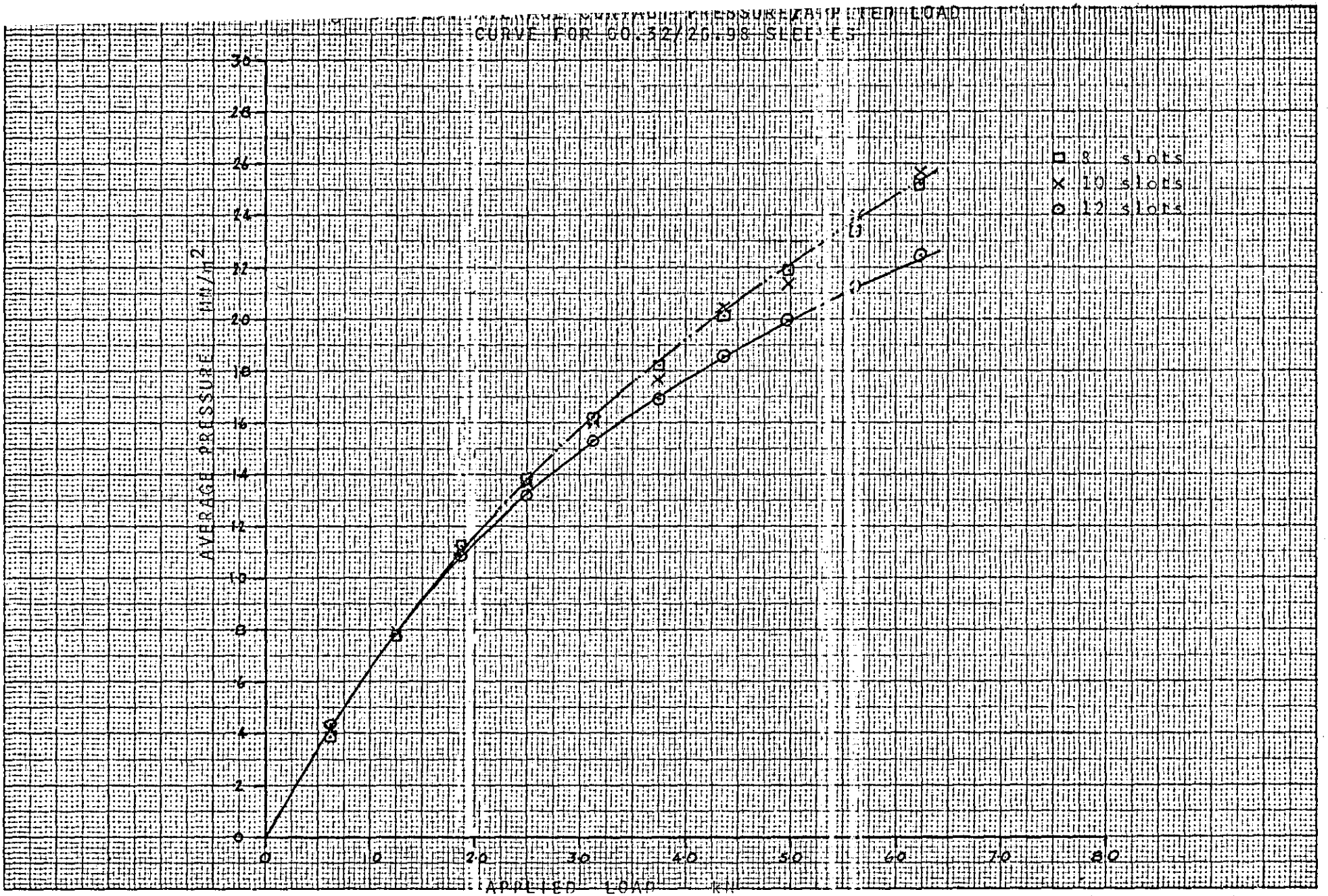
CURVE FOR 60.32/20.98 SLEEVES
AVERAGE PRESSURE KN/m2
APPLIED LOAD KN
8 slots
10 slots
12 slots
0
2
4
6
8
10
12
14
16
18
20
22
24
26
28
30
10
20
30
40
50
60
70
80

Figure 5.26. COMPARISON OF CONTACT PRESSURE/APPLIED LOAD FOR 8SLOT MANDRELS.

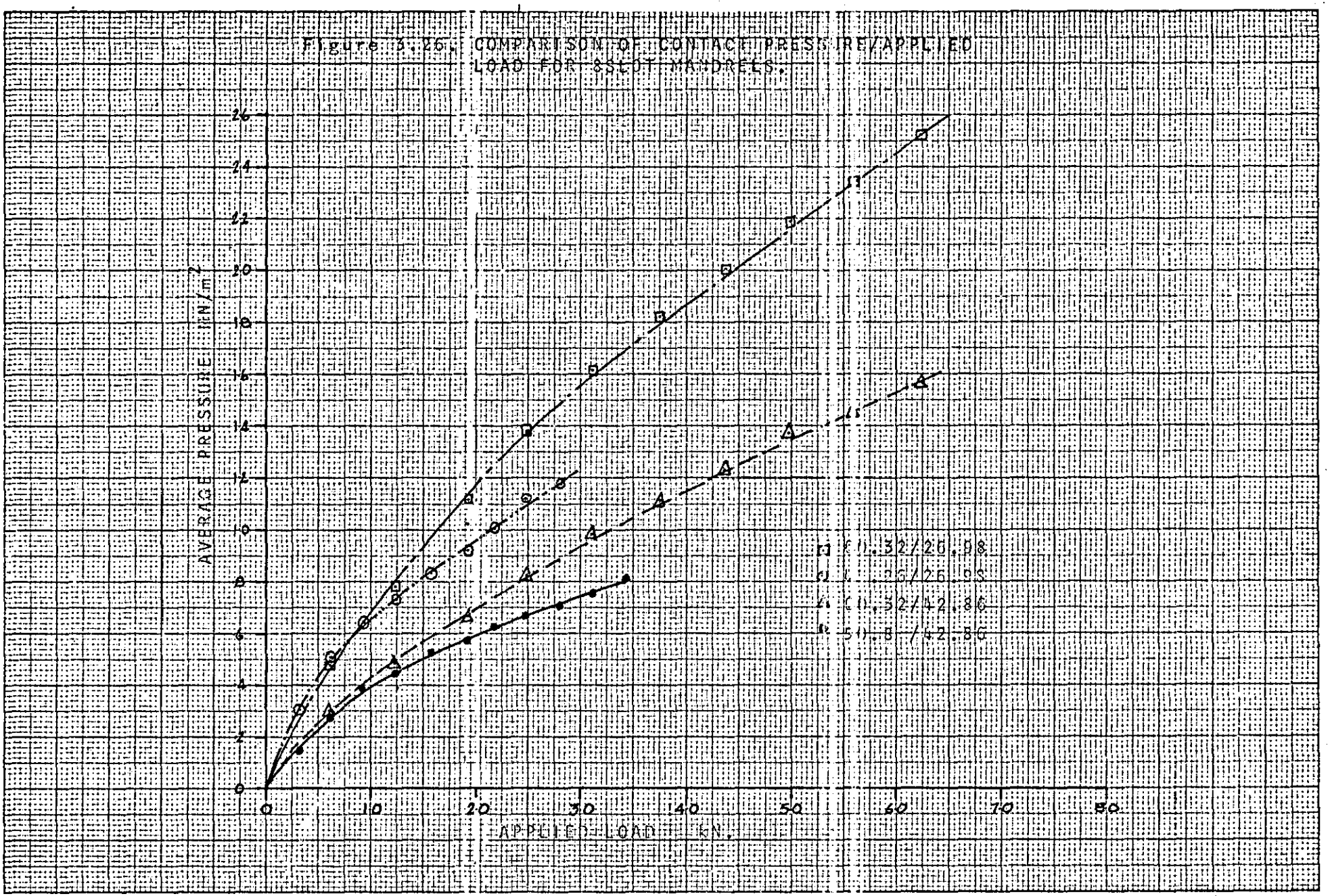

CHAPTER 1V

MATHEMATICAL MODEL OF THE MANDREL SLEEVE

4. Formulation of Mathematical Model of Sleeve

4.1 Analysis of the action of the Mandrel Sleeves

The mathematical model of the mandrel sleeve was formulated out of an analysis of the experimental work conducted. The load-radial expansion experimentation indicated that the relationship between the applied load and radial expansion was linear in nature, this initial experimentation and the qualitative photo-elasticity work gave rise to a first hypothesis defining the micro-deformation of certain elements within the mandrel sleeve. With the micro-deformation established the macro-deformation of the mandrel sleeve (circumferential expansion) is found by summating the micro-deformation of the beam elements.

Further experimental work, the load-extension of the linear models, was initiated to establish the validity of the first hypothesis. This work defined the limitations of the first hypothesis and further analysis of the deformations taking place within the mandrel sleeves lead to a second hypothesis. This second hypothesis took into account the micro-deformation of all elements making up the mandrel sleeve and enabled a mathematical model, which demonstrates the influence the design parameters have on the radial expansion of a sleeve for a given applied load, to be established.

4.1.1 First hypothesis of the deformation characteristics of some elements within a Mandrel Sleeve

The mandrel sleeve expands under load like a garter spring, and the deformations of the beam elements within the mandrel sleeve, taken in total, give rise to the circumferential expansion of the sleeve. The beam elements being considered, for the purpose of establishing their deformation for a given load, as a beam encastre at both ends and that any deformation of this beam is by a deflection of one end of the beam relative to the other which maintains a condition of zero slope at the supports, as shown in figure 4.1.

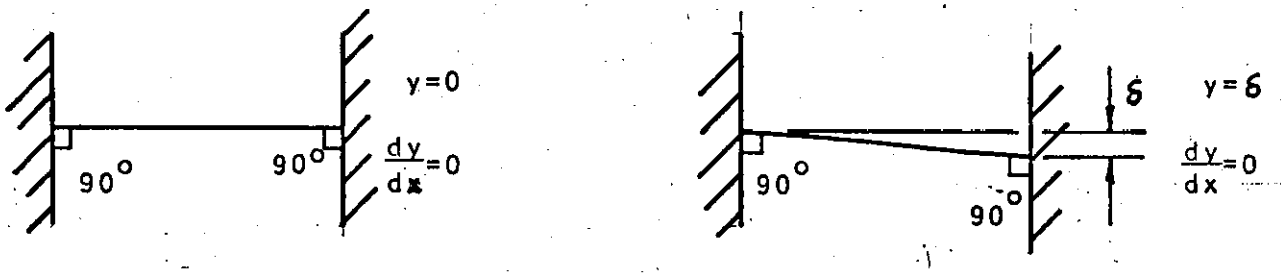

initial built in beam (a) — deflection mode (b)

Figure 4.1

The resulting load W to effect the change from situation (a) to (b) can be found thus

Consider the beam as a cantilever with a load W and a bending moment M_r at the free end, figure 4.2.

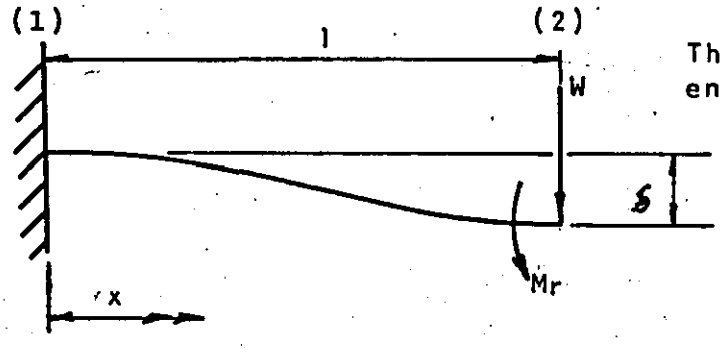

The end conditions are;
end (1), x=0, y=0, $\frac{dy}{dx}=0$.
(2), x=l, y=ℓ, $\frac{dy}{dx}=\delta$

Figure 4.2.

from Morley (62), the lateral deflection due to bending only may be determined by solving the differential equation of the elastic curve of the neutral axis

$$EI\frac{d^2y}{dx} = M_x \qquad (1)$$

The bending moment at any position x is given by

$$M_x = W(l-x) + M_r \qquad (2)$$

substituting for M_x in (1)

$$EI\frac{d^2y}{dx} = W(l-x) + M_r \qquad (3)$$

using double integration with respect to x, we get

$$EI\frac{dy}{dx} = W\left(lx-\frac{x^2}{2}\right) + M_r x + A \qquad (4)$$

$$EIy = W\left(\frac{lx^2}{2} - \frac{x^3}{6}\right) + M_r\frac{x^2}{2} + Ax + B \qquad (5)$$

using the end conditions $\frac{dy}{dx} = 0$ at $x = 0$ and substituting in (4) gives $A = 0$

also $y=0$ at $x=0$ substituting in (5) gives $B=0$

(5) becomes $$EIy = W\left(\frac{lx^2}{2} - \frac{x^3}{6}\right) + M_r\frac{x^2}{2} \qquad (5a)$$

using end condition $\frac{dy}{dx} = 0$ at $x = l$ and substituting in (4) we get

$$M_r = \frac{-Wl}{2} \qquad (6)$$

substituting (6) into (5a)

$$EIy = \frac{Wx^3}{3} - \frac{Wl^3}{4}$$

at $x = l$

$$EIy = \frac{Wl^3}{3} - \frac{Wl^3}{4}$$

$$EIy = \frac{Wl^3}{12}$$

$$y = \frac{Wl^3}{12EI} \qquad (7)$$

4.1.2 Second hypothesis of the deformation characteristics of the elements within a Mandrel Sleeve

The circumferential expansion of a sleeve under load is made up of the beam element deflection (as stated in the first hypothesis) and of a deflection caused by the change in slope of the end sections joining such beam elements. The end sections to be considered as a beam subjected to a bending moment at each end, as shown in figure 4.3.

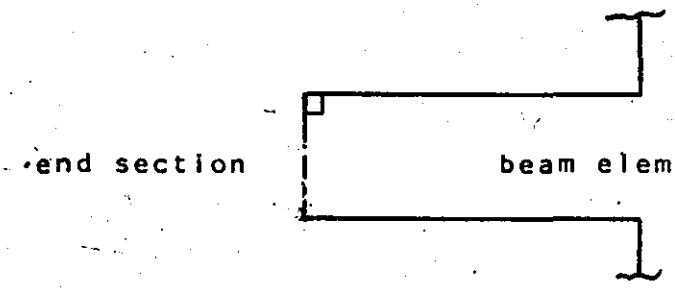

(a). Diagramatic representation of a mandrel sleeve.

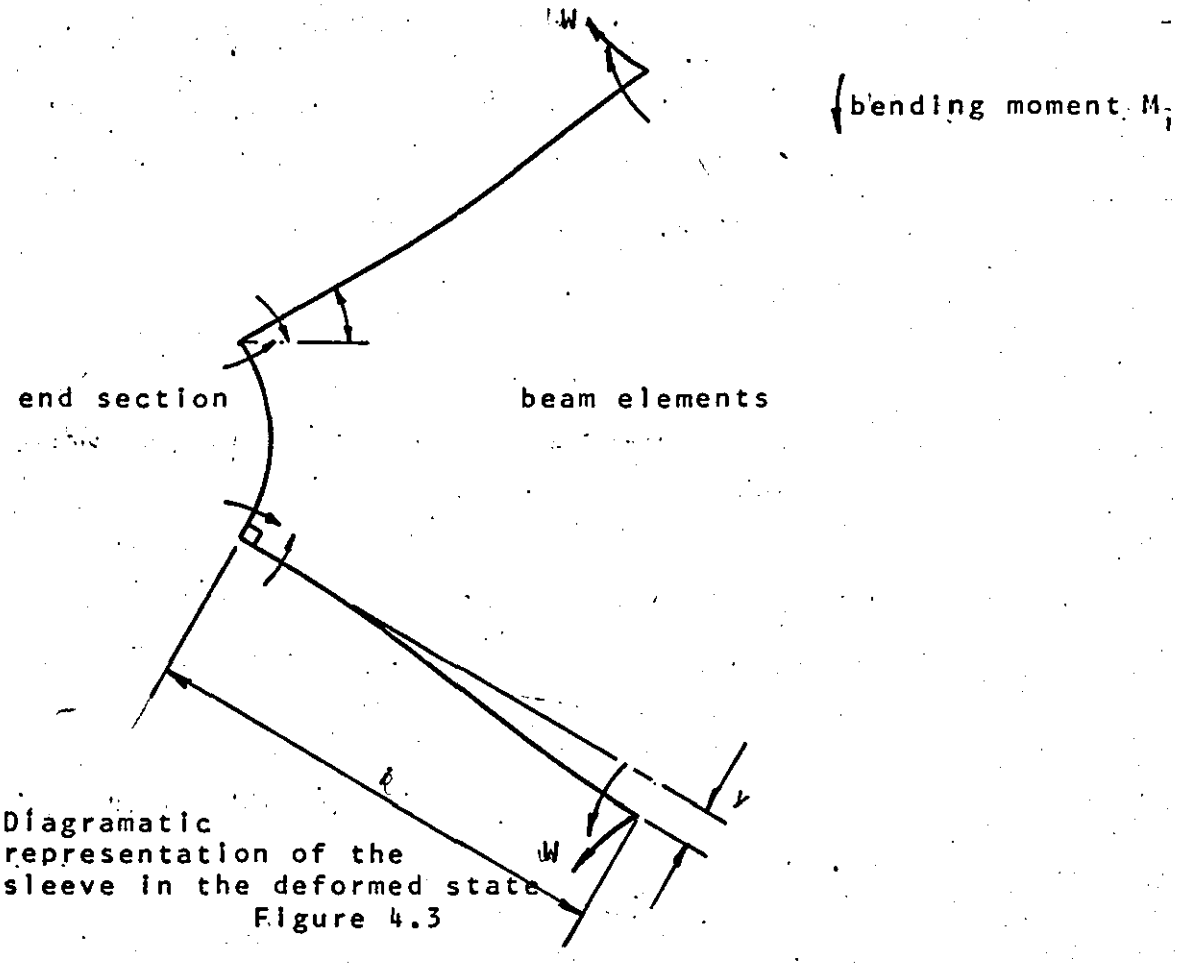

(b) Diagramatic representation of the sleeve in the deformed state

Figure 4.3

The end section under load is subjected to a bending moment at each end. This bending moment is the 'built in' moment

caused by the beam elements.

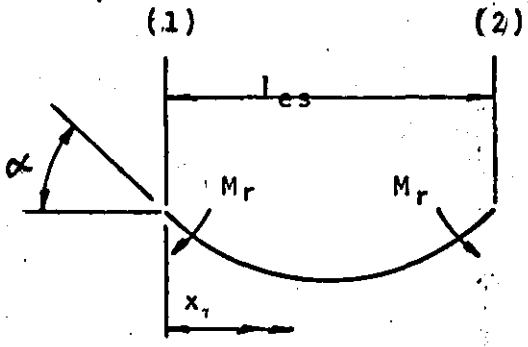

The end conditions are:
end (1), $x=0$, $\frac{dy}{dx}=\alpha$
(2), $x=l_{es}$, $\frac{dy}{dx}=\alpha$

Figure 4.3 (c):Deflection of end section.

from Morley (62), the slope due to bending only may be determined by solving the differential equation of the curve or the elastic neutral axis.

$$EI_{es}\frac{d^2y}{dx} = M_x \qquad (1) \text{ (from page 91)}$$

Integrating with respect to x

$$EI_{es}\frac{dy}{dx} = Mx + A \qquad (2) \text{ (from page 91)}$$

using the condition $\frac{dy}{dx} = 0$ at $x = l_{es}/2$ and substituting in (2) we get

$$0 = \frac{M_x l_{es}}{2} + A$$

$$A = -\frac{M_x l_{es}}{2} \qquad (7)$$

(2) becomes $EI_{es}\frac{dy}{dx} = Mx - \frac{M_x l_{es}}{2}$ (2a)

also $\frac{dy}{dx} = \alpha$ at $x = l$ substituting in (2a) gives

$$EI_{es}\alpha = M_x l_{es} - \frac{M_x l_{es}}{2}$$

$$\alpha = \frac{M_w l_{es.}}{2EI_{es.}} \qquad (8)$$

Now (6) gives $M_r = \frac{Wl}{2} = M_x$ (bending moment at support of ecastré beam)

substituting (6) into (8) gives

$$\alpha = \frac{W.l.l_{es}}{4E.I_{es.}} \qquad (9)$$

The deflection caused by end section bending is equal to the slope at the end of the end section multiplied by the length of the beam element, for small deflections

$$y_{es.} = \alpha L^* \qquad (10)$$

substituting (9) into (10)

$$y_{es.} = L^* \frac{W.l.l_{es.}}{4E.I_{es.}} \qquad (11)$$

Using the theorem of superposition the deflection, y_n, of one beam element and one end section for a given load W is

$$y_n = y + y_{es} \qquad (12)$$

substituting (7) and (11) in (12)

$$y_n = \frac{Wl}{12EI} + \frac{W L^*.l.l_{es.}}{4EI_{es.}} \qquad (12a)$$

The circumferential expansion of the sleeve is the sum of all the individual deflections.

$$\Delta C = N \cdot y_n \qquad (13)$$

substituting (12a) in (13)

$$\Delta C = N \left[\frac{Wl^3}{12EI} + \frac{WL^* l \cdot l_{es}}{4EI_{es}} \right] \qquad (14)$$

$$\Delta C = \frac{N \cdot W \cdot l}{4E} \left[\frac{l^2}{3I} + \frac{L^* \cdot l_{es}}{I_{es}} \right] \qquad (14a)$$

4.1.3 Mathematical Model of Sleeve

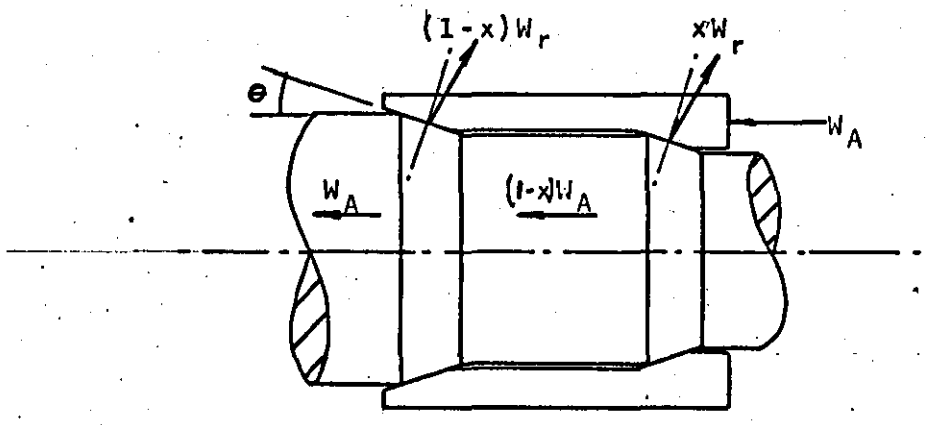

Figure 4.4.

Figure 4.4 shows the forces acting on the mandrel when a load W_A is applied to the mandrel sleeve. The total radial force W_o can be found by considering the mandrel system as a wedge, as shown in figure 4.5 below.

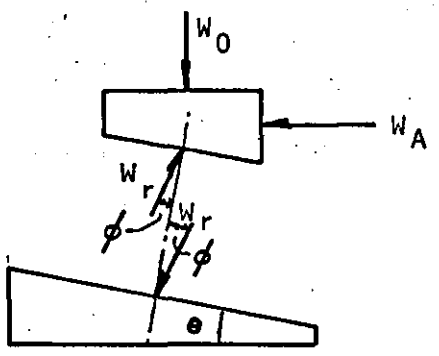

$$\phi = \tan^{-1}\mu$$

resolving the forces

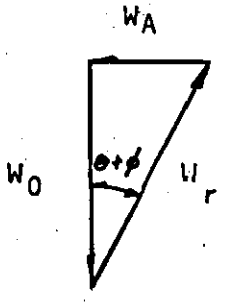

Figure 4.5:Forces acting on a wedge

$$W_o = \frac{W_A}{\text{Tan}(\theta+\phi)} \qquad (15)$$

Now W_o is the total outward load on the mandrel sleeve and the load per metreof circumference is(for unit length)

$$W_c = \frac{W_o}{\pi D} \qquad (16)$$

Now, if we consider a thin tube with internal pressure p

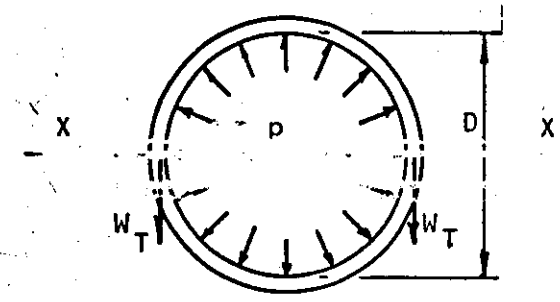

cutting the tube on line X-X and resolving forces

$$pD = 2W_T \text{(for unit length)}. \qquad (17)$$

Now consider the expanding mandrel

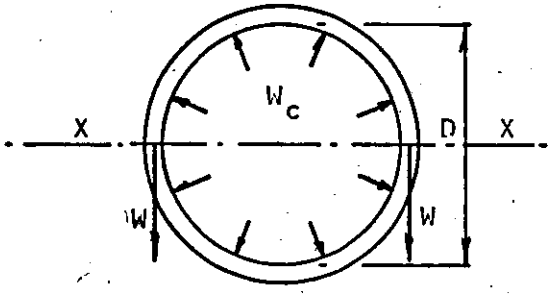

cutting the mandrel slee on line X-X and resolvin forces

$$W_c D = 2W \text{(for unit length)}. \qquad (18)$$

substituting (16) into (18)

$$\frac{W_o}{\pi} = 2W \qquad (18a)$$

substituting (15) into (18a)

$$\frac{W_A}{\pi \text{Tan}(\theta+\phi)} = 2W \qquad (19)$$

rearranging

$$W = \frac{W_A}{2\pi \text{Tan}(\theta+\phi)} \qquad (19a)$$

We now have an expression which relates the circumferential tension, W, in the mandrel sleeve with the applied axial load to the sleeve, W_A. Now the circumferential tension W is the load which causes the circumferential expansion in the mandrel sleeve.

from (14a) (page 96)

$$\Delta C = \frac{N.W.l}{4\ E}\left[\frac{l^2}{3I} + \frac{L^*.l_{es.}}{I_{es.}}\right]$$

substituting (19a) into (14a)

$$\Delta C = \frac{W_A}{2\pi \mathrm{Tan}(\theta+\phi)}\ \frac{N.l}{4E}\left[\frac{l^2}{3I} + \frac{L^*.l_{es}}{I_{es}}\right] \qquad (20)$$

also

$$\Delta C = 2.\pi.\Delta r. \qquad (21)$$

substituting (21) into (20)

$$2\pi\Delta r = \frac{W_A}{2\pi \mathrm{Tan}(\theta+\phi)}\ \frac{N.l}{4E}\left[\frac{l^2}{3I} + \frac{L^*.l_{es.}}{I_{es.}}\right] \qquad (20a)$$

equation (20a) now gives us a mathematical relationship between the increase in radius for a given applied load in terms of the number of slots in the mandrel sleeve, the length of the mandrel sleeve and the internal and external dimensions of the sleeve (these are represented in terms of the second moments of area of the beam elements and end sections of the mandrel sleeve).

CHAPTER V

ANALYSIS AND DISCUSSION OF RESULTS

5.1 Comparison of Experimental and Predicted Results

5.1.1 Predictions based on the Assumptions of the First Hypothesis for the Linear Models

Equation 4-(7) has been derived from the assumption of the first hypothesis and gives the deflection of one beam element for a given load W,

$$y = \frac{Wl^3}{12EI} \qquad 4\text{-}(7)$$

for N beam elements the total extension ΔC is the sum of the individual element deflections and equation 4-(7) becomes

$$\Delta C = \frac{N.Wl^3}{12EI} \qquad 5\text{-}(1)$$

Typical calculation of predicted extension for linear model 1

$I = .132 \times 10^{-9} m^4$ $\qquad N = 4$

$l = 31.46 \times 10^{-3} m$ $\qquad W = 500N$

$E = 207 \times 10^9$ N/m^2 (this value of Youngs Modulus is used throughout the following calculations, it is the accepted value for most steels).

substituting above in equation 5-(1)

$$\Delta C = \frac{4 \times 500 \times (31.46 \times 10^{-3})^3}{12 \times 207.9 \times 10^9 \times .1323 \times 10^{-9}}$$

$$= 189\ \mu m$$

Table 5.1 lists the predicted and experimental extensions for comparison.

Table 5.1

Linear Model	Load N	Predicted Extension μm	Experimental Extension μm	Maximum Error %
1	500	189	280	35
2	100	90	124	25
3	100	44	50	12

5.1.2 Prediction based upon the 2nd Hypothesis for the Linear Models

Equation 4-(20a) is the mathematical model of the mandrel sleeve based upon the assumptions of the second hypothesis.

$$2\pi\Delta r = \frac{W_A}{2\pi\tan(\theta+\phi)} \quad \frac{N.l.}{4E} \left[\frac{l^2}{3I} + \frac{L^* l_{es}}{I_{es}}\right] \qquad 4\text{-}(20a)$$

for the linear models equation 4-(20a) simplifies to the form of equation 4-(14a)

$$\Delta C = \frac{N.W.l.}{4C} \left[\frac{l^2}{3I} + \frac{L^* l_{es}}{I_{es}}\right] \qquad 4\text{-}(14a)$$

Where ΔC is now the total linear expansion

Figure 5.1., below, defines some of the symbols in equation 4-(14a) with respect to the linear models.

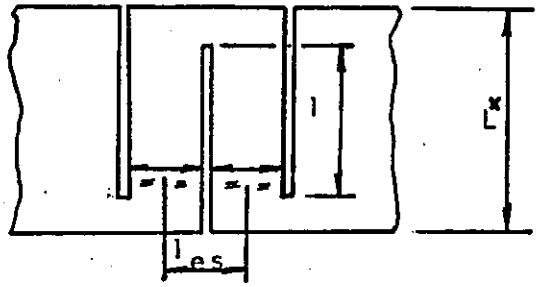

Figure 5.1

Typical calculation of predicted extension for linear model 2 note: the value of second moment of area for each end section of a linear model with the mandrel profile, is not the same. It can be shown, that by using the average of the two values, the same predicted result is obtained to that found by the use of an expanded form of equation 4-(14a) which includes separate terms for each end section.

The average value was therefore used.

$I_{es_1} = .135 \times 10^{9} m^4$ $\quad N = 4$

$I_{es_2} = .179 \times 10^{-9} m^4$ $\quad E = 207 \times 10^{9}\ N/m^2$

$I = 34.8 \times 10^{-12} m^4$ $\quad W = 100N$

$l_{es} = 6.16 \times 10^{-3} m$ $\quad I_{es} = \dfrac{I_{es_1} + I_{es_2}}{2}$

$l = 26.98 \times 10^{-3} m$ $\quad = \dfrac{(.135 + .179) \times 10^{-9}}{2}$

$= .157 \times 10^{-9} m^4$

$$\Delta C = \frac{4 \times 100 \times 26.98 \times 10^{-3}}{4 \times 207 \times 10^{9}} \left[\frac{(26.98 \times 10^{-3})^2}{3 \times 34.8 \times 10^{-12}} + \frac{42.86 \times 10^{-3} \times 6.16 \times 10^{-3}}{.157 \times 10^{-9}} \right]$$

$= 112.7\ \mu m$

Table 5.2 lists the predicted and experimental extensions for comparison

Table 5.2.

Linear Model	Load N	Predicted Extension μm	Experimental Extension μm	Maximum Error %
1	500	280	268	8
2	100	112.7	122	9
3	500	266	246	8

5.1.3 Assesment of Predictions for the Linear Models

Two mathematical models for the prediction of the extension of the linear models have been examined. The first model developed from the first hypothesis of mandrel sleeve deformation is not valid for any situation except where the

second moment of area of the beam element is considerably less than that of the end section, the maximum percentage error between predicted and experimental results was 35%. The second model derived from the assumption of the second hypothesis, is valid for all the linear models to which it was applied. Preductions being within experimental accuracy with a maximum error of 8% in the case of linear model 2.

The mathematical model of the linear model expressed by equation 4-(14a) has been shown to give solutions which correlate with the performance of the linear model, and based upon these findings the indications are that when applied to the mandrel sleeves a similar correlation will be obtained.

5.1.4 Prediction for the Mandrel Sleeves

The prediction of increase in radius for a given applied load is given by equation 4-(20a)

$$2\pi\Delta r = \frac{W_A}{2\pi\tan(\theta+\phi)} \cdot \frac{N.l.}{4E} \left[\frac{l^2}{3I} + \frac{L^* l_{es}}{I_{es}}\right] \qquad 4\text{-}(20a)$$

Note: The rules for determining the magnitude of several of the parameters specified in equation 4-(20a) are given below. The end section length: This the length of arc between the centre line of the beam elements taken on the mid-distance centre line between the inner and outer diameters of the end section as shown in figure 5.2 below.

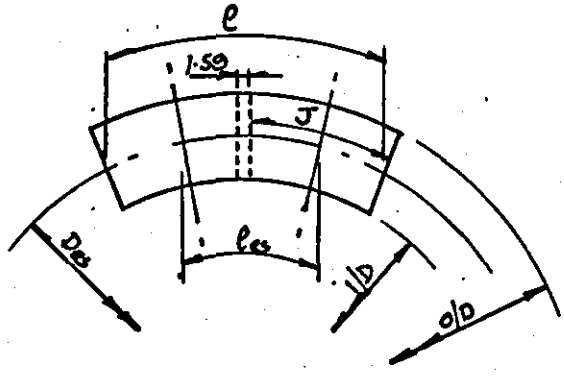

Figure. 5.2

$$D_{es} = \frac{\text{outside diameter} - \text{inside diameter}}{2}$$

For N slots the length of arc of end section at diameter D_{es} is

$$l = \frac{\pi . D_{es} - 1.59N}{N}$$

and $$J = \frac{l - 1.59N}{2}$$

$$l_{es} = J + 1.59$$

The second moment of area of the end sections : This is to be taken as the second moment of area about the axis X-X of the projected areas shown below in figure 5.3.

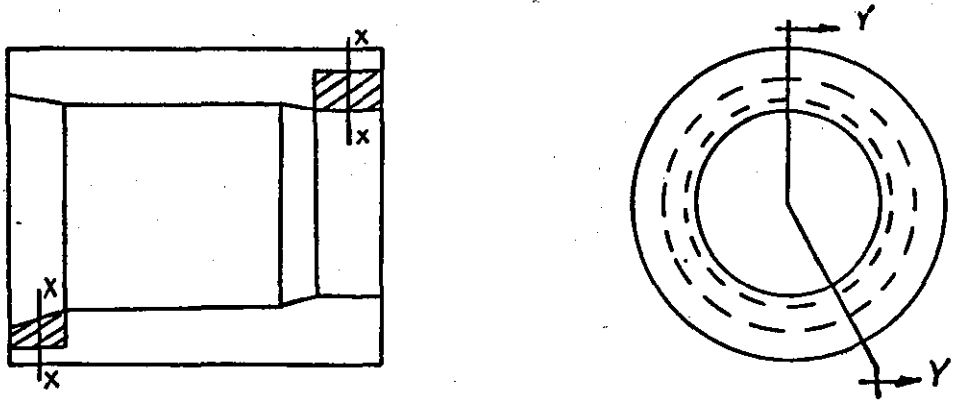

Figure 5.3

The second moment of area of the beam elements : The beam element in cross section is as shown in figure 5.4(a). below.

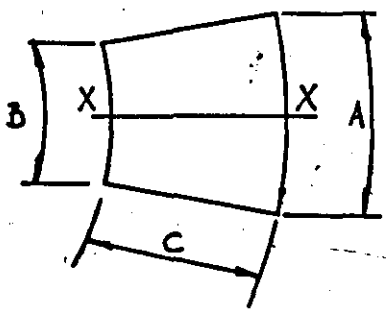

Figure. 5.4(a)

For the purpose of establishing the second moment of area about the axis X-X the segment is to be considered as a trapezium as shown in figure 5.4(b).

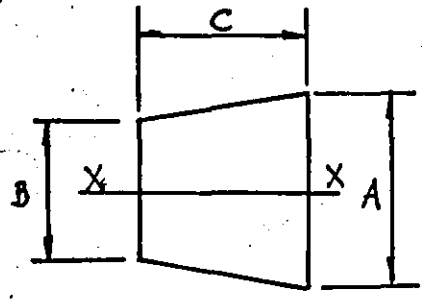

Figure 5.4(b)

It is important when calculating the predicted extensions to use the actual dimensions of the mandrel sleeves. Figure 5.5, gives the dimensions taken by measurement from the mandrel sleeves used in this investigation and is a supplement to the table given on figure 2.2., which gives the nominal (manufacturers) dimensions. Table 5.3. lists the values of the parameters for the mandrel sleeves.

Table 5.3.

Mandrel dia/length mm			N	I $m^4 \times 10^{-12}$	L* mm	l_{es} mm	I_{es} $m^4 \times 10^{-12}$	l mm
41.27	/	42.86	24	12.05	42.85	4.68	305	25.32
			20	29.26	42.62	5.61	249	26.36
			16	71.38	47.76	7.01	278	25.85
41.27	/	26.98	20	29.26	26.69	5.46	677	16.08
			16	71.38	26.21	7.01	595	16.08
50.80	/	42.86	24	40.01	43.01	4.68	305	25.80
			20	101	42.55	5.61	250	26.29
			16	238	42.64	7.01	296	25.43
50.80	/	26.98	24	40.01	27.05	4.68	689	16.43
			20	102	26.92	5.46	577	16.84
			16	238	76.79	7.01	768	16.08
60.32	/	42.86	24	94.90	43.98	4.68	203	26.98
			20	212	42.54	5.61	253	26.19
			16	560	42.67	7.01	300	25.63
60.32	/	20.98	20	246	26.95	5.46	639	16.61
			16	560	27.03	7.01	655	16.56

Typical calculation of predicted result for 41.27/42.86 12 slot mandrel

$$2\times\pi\times127\times10^{-6} = \frac{W_A}{2\times\pi\times.3249} \times \frac{24\times25.32\times10^{-3}}{4\times207\times10^{9}} \left[\frac{(25.32\times10^{-3})^2}{3\times12.05\times10^{-12}} + \frac{(42.62\times4.675)\times10^{-3}}{305\times10^{-12}} \right.$$

W_A = 119.5N

Table 5.4. lists the predicted and experimental extensions for the mandrel sleeves.

Table 5.4.

Experimental and Predicted Loads to produce an increase in radius of 127 um.

Mandrel dia/length mm / mm	N/2	Predicted Load N	Experimental Load N	$\theta+\phi$ degrees	μ
41.27 / 42.86	12	119.5	137	20.40	.047
	10	282.7	346	21.66	.073
	8	734.4	905	21.80	.075
41.27 / 26.98	10	815.5	975	21.23	.064
	8	1155	1465	22.39	.074
50.80 / 42.86	12	255	332	22.92	.098
	10	756	975	22.73	.094
	8	1604	2040	22.45	.088
50.80 / 26.98	10	1140	1425	22.10	.081
	8	1672	2235	23.40	.108
60.32 / 42.86	12	570	725	22.45	.088
	10	1187	1240	18.74	.015
	8	2018	2660	23.18	.103
60.32 / 26.98	10	1419	1820	22.62	.092
	8	1646	2020	21.74	.074

5.1.5 Assessment of the Prediction for Mandrel Sleeves

The mathematical model derived from the second hypothesis has been applied to sixteen mandrel sleeves and found to be valid for the prediction of extension. The predicted extensions are found to be lower than those obtained by experiment when a value of coefficient of friction of zero (μ=0) is used.

The average value of coefficient of friction required to raise the predicted values to the experimental values is .075, (the coefficients varied from .015 to .108 and had an

average value of .078 with a standard deviation of .021). Meek (65) gives the coefficient of friction between lubricated hard steel surfaces as ranging from .052 to .110. The figure of .075 is approximately in the middle of this range and indicates that it is of the right order for use in calculating the stiffness.

When applied with an appropriate value of coefficient of friction the mathematical model expressed by equation 4-(20a) has been shown to give solutions which correlate with the experimental performance of the mandrel sleeves.

5.2 Further Measurements of Mandrel System Action

Analysis of the results of the measurements to establish the variation in expansion down the length of the mandrel sleeves, Tables 8.37 -8.42, show that in the free state the mandrel expands uniformly down the length. For the six sleeves tested the maximum variation between the top and bottom diameters of the sleeve was 2.5 um. The distribution of load between the two conical tapers measurements, presented in Tables 8.43 - 8.48, indicate that the load is transmitted from the sleeve to the arbor equally across the contact areas on the two tapers. Although the loads applied produced small strains in the arbor the measurements at the higher loads produced strain reading of sufficient accuracy.

The mandrel sleeves when examined in the absolute free state, i.e., not mounted on the arbor, are found to have contracted from the nominal working diameter and to have taken the form of a frustrum of a cone with the small diameter of the frustrum being the top of the mandrel sleeve. It is thought to take this form because the machining stresses in the sleeve deform the sleeve more easily at the end of the mandrel with the weakest end section, this allows the opposite end to contract by the greatest amount. When placed upon the arbor the sleeve requires a small load to bring it to its nominal and uniform diameter, it is likely that this is not shared equally between the two tapers. This could not be confirmed by measurement as the load did not produce sufficient strain in the arbor to allow accurate readings. Once the sleeve reaches its nominal diameter the mandrel expands uniformly and the load is taken equally by the tapers, the indication being that the 'fit' between arbor and sleeve is very important and that for the mandrels tested this was so.

5.3. Analysis of Interface Pressure Results

Three separate but related sets of curves have been derived from the results of the interface pressure tests, Tables 8.53. to 8.64. The three sets of curves are,

1. Average contact pressure at interface/applied load, figures 3.22. to 3.26.
2. Total gripping load at interface/applied load to mandrel, figures 5.5. to 5.9.
3. Variation of contact pressure down the axial length of the mandrel sleeve, figures 5.10. to 5.21.

The average contact pressure/applied load curves, typically shown by figure 3.26, are found to be similar in form to the true stress-strain curve (tension and compression) of a ductile metal. The curves of contact pressure/load for the twelve mandrel sleeves tested all exhibit the same feature of firstly, rising with a constant $\Delta P/\Delta L$ (change in pressure for a given change of applied load) until a load in the region of .5 - 1.0KN has been applied, for a further increase in applied load of between .5 - 1.5KN the ratio $\Delta P/\Delta L$ falls rapidly until it again assumes an almost constant ratio as the curve continues in a linear manner.

It is well understood that some phenomenon takes place within a ductile metal upon application of an increasing tensile or compressive load, the phenomenon being strain-hardening, it is this strain-hardening which gives the true stress-strain curve its characteristic shape. It is believed therefore that some 'locking-up' mechanism, analogous to strain-hardening, is taking place within a mandrel sleeve when subjected to loading to hold a workpiece. The possible mechanism and causes of this 'locking-up' are discussed at the end of this chapter. It is interesting

to note however, that the true stress strain curves often follow the empirical relation ,

$$\text{stress} = K(\text{strain})^n \qquad 5\text{-}(2)$$

Where K is a constant for the material and n is the 'strain-hardening exponent'. Application of the empirical relationship to the loading of the mandrel sleeves, with the empirical relationship now in the form,

$$\text{contact pressure} = K(\text{applied load})^n \qquad 5\text{-}(3)$$

Where K is some constant and n the 'locking-up exponent', gives the following values for n,

Mandrel dia. x length (mm.)	n
60.32 x 26.98	.83
60.32 x 42.86	.76
50.00 x 42.86	.68
41.26 x 26.98	.57

Table 5.5

As is shown in Table 5. 5. exponent n is the lowest, .57, for the smallest diameter, whilst the largest has an average value of approximately .8 and the 50.00mm. diameter having a value of .68.

No definite indications as to the effect that the number of slots contained within a mandrel sleeve have upon the contact pressure at the interface are apparent from the results presented in figures 3.22. to 3.25. A comparison of the curves show that for the 60.32, 50.00, and 41.26mm. diameter mandrel sleeves the 10,8 and 12 slot mandrels respectively gave the highest contact pressures. The variation in contact pressure for a mandrel of similar diameter and length but with varying number of slots was shown to be a maximum for the 60.32mm. diameter 42.86mm. long

sleeve where a variation in contact pressure of 1.6MN/m^2 (some 15% of the average contact pressure) was obtained between the 10 slot (highest), and the 12 slot (lowest) mandrel sleeves. The average variation for the twelve mandrel sleeves being 4.5% of the average contact pressure.

As one would expect, an increase in length of a mandrel sleeve has the effect of reducing the contact pressure. Figures 3.24. and 3.25. demonstrate that for a mandrel sleeve of 60.32mm. diameter a higher contact pressure is to be found with sleeves that are shorter in length. The 26.98mm. long mandrel sleeves having a contact pressure some 100% greater than the 42.86mm. long sleeve at an applied load of 4.0KN.

Variation in contact pressure with respect to the diameter of the mandrel sleeve is shown by the results to infer that for mandrels of the same length, the larger the diameter, the higher the contact pressure. Figure 5.9. summarizes the effect of diameter for the 8 slot mandrels, we can see that the only true comparison can be made between mandrels of similar length. With this constraint in mind it is apparent that for the 42.86mm. long sleeves the 60.32mm. diameter has produced contact pressures greater than those found in the 50.80mm. diameter sleeve. This situation again appears when comparing the 26.98mm. long sleeves where the 60.32mm. diameter is shown to have higher contact pressures than the 41.26mm.

The presentation of the results in the form of total gripping force at the interface/applied load, figures 5.5. to 5.9., produce some interesting facts and results in an empirical relationship which expresses the contact pressure in terms of the diameter of the mandrel and the applied load. The total gripping force is found by integrating the pressure over the area and is

expressed by,

$$\text{Gripping force} = \int_A P\,dA \qquad 5\text{-}(4)$$

It will be shown below that the pressure does vary down the length of the mandrel sleeve but that this variation is small and that the use of an arithmetic average value will give acceptable results when calculating the gripping force. We can use therefore the simple relation

$$\text{Gripping force} = \text{average pressure} \times \text{area of contact} \qquad 5\text{-}(5)$$

The shape of the curves of total gripping load/applied load are of course, similar to the average contact pressure/applied load curves, the former being derived from the product of average contact pressure x surface area of mandrel. This has not altered the exponent n, in equation 5-(3), but has only altered the value of the constant K.

Figures 5.5. to 5.9. demonstrate that generally for the range of loading considered the gripping force increases as the number of slots in the mandrel sleeve decreases. A small exception to the above is shown in figure 5.6 ., where over a small range of loading the 10 slot mandrel produced a greater total gripping force than that produced by the 8 slot mandrel. The range of loading over which this occurs is small and the difference in the magnitude of the two total gripping forces is small and it is therefore considered that this conforms to the general finding stated above.

Gripping force values with respect to the diameter of the mandrel, figure 5.9 ., show that for mandrel sleeves with equal number of slots, the larger the diameter of the mandrel sleeve, the greater the total gripping force produced, this is true over the whole range of loading. It appears also, from the similarity

of the gripping force curves for the 60.32mm. diameter 42.86 and 26.98mm.long sleeves that this is independent of mandrel length. Figure 5.9. shows the gripping force/applied force curves for the four mandrel sleeves with 8 slots, a similar result would be obtained however, with the mandrel sleeves with 10 and 12 slots. We can expand the above statement to say that the larger the diameter of the mandrel sleeve the greater the total gripping force whatever the length or number of slots the sleeve has.

One of the main points of the investigation is whether, and to what extent does the contact pressure vary along the axial length of the mandrel sleeve. The results presented in Figure 5.10. to 5.21. indicate that there is a variation in local magnitude of contact pressure down the length of the mandrel sleeve.

The curves show in all cases that there is a reduction at the ends and in the centre, from the maximum value of contact pressure attained. The characteristic shape of the curves, starting at the near end of the sleeve, is of a rise from the contact pressure at the boundary at the end of the mandrel/work-piece which must be zero, to a maximum, which is generally arrived at to the end of the first quarter of the axial length, a fall to a lower value then occurs mid-way along the length rising again to a value approximately equal to the first maximum, at the beginning of the third quarter, and finally falling again as the far end of the mandrel/workpiece is reached.

MacDonald and Meek (60) show the distribution of contact stress in a shrink-fit for both the shaft and ring, it is interesting to note that the form of the radial stress dist-ribution for the shaft has a similar form to the curves of

contact pressure for the mandrel sleeves.

The curves, figures 5.10. to 5.21. all show that there is some variation in measured contact pressure along the length, the actual variation ranges from 28% of nominal contact pressure at a load of approximately 3KN for the 50.00mm. diameter 42.86mm. long , 12 slot sleeve, to 2% of nominal contact pressure for the 60.32mm. diameter 42.86mm. long, 10 slot sleeve. The indication is that the larger the diameter the smaller the variation.

The divergence between distribution of stress on the shaft and ring at the interface of a 'shrink-fit' are generally thought,(60), to be due to a compressive stress in the shaft and a tensile stress in the ring. The expansion of an expanding mandrel to hold a workpiece must, by virtue of the beam elements between the two tapers having to carry a load of approximately half the applied load, be also under a compressive stress. It is possible therefore that the beam section, which in this particular instance is acting like a slender column section, is buckling slightly in an axial manner and causing the contact pressure between sleeve and workpiece to be reduced in the area of deflection. The ability of a beam to resist buckling can be shown to be proportional to

$$\frac{I}{L^2} \qquad 5\text{-}(6)$$

where I is the second moment of area of the transverse section, L is the length.

It is apparent then, that in order to resist buckling, high values of I and low values of L are required. It therefore follows that we would expect that the larger the diameter and the shorter the length of a mandrel sleeve, (i.e.,high I,

low L) the higher the resistance to buckling. Analysis of the results show that the variation in pressure is greatest for the 50.00mm. diameter, 42.86mm. long and the 41.26mm. diameter 26.98mm. long mandrel sleeves, also there is a larger variation in the 60.32mm. diameter 41.26mm. long compared with the 26.98mm. long sleeve. The indications are therefore that a small deformation due to buckling is taking place and thereby causing a reduction in contact pressure.

The curve A-B shown dotted on figure 5.9. is the theoretical gripping force/ applied load curve for mandrels of 100% efficiency i.e., with no losses (efficiency defined as total gripping force out/ applied load). It is immediately apparent that the efficiency of all the mandrels decreases as the applied load increases, the 41.26mm. diameter sleeve is shown to have the lowest overall efficiency of the four diameters of mandrels tested. The efficiency is shown to increase as the diameter of the mandrel increases. It is shown above that the curves of gripping force/ applied load can be represented by equation 5.3 , the exponent of this equation, n, can be taken as some measure of the 'locking-up' of the mandrel system, analogous to the 'strain-hardening' of ductile metals. What is actually happening within the mandrel system to cause this 'locking-up' has not been fully established, but the results indicate that the larger the diameter of mandrel sleeve the higher the value of n and, as is shown below, the discussion and explanations as to the possible causes of the 'locking-up' provide similar indications.

It has been shown above that the beam elements of the mandrel sleeves are subjected to a compressive axial load which may cause the beam elements to deflect and thereby reduce the contact pressure, other internal deformations within the

mandrel system could also be taking place, these actions are therefore a possible contributor to the 'locking-up' of the mandrel sleeve. A further possible contributor to the 'locking-up' is the increase in coefficient of friction due to the increase in contact pressure on the tapers of the mandrel sleeve and arbor, (66) shows that for a 100% increase in contact pressure an increase in coefficient of friction of some 30% can be expected, if the coefficient of friction of the mandrel system increases to this extent then this would be a major contributor to the 'locking-up' of the mandrel system. A further minor contributor is the load required to expand the mandrel sleeve from the initial contact diameter to the expanded diameter. The increase in diameter for an increase in internal pressure of $\cdot 8$ MN/m^2 in the 50.80mm. diameter ring used in the experimentation would cause an expansion of the bore of some 3 μm, this would require from figure 3.14. an applied load of 5 N.

5.2.2. Formulation from the Experimental Data of an Empirical Expression Relating Gripping Force to Applied Load.

It is sometimes useful to present data which an engineer uses in the from of idealized curves, this is particularly apparent in the theory of plasticity where the use of the idealized stress-strain curve, as shown in figure 5.22, enables the theory to be used more easily but still giving answers that are within engineering limitations. The presentation of the curves shown in figure 5.9. in idealized form enables an empirical expression to be formulated relating the applied load and diameter of the mandrel sleeve to the gripping force produced at the interface of mandrel and workpiece.

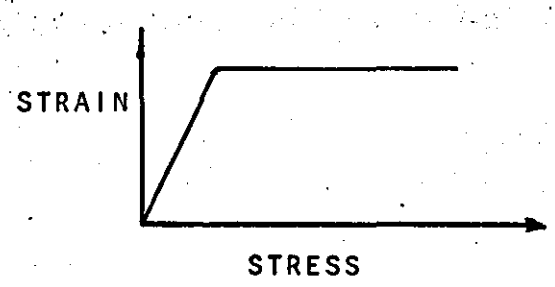

Figure 5.22

Figure 5.23. shows in idealized manner the gripping force/ applied load curves for each of the three diameters of mandrels. The curves are of the form of an initial linear section, A-B, which rises with a high value of slope to a turning point at B, the curve continues from B to C linearly but with a reduced value of slope.

Over the range of applied load $W \geq (4.125(D-41)^2+825)N$. (considered to be the working range for each mandrel) an approximation of the gripping force can be obtained from the following expression.

$$F_G=1600+10(D-41)^2+(.78+((D-41)^2.00112))(W-(4.125(D-41)^2+825))) \qquad 5\text{-}(7)$$

Where D is the diameter of the mandrel sleeve to the nearest millimetre.

Figure 5.24. gives a comparison of the gripping force predicted by the above expression and the experimental results for the 41.26mm. diameter, 26.98mm. long mandrels. The aim of the expression is to allow designers and production engineers to obtain a quick approximation of the gripping force knowing the diameter of the mandrel and applied load. Similar curves are obtained for the 60.32 and 50.80mm. diameter mandrels.

Figure 5.2 GRIPPING FORCE/APPLIED LOAD CURVE FOR 50.8/42.86 SLEEVES

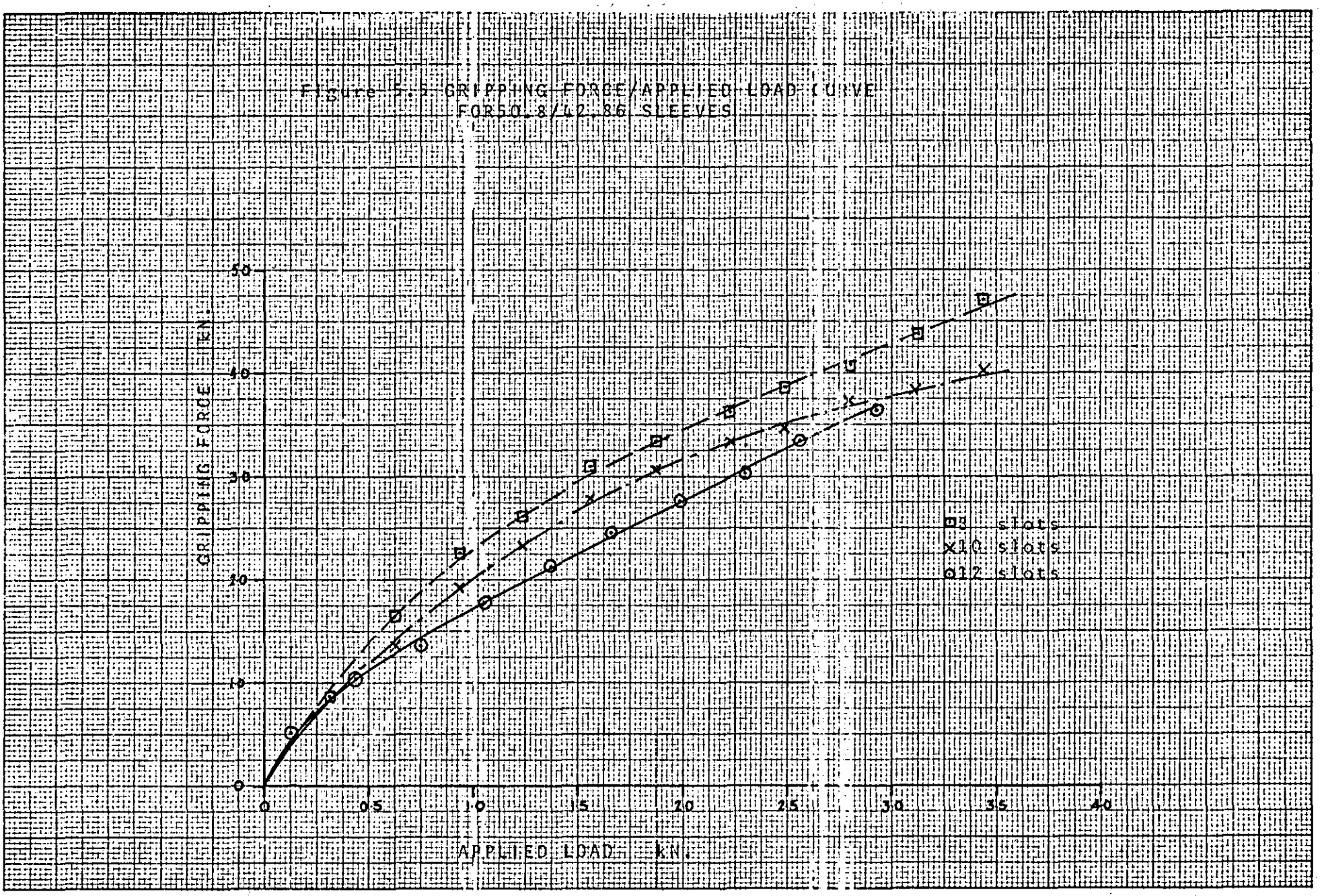

Figure 5.6. GRIPPING FORCE/APPLIED LOAD CURVE FOR 60.32/42.SC SLEEVES

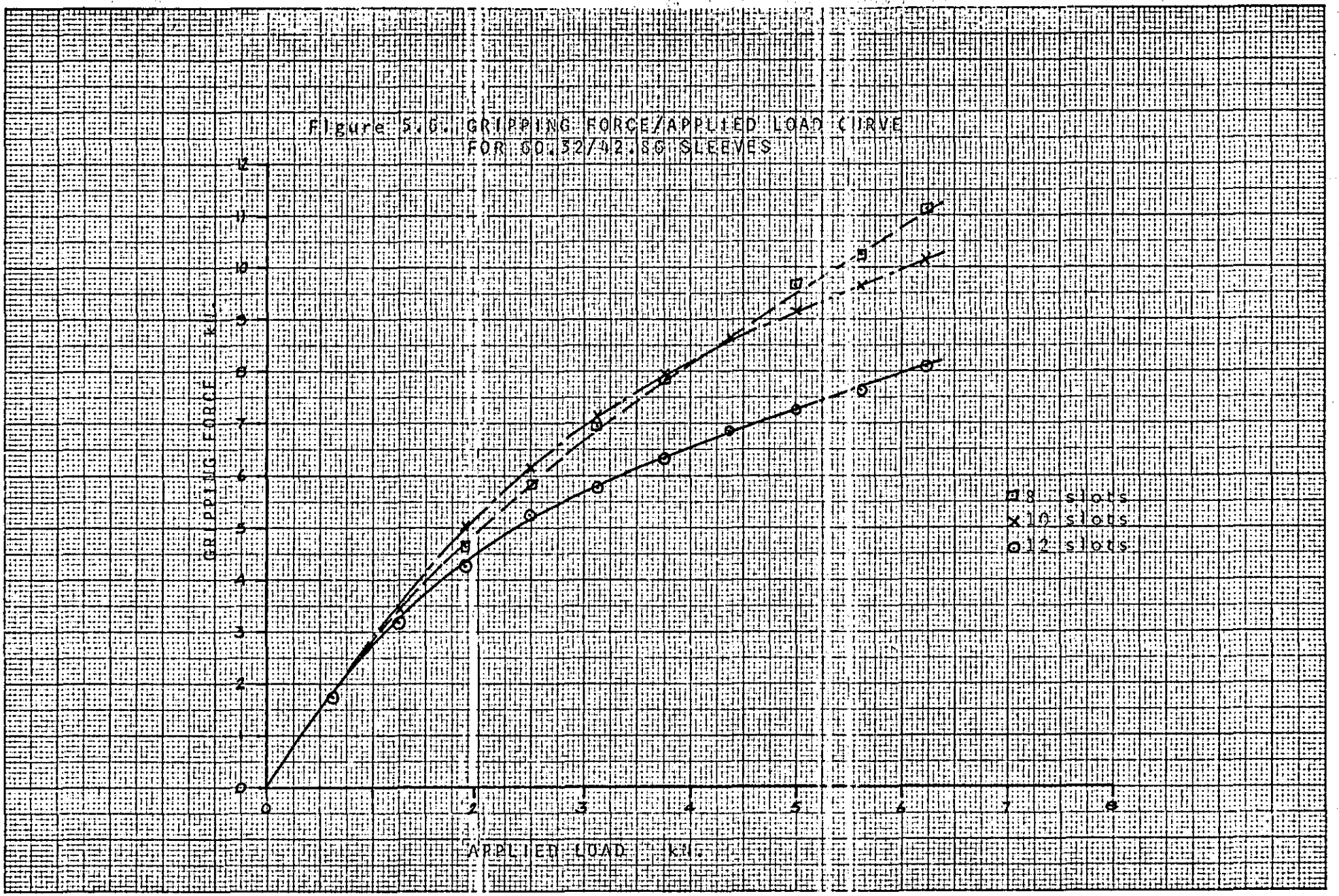

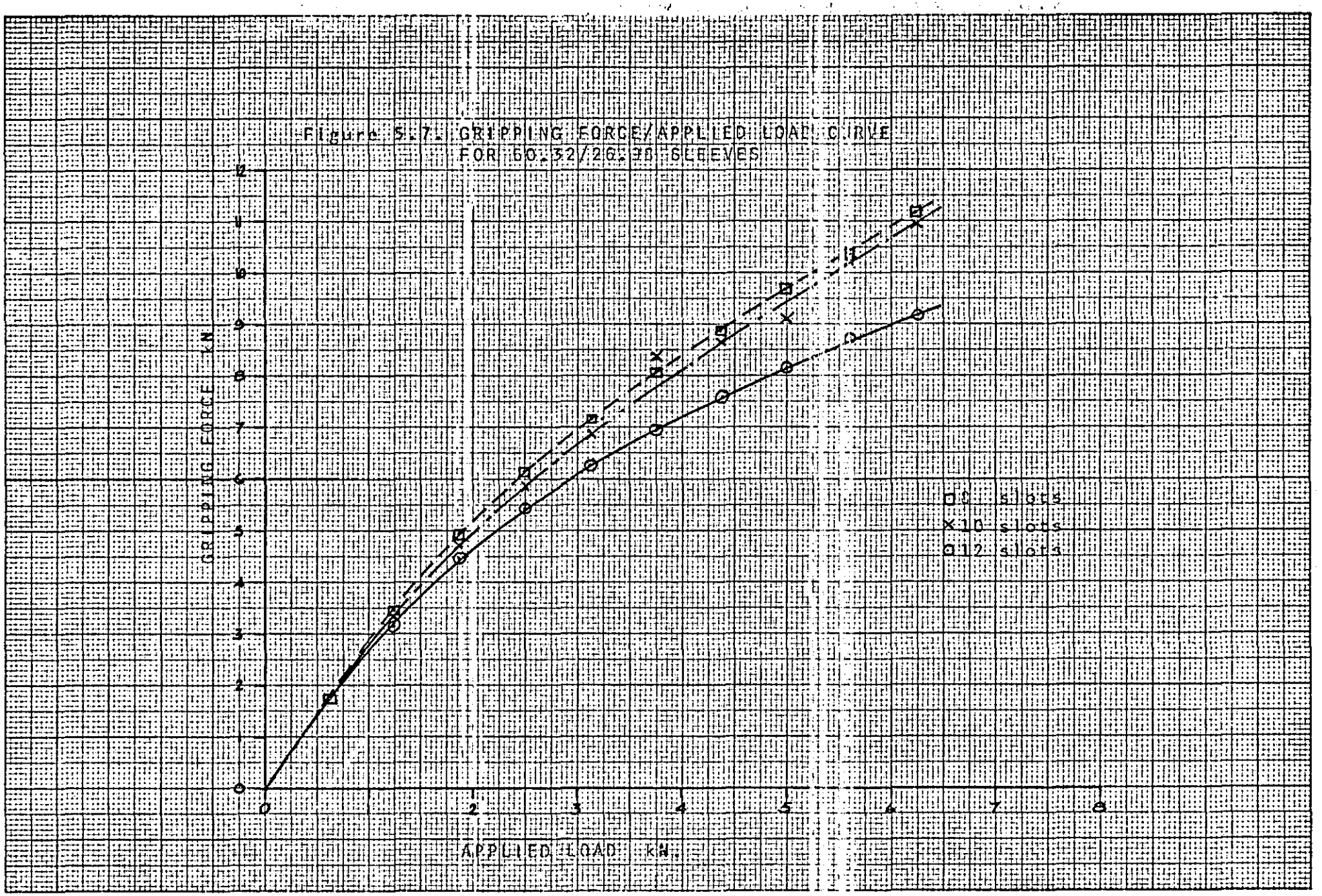

Figure 5.7. GRIPPING FORCE/APPLIED LOAD CURVE FOR 60.32/26.70 SLEEVES

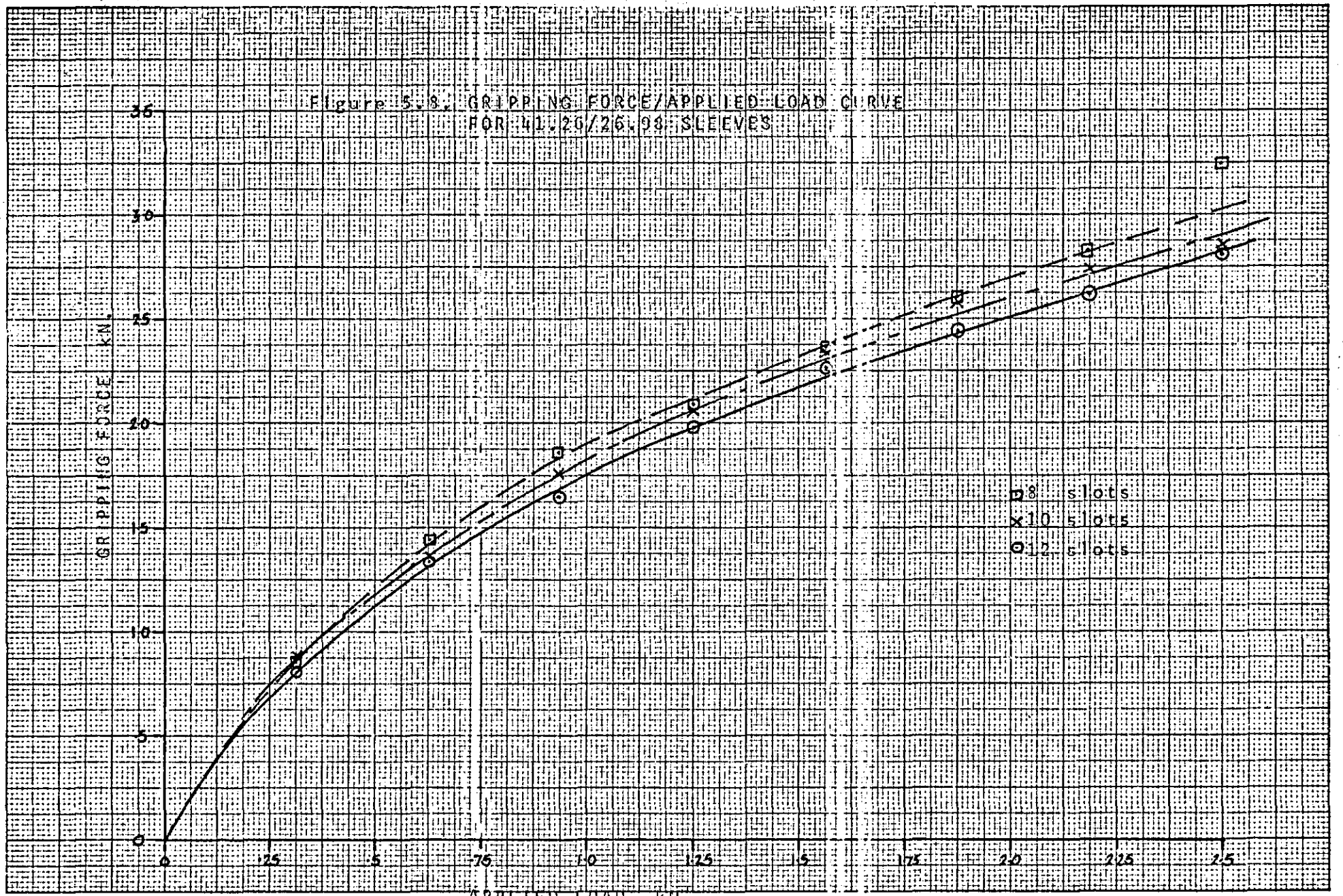

Figure 5.8. GRIPPING FORCE/APPLIED LOAD CURVE FOR 41.26/26.98 SLEEVES

Figure 5.9. COMPARISON OF GRIPPING FORCE/APPLIED LOAD FOR 8 SLOT SLEEVES

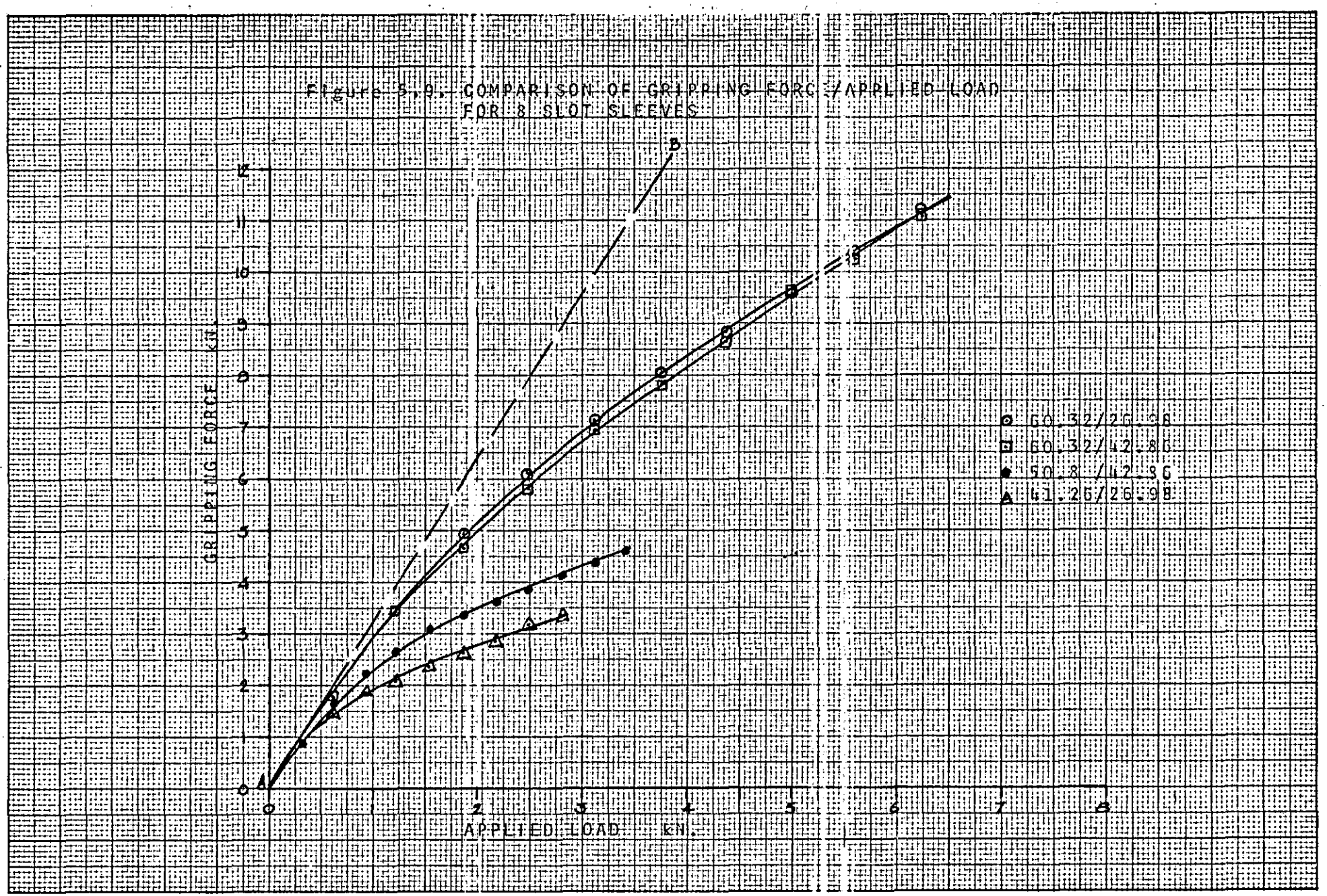

Figure 5.10. VARIATION OF CONTACT PRESSURE FOR 6D.32/42.86/12 SLEEVE

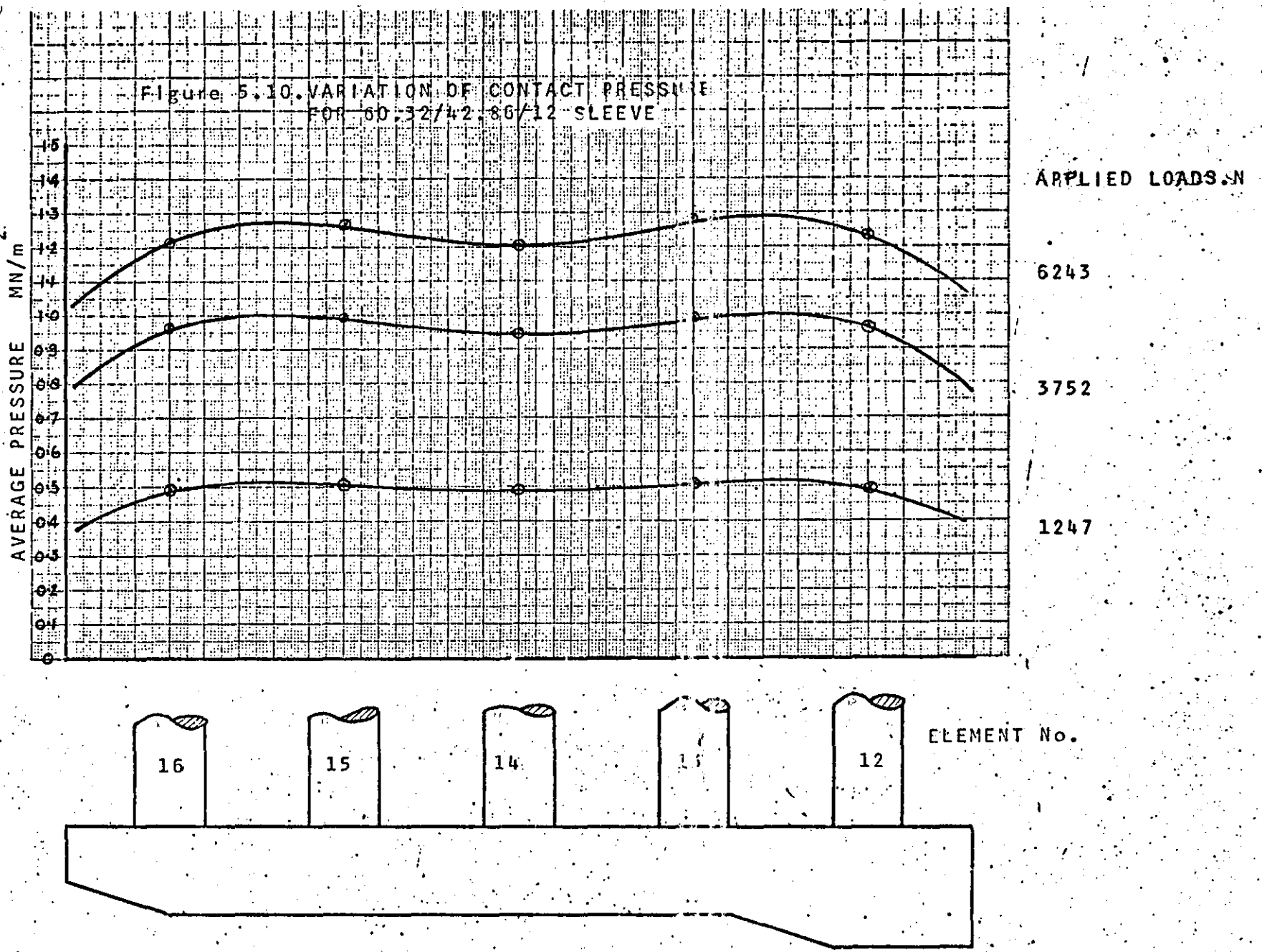

Figure 5.11. VARIATION IN CONTACT PRESSURE FOR 60.32/42.86/10 SLEEVE

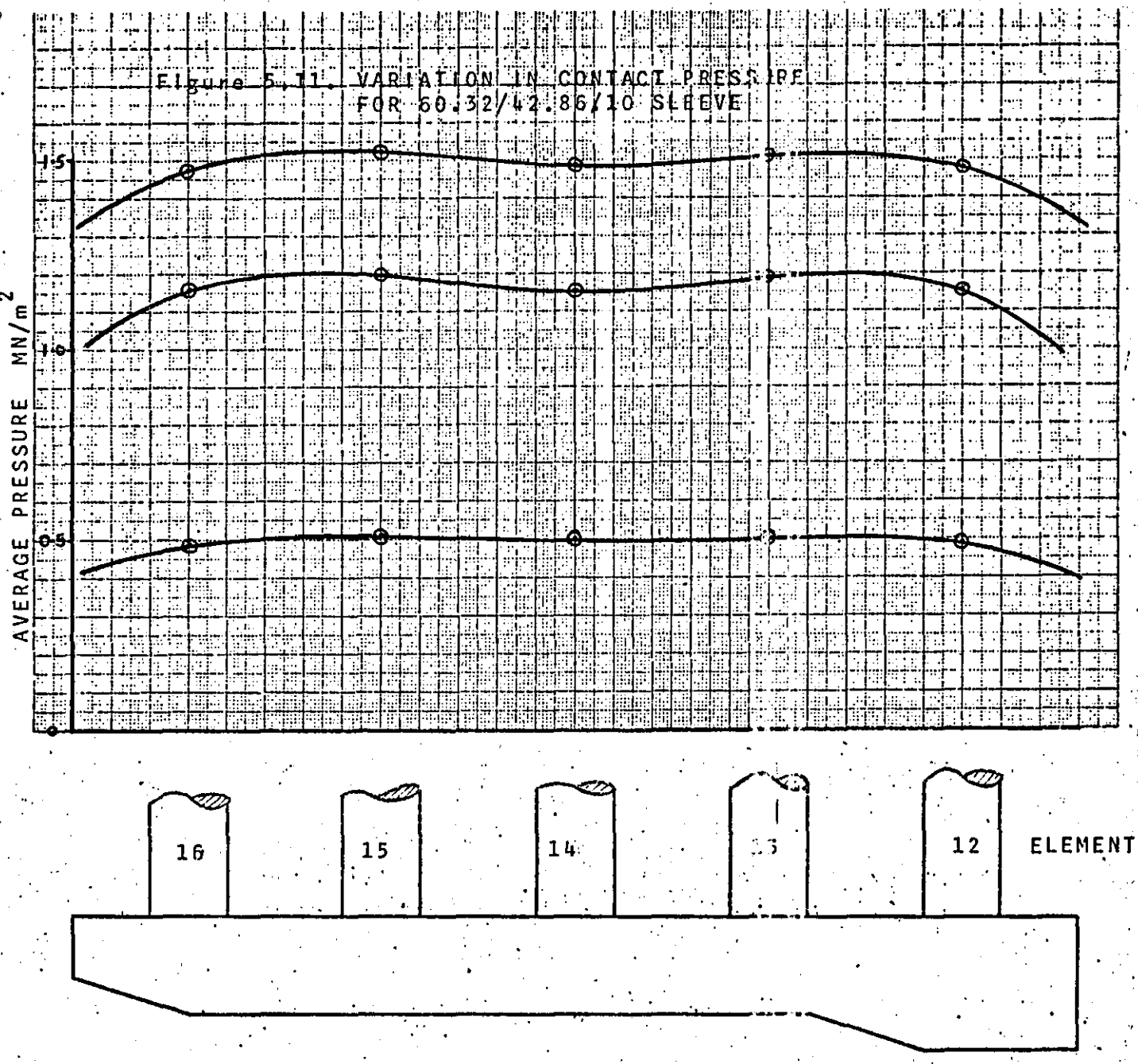

Figure 5.12. VARIATION IN CONTACT PRESSURE FOR 60.32/42.86/8 SLEEVE

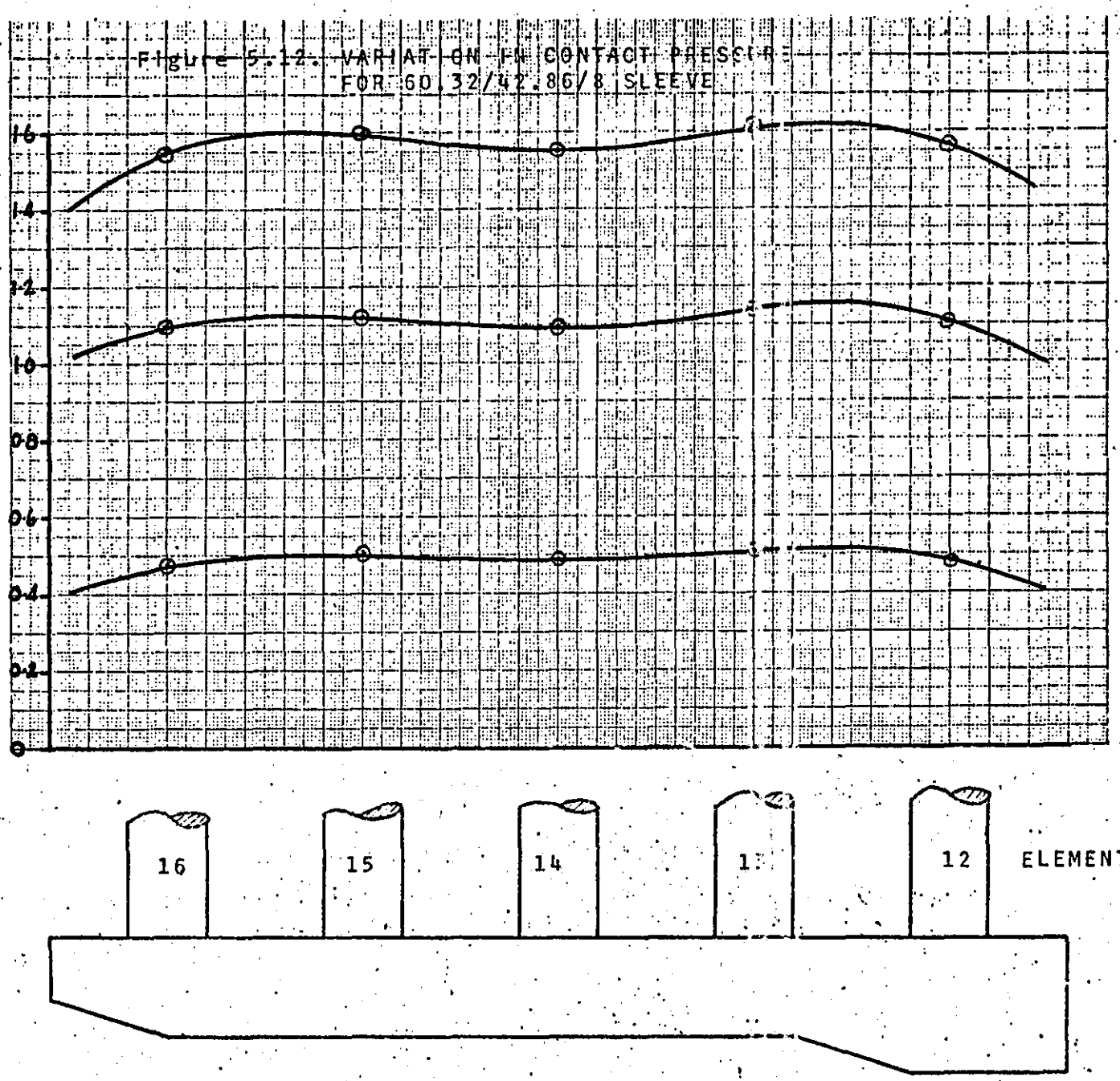

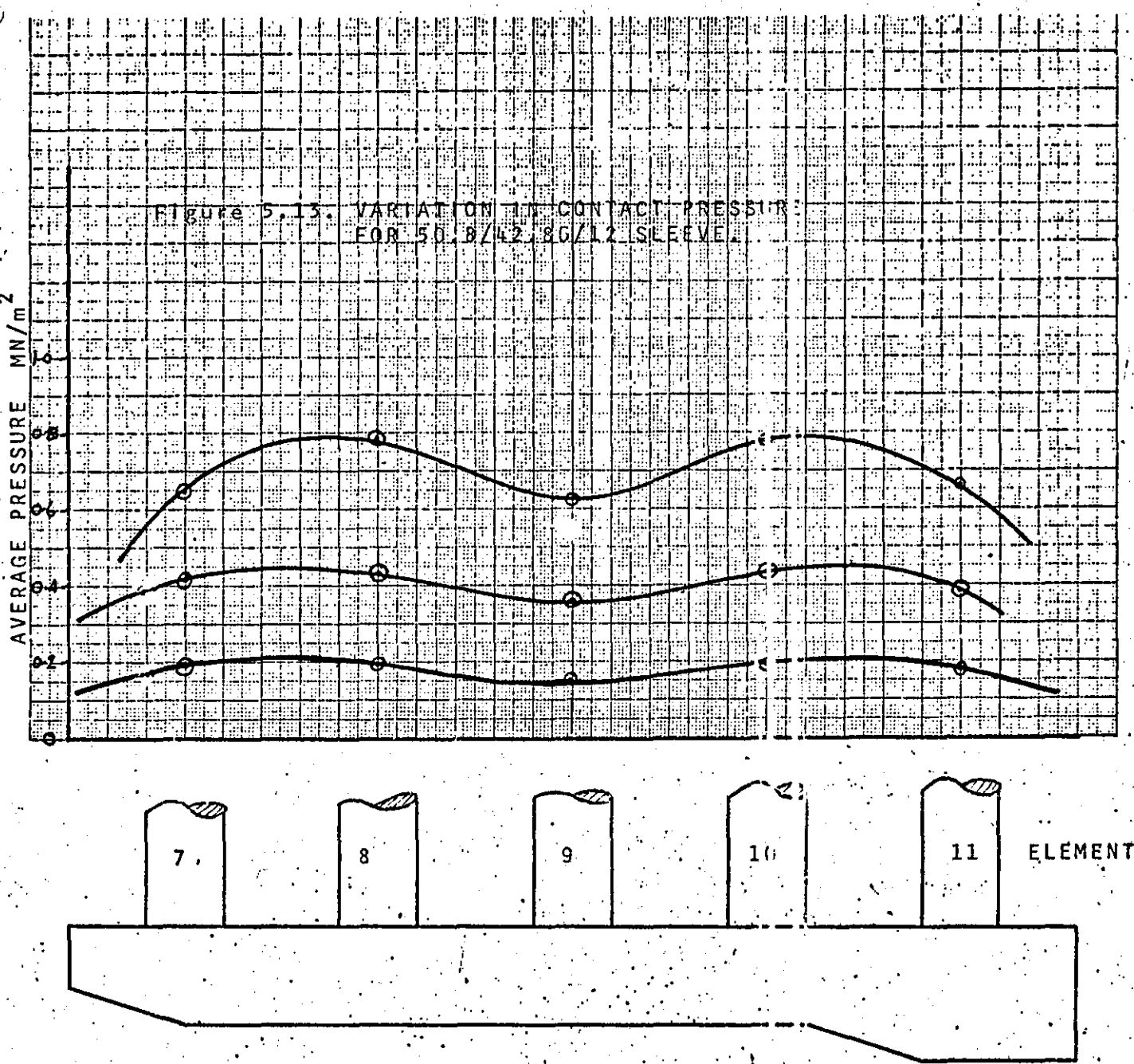

Figure 5.13. VARIATION IN CONTACT PRESSURE FOR 50.8/42.86/12 SLEEVE.

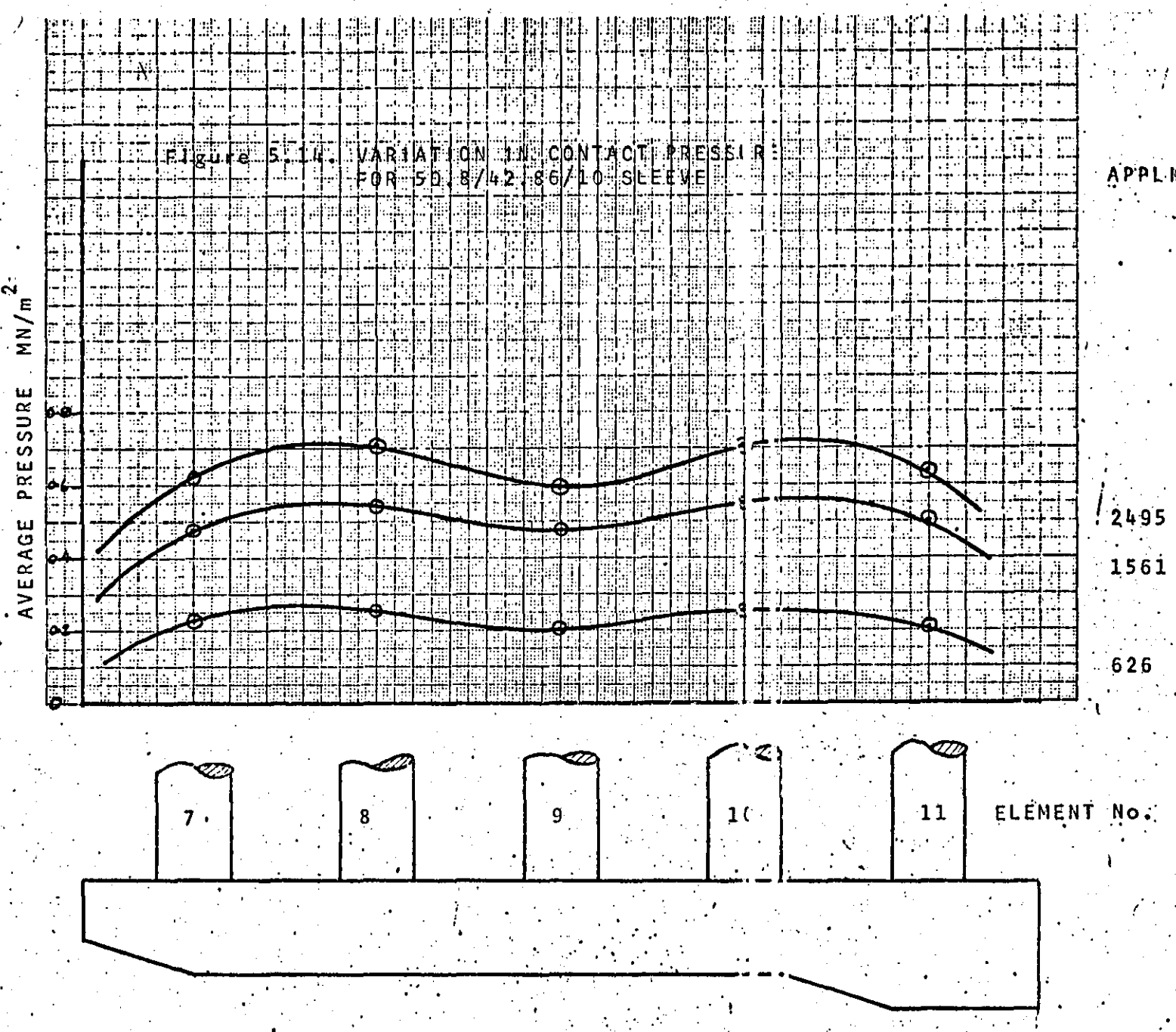
Figure 5.14. VARIATION IN CONTACT PRESSURE FOR 50.8/42.86/10 SLEEVE
AVERAGE PRESSURE MN/m²
APPLIED LOADS N.
2495
1561
626
7
8
9
10
11
ELEMENT No.

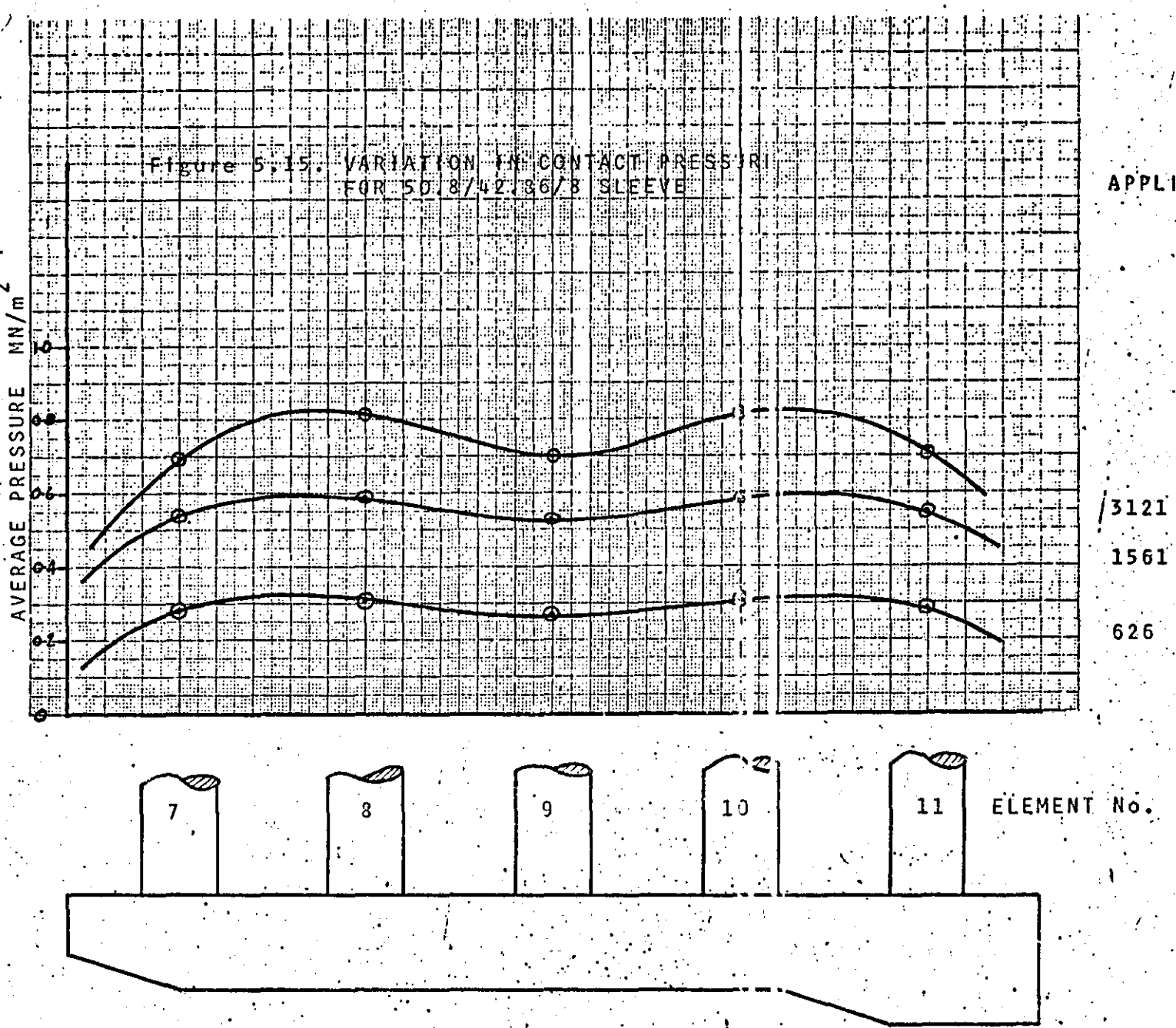

Figure 5.15. VARIATION IN CONTACT PRESSURE FOR 50.8/42.86/8 SLEEVE

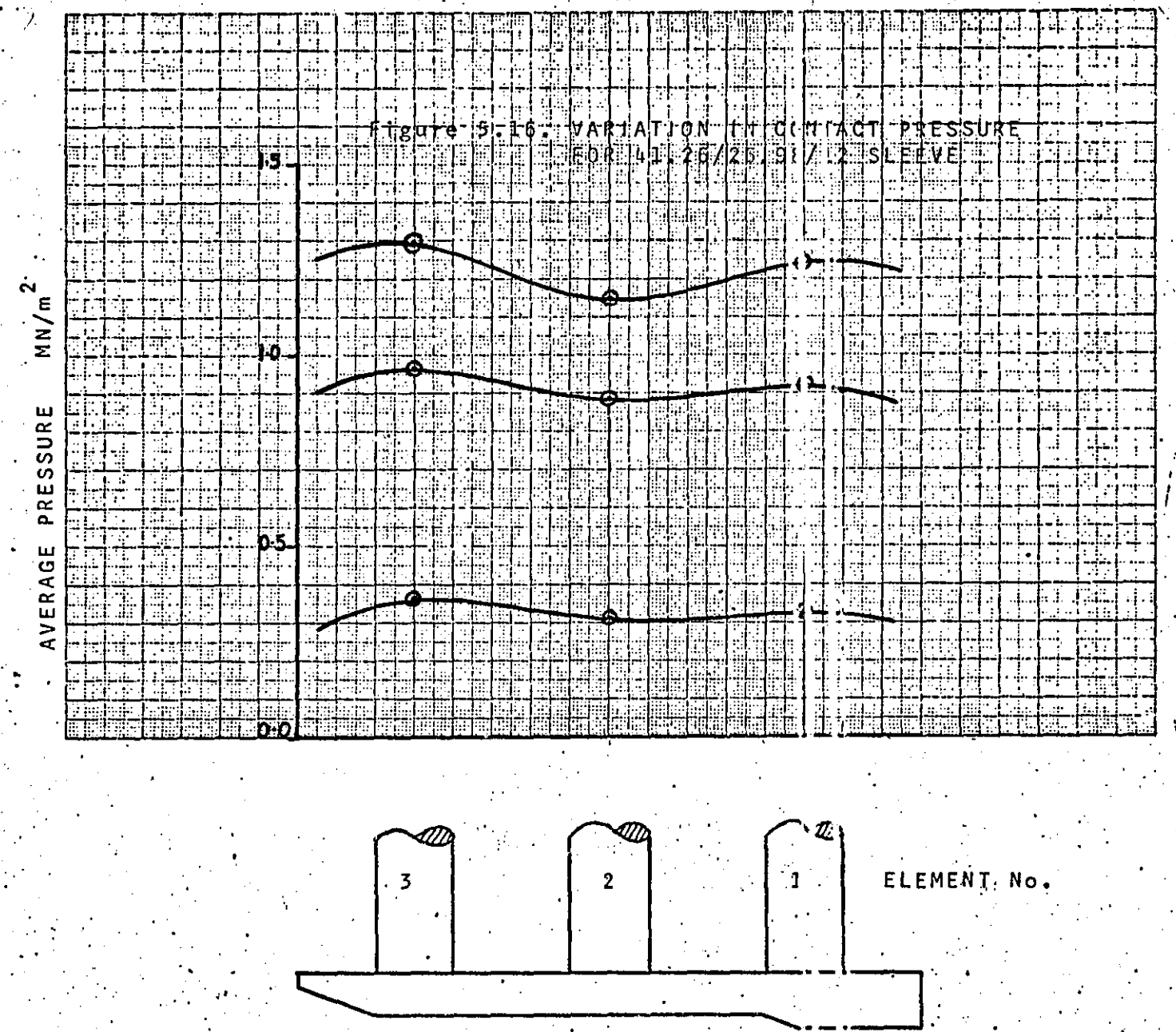

Figure 5.16. VARIATION IN CONTACT PRESSURE FOR 41.26/25.91/.2 SLEEVE

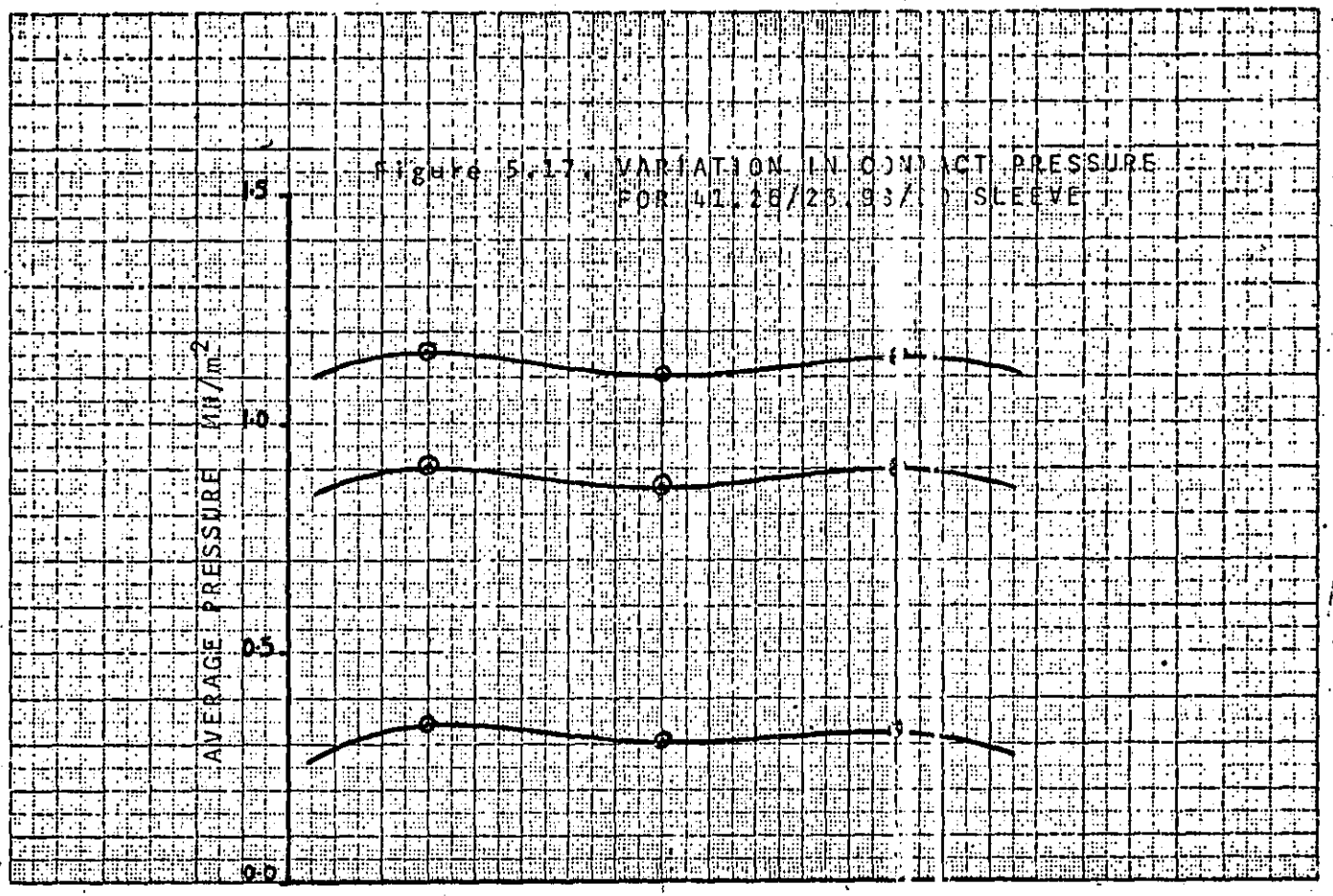

Figure 5.17. VARIATION IN CONTACT PRESSURE FOR 41.26/25.93/ SLEEVE

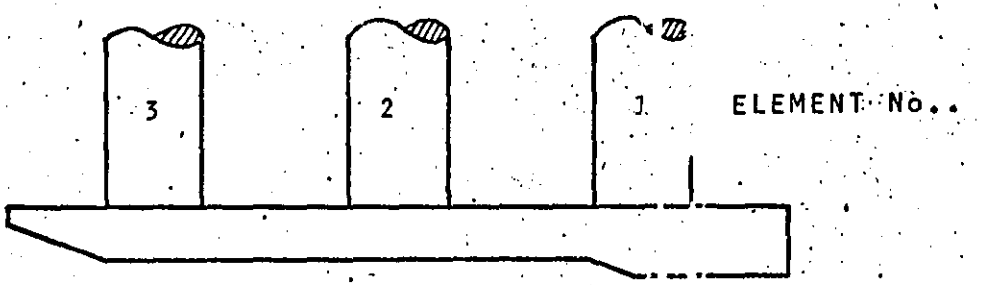

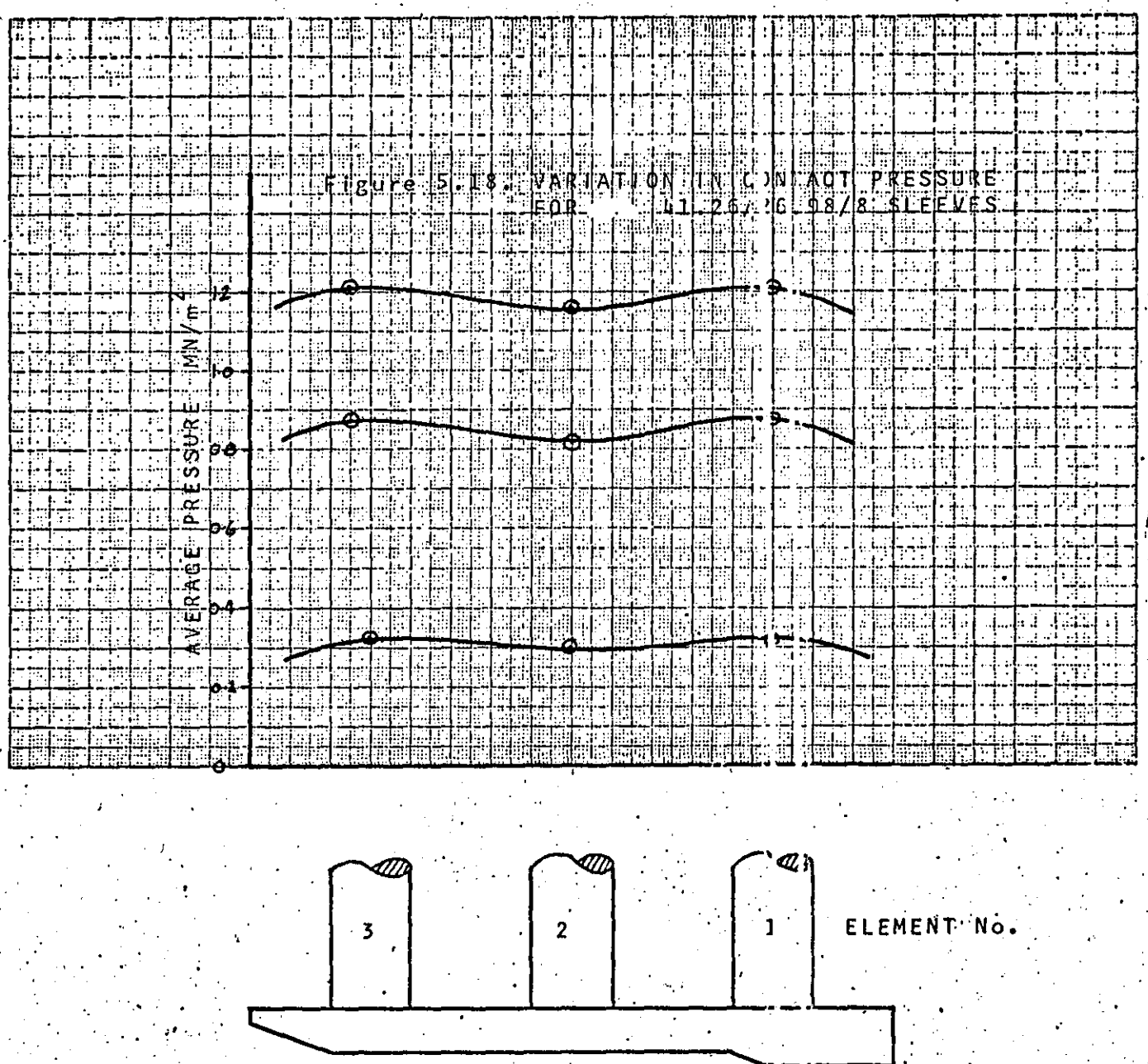

Figure 5.18. VARIATION IN CONTACT PRESSURE FOR 41.26/26.98/8 SLEEVES

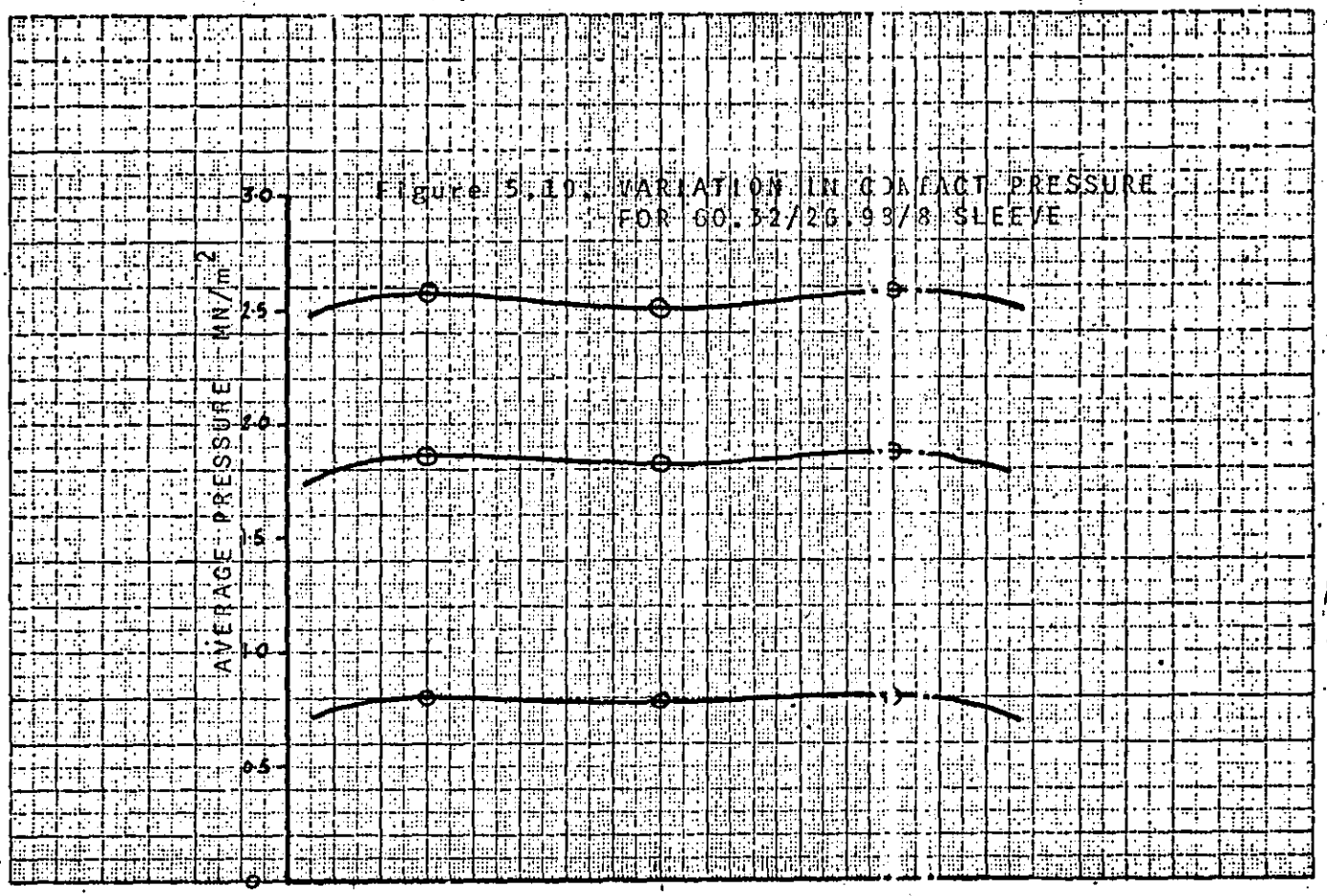

Figure 5.10. VARIATION IN CONTACT PRESSURE FOR 60.52/26.98/8 SLEEVE

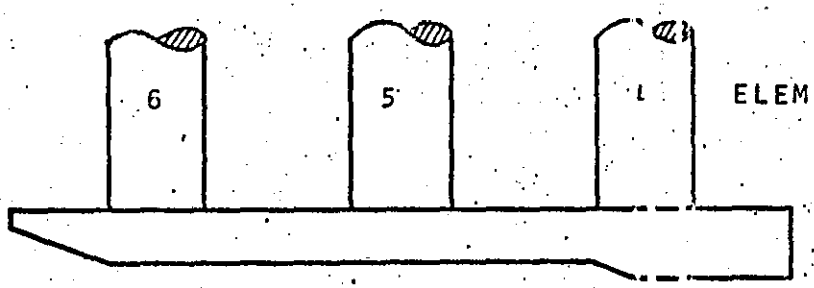

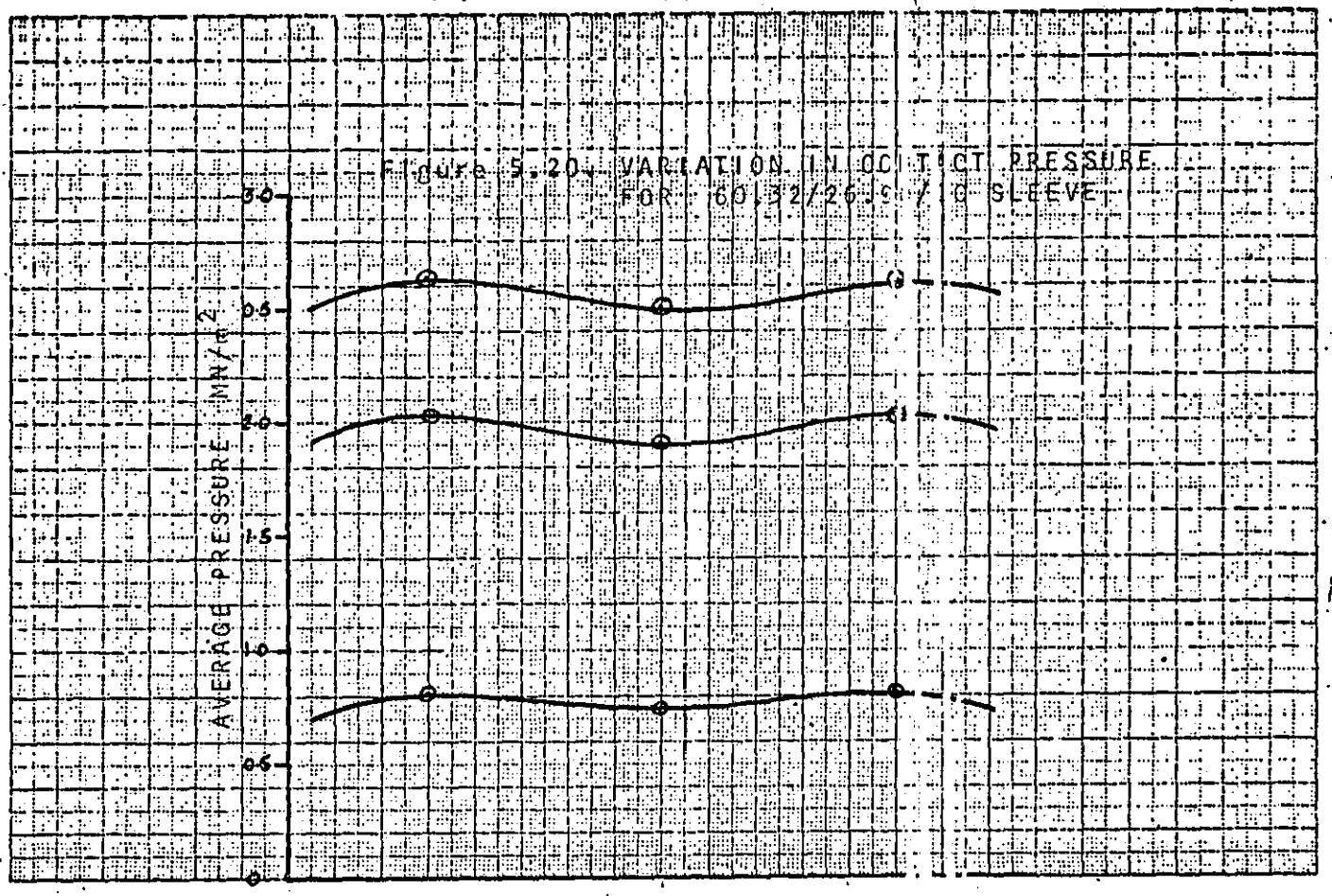
Figure 5.20 VARIATION IN CONTACT PRESSURE FOR 60/32/26 S/C SLEEVE
AVERAGE PRESSURE MN/m2
3.0
2.5
2.0
1.5
1.0
0.5
0
APPLIED LOADS N.
6243
3752
1247

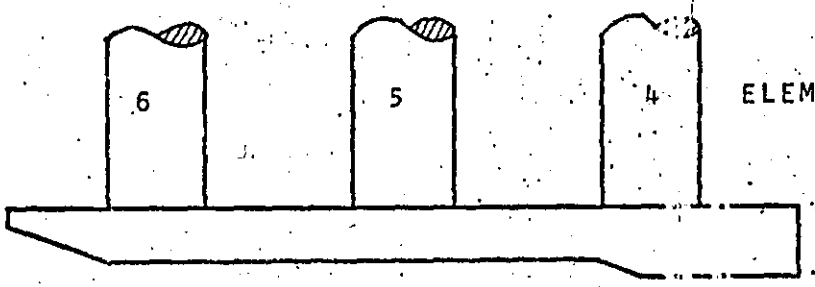
6
5
4
ELEMENT No.

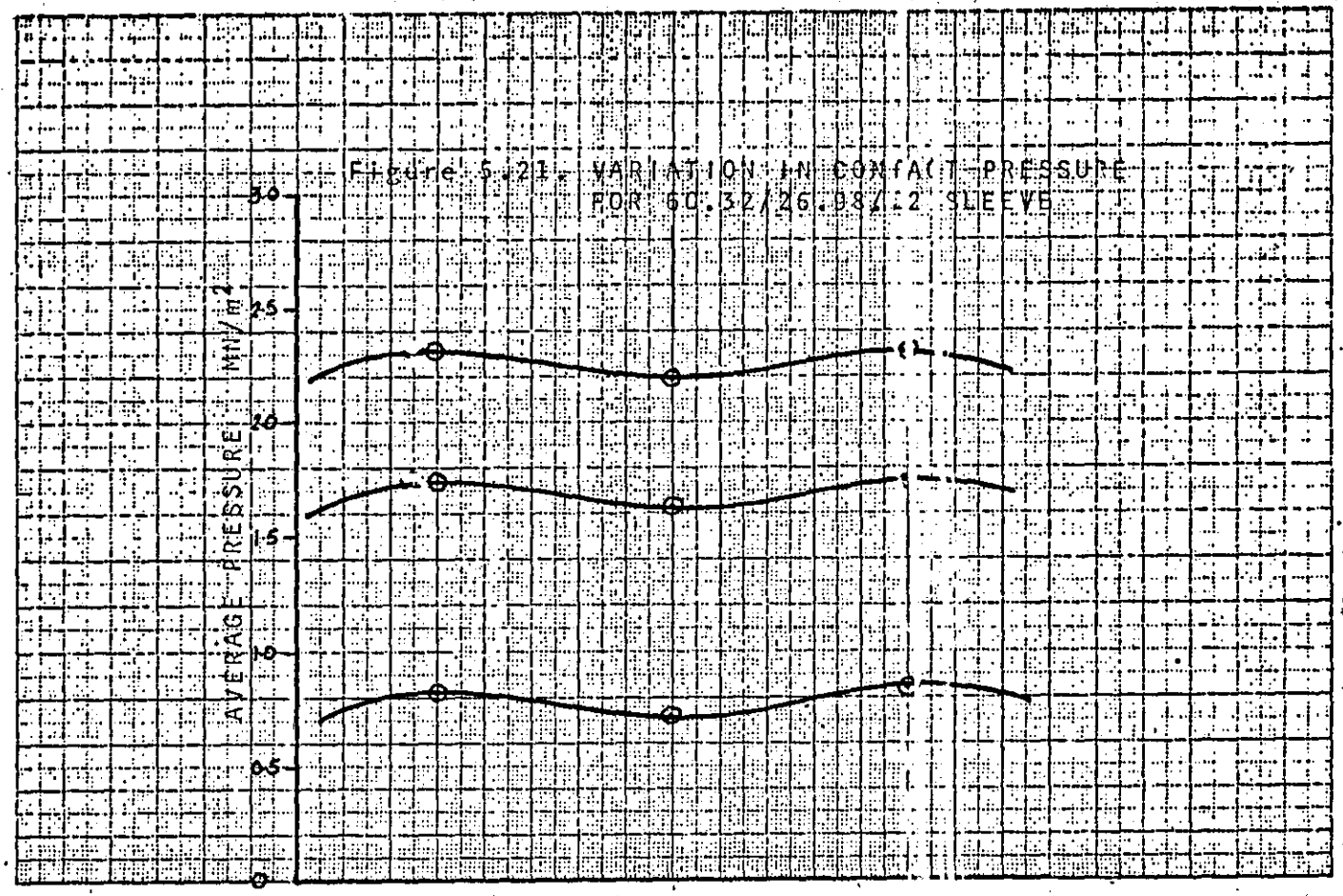

Figure 5.21 VARIATION IN CONTACT PRESSURE FOR 60.32/26.98/2 SLEEVE

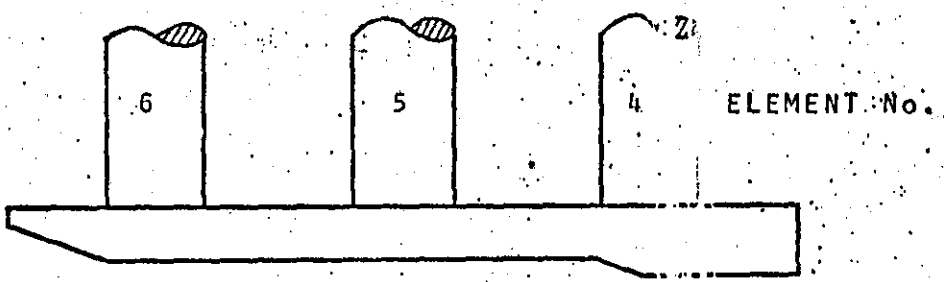

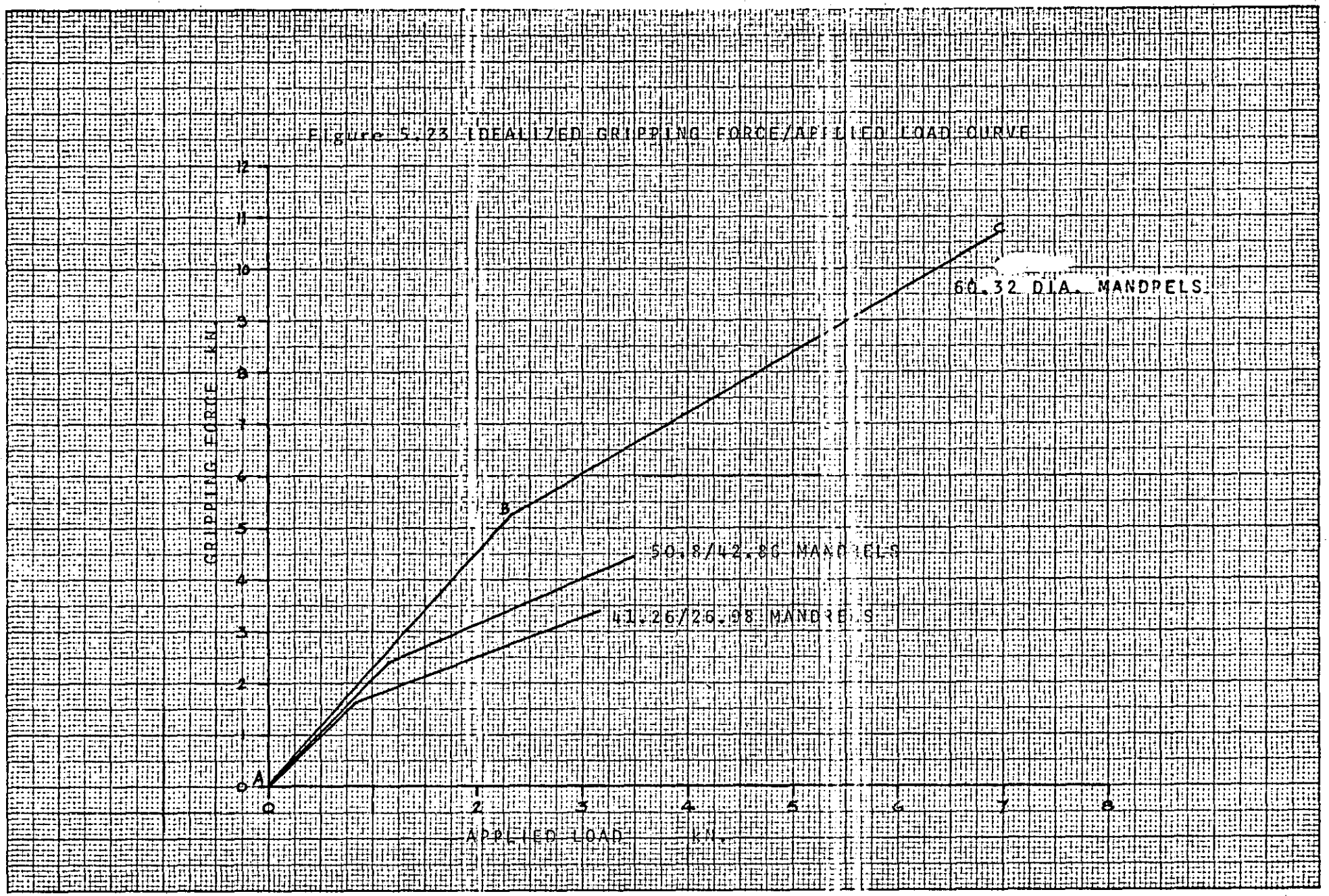

Figure 5.23 IDEALIZED GRIPPING FORCE/APPLIED LOAD CURVE

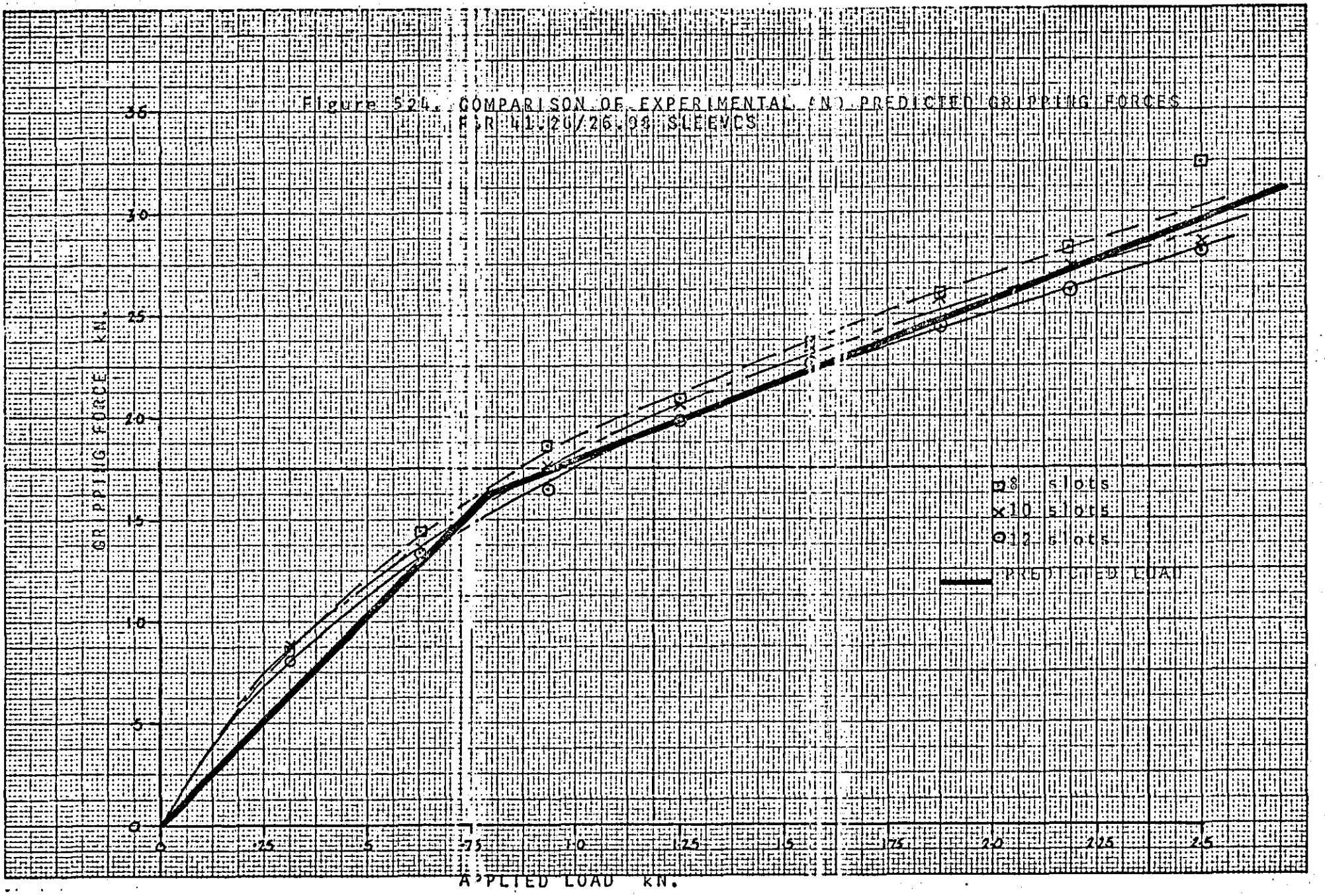

Figure 52. COMPARISON OF EXPERIMENTAL AND PREDICTED GRIPPING FORCES FOR 41.20/26.03 SLEEVES

CHAPTER VI

CONCLUSIONS AND SUGGESTIONS FOR FURTHER WORK

6. Conclusions and Suggestions for Further Work

6.1 Conclusions

1. The mandrel sleeve has been shown to behave elastically during unrestricted expansion. An expression has been formulated which relates the diametral expansion of the sleeve to the applied load. Close correlation has been achieved between predicted and experimental results.

2. The expression allows the relative importance of the design parameters, diameter, length, no. of slots, of the mandrel sleeve to be established in the design stage. The major factors in determining the stiffness of a mandrel sleeve are shown to be the size of the end section and the cross-section of the beam elements.

3. The mandrel has been shown to have uniform radial expansion down the length of the mandrel and the distribution of load between the two tapers is shown to be equal, within the limitations of the measuring system.

4. The contact pressure at the interface of mandrel sleeve/workpiece has been shown to vary down the axial length of the mandrel sleeve, the variation decreases as the diameter of the mandrel increases. Similarities between a 'shrink-fit' of a shaft and ring and an expanded-fit between the mandrel and workpiece have been established.

5. The magnitude of the contact pressure increases as the diameter of the mandrel increases, and decreases as the length of the mandrel increases. The effect on the contact pressure of the number of slots within the mandrel sleeve was inconclusive.

6. The gripping force produced by a mandrel system between the mandrel sleeve and workpiece is shown, for mandrels with the same number of slots, to be a function of the diameter of the mandrel sleeve only. The larger the diameter of sleeve the greater the output of gripping force for any given load. The gripping force for a given load is reduced as the number of slots in the mandrel sleeve increases.

7. An empirical linear expression has been derived from the experimental data which relates the gripping force produced by the mandrel system to the applied load and diameter of the mandrel sleeve. The expression is applicable over the working range of the mandrels and gives a fast approximation of the gripping force to the designer.

6.2. Suggestions for Further Work

The expanding mandrel system has not been subjected to any substantial amount of scientific investigation. This project has investigated one particular type of expanding mandrel, when in fact, there are several proprietary designs of mandrels on sale in the United Kingdom. A scientific assessment of the advantages and disadvantages of the different mandrels in use today would provide useful and needed knowledge. Further research is needed to determine an optimal angle(s) for the mandrel system. Is the continuous taper or saw section taper better than the parallel angle? This and other questions require investigation.

The research has dealt, in general, with the expansion of, and the gripping force produced by a mandrel sleeve. This work can now be extended to establish slipping torques of the workpieces on the mandrels by further experimentation, the results could then be correlated to the known values of gripping force and values of coefficient of friction established.

CHAPTER V11

REFERENCES

References:

1. R.H. Thornley and B. Wilson,
A Review of Some of the Aspects Involved in Chuck Design,
Production Engineer. Vol. 51, No.3, March 1972, pp. 87-91

2. H.J. Warnecke,
Operation Limits of 3-jaw Chucks in Respect to their Dynamic Stress,
4th International M.T.D.R. Conference, Sept. 1963.

3. G. Pahlitzsch and H.J. Warnecke,
Tests of Rigidity in Hand-operated Three-jaw Chucks,
Werkstatt and Betrieb, Vol. 94, No. 4, April 1961,
pp. 177-185.

4. A. Clegg,
The Design of Concentric Chucks,
Machinery (L), June 5 1919, pp. 277-281.

5. Anon.,
Universal Chuck Manufacture,
Machinery (L), April 10 1919.

6. R. Rigeswaren,
Design Requirements for 3-jaw Chucks,
Production Engineer, Vol. 52, No. 10, November 1973.

7. Wilson and Holt
Fundamentals of Tool Design,
McGraw Hill,
London. 1962.

8. J.B. Snell,
Railways: Mechanical Engineering,
Arrow Books, p. 85.

9. Anon.,
The Expanding Mandrel,
The Engineer, Vol. 12, Aug. 9 1861, p. 77.

10. CLUTHA.,
Letter to the Editor,
The Engineer, Vol. 11, Nov. 30 1860, p. 361.

11. J. Jewsbury and K.R.U.,
Letters to the Editor,
The Engineer, Vol. 11, Dec. 7 1860, p. 375.

12. K.R.U. and A. Dixon,
Letters to the Editor,
The Engineer, Vol. 11, Dec. 14 1860,

13. J. Jewsbury,
Letter to the Editor,
The Engineer, Vol. 11, Dec. 21 1860, p. 405.

14. A. Alan,
Expanding Mandrels,
The Engineer, Vol. 11, May 3 1861, p. 276.

15. A. Alan,
Letter to the Editor,
The Engineer, Vol. 11, May 10 1861, p. 293.

16. A. Alan,
Letter to the Editor,
The Engineer, Vol. 11, June 21 1861, p. 377.

17. J. Inshaw,
Letter to the Editor,
The Engineer, Vol. 11, June 28 1861, p. 391.

18. K.R.U.,
Letter to the Editor,
The Engineer, Vol. 12, July 19 1861, p. 37.

19. J. Inshaw,
Letter to the Editor,
The Engineer, Vol. 12, July 26 1861, p. 51.

20. J. Inshaw and K.R.U.,
Letters to the Editor,
The Engineer, Vol. 12, Aug. 2 1861, p. 77.

21. A.E. Bloofield,
Mandrel for Turning Parallel Surfaces,
Machinery (U.S.), Dec. 1914, p. 340.

22. E.F. Lake,
Air-Operated Chucks and Mandrels,
Machinery (U.S.), Feb. 1915, pp. 476-479.

23. A.A. Dowd,
Compensating and Quick-Acting Devices,
Machinery (U.S.), Jan. 1915, pp. 355-359.

24. H. Baxter,
Personal Communication.

25. E. Chapman,
Nonslip Expanding Mandrel,
American Machinist, Mar. 21 1918, p. 506.

26. N. Hall,
Design of Expanding Arbors,
American Machinist, Mar. 8 1923, p. 385.

27. E.A. Dixie,
Expanding Arbors,
American Machinist, Oct. 7 1920, p. 664.

28. C.C. Tomney,
An Expansion Mandrel,
American Machinist, Dec. 1935, p. 926.

29. O.H. Gitter,
Expanding Mandrel Permits Quick Work Changes,
American Machinist, Vol. 40, Dec. 19 1946, p. 140.

30. D.J. Mulholland,
Expanding Mandrel Tightens in Blind Holes,
American Machinist, Vol. 91, June 19 1947, p. 153.

31. R.B. Courtney,
Expansion Arbor for Secondary Lathe Operations,
Machinery (U.S.), Vol. 58, June 1952, p. 203.

32. R.B. Courtney,
Expanding Mandrel is Practical and Inexpensive in its Simplicity,
American Machinist, Vol. 100, Nov. 19 1956, p. 159.

33. J.J. Baule,
Expanding Arbor for Second-Operation Lathe Work,
Machinery (U.S.), Dec. 1951, p. 194.

34. F. Schroeder,
Self-centering Mandrels and Chucks,
Mechanical World, Vol. 117, Feb. 23 1945, pp. 221-222.

35. Anon.,
An Expanding Mandrel,
The Engineer, April 28 1960, p. 516.

36. L.J. Herriman,
Expanding Arbor with Rubber Gripping Member,
Machinery (U.S.), Vol. 43, Nov. 1936, p. 200.

37. Handbook on Fixture Design,
A.S.T.M.E.,
Mcgraw-Hill.

38. A.R. Jones,
An Expanding Mandrel,
American Machinist, Dec. 13 1917, p. 1035.

39. H.L. Wheeler,
Expansion Mandrel for Long Bushings,
American Machinist, Dec. 1936, p. 1016.

40. H. Fletcher,
Expanding Mandrel,
Machinery (U.S.), June 19 1919, p. 313.

41. J.H. Hahn,
Special Tools and Devices for Railway Shops,
Machinery (U.S.), March 1930, pp. 511-512.

42. G.M. Dick,
Expanding Mandrel,
Machinery (U.S.), May 2 1918, p. 761.

43. J.R. Whittle,
Expanding Mandrel,
American Machinist, Aug. 25 1935, pp. 743-744.

44. H.J. Gerber,
Differential Expanding Mandrel,
Tool Engineer, Vol. 38, May 1956, p. 82.

45. F. Heise,
Selbstzentrierende Sponndorne,
U.D.I. Zeitschrift, March 1934, p. 298.

46. H. Conn,
Work Holders and Drivers,
Grinding and Finishing, Vol. 2, Sept. 1956, pp. 45-48,

47. Anon.,
'Efficiency' Self-Gripping Mandrel,
American Machinist, Vol. 51, Oct. 30 1919, p. 804.

48. Wilson et.al.,
Handbook of Fixture Design,
A.S.T.M.E., Mcgraw-Hill,

49. Letter to Author from Tobler S.A., Montrouge, France,
April 2 1973.

50. F.H. Charlton,
Use and Abuse of Expansion Mandrels.
Machinery (U.S.), April 1917, pp. 712-713.

51. W.S. Rowell,
Expanding Mandrels,
American Machinist, Ap. 22 1936, p. 317.

52. J.G. Jergens,
Expanding Arbors for Lathe Work,
The Machinist, 1942, pp. 438-439.

53. R.R. Holmes,
Expanding Mandrel for Bevel Gear Blanks,
Machinery (U.S.), Aug. 1935, p. 745,

54. J.R. Whittles,
Expansion Mandrels for Holding Tubing,
American Machinist, June 1936, pp. 560-561.

55. F.C. Hudson,
Chuck Operates Expanding Mandrel,
American Machinist, Mar. 3 1941, pp. 162-163.

56. G.W. Mason,
Bristol-Erickson Collets and Expanding Mandrels,
Machinery (L), April 7 1965, pp. 741-747.

57. Anon.,
Expanding Mandrels in the Evolution of Modern Machining Methods,
Machine Modern, April 1972.

58. Anon.,
The Close Relationship between Precision Expanding Mandrels and Increased Productivity,
Tobler Sales Publication,
Tobler S.A., Montrouge, France.

59. Anon.,
Examples of Applications of Expanding Mandrels,
Tobler Sales Publication,
Tobler S.A., Montrouge, France.

60. D.M. MacDonald and R.M.G. Meek,
A Photoelastic Study of Shrink-fit and Bending Stresses in Shaft and Ring Assemblies,
N.E.L. Report No. 545, June 1973,
Department of Trade and Industry.

61. Roark,
Formulas for Stress and Strain,
Mcgraw-Hill, London 1954.

62. Morley,
Strength of Materials,
Longmans.

63. Hall et.al.,
Machine Design,
Mcgraw-Hill,

64. G.Ya. Andreev and I.I. Shat'ko,
Distribution of the Contact Pressure in Interface Fits,
Russian Engineering Journal, Vol. XLVII, No. 5, pp. 36-38

65. Baumeester,
Marks Mechanical Engineering Handbook,
Mcgraw-Hill, London, 6th Ed.

66. Machinerys Handbook,
Fourteenth Edition,
Machinery Publications Co,
Brighton,
England.

CHAPTER V111

APPENDICES

8.1 Calibration

8.1.1 Calibration of Strain Gauge Proving Rings

Instrument Data.

Techequipment Strain Bridge model 11
Manufactured by Techequipment, Nottingham

Mean sensitivity at gain factor 1 = 1 με

Clockhouse proving ring model 200.

Dial gauge number 7513. Last calibrated 1971.

Mean sensitivity .59N (.133lbf) per division.

The experimental set up for the calibration of the strain gauge proving rings is shown on plate 9, the rig consists of a load application apparatus which is a standard piece of equipment in the Centre for Industrial Studies, the design of this apparatus enables a known axial load (this loading condition is required) to be applied to a specimen. The proving ring strain gauges are wired to the Techequipment strain bridge.

The following method was used in the calibration of the strain gauge proving rings. Initially the proving ring was positioned in the rig, axial alignment being established by the use of a set-square to position the vertical centre line marked on the proving ring. The strain reading displayed on the strain bridge was set to a zero datum with the system in the no load mode. With the zero datum set, the Clockhouse proving ring was positioned above the thrust shaft and under the loading screw, the system in this state gives a 2.62N (.59lbf) load to the strain gauge proving ring, the strain reading, corresponding to this load, displayed on the strain bridge was recorded.

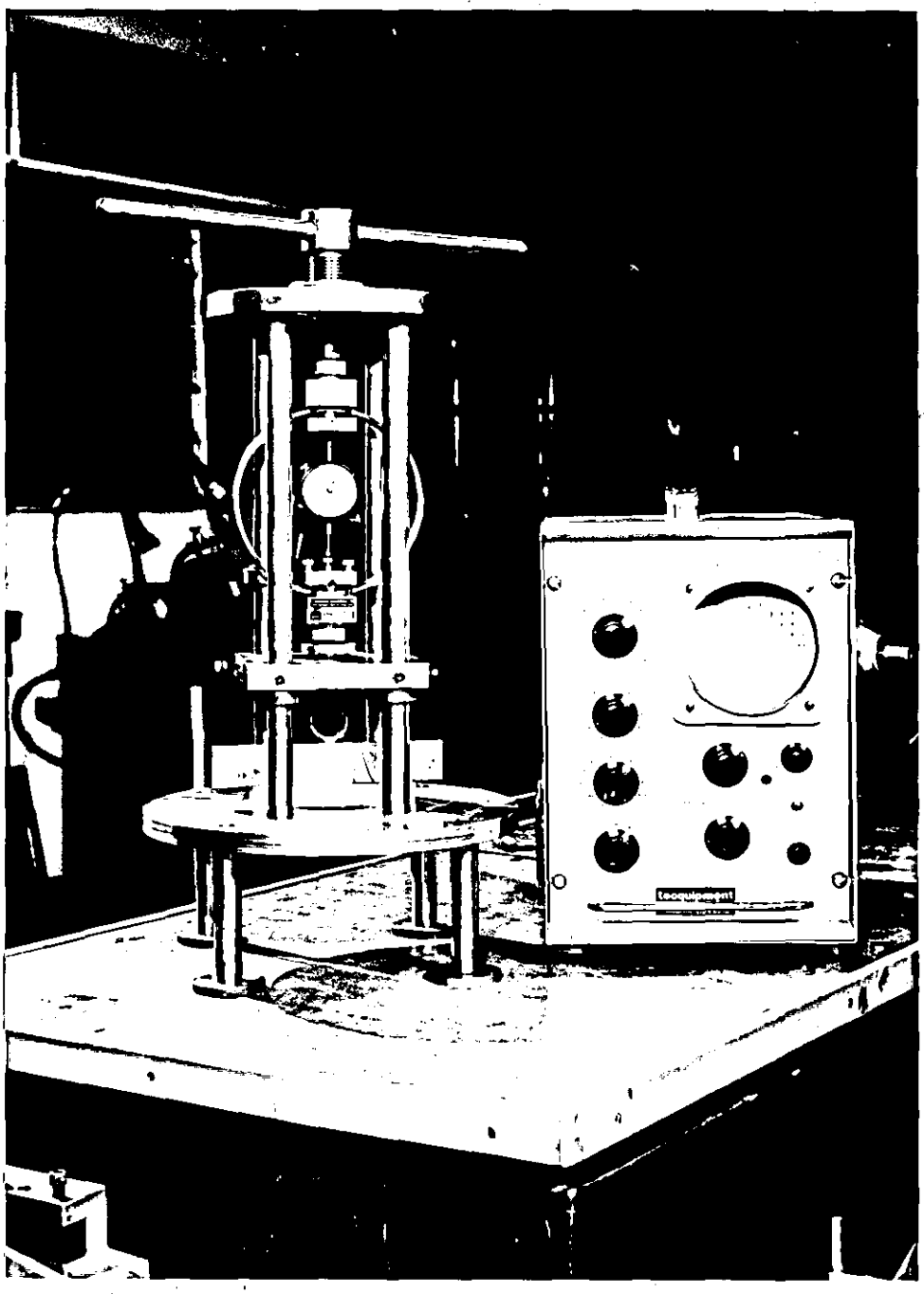

Plate 9. Calibration rig for strain gauge proving rings.

The strain gauge proving ring was then further loaded in incremental steps of 22.24N (5lbf) up to a maximum load of 91.58N (20.59lbf) for each increase in load, the resulting strain reading was recorded. The calibration was repeated five times for each of the three strain gauge proving rings, the average strain reading for each incremental load being used to produce the calibration curve.

Tables 8.1, 8.2. and 8.3. and figures 8.1, 8.2. and 8.3., show the readings and calibration curves respectively.

Table 8.1.

Calibration of the 41.27 mm. (1.625in.) diameter strain gauge proving ring

Strain bridge gain setting 1

Applied load N	Proving ring strain reading με 1st	2nd	3rd	4th	5th	Average strain reading με
2.62	3	3	4	4	5	4.2
24.86	46	43	44	46	48	45.4
47.10	88	87	88	88	87	87.6
69.34	134	130	127	133	129	130.6
91.58	175	171	173	174	175	173.6

Table 8.2.

Calibration of the 50.8 mm. (2in.) diameter strain gauge proving ring

Strain bridge gain setting 1

Applied load N	Proving ring strain reading με 1st	2nd	3rd	4th	5th	Average strain reading με
2.62	7	8	9	8.5	9	8.3
24.86	77	76	76	77.0	76	76.4
47.10	136	134	137	139.0	135	136.2
69.34	211	209	212	211.5	208	210.3
91.58	270	268	272	272.0	268	270.0

Table 8.3.

Calibration of the 60.32 mm. (2.375in.) diameter strain gauge proving ring

Strain bridge setting 1

Applied load N	Proving ring strain reading με 1st	2nd	3rd	4th	5th	Average strain reading με
2.62	11	13	11	12	13	12.0
24.86	99	99	96	98	99	97.8
47.10	186	180	185	180	184	182.6
69.34	260	263	268	264	267	264.4
91.58	353	350	351	356	356	353.2

Figure 8.1. CALIBRATION OF 60.32mm. (2.375 in.) STRAIN GAUGE PROVING RING

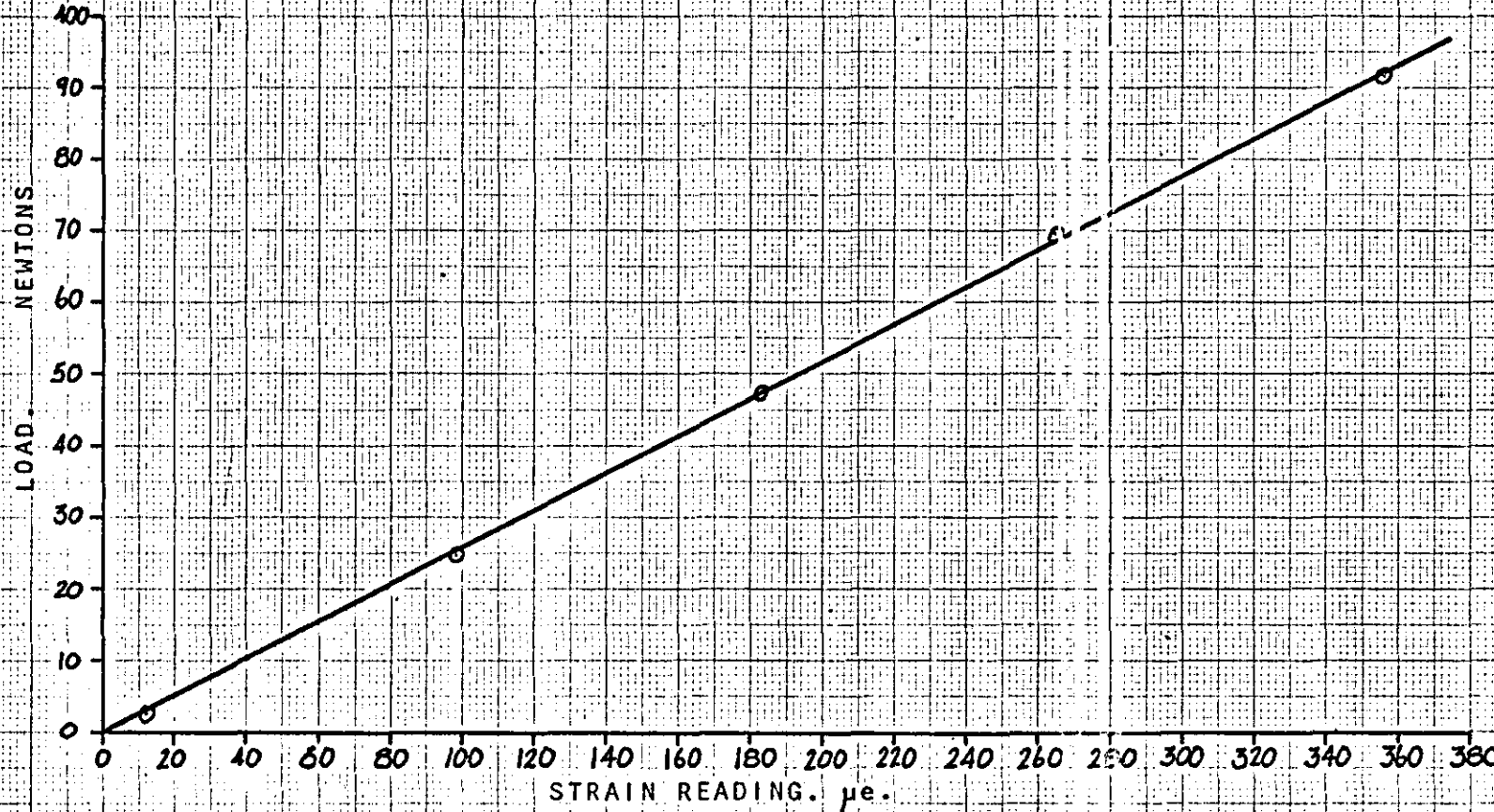

Figure 8.2 CALIBRATION OF 50.8mm (2.0in.) STRAIN GAUGE PROVING RING

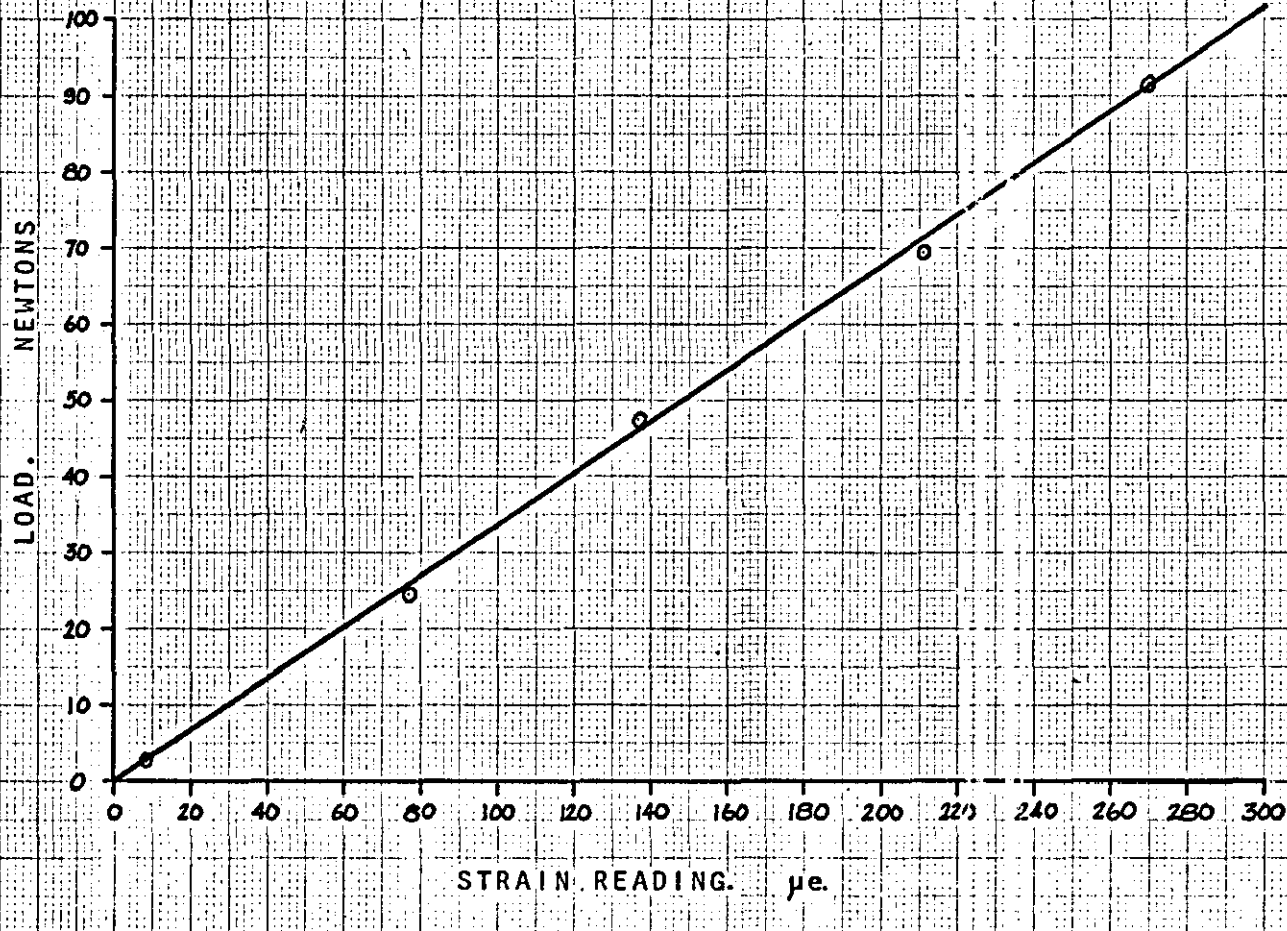

Figure 8.3 CALIBRATION OF 41.27MM.(1.625 in.) STRAIN GAUGE PROVING RING

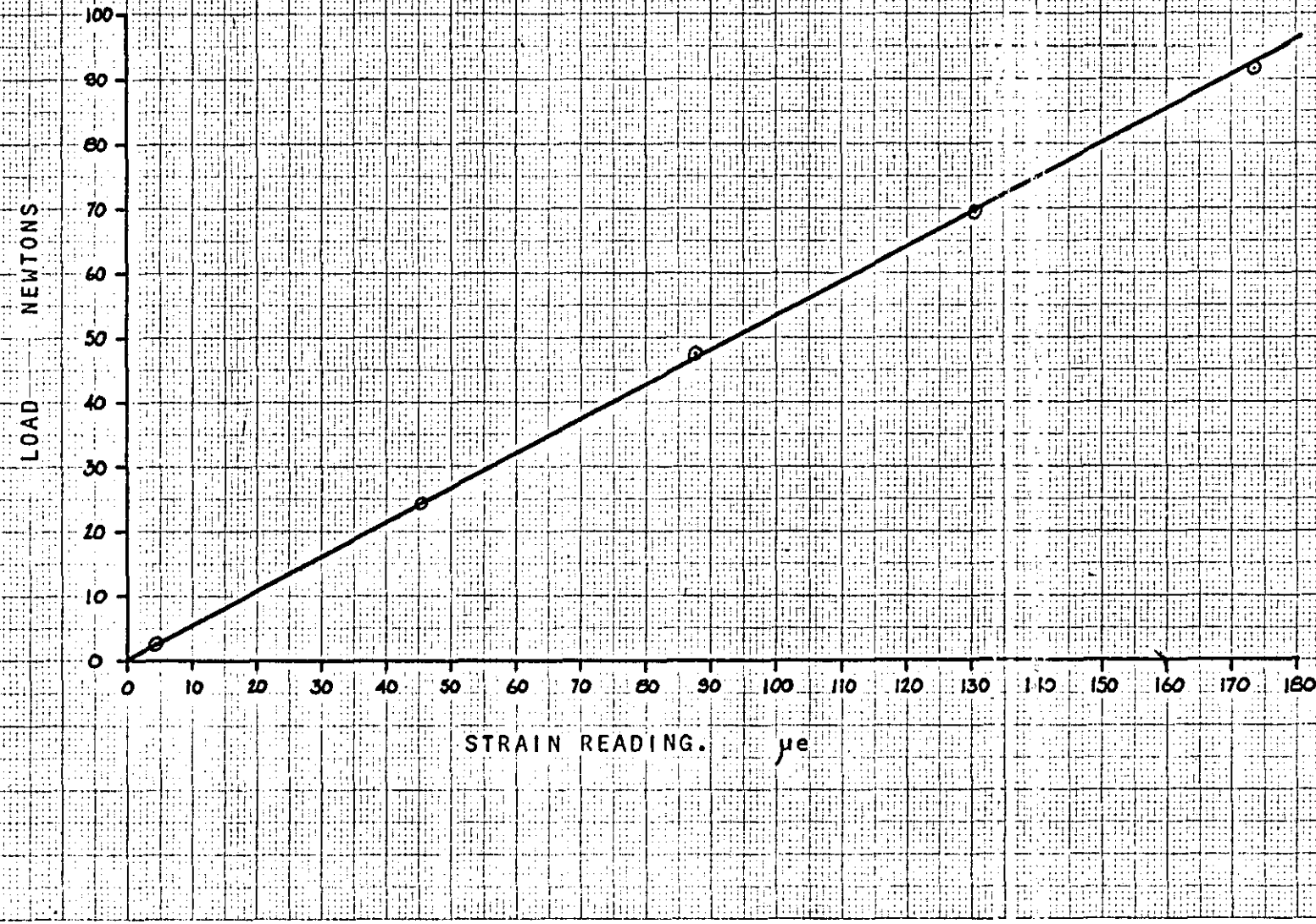

8.1.2 Calibration of the Pressure Transducer Elements

Instrument Data.

Techequipment Strain Bridge model 11
Manufactured by Techequipment, Nottingham

Mean sensitivity at gain factor 1 = 1 με

Strain gauge proving rings shown in figure 2.18.

Interface pressure rigs shown in figure 2.15.

The transducer elements were calibrated in situ in the interface pressure rigs, the strain gauge proving rings having been designed to facilitate in situ calibration, this method enabled the calibration to be undertaken simply and with the minimum of disturbance to the wiring to the strain gauges on the elements.

The method used in the calibration was to place the interface pressure rigs containing the transducer elements wired to the strain bridge, on a flat horizontal surface, a flat horizontal surface enabled the bore to be 'square' to some datum surface and also to provide a datum from which the horizontal alignment of the proving rings could be set, a surface table was used in this instance. Slip gauges were then placed in the bore of the pressure rigs, the height of the gauges being set to position, the horizontal centre line of the strain gauge proving ring with the horizontal centre line of the elements, as shown in figure 8.4. The appropriate strain gauge proving ring, wired to the strain bridge, was then placed in the bore of the interface pressure rig until it was supported by the slip gauges, axial alignment of the proving ring and the transducer elements was facilitated by matching, by eye, the vertical centre line marked on the strain gauge proving ring with the marked centre line of the

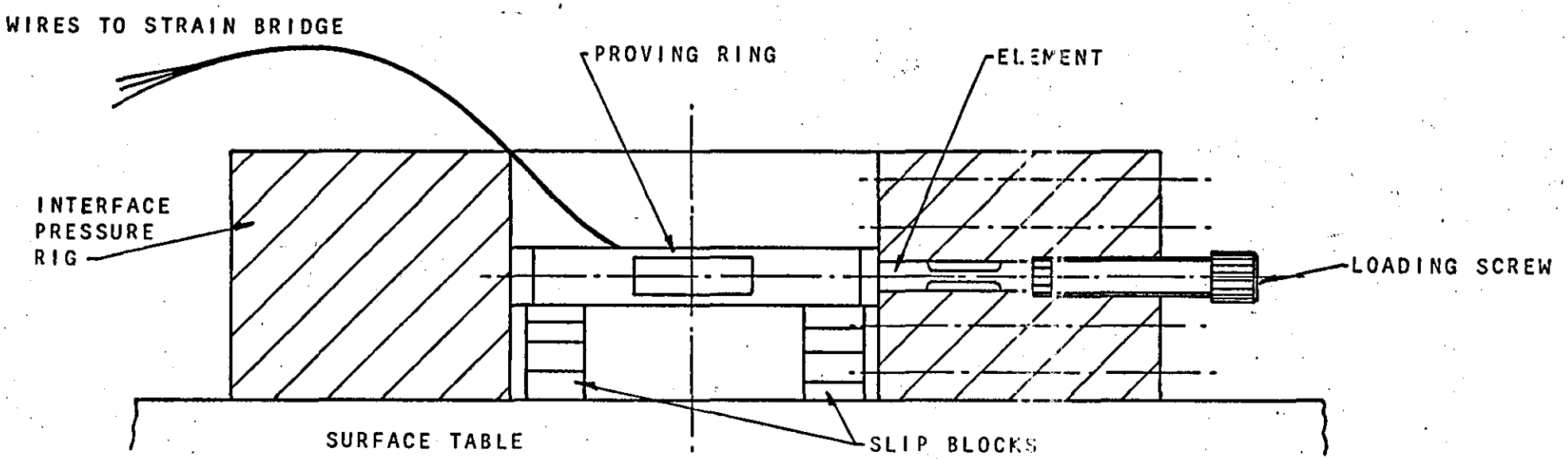

Figure 8.4.:TRANSDUCER ELEMENT CALIBRATION SET-UP.

interface pressure rig, the centre line of the interface pressure rigs passing through the centre line of the transducer elements. In this no load situation the strain readings of the elements and the strain gauge proving ring were noted.

Load application for the calibration was by means of a thrust screw positioned behind the element, see figure 2.15, clockwise rotation of the screw moves the element radially inwards thereby subjecting the strain gauge proving ring to a deflection, measurement of the resulting strain induced establishes the magnitude of the applied load.

The actual method used for load application was to set the reading on the strain bridge to the value of load required, advancement of the measuring switches on the strain bridge to the value of strain required (i.e., the new load) causes the trace line on the C.R.T. (Cathode Ray Tube) to be at an angle relative to the horizontal, upon loading the trace line moves toward the horizontal and reaches the horizontal when the strain required (load) is obtained. The measurement of the strain in the transducer elements for any given loading was made by changing to the appropriate channel on the strain bridge, the transducer element strain displayed was now measured using the measuring switches to bring the trace line on the C.R.T. to the horizontal.

Strain readings for the element were taken for several values of load and from the results a calibration curve for the element was plotted. The whole procedure was repeated for 16 elements in the four interface pressure rigs. Tables 8.4 to 8.19. present the results and figures 8.5. to 8.20. show the calibration curves.

Table 8.4

Calibration of Transducer Element Number 1

Proving Ring Strain με	Element Strain Reading με					Average Elemen Strain με
	1st	2nd	3rd	4th	5th	
20	19	22	20	20	24	21
40	39	41	43	42	40	41
60	61	58	63	57	61	60
80	79	77	76	80	78	78
100	94	97	95	96	98	96
120	112	118	116	113	116	115
140	133	131	135	130	131	132
160	153	153	150	150	149	151
180	173	174	178	177	173	175

Table 8.5

Calibration of Transducer Element Number 2

Proving Ring Strain με	Element Strain Reading με					Average Elemen Strain με
	1st	2nd	3rd	4th	5th	
20	15	12	15	15	13	14
40	33	30	31	34	30	32
60	46	43	45	44	42	44
80	57	63	58	57	60	59
100	77	75	73	79	77	76
120	92	94	90	92	92	92
140	103	110	106	109	106	107
160	118	121	122	124	119	121
180	134	136	133	137	135	135

Table 8.6

Calibration of Transducer Element Number 3

Proving Ring Strain με	Element Strain Reading με					Average Element Strain με
	1st	2nd	3rd	4th	5th	
20	16	17	16	15	16	16
40	30	32	34	35	34	33
60	53	50	50	51	51	51
80	75	73	69	73	70	72
100	87	85	89	90	89	88
120	108	105	109	107	106	107
140	123	124	126	121	121	123
160	136	138	140	134	137	137
180	160	157	165	158	157	159

Table 8.7

Calibration of Transducer Element Number 4

Proving Ring Strain με	Element Strain Reading με					Average Element Strain με
	1st	2nd	3rd	4th	5th	
50	37	38	34	35	34	35.6
100	72	74	70	72	71	71.8
150	102	105	101	105	102	103.0
200	144	145	144	144	140	143.4
250	178	180	181	178	175	178.4
300	211	213	214	210	208	211.2
350	255	257	258	253	250	254.6

Table 8.8

Calibration of Transducer Element Number 5

Proving Ring Strain με	Element Strain Reading με					Average Element Strain με
	1st	2nd	3rd	4th	5th	
50	32	33	29	33	29	31.2
100	64	65	60	60	64	62.6
150	90	90	87	89	87	88.6
200	119	118	117	116	119	117.8
250	150	149	149	152	150	150.0
300	184	183	180	181	180	181.6
350	212	211	208	212	208	210.2

Table 8.9

Calibration of Transducer Element Number 6

Proving Ring Strain με	Element Strain Reading με					Average Element Strain με
	1st	2nd	3rd	4th	5th	
50	21	25	24	22	22	22.8
100	46	47	50	49	49	48.2
150	71	71	74	73	71	72.0
200	95	97	100	98	99	97.8
250	121	121	125	124	125	123.2
300	148	149	150	149	150	149.2
350	171	174	175	175	173	173.6

Table 8.10

Calibration of Transducer Element Number 7

Proving Ring Strain με	Element Strain Reading με					Average Elemen Strain με
	1st	2nd	3rd	4th	5th	
40	20	22	23	20	23	21.6
80	42	41	41	40	40	40.8
120	63	66	66	64	65	64.8
160	85	86	84	86	85	85.2
200	105	105	106	104	106	105.2
240	126	127	128	125	126	126.4
280	149	149	147	149	148	148.0

Table 8.11

Calibration of Transducer Element Number 8

Proving Ring Strain με	Element Strain Reading με					Average Elemen Strain με
	1st	2nd	3rd	4th	5th	
40	25	24	25	26	23	24.6
80	50	48	49	50	47	48.8
120	76	75	76	76	74	75.4
160	98	97	99	96	98	97.6
200	124	123	122	122	123	122.8
240	149	149	152	151	152	150.6
280	174	173	176	177	176	175.0

Table 8.12

Calibration of Transducer Element Number 9

Proving Ring Strain με	Element Strain Reading με					Average Element Strain με
	1st	2nd	3rd	4th	5th	
40	23	24	25	24	26	24.4
80	45	46	46	45	47	45.8
120	67	69	70	68	71	69.0
160	86	88	89	89	88	88.0
200	109	109	112	111	111	110.4
240	132	133	134	131	133	132.2
280	156	159	159	158	158	158.0

Table 8.13

Calibration of Transducer Element Number 10

Proving Ring Strain με	Element Strain Reading με					Average Element Strain με
	1st	2nd	3rd	4th	5th	
40	25	23	23	26	24	24.2
80	47	44	45	48	43	45.4
120	71	69	70	72	68	70.0
160	95	93	96	95	91	94.0
200	118	117	117	117	115	116.8
240	138	136	139	137	135	137.0
280	171	170	171	169	168	169.8

Table 8.14

Calibration of Transducer Element Number 11

Proving Ring Strain με	Element Strain Reading με					Average Elemen Strain με
	1st	2nd	3rd	4th	5th	
40	17	18	17	19	19	18.0
80	35	36	35	37	37	36.0
120	53	55	52	55	54	54.0
160	67	68	67	69	69	68.0
200	86	88	86	87	89	87.2
240	102	104	106	105	104	104.5
280	124	125	126	124	126	125.0

Table 8.15

Calibration of Transducer Element Number 12

Proving Ring Strain με	Element Strain Reading με					Average Elemen Strain με
	1st	2nd	3rd	4th	5th	
50	25	26	26	24	26	25.4
100	46	48	48	45	47	46.8
150	71	72	72	70	71	71.2
200	96	97	96	95	96	96.0
250	121	122	121	120	120	120.8
300	143	145	143	143	145	143.8
350	168	170	169	167	168	168.4

Table 8.16

Calibration of Transducer Element Number 13

Proving Ring Strain με	Element Strain Reading με					Average Elemen Strain με
	1st	2nd	3rd	4th	5th	
50	18	22	21	19	19	19.8
100	40	41	43	42	42	41.6
150	61	61	64	63	61	62.0
200	82	83	86	84	85	84.0
250	104	104	107	106	107	105.7
300	127	128	129	128	129	128.2
350	147	149	150	150	149	149.0

Table 8.17

Calibration of Transducer Element Number 14

Proving Ring Strain με	Element Strain Reading με					Average Elemen Strain με
	1st	2nd	3rd	4th	5th	
50	26	27	24	25	24	25.2
100	51	52	49	51	50	50.6
150	72	74	71	74	72	72.6
200	101	102	101	101	98	100.6
250	125	126	127	125	123	125.2
300	148	149	150	147	146	148.0
350	179	180	181	177	175	178.4

Table 8.18

Calibration of Transducer Element Number 15

Proving Ring Strain με	Element Strain Reading με					Average Elemen Strain με
	1st	2nd	3rd	4th	5th	
50	25	26	23	23	26	24.6
100	50	51	47	47	50	49.0
150	70	70	68	69	68	69.0
200	93	92	91	90	93	91.8
250	117	116	116	118	117	116.8
300	143	142	140	141	140	141.2
350	166	164	162	165	162	163.8

Table 8.19

Calibration of Transducer Element Number 16

Proving Ring Strain με	Element Strain Reading με					Average Elemen Strain με
	1st	2nd	3rd	4th	5th	
50	21	18	22	19	18	19.6
100	42	40	43	40	39	40.8
150	63	60	65	61	60	61.8
200	86	84	87	85	83	85.0
250	107	105	109	106	104	106.2
300	123	122	126	124	121	123.3
350	148	145	149	148	144	146.8

Figure 8.5. CALIBRATION OF ELEMENT No. 1

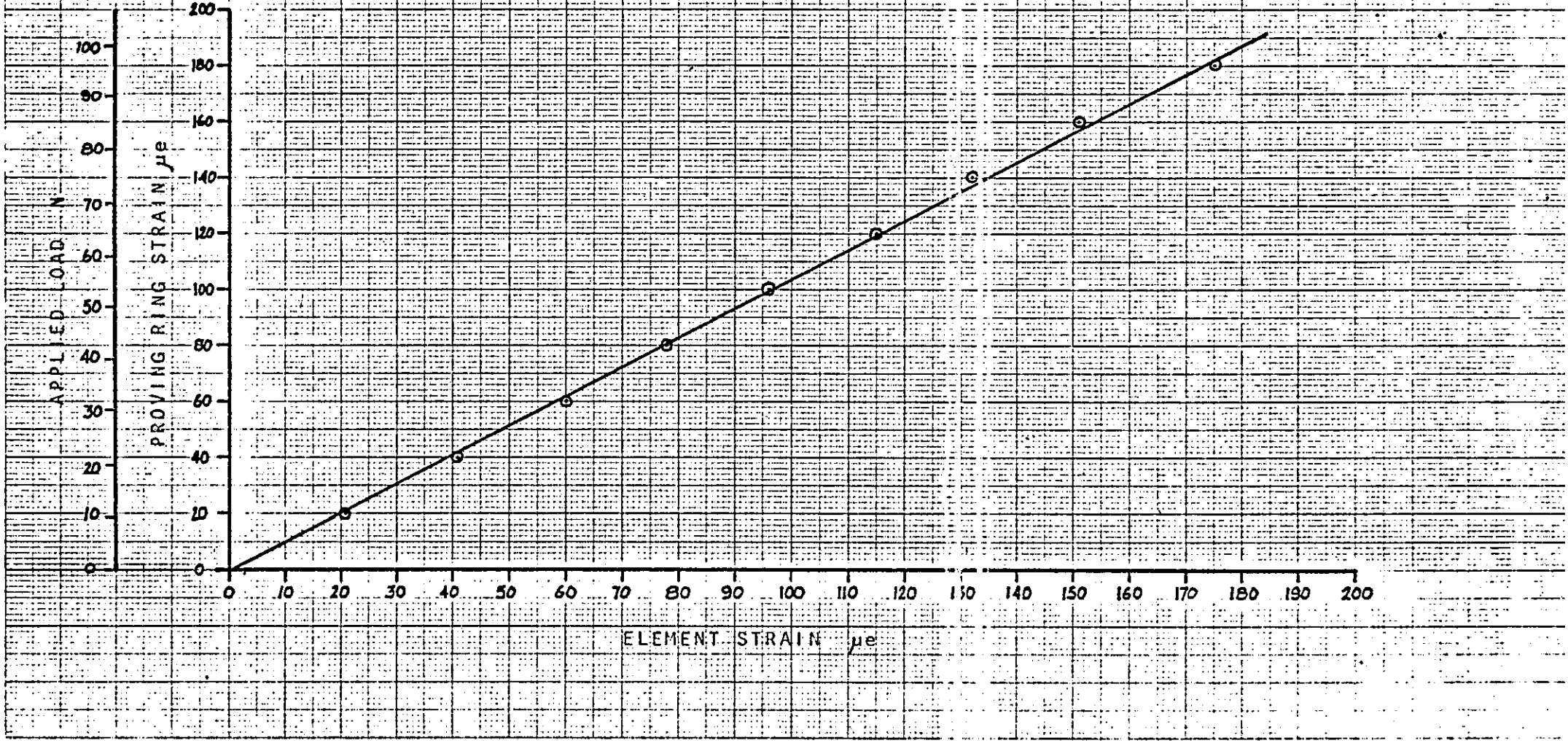

Figure 8.6. CALIBRATION OF ELEMENT No. 2

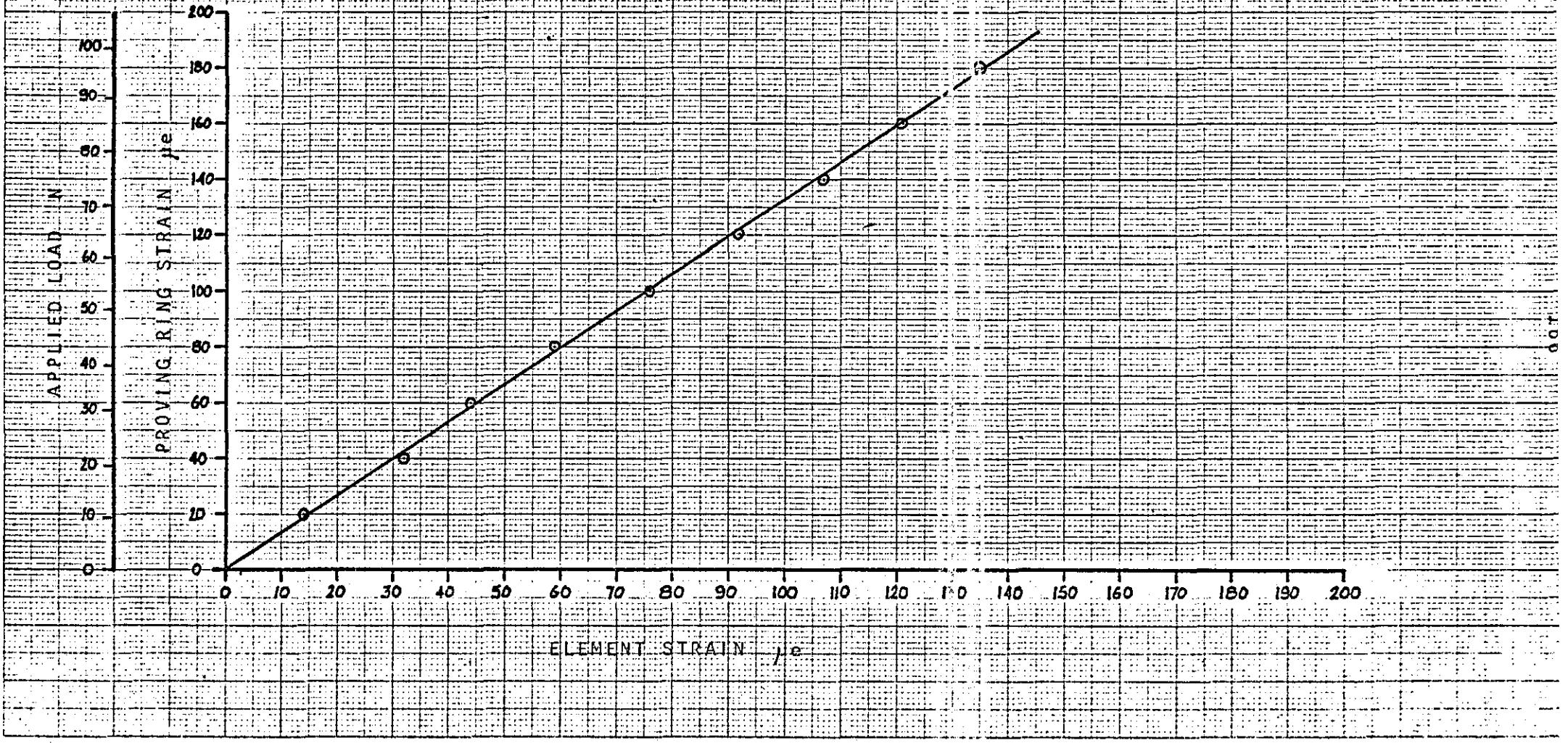

Figure 8.7. CALIBRATION OF ELEMENT No. 3

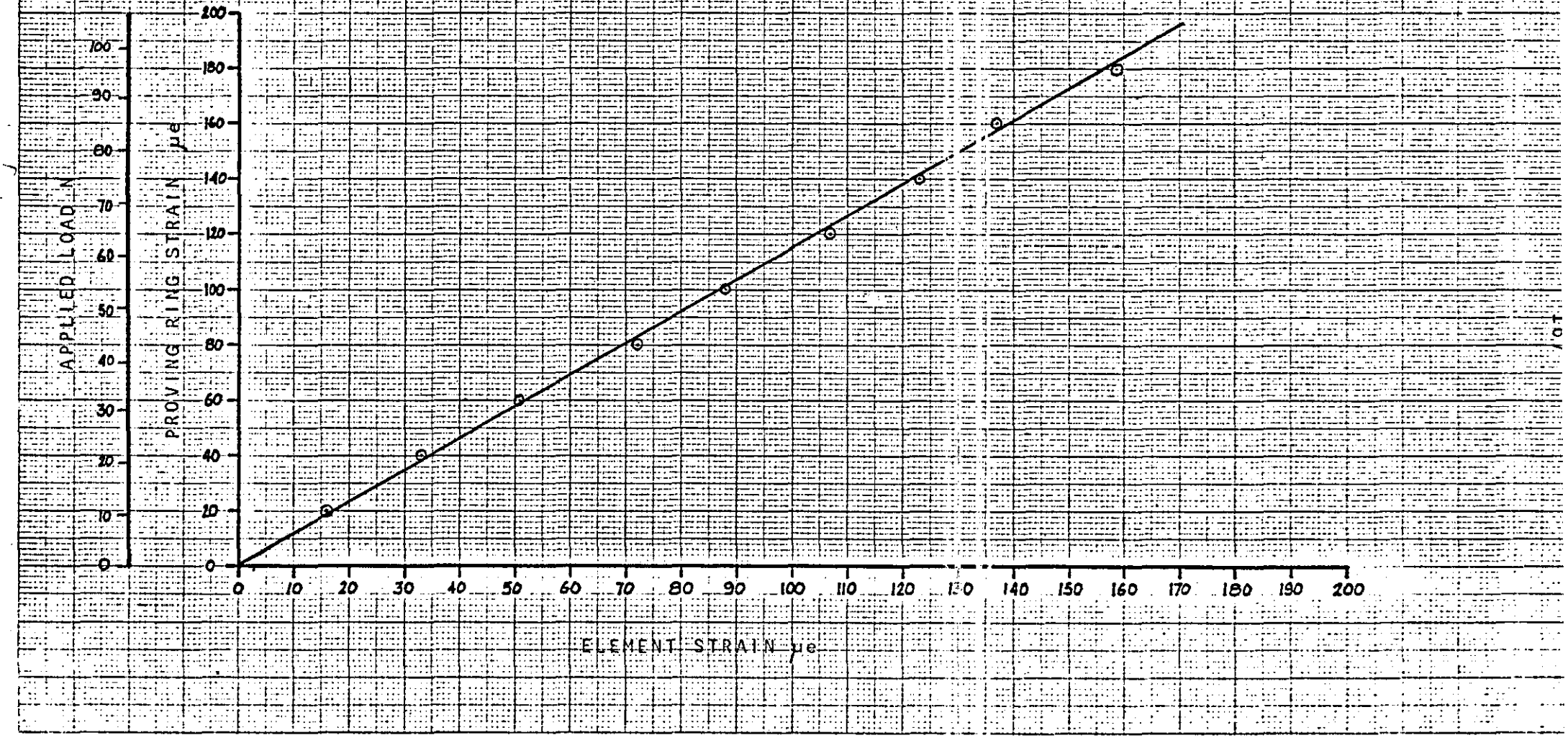

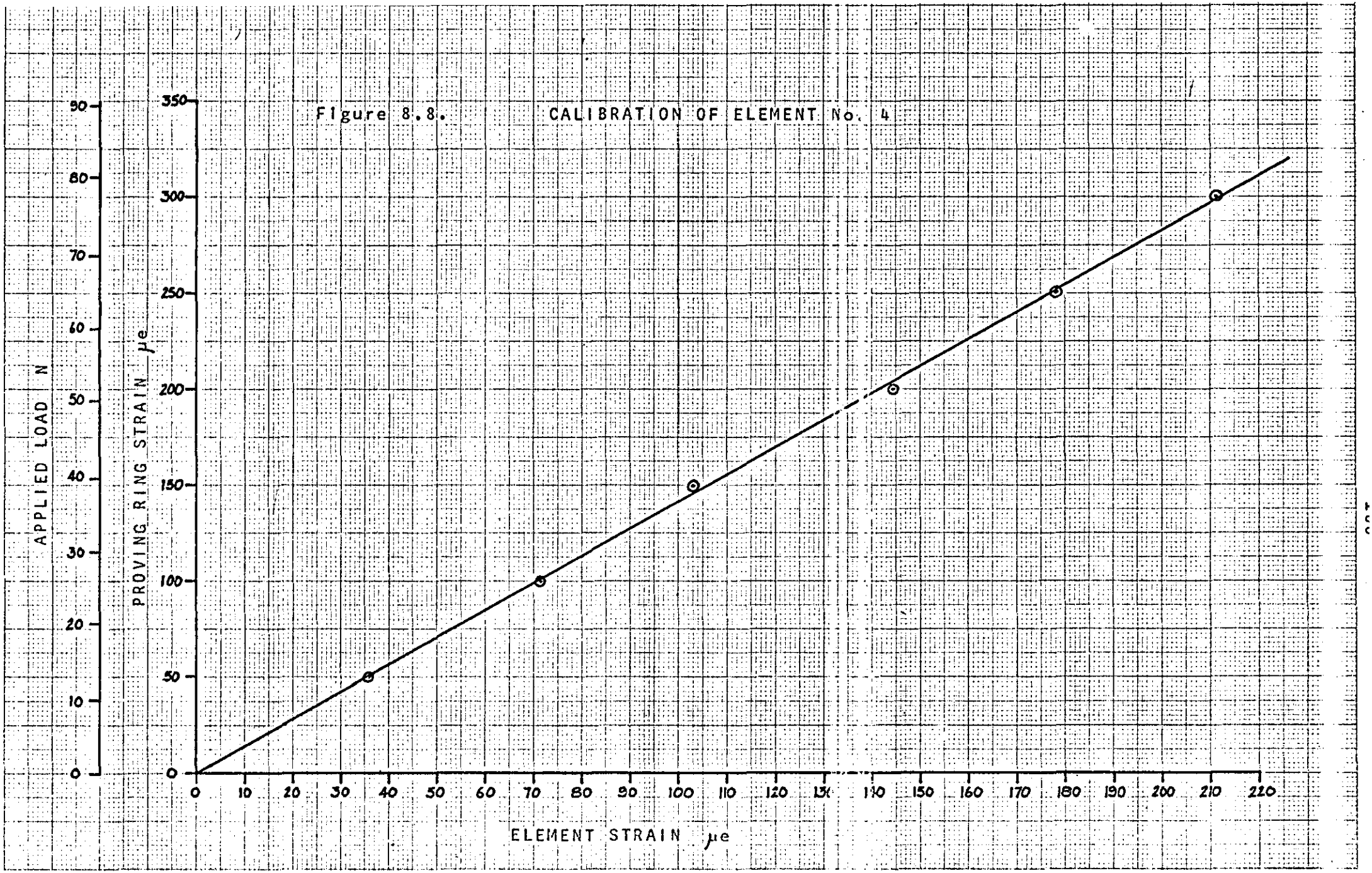
Figure 8.8. CALIBRATION OF ELEMENT No. 4
APPLIED LOAD N
0
10
20
30
40
50
60
70
80
90
PROVING RING STRAIN με
0
50
100
150
200
250
300
350
ELEMENT STRAIN με
0
10
20
30
40
50
60
70
80
90
100
110
120
130
140
150
160
170
180
190
200
210
220

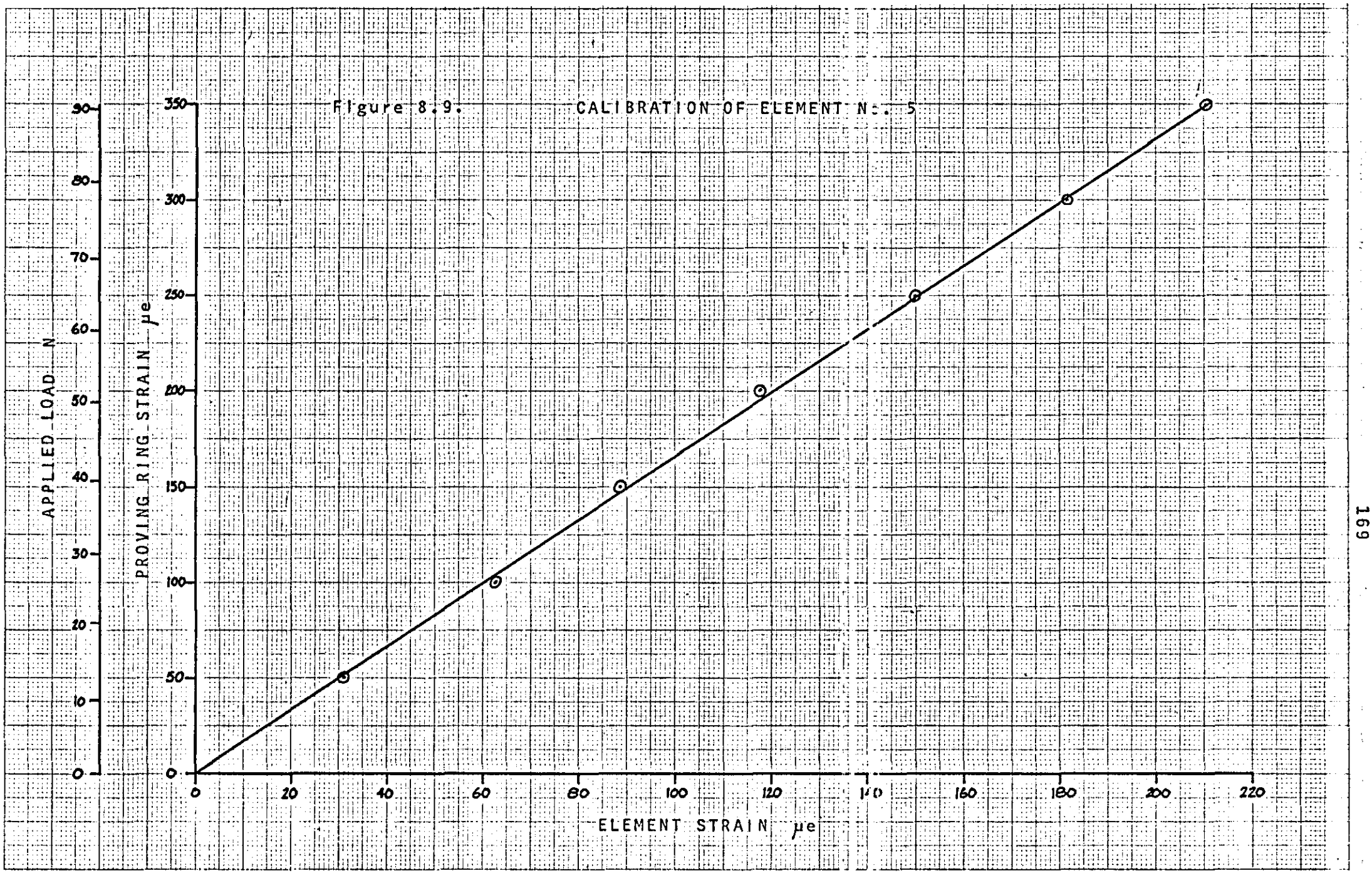

Figure 8.9. CALIBRATION OF ELEMENT No. 5

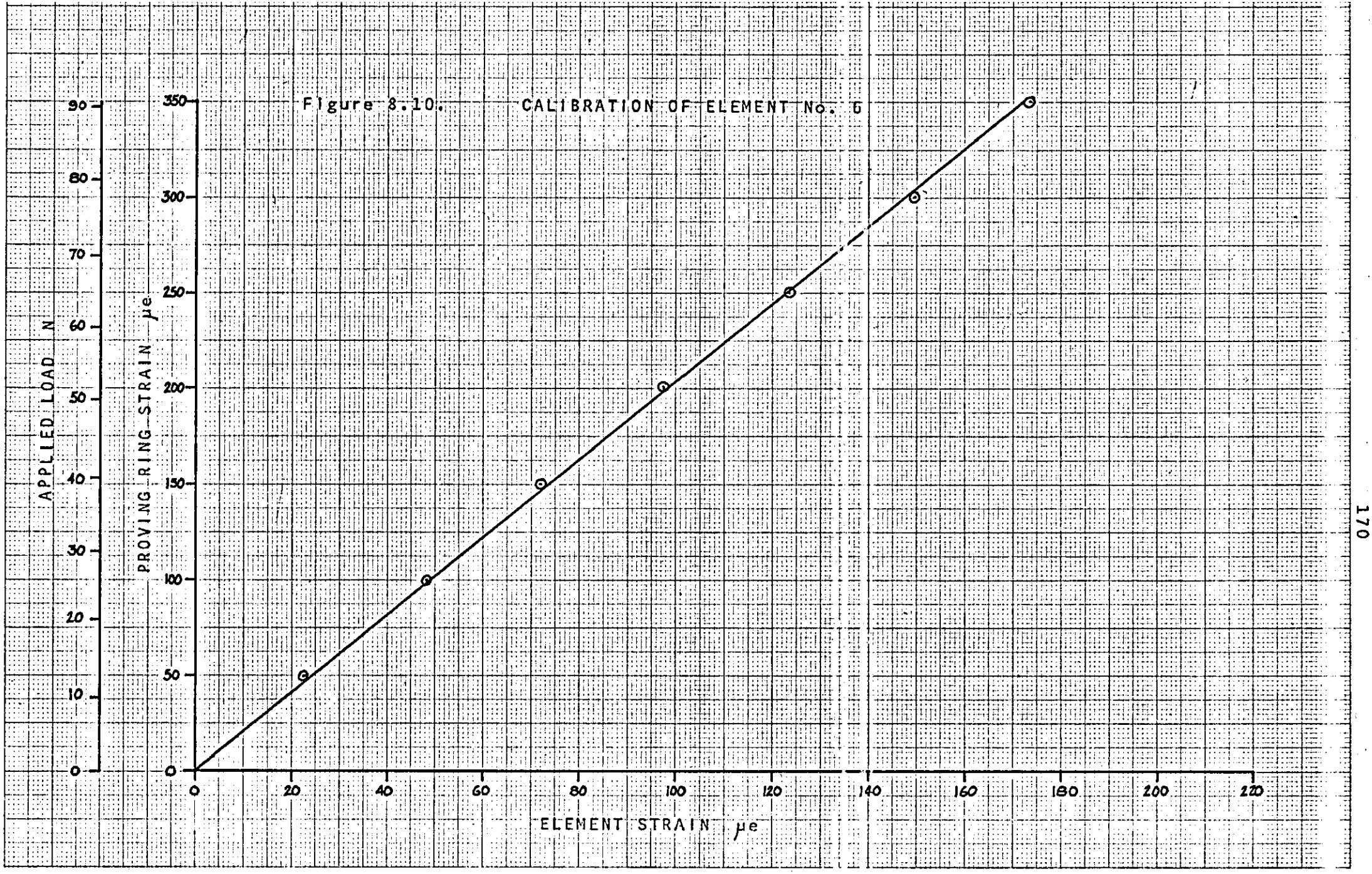
Figure 8.10. CALIBRATION OF ELEMENT No. 6
APPLIED LOAD N
PROVING RING STRAIN με
ELEMENT STRAIN με
0
10
20
30
40
50
60
70
80
90
50
100
150
200
250
300
350
0
20
40
60
80
100
120
140
160
180
200
220

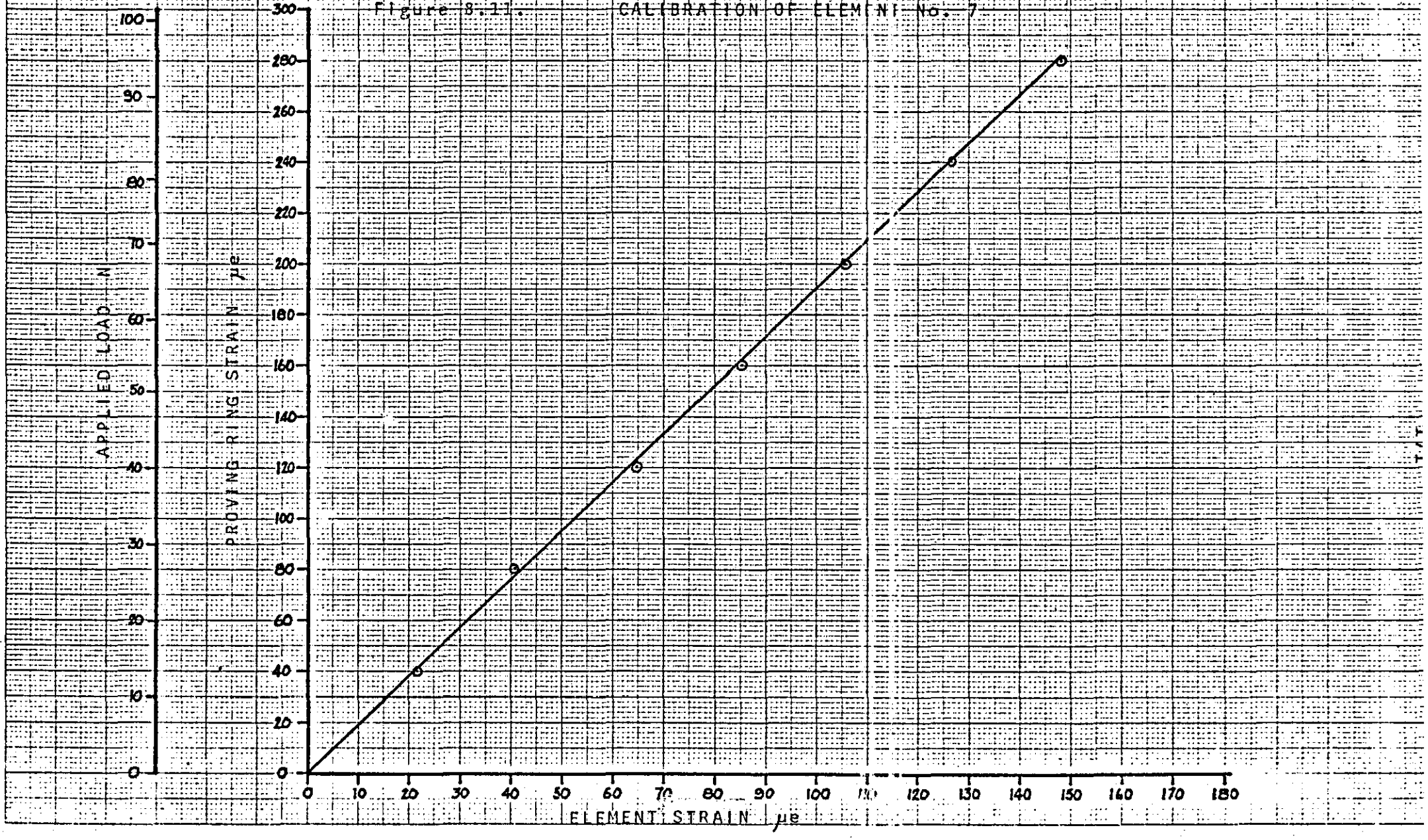

Figure 8.11. CALIBRATION OF ELEMENT No. 7

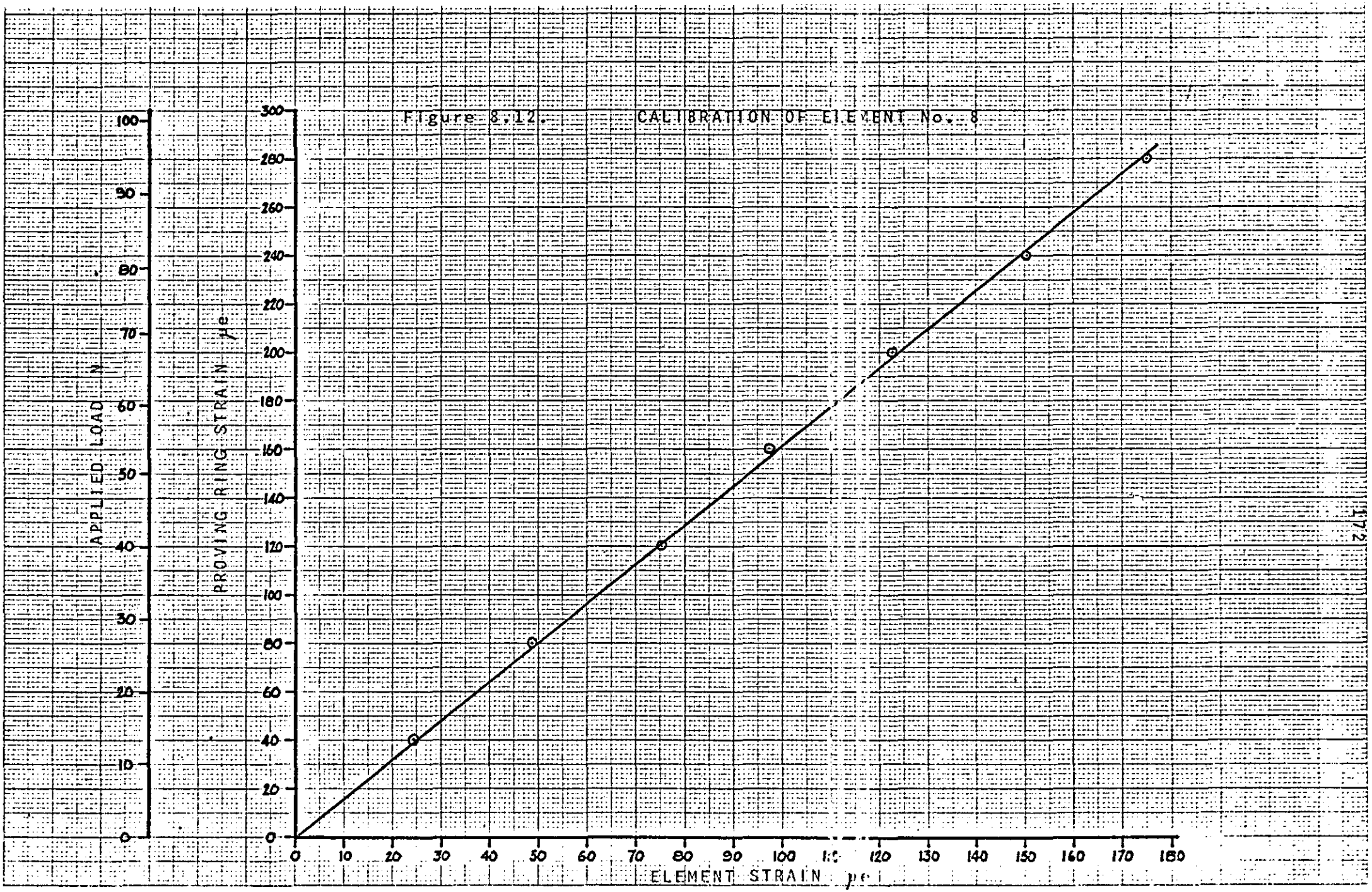
Figure 8.12. CALIBRATION OF ELEMENT No. 8
APPLIED LOAD N
PROVING RING STRAIN με
ELEMENT STRAIN με
0
10
20
30
40
50
60
70
80
90
100
120
130
140
150
160
170
180
200
220
240
260
280
300

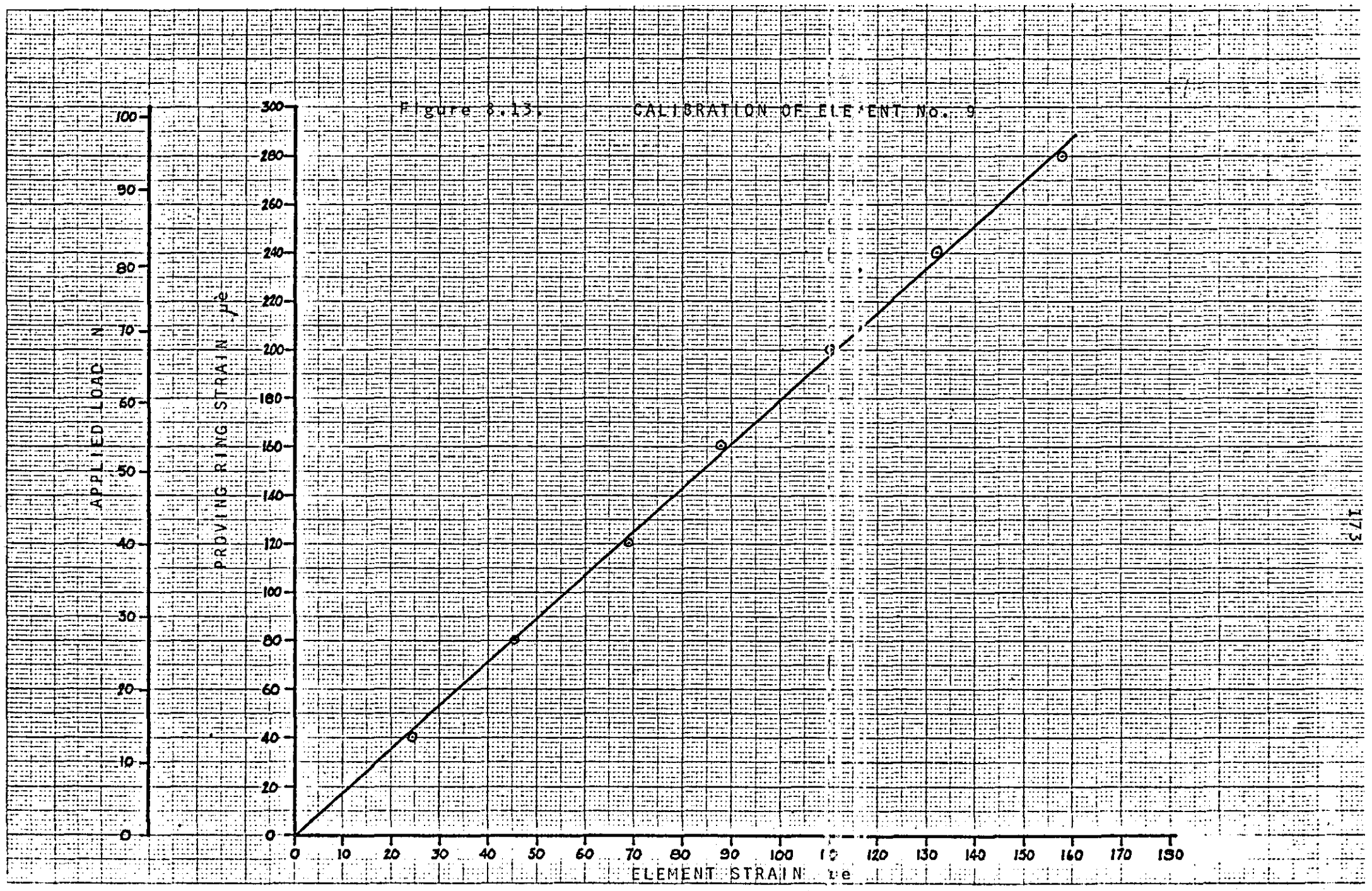
Figure 8.13. CALIBRATION OF ELEMENT No. 9
APPLIED LOAD N
PROVING RING STRAIN μe
ELEMENT STRAIN μe
0
10
20
30
40
50
60
70
80
90
100
110
120
130
140
150
160
170
180
200
220
240
260
280
300

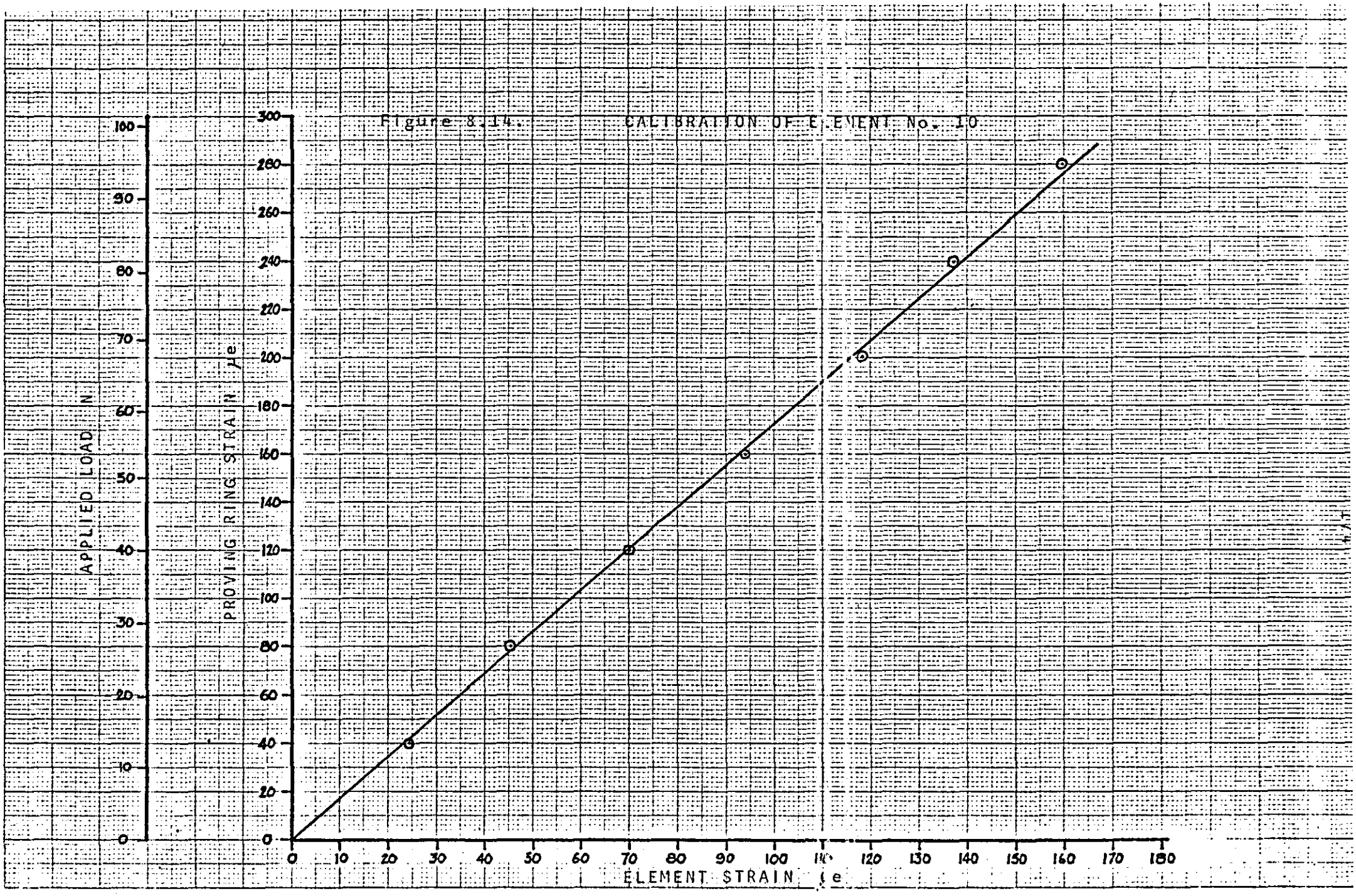

Figure 8.14. CALIBRATION OF ELEMENT No. 10

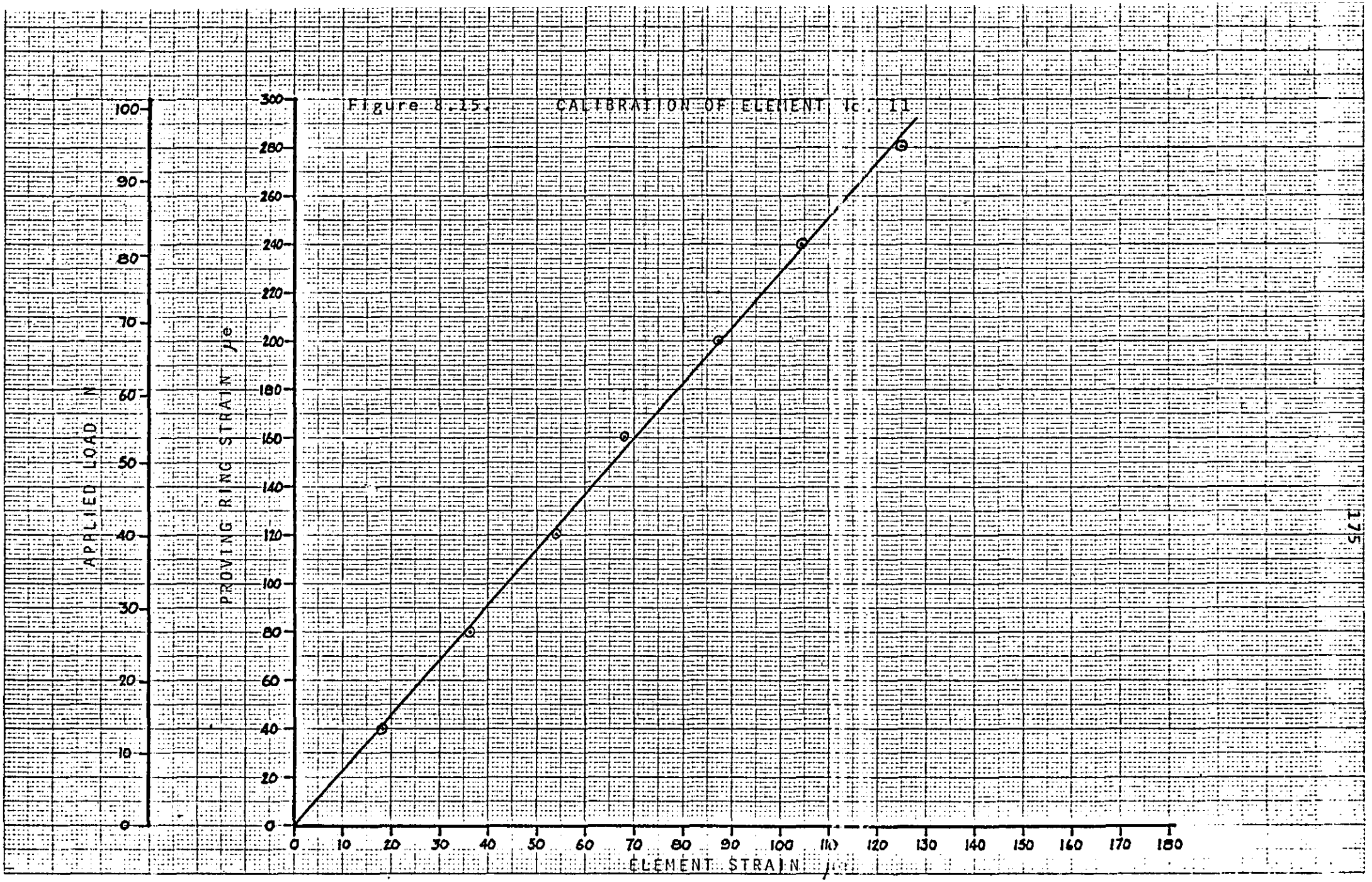
Figure 8.15 CALIBRATION OF ELEMENT Ic. 11
APPLIED LOAD N
PROVING RING STRAIN με
ELEMENT STRAIN με
0
10
20
30
40
50
60
70
80
90
100
110
120
130
140
150
160
170
180
0
10
20
40
60
80
100
120
140
160
180
200
220
240
260
280
300

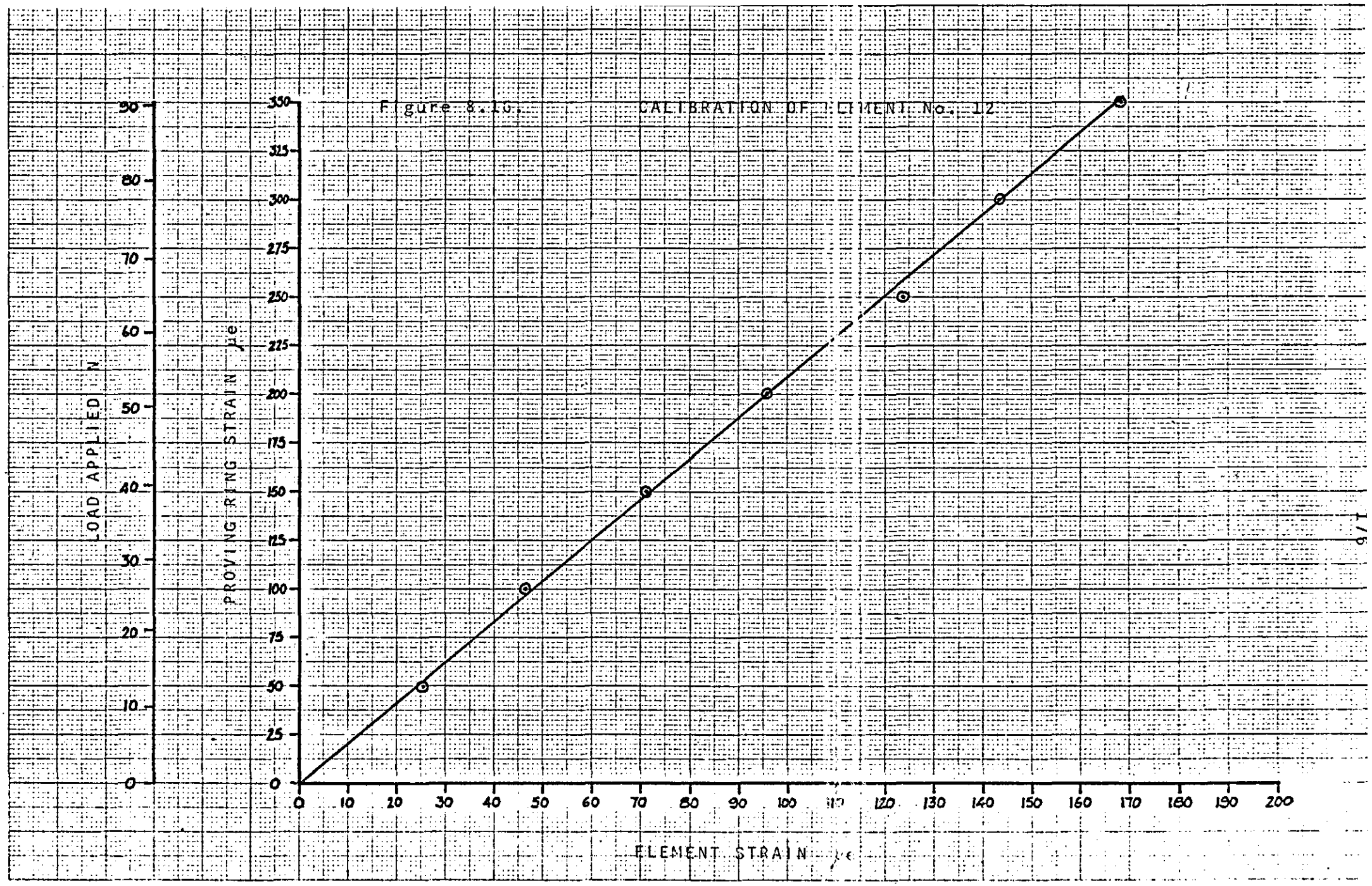
Figure 8.10. CALIBRATION OF ELEMENT No. 12
LOAD APPLIED N
PROVING RING STRAIN με
ELEMENT STRAIN με
0
10
20
30
40
50
60
70
80
90
100
110
120
130
140
150
160
170
180
190
200
25
75
125
175
225
275
325

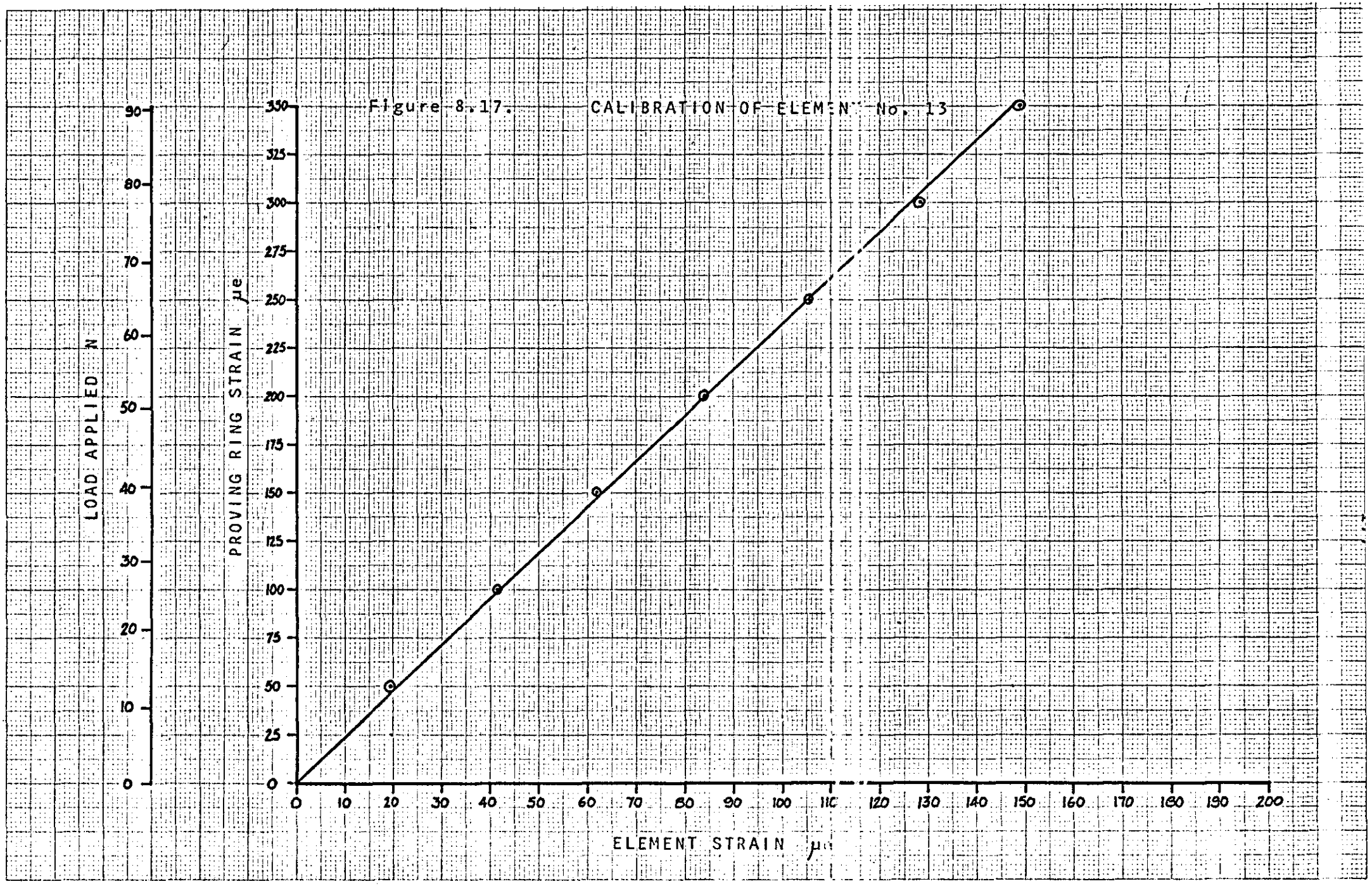
Figure 8.17. CALIBRATION OF ELEMENT No. 13
LOAD APPLIED N
PROVING RING STRAIN με
ELEMENT STRAIN με
0
10
20
25
50
75
100
125
150
175
200
225
250
275
300
325
350
30
40
60
70
80
90
110
120
130
140
150
160
170
180
190

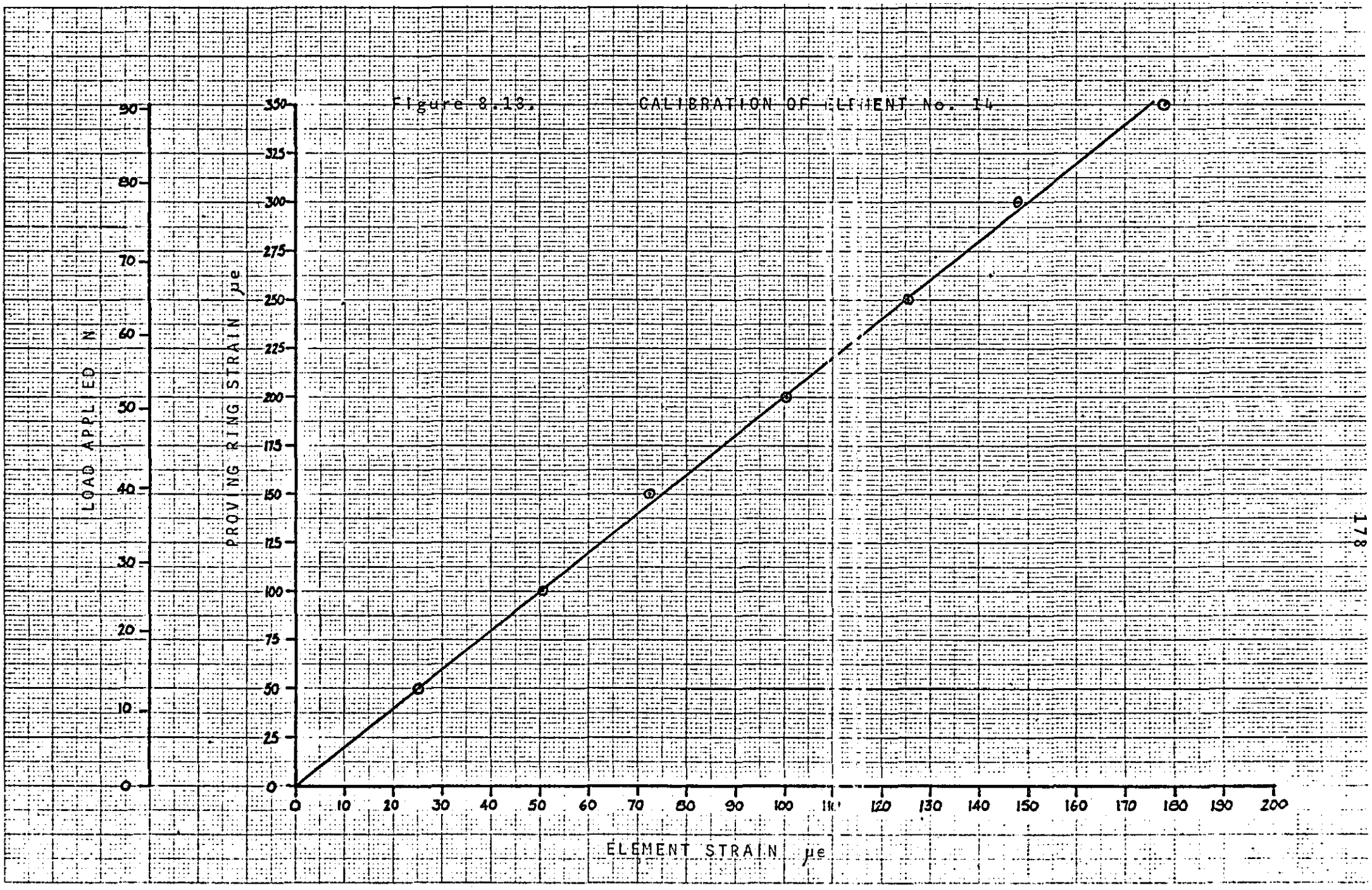
Figure 8.13. CALIBRATION OF ELEMENT No. 14
LOAD APPLIED N
PROVING RING STRAIN με
ELEMENT STRAIN με
0
10
20
30
40
50
60
70
80
90
100
120
130
140
150
160
170
180
190
200
25
75
125
175
225
275
300
325
350

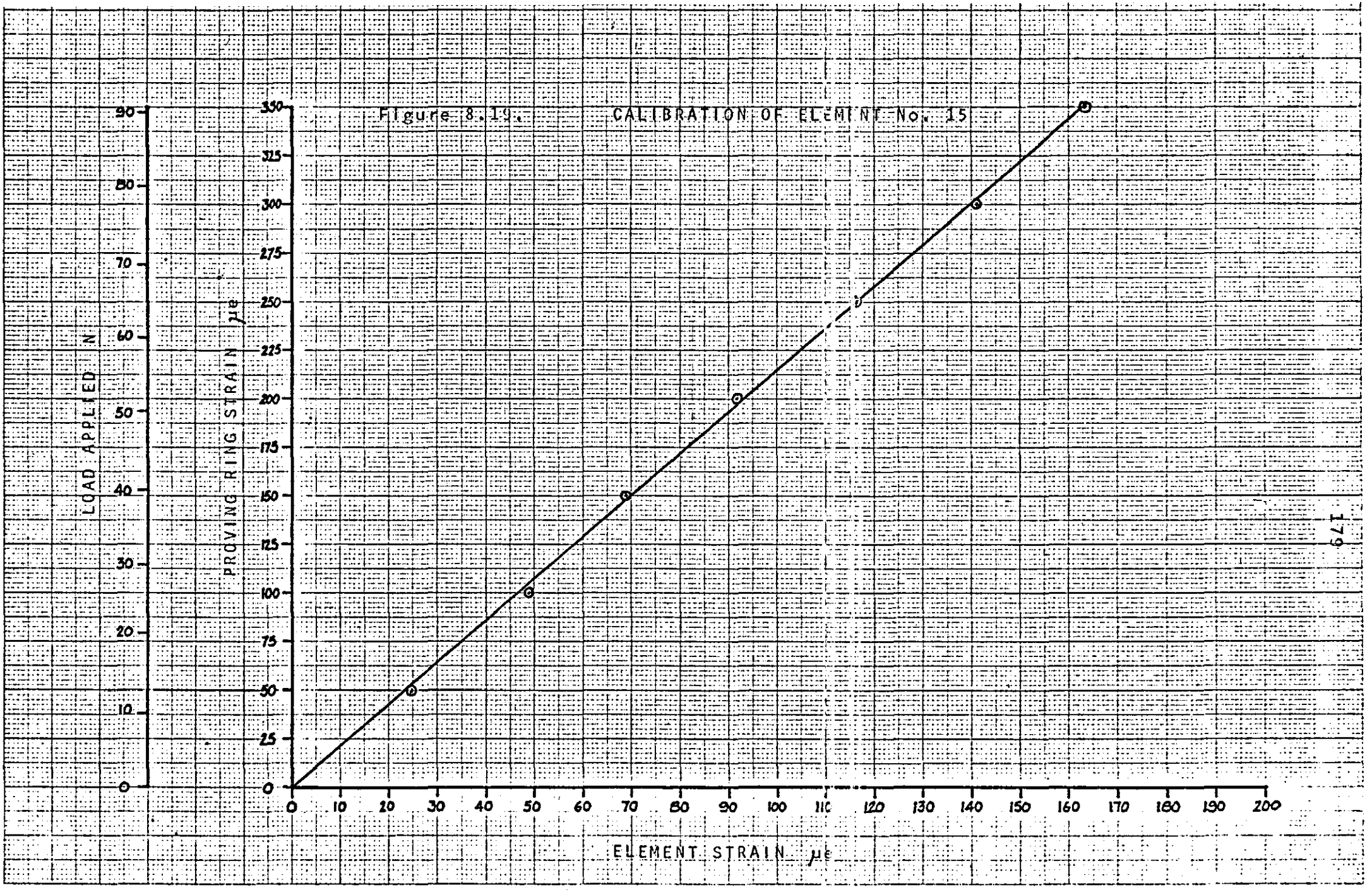
Figure 8.19. CALIBRATION OF ELEMENT No. 15
LOAD APPLIED N
PROVING RING STRAIN με
ELEMENT STRAIN με
0
10
20
30
40
50
60
70
80
90
100
110
120
130
140
150
160
170
180
190
200
25
75
125
175
225
275
325

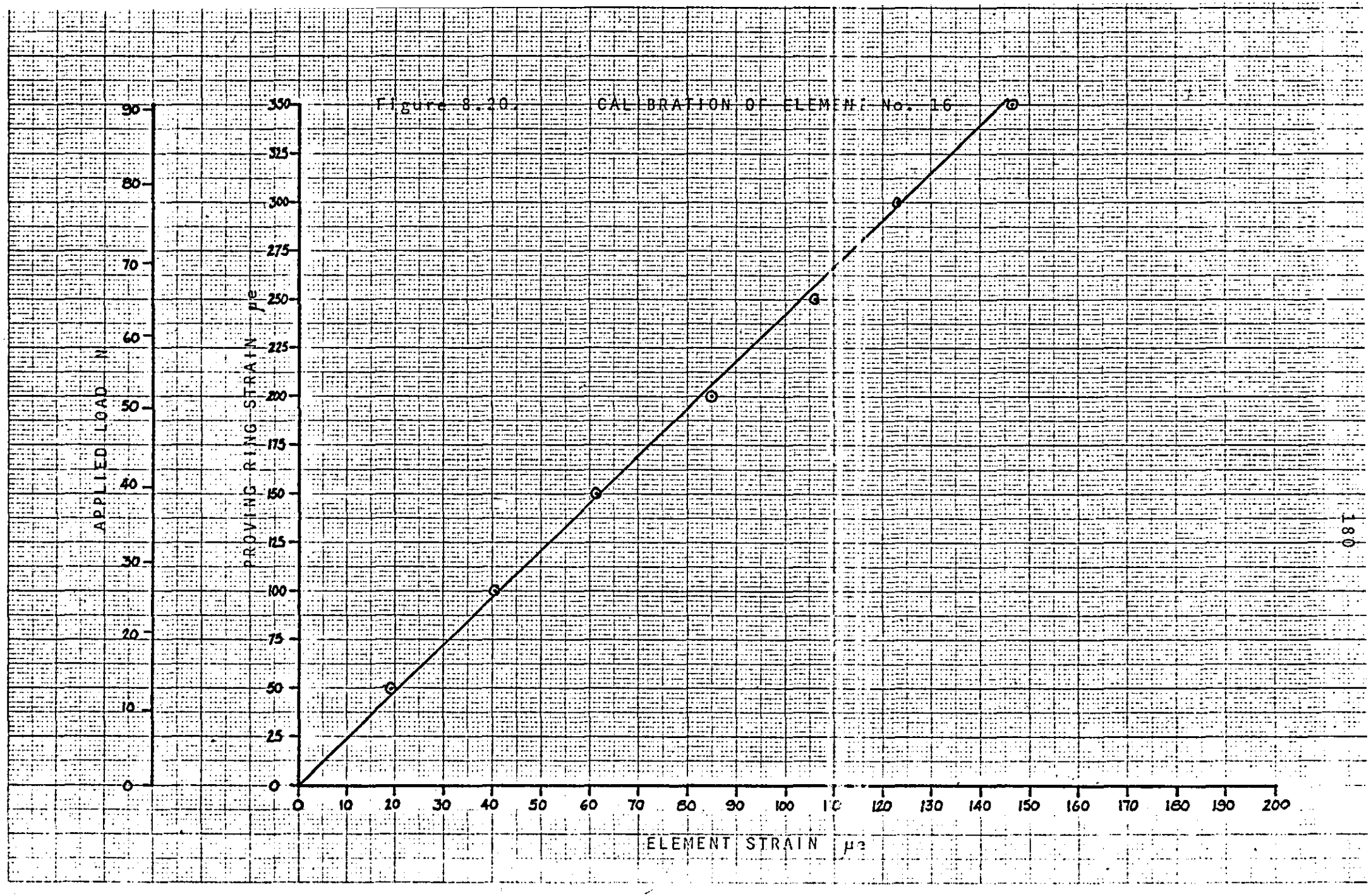
Figure 8.20. CALIBRATION OF ELEMENT No. 16
APPLIED LOAD N
PROVING RING STRAIN με
ELEMENT STRAIN με
0
10
20
30
40
50
60
70
80
90
100
110
120
130
140
150
160
170
180
190
200
25
75
125
175
225
275
325
350
180

8.1.3 Calibration of the Arbor for the 42.86mm. long Mandrel Sleeves

Instrument Data.

Techequipment Strain Bridge model 11
Manufactured by Techequipment, Nottingham.

Mean sensitivity at gain factor 1 = 1 με

Clockhouse proving ring model 2000.

Dial gauge number 1537. Last calibrated October 1972.

Mean sensitivity 5.9N (1.331bf) per division.

The experimental set up for the calibration of the arbor for the 42.86mm.(1.6875in.) long mandrel sleeves is shown in figure 8.21., the set up is similar to, and the load application apparatus and method the same as that used in the Load-Radial Expansion measurement rig described in Chapter 2. section 2. The set up consists of the arbor, the strain gauges wired to the Techequipment strain bridge, positioned on the table of the load application apparatus. On the uppermost taper of the arbor is a hardened steel collar with a 36^{o} included angle female taper in one end, this taper mates with the uppermost taper of the arbor for load application. During normal use the mandrel sleeve transfers its load to the arbor through contact on the tapers, for calibration therefore this situation has to be reproduced, but on one taper only. Positioned on top of the collar is the Clockhouse proving ring, used for verification of the magnitude of the applied load, the free end of the proving ring being positioned against a thrust bar which restrains upward movement. A load is applied when the table of the loading apparatus is moved upward and toward the restrained thrust bar, this subjects the proving ring to a deflection

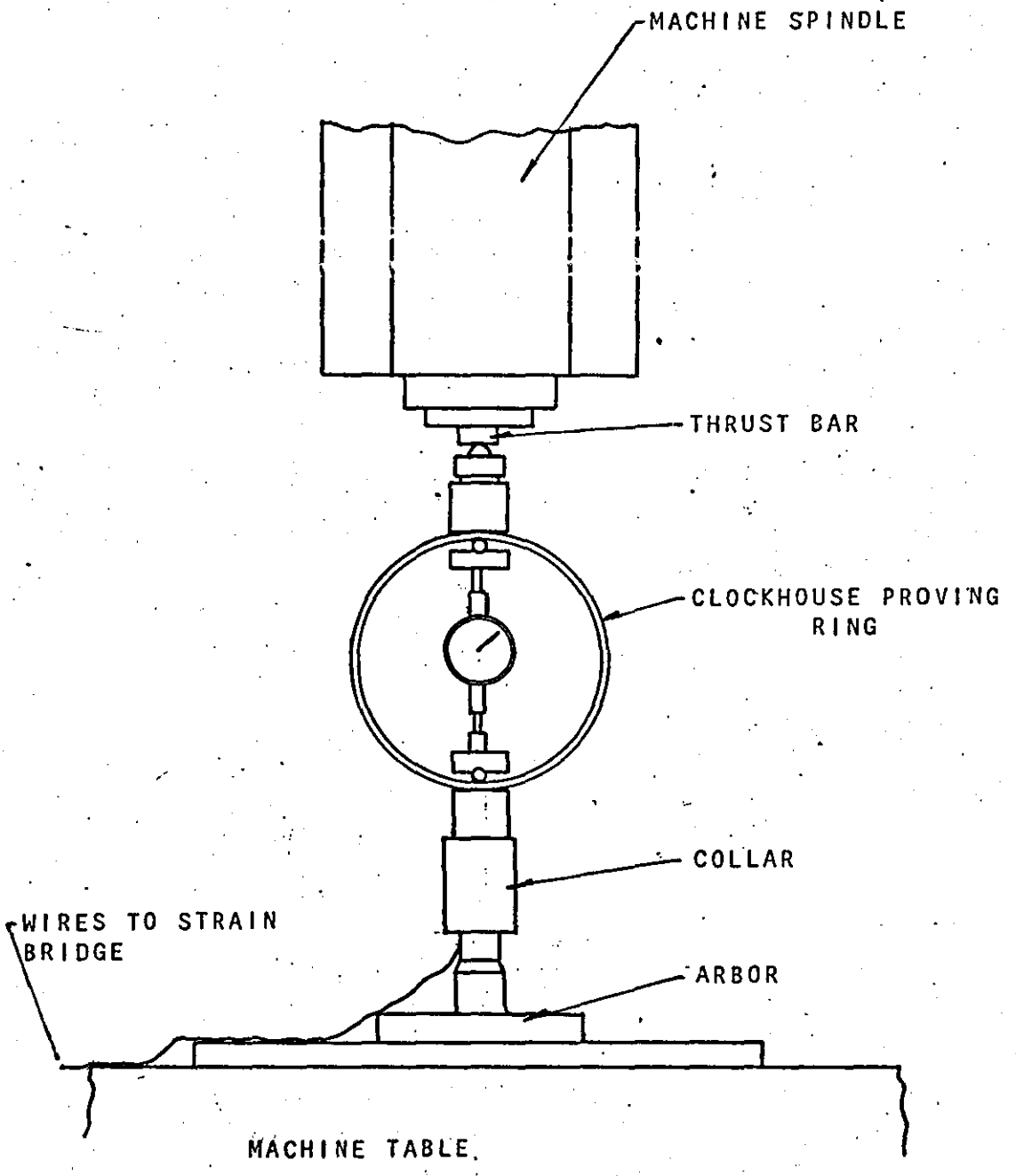

Figure 8.21: CALIBRATION OF ARBOR

and creates a load of known magnitude on the arbor.

The arbor was calibrated in the following manner, with the arbor subjected to no load the strain reading was measured and recorded, loads were then applied to the arbor in increments of 445N (100lbf) up to a maximum of 5340N (1200lbf), the strain readings corresponding to each load were measured and recorded. The calibration was repeated five times, the average value of strain for each load being used to plot the calibration curve. Table 8.20. and figure 8.22. show the experimental results and calibration curve respectively.

Table 8.20

Calibration of the arbor for the 42.86 mm. mandrel sleeve

Applied Load N	Strain bridge readings με 1st	2nd	3rd	4th	5th	Average Strain με
445	9	7	6	7	8	7.4
890	22	19	16	21	22	20.0
1334	31	28	27	27	30	28.6
1792	39	35	35	35	38	36.4
2240	47	45	44	46	46	45.6
2669	57	55	55	56	56	55.8
3174	67	64	63	65	66	65.0
3558	76	73	73	73	75	74.4
4005	85	83	82	85	84	84.0
4448	95	92	92	93	93	93.0
4893	104	102	101	102	103	102.4
5377	113	110	109	111	111	111.0

Figure 8.22. CALIBRATION OF ARBOR

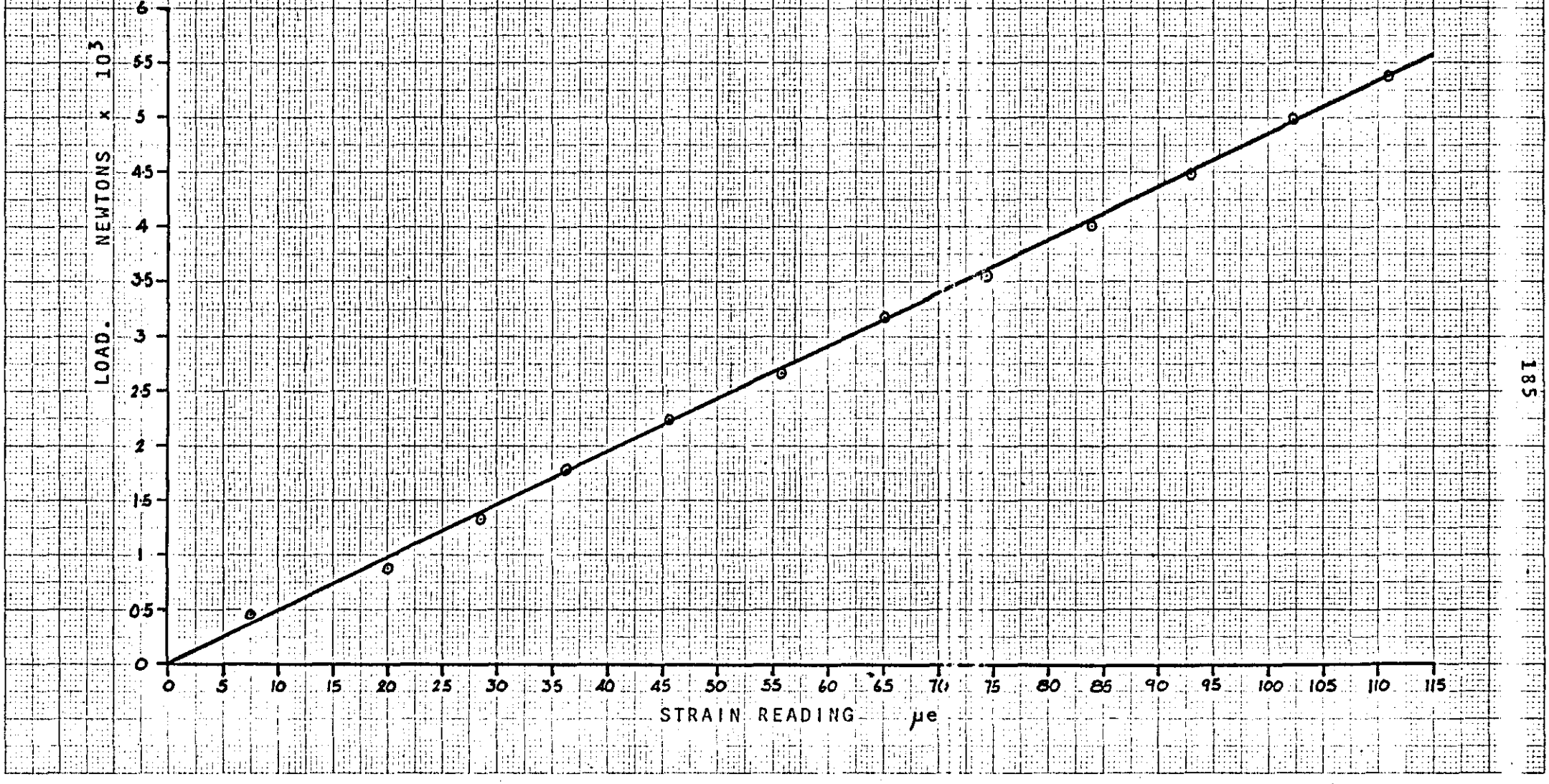

Table 8.21.

Mandrel dia. 60.32 mm. (2.375 in.). Length 26.99 mm. (1.0625 in.)
Number of slots 8. Initial dia. 60.30 mm. (2.3744 in.)
Initial preload 45N.

Applied Load Newtons	Increase in Radius Δr., μm.						Average Δr., μm.
98	8.12	7.87	8.89	8.89	9.14	7.87	8.38
347	24.89	25.40	24.13	24.89	25.65	23.36	24.63
595	37.84	38.10	38.10	39.11	39.62	38.60	38.60
843	52.57	53.84	52.57	53.59	55.11	52.32	53.34
1090	68.07	65.53	66.80	69.85	70.86	67.31	68.07
1338	85.09	83.82	83.82	86.10	87.12	83.05	84.83
1584	100.83	100.33	99.31	101.34	102.61	100.58	100.83
1817	117.34	116.33	115.82	118.36	119.12	116.07	117.09

Table 8.22.

Mandrel dia. 60.32 mm. (2.375 in.). Length 26.99 mm. (1.0625 in.)
Number of slots 10 Initial dia. 60.19 mm. (2.3697 in.)
Initial preload 45N.

Applied Load Newtons	Increase in Radius Δr., μm.						Average Δr., μm.
187	13.71	13.46	15.24	13.46	13.46	11.43	13.46
340	24.38	26.67	26.16	25.65	25.14	24.63	25.40
496	33.78	35.81	36.32	36,06	35,05	34,29	35.30
650	42.67	45.97	45.97	45.21	45.46	44,19	44.70
802	52.83	56.67	56.13	55.11	54.10	53.84	54.86
958	62.73	67.81	67.31	65.53	65.53	61.46	65.02
1112	73.40	76.45	75.94	75.43	77.47	75.69	75.69
1266	82.29	86.86	87.12	88.90	96.77	84.58	87.63
1486	101.34	100.33	99.82	103.37	99.82	96.57	100.07
1574	115.31	115.57	114.55	119.12	121.15	115.06	116.84
1730	119.12	123.95	126.74	125.22	123.44	121.41	123.19

Table 8.23.

Mandrel dia. 50.8 mm.(2 in.). Length 26.99 mm.(1.0625 in.)
Number of slots 8. Initial dia. 50.63 mm.(1.993 in.)
Initial preload 45N.

Applied Load Newtons	Increase in Radius Δr., μm.						Average Δr., μm.
162	10.41	9.65	12.19	10.16	11.68	10.66	11.25
449	25.14	24.89	27.43	26.41	27.17	25.90	26.16
723	38.35	38.10	41.65	39.62	40.38	39.62	39.62
1003	53.08	54.35	56.64	54.61	56.13	54.35	54.86
1281	71.37	70.86	74.42	71.88	73.66	70.61	72.13
1560	86.36	88.90	87.12	88.64	90.17	87.63	88.13
1841	104.39	106.68	108.71	104.39	108.20	104.39	105.92
2120	123.19	124.46	125.98	122.68	124.46	120.65	123.44
2395	144.27	142.24	141.73	141.22	140.97	137.66	141.48

Table 8.24.

Mandrel dia. 50.8 mm.(2in.). Length 26.99mm.(1.0625 in.)
Number of slots 10 Initial dia. 50.69 mm.(1.996 in.)
Initial preload 45N.

Applied Load Newtons	Increase in Radius Δr., μm.						Average Δr., μm.
176	15.74	16.50	17.52	16.25	16.25	17.02	16.51
324	28.19	30.23	28.96	28.96	29.72	30.99	29.46
474	41.14	43.18	43.18	41.65	42.24	43.37	42.67
617	52.57	54.86	57.65	53.34	55.37	54.61	58.86
764	65.53	66.80	67.05	67.56	66.54	68.07	67.06
912	78.23	80.01	78.23	79.76	80.26	82.29	79.76
1058	91.94	92.96	92.71	95.25	94.23	93.98	93.47
1206	107.95	107.95	108.96	107.95	107.69	109.22	108.20
1354	123.44	125.98	123.19	124.46	123.69	126.49	124.46
1500	139.19	134.62	138.43	140.71	140.71	139.70	138.94

Table 8.25.

Mandrel dia. 50.8 mm.(2 in.). Length 26.99 mm.(1.0625 in.)
Number of slots 12. Initial dia. 50.673 mm.(1.995 in.)
Initial preload 45N.

Applied Load / Newtons	Increase in Radius Δr., μm.						Average Δr., μm.
19	2.28	3.04	1.27	3.30	3.04	4.06	2.54
89	13.20	13.20	6.85	11.93	12.70	13.20	11.17
157	20.82	23.36	16.00	21.08	21.33	22.09	20.87
228	29.71	33.02	24.89	30.99	30.98	30.98	29.97
299	38.10	42.16	34.04	38.86	39.16	39.88	38.61
369	45.90	50.80	42.41	47.49	48.00	47.75	46.99
440	52.83	59.18	51.30	56.13	54.35	56.38	54.86
510	58.93	68.58	61.72	65.53	69.09	68.58	65.29
579	66.55	76.70	69.85	78.23	72.89	72.89	72.64
649	75.69	85.09	78.23	81.28	92.45	94.74	84.58
716	82.55	96.77	87.88	98.29	93.98	96.01	92.46
790	88.90	102.36	99.06	100.33	101.60	99.06	98.55
858	98.55	111.25	105.41	110.49	111.76	129.54	111.25
927	102.36	115.29	113.06	116.60	117.35	125.54	110.35
1000	130.11	120.54	123.19	127.76	134.60	131.57	130.05

Table 8.26.

Mandrel dia. 41.27 mm.(1.625 in.). Length 26.99 mm.(1.0625 in.)
Number of slots 8 Initial dia. 41.15 mm.(1.6204 in.)
Initial preload 45N.

Applied Load Newtons	Increase in Radius Δr., μm.						Average Δr., μm.
153	16.00	17.27	15.24	14.22	14.89	15.24	15.73
282	27.43	28.70	26.42	26.42	27.43	25.90	26.97
408	38.10	40.13	38.60	38.60	36.83	36.83	38.18
536	49.78	48.00	48.76	48.76	50.80	48.00	49.02
665	59.44	58.16	59.94	58.42	62.74	58.16	59.48
792	70.10	69.34	70.10	70.36	73.66	69.08	70.44
921	82.55	82.29	82.80	82.80	85.09	79.25	82.39
1048	90.67	94.48	93.47	86.61	92.71	86.10	90.67
1177	97.02	99.31	99.31	100.58	103.63	96.52	99.99
1304	111.76	109.22	113.03	107.69	114.30	105.41	110.23
1431	122.43	120.90	122.42	118.36	123.44	119.38	121.16

Table 8.27.

Mandrel dia. 41.27mm.(1.625 in.). Length 26.99 mm.(1.0625in.)
Number of slots 10. Initial dia. 41.148 mm.(1.620 in.)
Initial preload 45N.

Applied Load Newtons	Increase in Radius Δr.,μm.					Average Δr.,μm.
101	12.70	12.70	15.24	13.46	12.70	13.46
202	26.40	27.43	27.94	27.68	28.19	27.43
303	36.83	38.35	41.66	39.62	39.12	39.11
405	49.78	52.83	55.12	53.59	52.58	52.83
506	64.77	64.77	69.08	66.80	65.79	66.29
607	78.99	79.50	77.98	78.99	78.74	78.74
708	91.94	93.47	89.41	91.69	91.95	91.69
810	103.63	106.68	100.83	102.87	100.83	102.87
911	116.84	119.38	115.57	118.62	114.80	117.09
1013	136.14	132.33	133.38	129.79	130.55	132.43

Table 8.28.

Mandrel dia. 60.32 mm.(2.375in.). Length 48.86mm.(1.6875 in.)
Number of slots 8 Initial dia. 60.23 mm.(2.3715 in.)
Initial preload 45N.

Applied Load Newtons	Increase in Radius Δr.,μm.						Average Δr.,μm.
171	9.14	8.12	7.87	8.12	8.12	7.11	8.12
458	23.36	21.84	20.32	20.06	21.84	19.55	21.08
741	34.29	33.78	32.25	31.75	33.78	30.98	32.76
1027	48.51	46.22	43.69	43.69	45.47	42.16	44.96
1311	62.48	60.19	59.18	57.66	58.42	53.84	58.67
1595	76.71	76.96	76.20	76.71	75.69	72.89	75.94
1881	94.99	96.52	95.25	88.13	95.25	97.03	94.49
2166	111.18	113.54	101.09	115.06	108.71	101.60	108.53
2417	118.78	126.39	124.60	106.33	124.62	126.14	121.06

Table 8.29.

Mandrel dia. 60.32 mm. (2.375 in.). Length 48.86 mm. (1.6875 in.)
Number of slots 10. Initial dia. 60.23 mm. (2.3715 in.)
Initial preload 45N.

Applied Load Newtons	Increase in Radius Δr., μm.						Average Δr., μm.
203	21.33	20.32	20.32	20.06	20.32	20.32	20.45
373	38.86	37.59	38.61	38.61	37.08	37.34	38.01
543	58.42	55.88	56.39	56.39	54.36	55.88	56.13
712	72.89	70.36	71.12	70.86	70.35	71.62	71.20
882	89.15	86.86	88.90	88.13	84.84	86.36	87.33
1052	108.71	107.19	108.71	107.44	104.90	107.19	107.36
1222	122.43	124.46	124.71	124.71	124.20	124.97	124.21
1392	142.49	142.49	145.29	142.74	144.02	144.02	143.25

Table 8.30.

Mandrel dia. 60.32 mm. (2.375 in.). Length 48.86 mm. (1.6875 in.)
Number of slots 12 Initial dia. 60.26 mm. (2.3725 in.)
Initial preload 45N.

Applied Load Newtons	Increase in Radius Δr., μm.						Average Δr., μm.
138	25.65	24.38	24.38	22.35	23.62	23.87	24.13
278	48.77	48.51	48.77	46.73	46.73	49.78	48.26
416	71.62	72.89	73.66	71.12	74.17	73.41	72.89
556	99.82	101.09	102.36	99.06	98.30	100.83	100.33
694	119.88	122.43	121.92	120.14	119.88	119.38	120.66
834	142.49	146.81	148.84	143.26	146.30	146.56	145.79

Table 8.31.

Mandrel dia.50.80 mm.(2 in.). Length 48.86 mm.(1.6875 in.)
Number of slots 8. Initial dia. 50.66 mm.(1.9945in.)
Initial preload 45N.

Applied Load Newtons	Increase in Radius Δr.,μm.						Average Δr.,μm.
178	10.40	10.66	11.17	10.66	11.17	10.92	10.83
476	25.40	29.97	29.97	28.45	29.97	28.44	28.70
773	42.67	43.69	43.69	43.69	45.97	43.69	43.90
1081	60.45	64.00	64.77	62.23	65.02	61.72	63.03
1366	79.50	83.82	84.58	83.31	86.36	80.52	83.48
1664	100.33	105.41	105.92	104.14	106.17	100.84	103.80
1960	120.65	126.50	127.00	124.96	127.76	123.19	124.75
2257	142.24	148.60	148.80	146.81	149.60	146.30	147.06

Table 8.32.

Mandrel dia. 50.80 mm.(2 in.). Length 48.86mm.(1.6875 in.)
Number of slots 10 Initial dia.50.703 mm.(1.9962in.)
Initial preload 45N.

Applied Load Newtons	Increase in Radius Δr.,μm.						Average Δr.,μm.
136	19.56	15.74	17.78	16.50	17.02	15.74	17.05
273	38.60	35.56	35.05	38.10	37.59	36.06	36.83
409	57.91	54.36	51.56	51.56	51.56	48.26	52.54
550	77.97	70.35	70.36	67.82	65.77	63.24	69.26
681	96.01	90.17	84.33	88.39	82.55	91.44	91.44
819	111.25	109.22	105.16	109.72	103.63	107.44	107.75
955	127.76	129.54	124.21	124.21	122.68	124.46	125.47
1092	144.27	142.75	143.00	143.00	143.00	142.74	143.12

Table 8.33.

Mandrel dia. 50.80mm.(2in.). Length 48.86mm.(1.6875 in.)
Number of slots 12. Initial dia. 50.596mm.(1.992 in.)
Initial preload 45N.

Applied Load Newtons	Increase in Radius Δr., μm.						Average Δr., μm.
52	20.82	20.06	20.32	19.56	24.63	20.82	21.04
105	39.88	38.86	38.86	38.86	40.13	38.86	39.24
159	60.20	60.45	60.20	56.38	60.45	60.71	59.73
212	81.53	81.53	82.04	81.28	80.77	80.77	81.43
266	102.36	101.09	99.82	101.60	101.09	101.09	101.17
319	122.43	124.21	121.16	118.11	121.16	122.43	121.58
371	142.24	145.54	141.73	142.24	141.73	143.26	142.79

Table 8.34.

Mandrel dia. 41.275mm.(1.625 in.). Length 48.86 mm.(1.6875in.)
Number of slots 8 Initial dia. 41.163 mm.(1.6206in.)
Initial preload 45N.

Applied Load Newtons	Increase in Radius Δr., μm.						Average Δr., μm.
53	5.84	8.38	7.87	7.62	7.11	7.87	7.47
123	16.00	18.03	17.27	17.27	16.00	17.27	16.97
194	20.65	27.17	26.16	25.91	25.40	25.91	26.03
263	35.05	36.06	35.05	35.56	33.53	34.29	34.92
332	44.45	45.21	43.68	43.68	43.18	43.68	44.04
402	54.61	54.10	51.56	52.57	52.32	54.10	53.08
473	62.73	66.04	65.27	64.26	65.27	64.00	64.59
543	70.61	74.16	75.69	74.16	72.89	75.90	74.09
612	73.15	84.58	82.55	84.58	88.90	81.28	82.51
682	79.25	93.22	97.28	97.28	100.84	100.84	94.78
753	97.28	104.90	102.36	102.36	103.63	103.63	102.36
822	115.06	116.33	118.62	122.17	119.89	124.21	119.38
962	124.97	125.22	126.49	124.46	129.54	124.96	125.94
1032	137.66	138.94	140.21	144.78	137.92	145.54	140.84

Table 8.35.

Mandrel dia. 41,275 mm. (1.625 in.). Length 48.86 mm. (1.6875 in.)
Number of slots 10. Initial dia. 41.193 mm. (1.6218 in.)
Initial preload 45N.

Applied Load Newtons	Increase in Radius Δr., μm.						Average Δr., μm.
53	16.00	20.32	17.78	19.56	21.59	19.30	19.35
89	27.68	33.02	30.22	30.99	34.29	32.51	31.45
124	39.88	44.45	41.91	42.92	45.72	42.16	42.84
159	54.61	56.38	53.59	55.10	58.42	56.64	55.79
195	68.58	71.88	67.56	72.39	75.94	74.67	71.84
229	78.74	84.00	82.29	83.05	86.61	86.36	83.51
265	86.87	96.77	98.04	97.03	99.06	99.56	100.58
300	102.87	106.93	110.49	109.98	112.27	113.79	109.38
335	118.11	125.22	128.78	128.78	132.59	130.30	127.29

Table 8.36.

Mandrel dia. 41,275 mm. (1.625 in.). Length 48.86 mm. (1.6875 in.)
Number of slots 12 Initial dia. 41.099 mm. (1.6181 in.)
Initial preload 45N.

Applied Load Newtons	Increase in Radius Δr., μm.						Average Δr., μm.
18	10.67	14.22	18.28	18.54	15.74	13.97	15.23
36	24.13	29.21	32.25	31.24	27.94	30.45	29.20
53	41.14	44.70	49.78	43.43	43.68	45.72	44.74
71	59.94	62.99	67.06	64.77	61.72	64.77	63.54
89	74.42	85.09	87.88	86.61	82.80	84.58	83.56
106	88.13	103.63	107.88	103.88	98.29	103.37	100.86
123	113.53	119.38	124.21	123.19	118.11	122.17	120.09
141	118.87	134.11	138.18	140.46	132.08	133.60	132.88
159	135.13	151.13	152.15	154.69	143.00	153.16	149.13

Table 8.37.

Mandrel Sleeve dia. 41.26mm. Length 42.86mm. No. of Slots 12

Position from Top of Sleeve mm.	Radial Expansion μm				Average Radial Expansion μm
1	127	127	127	127	127
6	126.8	124.3	124.6	125.1	125.2
11	127.3	126.4	127.2	126.9	126.9
16	124.7	125.8	125.1	124.6	125.0
21	126.9	125.3	127.3	124.9	126.1
26	125.4	127.3	124.1	127.1	125.9
31	126.1	125.8	127.3	128.3	126.9
36	124.2	123.8	125.9	125.8	124.9
41	127.1	127.3	126.3	126.2	126.7

Table 8.38.

Mandrel Sleeve dia. 60.32mm. Length 42.86mm. No. of Slots 10

Position from Top of Sleeve mm.	Radial Expansion μm				Average Radial Expansion μm
1	127	127	127	127	127
6	127.3	127.6	126.8	127.5	127.3
11	126.8	125.8	126.3	126.1	126.2
16	125.3	125.1	126.7	126.1	125.8
21	127.6	126.1	125.9	127.6	126.8
26	127.8	128.2	127.6	127.3	127.7
31	127.6	126.8	125.5	127.1	126.8
36	126.8	124.9	125.8	125.3	125.7
41	127.4	126.8	127.3	128.2	127.4

Table 8.39.

Mandrel Sleeve dia. 50.80mm. Length 42.86mm. No. of Slots 8

Position from Top of Sleeve mm.	Radial Expansion μm				Average Radial Expansion μm
1	127	127	127	127	127
6	124.8	125.3	127.4	127.6	126.3
11	126.9	126.5	125.4	126.3	126.3
16	125.1	126.8	126.4	126.1	126.1
21	127.4	126.1	127.7	127.6	127.2
26	126.8	125.4	128.5	125.9	126.7
31	127.1	127.1	126.5	126.1	126.7
36	126.0	123.8	126.7	128.2	126.2
41	126.5	125.8	126.3	125.5	126.0

Table 8.40.

Mandrel Sleeve dia. 41.26mm. Length 26.98mm. No. of Slots 8

Position from Top of Sleeve mm.	Radial Expansion μm				Average Radial Expansion μm
1	127	127	127	127	127
6	126.5	127.3	126.9	125.1	126.5
11	126.8	125.8	127.3	124.9	126.8
16	127.8	127.3	124.1	127.3	126.6
21	125.3	124.7	127.1	128.3	126.3
26	127.3	124.3	127.3	126.5	126.3

Table 8.41.

Mandrel Sleeve dia. 50.80mm. Length 26.98mm. No. of Slots 1(

Position from Top of Sleeve mm.	Radial Expansion μm				Average Radial Expansion μm
1	127	127	127	127	127
6	126.8	127.1	125.1	126.5	126.4
11	126.4	126.8	127.4	127.3	127.0
16	124.6	127.3	127.1	128.2	126.8
21	126.8	126.9	125.8	127.2	126.6
26	127.3	124.6	124.2	125.4	125.3

Table 8.42.

Mandrel Sleeve dia. 60.32mm. Length 26.98mm. No. of Slots 12

Position from Top of Sleeve mm.	Radial Expansion μm				Average Radial Expansion μm
1	127	127	127	127	127
6	127.3	126.1	126.7	127.6	127.0
11	125.8	126.3	125.3	126.8	126.0
16	126.8	127.7	125.5	127.1	126.8
21	127.5	128.5	126.1	127.3	127.3
26	126.1	126.5	126.8	125.8	126.3

Table 8.43.

Mandrel dia. 60.32mm. Length 42.86mm. No. of Slots 8.

Applied Load N	Strain Reading με					Average Strain με	Load Between Tapers N
500	4	5	5	4	5	4.6	230
1000	9	9	10	10	9	9.4	460
1500	13	14	15	14	14	14.0	700
2000	20	21	21	19	20	20.2	1000
2500	25	26	27	25	25	25.6	1250

Table 8.44.

Mandrel dia. 60.32mm. Length 42.86mm. No. of Slots 10.

Applied Load N	Strain Reading με					Average Strain με	Load Between Tapers N
300	2	2	2	2	2	2.0	100
600	5	5	6	5	6	5.4	270
900	9	9	8	8	9	8.6	430
1200	12	12	11	11	11	11.4	570

Table 8.45.

Mandrel dia. 60.32mm. Length 42.86mm. No. of Slots 12.

Applied Load N	Strain Reading με					Average Strain με	Load Between Tapers N
200	1	1	1	1	1	1.0	60
400	3	4	4	3	3	3.4	180
600	6	5	5	5	6	5.4	270
800	8	8	7	7	8	7.6	370

Table 8.46.

Mandrel dia. 50.80mm. Length 42.86mm. No. of Slots 10.

Applied Load N	Strain Reading με					Average Strain με	Load Between Tapers N
250	2	3	3	2	3	2.6	120
500	5	5	5	4	4	4.6	230
750	7	7	7	7	8	7.2	360
1000	10	9	10	9	9	9.4	470

Table 8.47.

Mandrel dia. 50.80mm. Length 42.86mm. No. of Slots 12

Applied Load N	Strain Reading με					Average Strain με	Load Between Tapers N
100	1	1	1	1	1	1.0	50
200	1	2	2	2	1	1.6	80
300	1	2	2	2	2	1.8	105
400	3	3	4	4	4	3.6	175

Table 8.48.

Mandrel dia. 50.80mm. Length 42.86mm. No. of Slots 8

Applied Load N	Strain Reading με					Average Strain με	Load Between Tapers N
500	4	5	5	5	4	4.6	230
1000	10	10	9	10	11	10.0	500
1500	15	14	15	15	15	14.8	720
2000	20	20	19	20	21	20.0	970

Table 8.49.

Linear Sleeve 1 as per figure 2.9.

Load N	Extension μm						Average μm
0	0	0	0	0	0	0	0
49	33	30	28	30	30	30	30.16
98	61	58	58	58	56	58	58.16
147	91	90	84	86	81	86	86.33
196	119	117	114	114	109	114	114.50
245	147	145	140	142	134	140	141.33
294	178	173	170	172	163	168	170.66
343	206	201	198	203	188	193	198.16
392	234	231	226	231	213	221	226.00
441	262	259	254	259	239	249	253.66
490	290	287	282	287	264	274	280.66
539	320	315	310	315	290	300	308.33

Table 8.50.

Linear Sleeve 2 as per figure 2.9.

Load N	Extension μm						Average μm
0	0	0	0	0	0	0	0
49	61	66	58	51	61	61	59.66
98	122	127	119	109	122	124	120.50
147	183	191	183	170	183	185	182.50
196	244	269	241	231	246	249	246.66

Table 8.51.

Linear Sleeve 3 as per figure 2.9.

Load N	Extension μm						Average μm
0	0	0	0	0	0	0	0
49	25	25	28	25	23	23	24.83
98	51	51	48	51	46	46	49.00
147	76	76	71	74	69	69	72.50
196	102	102	97	97	91	94	97.16
245	127	127	122	122	114	117	121.50
294	152	150	145	145	137	142	145.16
343	178	175	168	168	160	165	169.00
392	203	198	191	193	183	188	192.66
441	223	221	213	216	208	213	213.36
490	249	246	236	238	231	236	239.33
539	269	269	259	261	254	259	261.83

Table 8.52.

Trial Interface Pressure Rig.

Transducer Element No.14.

Mandrel Sleeve dia. 60.32mm. Length 42.86mm. No. of Slots 8

Load N	626	1873	3120	4369
Strain με	16	41	60	74

Mandrel Sleeve dia. 60.32mm. Length 42.86mm. No. of Slots 10

Load N	626	1873	3120	4369
Strain με	13	44	62	75

Mandrel Sleeve dia. 60.32mm. Length 42.86mm. No. of Slots 12

Load N	626	1873	3120	4369
Strain με	17	41	56	66

Table 8.53.

Interface Pressure Results

Mandrel dia. 60.32mm. Length 26.98mm. No. of Slots 8.

Applied Load N	Average Element Strain με Element No. 6	5	4
626	24	28	34
1247	48	58	69
1873	68	81	97
2495	84	101	120
3120	98	118	140
3752	110	134	160
4369	121	147	175
4995	132	160	191
5616	142	172	206
6243	155	186	224

Table 8.54.

Interface Pressure Results

Mandrel dia. 60.32mm. Length 26.98mm. No. of Slots 10.

Applied Load N	Average Element Strain με Element No. 6	5	4
626	25	30	37
1247	48	57	69
1873	67	81	97
2495	84	101	120
3120	98	118	139
3752	121	141	175
4369	125	149	180
4995	131	156	189
5616	148	177	212
6243	157	185	225

Table 8.55.

Interface Pressure Results

Mandrel dia. 60.32mm. Length 26.98mm. No. of Slots 12

Applied Load N	Average Element Strain με Element No. 6	5	4
626	27	30	40
1247	49	52	73
1873	67	79	96
2495	81	96	117
3120	94	112	134
3752	104	120	151
4369	114	135	163
4995	122	146	175
5616	129	156	188
6243	138	163	199

Table 8.56.

Interface Pressure Results

Mandrel dia. 60.32mm. Length 42.86mm. No. of Slots 8

Applied Load N	Average Element Strain με Element No. 16	15	14	13	12
626	12	15	15	19	14
1247	24	29	29	26	28
1873	32	39	40	35	37
2495	43	48	49	43	47
3120	49	57	59	52	56
3752	55	64	67	59	65
4369	61	72	74	65	71
4995	68	79	82	72	79
5616	72	85	88	77	84
6243	78	91	95	83	92

Table 8.57.

Interface Pressure Results

Mandrel dia. 60.32mm. Length 42.86mm. No. of Slots 10

Applied Load N	Average Element Strain με				
Element No.	16	15	14	13	12
626	12	15	14	15	13
1247	25	29	31	26	28
1873	37	43	44	39	43
2495	45	53	55	48	53
3120	52	61	63	56	61
3752	59	68	70	61	68
4369	63	74	76	66	73
4995	67	79	81	71	78
5616	71	83	86	75	82
6243	75	87	91	78	87

Table 8.58.

Interface Pressure Results

Mandrel dia. 60.32mm. Length 42.86mm. No.of Slots 12

Applied Load N	Average Element Strain με				
Element No.	16	15	14	13	12
626	13	16	16	14	17
1247	24	29	30	26	28
1873	33	38	39	34	38
2495	39	46	47	41	45
3120	44	52	54	47	51
3752	49	57	58	51	56
4369	52	62	63	56	60
4995	56	66	67	60	65
5616	58	68	70	61	67
6243	62	72	74	66	73

Table 8.59.

Interface Pressure Results

Mandrel dia. 50.80mm. Length 42.86mm. No. of Slots 8

Applied Load N	Average Element Strain με				
	Element No. 7	8	9	10	11
313	7	9	7	9	6
626	13	18	14	16	12
934	18	24	20	22	15
1247	21	28	23	27	18
1561	25	34	27	32	22
1873	26	35	29	34	23
2181	28	39	32	37	25
2495	30	42	34	39	26
2808	32	45	36	42	28
3121	33	47	38	44	29

Table 8.60

Interface Pressure Results

Mandrel dia. 50.80mm. Length 42.86mm. No. of Slots 10

Applied Load N	Average Element Strain με				
	Element No. 7	8	9	10	11
313	7	10	7	9	6
626	11	15	11	15	9
934	16	22	17	20	14
1247	19	27	21	25	17
1561	23	31	25	30	21
1873	25	35	28	33	22
2181	27	38	30	36	24
2495	28	40	31	38	25
2808	30	43	34	40	26
3121	31	43	34	40	27

Table 8.60.

Interface Pressure Results

Mandrel dia. 50.80mm. Length 42.86mm. No. of Slots 12

Applied Load N	Average Element Strain με Element No. 7	8	9	10	11
436	9	12	8	10	7
750	11	17	13	16	10
1060	15	22	17	21	13
1373	18	27	20	24	16
1685	20	30	23	28	18
1997	23	35	26	33	20
2309	25	38	28	36	22
2621	28	42	31	39	24
2934	30	45	33	42	27

Table 8.61.

Interface Pressure Results

Mandrel dia. 41.28mm. Length 26.98mm. No. of Slots 8

Applied Load N	Average Element Strain με Element No. 3	2	1
313	16	13	18
626	27	22	30
934	34	27	37
1247	39	31	42
1561	45	36	50
1873	49	39	55
2181	53	43	60
2495	59	48	66
2808	63	51	69

Table 8.62.

Interface Pressure Results

Mandrel dia. 41.28mm. Length 26.98mm. No. of Slots 10

Applied Load N	Average Element Strain με		
Element No.	3	2	1
313	18	14	20
626	28	22	30
934	35	28	39
1247	42	33	46
1561	47	38	52
1873	51	42	57
2181	55	45	60
2495	57	47	63
2808	59	49	66

Table 8.63.

Interface Pressure Results

Mandrel dia. 41.28mm. Length 26.98mm. No. of Slots 12

Applied Load N	Average Element Strain με		
Element No.	3	2	1
313	18	14	19
626	29	23	32
934	35	28	39
1247	42	33	47
1561	50	39	53
1873	52	41	58
2181	57	44	62
2495	63	48	68
2808	67	51	71

8.3 'Scrap-Pad' Computer Program for the Calculation of the Axial Load to Produce a Diametral Expansion of 254 um

Program.

Program Step	Operation Key	Program Step	Operation Key	Program Step	Operation Key
1	S/S	26	4	51	*
2	St	27	*	52	Rc
3	2	28	S/S	53	2
4	a^x	29	*	54	*
5	3	30	Rc	55	S/S
6	=	31	2	56	
7	*	32		57	1.65
8	S/S	33	1.65	58	EXP
9	St	34	EXP	59	12
10	1	35	12	60	
11		36		61	S/S
12	2.48	37	S/S	62	1
13	EXP	38	1	63	=
14	12	39	=	64	+
15		40	+	65	Rc
16	S/S	41	Rc	66	9
17	1	42	9	67	=
18	=	43	=	68	1/X
19	St	44	St	69	*
20	9	45	9	70	.399
21	Rc	46	Rc	71	EXP
22	1	47	1	72	-
23	*	48	*	73	6
24	S/S	49	Rc	74	=
25	St	50	4	75	S/S

Execution of Program.

Step	Operation	Step	Operation
1	Press S/S	10	Enter value l_{es}
2	Enter value l	11	Press S/S
3	Press S/S	12	Enter value l_{es}
4	Enter value N	13	Press S/S
5	Press S/S	14	Enter value les_2
6	Enter value l	15	Press S/S
7	Press S/S	16	Enter value l_{es2}
8	Enter value L*	17	Press S/S Answer
9	Press S/S		W_A displayed.

8.4. Calculated Loading Data based upon the Maximum Load used in the Interface Pressure Experiments

8.4.1. Calculation of the Torque Required in Thread Loading to Produce the Maximum Experimental Load used

It is useful th have some comparison between the maximum load used in the interface pressure experimentation and that which might be effected by a workman using a wrench to tighten the nut on the arbor.

The standard formula for the torque required to produce an axial load by a screwthread against the load is given in (63) as

$$T = W\left[r_m\left(\frac{\tan\alpha + \mu/\cos\theta_n}{1-\mu\tan\alpha/\cos\theta_n}\right) + \mu_c\, r_c\right]$$

Where T = torque required to turn screw or nut
r_m = radius of the pitch circle
W = load
r_c = effective radius of rubbing surface against which load bears, called collar radius
μ = coefficient of friction
μ_c = coefficient of friction for collar
$\tan\alpha$ = $\frac{\text{screwthread lead}}{2\pi r_m}$
θ_n = helix angle of thread

From (63) typical values of μ and μ_c are .15 and .3 respectively.

Screwthread details.

Outside diameter - 25.4mm. (1 in.)

Tread form: American Threads, Unified. National-Fine.

Root dia. - 22.804mm. (.8978in.)

r_m - 12.013mm. (.4430in.)

Number of threads per inch = 12 (lead = 1/2in. = 2.1166mm.).

$$\text{Tan}\,\alpha = \frac{2.1166}{2\times\pi\times12.013} = .02804$$

r_c = O/D/2 = 25.4/2 = 12.7

$\theta_n = \theta = 30^\circ$ since the helix angle is so small

(American form threads have an included angle of 60°)

For a load of 5500N (1236lbf), the maximum applied to the 60.32mm. mandrels.

$$T = 5500\left[12.013\left[\frac{.028+(.15/.866)}{1-(.028x.15)/.866}\right] + (.3 \times 12.7)\right]$$

$$= 34.48 \text{ N-m}$$

For a 230mm(9in.) spanner the load required to produce the above torque is 150N (33.7lbf).

8.4.2 Diameter of Air Cylinder Required

The compressed air line pressure available in most workshops is of the order of .689 MN/m^2 (100lbf/in^2), the diameter of an air cylinder to effect a 5500N load on the mandrel system is given by $D = \sqrt{\frac{\text{Load} \times 4}{\text{airline pressure} \times \pi}}$

Substituting values into the above equation

$$D = \sqrt{\frac{5500 \times 4}{.6895 \times 10^6 \times \pi}}$$

$$= 100\text{mm.}$$

8.5. Strain Gauges

The use of strain gauges in this project was to allow transducers of simple design to be manufactured. The transducers manufactured, proving rings etc., rely on strain measurement to convert some deformation into information which is usable and presented in a readable form. It was at no time required to make absolute strain measurements to establish stress levels etc., in components, even when direct stress readings were being taken, (e.g. load measurement on arbor), a load-strain curve was established by calibration, therefore it is not felt necessary to present detailed information about either the strain bridge or strain gauge theory.

The strain gauges used were foil gauge type, gauge factor approximately 2.1, manufactured by Tokyo Sokki Kenkyujo Co. Ltd, Japan. Although the strain gauges used were the temperature compensated type, the effects of temperature on strain readings was eliminated in every application by either the use of a dummy gauge mounted to a strip of unstrained material positioned near and in a similar environment to the active gauge, or by the use of two active gauges one in each arm of the strain bridge. The gauges were attached to the transducer with an adhesive (P-2) supplied by the manufacturers of the strain gauges, the standard procedure for mounting strain gauges being used for every strain gauge application.